Collective Excitations with Chiral NN+3N Interactions from Coupled-Cluster and In-Medium SRG

Vom Fachbereich Physik
der Technischen Universität Darmstadt

zur Erlangung des Grades
eines Doktors der Naturwissenschaften
(Dr. rer. nat.)

genehmigte Dissertation von
M.Sc. Richard Trippel
aus Langen

Darmstadt 2016
D17

Referent:	Prof. Dr. Robert Roth
Korreferent:	Prof. Achim Schwenk, Ph.D.
Tag der Einreichung:	22.11.2016
Tag der Prüfung:	19.12.2016

Abstract

A broad variety of many-body methods exists for the investigation of ground-state properties, ranging from sophisticated ab initio approaches to traditional, phenomenological models. The description of low-lying excited states of medium-mass nuclei with ab initio methods has also become possible through recent progress in many-body theory. For collective modes at higher energies, however, these methods usually cannot be applied. Therefore, when describing collective excitations either completely phenomenological, macroscopic models are employed or microscopic models using phenomenological interactions.

One of the microscopic models well suited for the calculation of collective properties is the random-phase approximation (RPA). In the past, the use of phenomenological interactions for RPA has shown promising results. However, the application of chiral NN interactions yielded transitions at significantly too high energies, far from agreement with experimental data.

This thesis focuses on the description of collective modes using both RPA and its second-order extension, SRPA. In contrast to previous research endeavors, we employ chiral NN+3N interactions. The use of chiral interactions is an important first step for describing ground-state, excitation and collective properties on an equal foundation. We find that the inclusion of 3N terms is crucial for RPA calculations and the prediction for collective modes is drastically improved through the 3N terms. For SRPA we show first-ever results with chiral interactions, again leading to an improvement in the predictions.

For a successful ab initio description of ground-state properties the inclusion of correlations is of paramount importance. Past RPA calculations have been performed using the quasi-boson approximation, effectively neglecting ground-state correlations. Using RPA, the next step along the path towards an ab initio description of collective properties will, therefore, be the inclusion of correlations. To that end, we extend the RPA formalism to include ground-state correlations from two different many-body methods, the in-medium similarity renormalization group (IM-SRG) and coupled-cluster theory with singles and doubles excitations (CCSD). Both methods have been applied with great success for the calculation of ground-state energies. We develop a formalism based on density matrices for CC-RPA that enables RPA based on an CCSD ground state. The use of IM-SRG transformed matrix elements gives us the possibility to include ground-state correlations even at the level of SRPA.

For both methods we observe a strong upward shift in the strength distributions, and, unexpectedly, we find a good agreement between IM-RPA and CC-RPA results. The structure of the transitions remains largely unchanged. We conclude that correlations have significant impact on the energetic positions, but not on the structure of the strength distributions.

Employing IM-SRPA we find a strong downward shift in energy similar to the case of SRPA. The agreement of both methods with experiment is comparable.

Zusammenfassung

Für die Beschreibung von Grundzustandseigenschaften existiert eine große Fülle an Vielteilchenmethoden, welche von komplizierten ab initio Ansätzen bis hin zu traditionellen, phänomenologischen Modellen reicht. Auch die Beschreibung von niedrig liegenden, angeregten Zuständen von Kernen im mittleren Massenbereich mit ab initio Methoden ist durch den Fortschritt der Vielteilchen-Theorien möglich geworden. Für kollektive Anregungen in höheren Energiebereichen können diese jedoch meist nicht angewendet werden. Aus diesem Grund werden hierzu entweder gänzlich phänomenologische, makroskopische Modelle oder aber mikroskopische Modelle mit phänomenologischen Wechselwirkungen eingesetzt.

Eines dieser mikroskopischen Modelle, welches für die Beschreibung kollektiver Anregungen gut geeignet ist, ist die random-phase approximation (RPA). In der Vergangenheit haben numerische Anwendungen der RPA mit phänomenologischen Wechselwirkungen vielversprechende Resultate ergeben. Die Verwendung chiraler Wechselwirkungen führte jedoch zu Vorhersagen, welche weit entfernt von den experimentellen Ergebnissen lagen.

In dieser Dissertation befassen wir uns mit der Beschreibung kollektiver Anregungen mithilfe sowohl der RPA, als auch ihrer Erweiterung zur zweiten Ordnung, der Second RPA (SRPA). Im Gegensatz zu früheren Forschungen verwenden wir hierzu chirale NN+3N Wechselwirkungen. Der Einsatz von chiralen Wechselwirkungen stellt einen wichtigen ersten Schritt für eine konsistente Beschreibung von Grundzustandseigenschaften sowie Eigenschaften angeregter Zustände und kollektiver Moden dar. Es zeigt sich, dass die Verwendung von 3N Beiträgen für die Beschreibung kollektiver Anregungen essentiell ist und zu einer drastischen Verbesserung der Vorhersage führt. Für SRPA zeigen wir allererste Ergebnisse mit chiralen Wechselwirkungen, welche gleichfalls zu einer weiteren Verbesserung der Vorhersagen führen.

Es ist bekannt, dass für eine erfolgreiche Beschreibung von Grundzustandseigenschaften die Berücksichtigung von Korrelationen von höchster Wichtigkeit ist. In früheren Anwendungen von RPA wurde die Quasi-Bosonen Näherung verwendet, welche zu einer Vernachlässigung von Grundzustandskorrelationen führt. Der nächste Schritt für eine ab initio basierte Beschreibung von Grundzustandseigenschaften ist daher die Berücksichtigung von Grundzustandskorrelationen. Um dieses Ziel zu erreichen entwickeln wir zwei Erweiterungen des RPA Formalismus, welche in der Lage sind Grundzustandskorrelationen der in-medium renormalization group (IM-SRG) sowie der coupled-cluster Theorie mit Einfach- und Zweifachanregungen (CCSD) zu verwenden. Beide Methoden wurden bereits mit großem Erfolg für die Berechnung von Grundzustandseigenschaften verwendet. Wir entwickeln einen Formalismus basierend auf Grundzustandsdichtematrizen für CC-RPA, welcher RPA Rechnungen ermöglicht welche auf dem CCSD Grundzustand basieren. Die Verwendung von IM-SRG transformierten Matrixelementen gibt uns die Möglichkeit Grundzustandskorrelationen sogar auf dem Niveau von SRPA Rechnungen zu verwenden.

Für beide Methoden sehen wir eine starke Verlagerung der kollektiven Anregungen hin zu höheren Energien und beobachten, unerwarteterweise, eine guter Übereinstimmung zwischen IM-

RPA und CC-RPA Ergebnissen. Die Struktur der Anregungen bleibt großteils unverändert. Wir schließen daraus, dass die Berücksichtigung von Korrelationen in der Tat wichtige Folgen für die energetische Vorhersage kollektiver Anregungen hat, für die Struktur dieser jedoch von untergeordneter Bedeutung ist.

Berechnungen mit IM-SRPA zeigen eine starke Verlagerung hin zu niedrigeren Energien, ähnlich dem Fall für SRPA. Die Übereinstimmung beider Methoden mit experimentellen Befunden ist auf einem ähnlichen Niveau.

Contents

Chapter 1

Introduction

Theoretical nuclear structure physics tries to explain the properties of nuclei that have already been measured by experiment, as well as to predict the yet unknown properties of, e.g., exotic nuclei. The theoretical interpretation of known qualities serves the purpose of validating the respective theories and models, while the prediction of so far unexplored characteristics is important to obtain information about the properties of nuclei that are not — or only with great effort — accessible to an experimental investigation. Additionally, theoretical predictions also provide guidance for the design of future experiments.

A broad variety of many-body methods exists for the investigation of ground-state observables, ranging from sophisticated ab initio approaches to traditional, phenomenological models. The description of low-lying excited states of medium-mass nuclei with ab initio methods has become possible through recent progress in various many-body frameworks. For collective modes at higher energies, however, these methods usually cannot be applied. Collective modes are important for the determination of macroscopic, bulk properties of nuclei such as the compression modulus [HV01], and given that they cannot be reached by most ab initio methods, either completely phenomenological, macroscopic models are employed for their description or microscopic models using phenomenological input. The random-phase approximation (RPA) provides a framework, which allows for the investigation of collective excitations. RPA allows for a computationally reasonable description of excited collective states and their transitions for closed-subshell nuclei across the nuclear chart [SJ03]. Thus, the RPA provides a theoretical approach to a class of observables which are experimentally well accessible but cannot be reached via ab initio methods such as the no-core shell model (NCSM), coupled-cluster theory (CC) or the in-medium similarity renormalization group (IM-SRG).

RPA is an improvement of the Tamm-Dancoff approximation (TDA). Within both, the RPA as well as the TDA, the excited states of nuclei are described via n-particle-n-hole ($np n$h) excitations of the ground state. The difference between these two methods lies in the formulation of their respective excitation creation operators. In the TDA, the excitation creation operator is a linear combination of particle-hole excitations, while in the RPA this operator also includes hole-particle excitations. Therefore, the RPA can be considered an extension of the TDA, as the excitation creation operator has a more general structure, allowing for more degrees of freedom. In fact, the hole-particle excitations produce a correlated ground state with a complicated structure, which cannot be expressed as a single Slater-determinant. In principle, all ApAh excitations have to be taken into account, for medium-mass nuclei, however, this is unfeasible. For practical applications the model space is truncated to 1p1h excitations, defining first-order RPA. The next step for a systematic extension is the inclusion of second-order 2p2h (de)excitations, leading to Second RPA (SRPA). Besides the "standard" (S)RPA for closed-

subshell nuclei, there are several modifications such as quasi-particle RPA (QRPA), which uses the Bogoliubov quasi-particle formalism.

In the past, many RPA calculations that have been conducted on the level of two-body (2B) forces or phenomenological three-body (3B) forces (see e.g. [PRP07; Gün11; Erl12; HPR11; Pap$^+$12; GPR14]) or using density-functional theories [TS04; GGC10; Gam$^+$12; Col$^+$13; Tse13]. Such calculations yield results that are in relative good agreement with experimental data.

The next step along the path towards a consistent description of all classes of nuclear observables is to employ the same chiral interactions for collective properties that have been applied with great success within initio methods such as the NCSM or CC for ground-state properties. It turns out that using chiral 2B interactions within RPA, however, leads to results far from agreement with experimental data. Through recent progress RPA has been extended to both normal-ordered as well as explicit 3B forces [Tri13]. We found that the inclusion of 3B forces shifts the strengths towards significantly lower energies. Furthermore, it can be shown that for RPA the use of explicit 3B forces is identical to the use of a normal-ordered 2B force.

The purpose of this work is to continue along this path in order to enable similar calculations for SRPA. In addition, we will also tackle the long-standing issue of missing ground-state correlations for the description of collective properties within RPA theories. Correlations have been found to be of great importance for the description of ground-state properties. The significance of correlations for collective modes can be expected to be considerable as well. Both ventures, the extension of (S)RPA to chiral 3B forces and the inclusion of ground-state correlations, will help in establishing a method for an ab initio description of collective properties that is consistent in physical input as well as methodology with state-of-the-art methods for ground-state properties.

For the inclusion of ground-state correlations we will pursue two completely independent approaches. The first will utilize ground-state densities from CC as input to RPA, defining the CC-RPA formalism. Though we will use CC densities, in principle density matrices from any ground-state method can be used as input. This offers the flexibility to perform calculations of collective properties based on different ab initio methods. Within the second approach, we use matrix elements transformed by IM-SRG, establishing the IM-RPA. This allows us to include correlations even on the level of second-order contributions, i.e., IM-SRPA.

The outline of this thesis will be as follows: Our discussion starts with a brief introduction to nuclear interactions, the SRG and basic principles and properties of normal ordering in chapter 2. We will then continue to discuss the Hartree-Fock (HF) approximation on which we build the standard, uncorrelated RPA and SRPA methods in chapter 3. After a short introduction on density matrices and the CC method, we derive the correlated CC-RPA as an extension of standard RPA in chapter 4. Subsequently, in chapter 5, we turn to IM-SRG leading to a second correlated version of RPA, the IM-RPA. We will then focus on electromagnetic transitions and how those can be calculated from the results of preceding RPA calculations in chapter 6. After these formal discussions we examine the results of HF, CC and IM-SRG calculations for ground-state properties in chapter 7. The results from the different, newly developed RPA methods will be studied and compared in chapter 8. We perform numerical applications for a series of closed-subshell medium-mass nuclei (^{16}O, ^{24}O, ^{40}Ca, ^{48}Ca, ^{56}Ni, ^{68}Ni, ^{78}Ni) and compare the results to experimental values. Finally, we will close this thesis with a short summary and an outlook towards possible topics for future research in chapter 9.

Chapter 2

Initial Hamiltonian and the Similarity Renormalization Group

In this chapter, we will first discuss the initial, "bare" interactions which we will use for the Hamiltonian. Afterwards we will introduce the *Similarity Renormalization Group* (SRG). The SRG is a method to improve the convergence behaviour of many-body calculations, which is necessary for nuclear structure calculations in order to improve, e.g., the Hartree-Fock approximation (cf. section 3.1) for a given basis size. The SRG uses a continuous flow equation to transform operators to a band-diagonal form, which can be interpreted as pre-diagonalization. Physically speaking, this pre-diagonalization aims at reducing the explicit short-range correlations in the nuclear wave functions by embedding them into the interaction, while at the same time leaving the long-range correlations and properties untouched [RNF10]. Since computational resources are limited, the SRG has become an important tool in nuclear structure calculations, especially for 3B interactions. The following notation and the steps of the derivation are largely taken from [Cal10]. Last but not least, we will briefly discuss the normal-ordering (NO) technique. The concept of NO has become a very important standard tool for many applications in nuclear theory and will be helpful in RPA, CC as well as IM-SRG.

2.1 The Initial Hamiltonian

Before we start with the review of the SRG in the next section, we will discuss the nuclear interactions entering the initial Hamiltonian. In this thesis, both the two-body (NN) and the three-body (3N) interaction have been derived from chiral effective field theory (χEFT), which is based on quantum chromodynamics (QCD). In the latter, quarks and gluons interact with each other via the "strong" or "color" force. This works very well for the high-energy regime in which the QCD coupling constant becomes small and thus the interaction can be treated perturbatively. This situation is often referred to as the "asymptotic freedom" of QCD. However, in the low-energy regime, which is relevant for nuclear physics, the coupling constant increases in strength with decreasing energy, making a perturbative description of QCD processes impossible. Hence, for the low-energy interactions between confined systems such as baryons we apply the χEFT instead.

Within the χEFT, a different approach is chosen as compared to QCD: Rather than concentrating on quarks and gluons, we focus on the relevant degrees of freedom, in this case the nucleons as well as the pions. The basic ideas of χEFT were introduced by S. Weinberg in [Wei79].

Weinberg proposed to use the most general Lagrangian that is consistent with the symmetries of the underlying theory.

A crucial factor in this consideration is the breaking of the so-called chiral symmetry (hence the name). For massless up and down quarks, the Lagrangian for nucleon-pion interactions would exhibit perfect chiral symmetry (cf. e.g [ME11; Koc97]). In reality, this is not the case due to the fact that the up and down quarks have a mass of about 5 MeV and, therefore, this symmetry is formally broken. Nevertheless, these quark masses are rather small compared to the masses of nucleons or pions, and the chiral symmetry may be considered an (approximate) symmetry. Prior to the χEFT there have been other meson-exchange theories. While methods using the one-pion-exchange were relatively successful in explaining some of the properties of the nuclear interaction, the multi-pion-exchange theories produced problematic results. The issues with multi-pion-exchange were due to the lack of the — at that time yet unknown — constraint of chiral symmetry [TMO52; BW53; ME11].

In principle there is an infinite number of possible terms and corresponding Feynman diagrams, consistent with the required symmetries, that contribute to the Lagrangian of χEFT. Weinberg, however, showed that a systematic expansion of the Lagrangian in terms of $\left(\frac{Q}{\Lambda_\chi}\right)^\nu$ is possible, where Q is a typical momentum, $\Lambda_\chi \approx 1\,\text{GeV}$ the breakdown scale of the effective theory and $\nu \geq 0$ the order the expansion. He further showed that for each order ν there is only a finite number of terms which contribute to the Lagrangian (cf. Figure 2.1). The first order ($\nu = 0$) is also-called leading order (LO). Due to symmetry requirements, the second order ($\nu = 1$) produces no contributions, which is why the third order ($\nu = 2$) is actually called next-to-leading order (NLO). This scheme continues accordingly for higher orders, i.e. $\nu = 3$ corresponds to the next-to-next-to-leading order (NNLO or N^{2}LO) etc.

In order for the expansion in terms of $\left(\frac{Q}{\Lambda_\chi}\right)^\nu$ to work properly, it is important to have a "separation of scales" between the "soft scale" Q and the "hard scale" Λ_χ. For this, we use the rather large gap in the hadron spectrum between the light pions (with masses of $\approx 135\,\text{MeV} \approx Q$) and the heavier mesons such as the ρ ($\approx 770\,\text{MeV}$) and ω ($\approx 782\,\text{MeV} \approx \Lambda_\chi$) [ME11]. Therefore, we introduce a momentum cutoff Λ_C between the soft and the hard scale, usually around 500 MeV. The details of QCD that cannot be resolved explicitly by χEFT, i.e. contributions from processes with $Q > \Lambda_C$, are absorbed in a set of low-energy constants (LECs). These can either be obtained via QCD lattice calculations (in future) (cf. [EMN10]) or fitted to experimental data. For the latter usually nucleon-nucleon and pion-nucleon scattering data as well as properties of the deuteron or few-nucleon systems are used. The systematic determination of theoretical uncertainties for different chiral orders is subject of ongoing research [EKM15a; EKM15b; Bin$^+$16].

The χEFT has two significant advantages over phenomenological high-precision potentials such as the Argonne V18 or the charge-dependent Bonn potential. The first one is the fact that the χEFT has its foundation in QCD, and the second one that higher-order interactions emerge automatically at higher expansion orders ν, in a derivation consistent with the NN interaction.

In this thesis, we will use two different chiral interactions. The first we call EM400. It consists of a non-local 2B interaction derived by Entem and Machleidt [EM03] up to the fourth order (N^{3}LO), supplemented by a local 3B force at third order (N^{2}LO) [Nav07]. This implies a small inconsistency for the use of NN+3N interactions. Ideally, both interactions would be derived up to the same order in χEFT, but unfortunately as of today there are no corresponding matrix elements for the 3N interaction at N^{3}LO. On the other hand, the use of a NN interaction derived at (only) N^{2}LO would lead to a significant loss in the precision [EM03]. The momentum cutoff for the 2B interaction is 500 MeV and that for the 3B force 400 MeV, see [GQN09; Rot$^+$12]. For

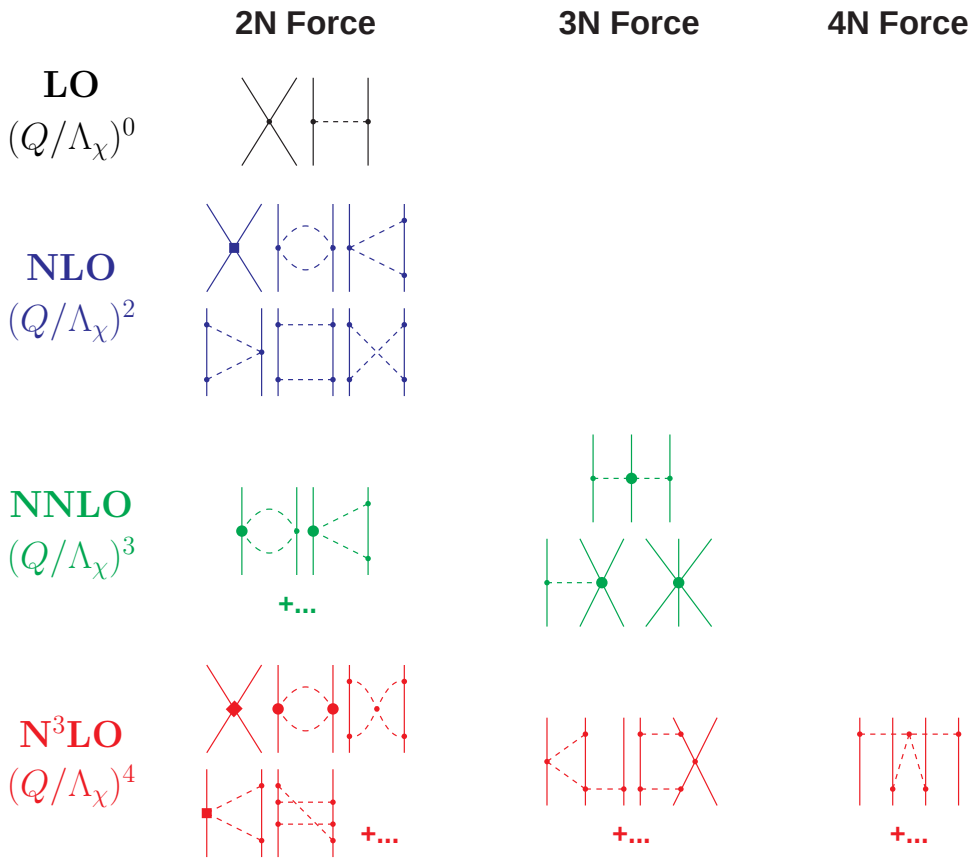

Figure 2.1: Diagrams for nuclear forces from χEFT for different particle-rank and different orders. Taken from [ME11], refer text or reference for further information.

the NN interaction at N^{3}LO there is a total of 29 LECs which are constrained via two-body scattering data. For reasons of consistency, the LECs for the 3N interaction have to be the same as for the NN interaction, and at the given order only two LECs remain to be determined for the 3N interaction [Cal10].

The second interaction that we use is the N^{2}LO$_{\text{sat}}$ [Eks+15], which in short we will call SAT. It is consistently derived up to N^{2}LO for both the 2B and the 3B force. Different from the EM400, the SAT interaction is obtained via a simultaneous fitting of all LECs together for the NN and 3N force. In addition, the fit also includes data of heavier nuclei, namely binding energies and charge radii of carbon and oxygen isotopes. The SAT interaction produces similar results for ground-state energies but yields substantially larger radii, in line withe experiment.

2.2 Similarity Renormalization Group

In this section, we will derive the mathematical foundations of the free-space SRG. Let $\hat{H}_0$ be an arbitrary Hamiltonian or, more generally, any Hermitian operator to be transformed, e.g. our initial, bare interaction. Given that the transformation is a unitary transformation, we can

write the transformed Hamiltonian $\hat{H}_\alpha$ as

$$\hat{H}_\alpha = \hat{U}_\alpha^\dagger \hat{H}_0 \hat{U}_\alpha, \tag{2.1}$$

with the unitary operator $\hat{U}_\alpha$. Differentiating expression (2.1) with respect to α gives

$$\frac{\mathrm{d}\hat{H}_\alpha}{\mathrm{d}\alpha} = \frac{\mathrm{d}}{\mathrm{d}\alpha}(\hat{U}_\alpha^\dagger \hat{H}_0 \hat{U}_\alpha) = \frac{\mathrm{d}\hat{U}_\alpha^\dagger}{\mathrm{d}\alpha}\hat{H}_0\hat{U}_\alpha + \hat{U}_\alpha^\dagger \underbrace{\frac{\mathrm{d}\hat{H}_0}{\mathrm{d}\alpha}}_{=0}\hat{U}_\alpha + \hat{U}_\alpha^\dagger \hat{H}_0 \frac{\mathrm{d}\hat{U}_\alpha}{\mathrm{d}\alpha} \tag{2.2}$$

$$= \frac{\mathrm{d}\hat{U}_\alpha^\dagger}{\mathrm{d}\alpha}\hat{H}_0\hat{U}_\alpha + \hat{U}_\alpha^\dagger \hat{H}_0 \frac{\mathrm{d}\hat{U}_\alpha}{\mathrm{d}\alpha} \tag{2.3}$$

where the bare or initial Hamiltonian $\hat{H}_0$ obviously does not depend on the quantity α that characterizes the transformation. Since $\hat{U}_\alpha$ is a unitary operator, it holds that

$$\hat{U}_\alpha^\dagger \hat{U}_\alpha = \hat{\mathbb{1}}, \tag{2.4}$$

which leads to

$$\frac{\mathrm{d}}{\mathrm{d}\alpha}(\hat{U}_\alpha^\dagger \hat{U}_\alpha) = \frac{\mathrm{d}\hat{U}_\alpha^\dagger}{\mathrm{d}\alpha}\hat{U}_\alpha + \hat{U}_\alpha^\dagger \frac{\mathrm{d}\hat{U}_\alpha}{\mathrm{d}\alpha}, = \frac{\mathrm{d}}{\mathrm{d}\alpha}\hat{\mathbb{1}} = 0 \tag{2.5}$$

$$\Rightarrow \frac{\mathrm{d}\hat{U}_\alpha^\dagger}{\mathrm{d}\alpha} = -\hat{U}_\alpha^\dagger \frac{\mathrm{d}\hat{U}_\alpha}{\mathrm{d}\alpha}\hat{U}_\alpha^\dagger. \tag{2.6}$$

Eq. (2.6) gives a connection between the derivative of $\hat{U}_\alpha$ and the derivative of its Hermitian conjugate $\hat{U}_\alpha^\dagger$. Inserting relation (2.6) into (2.3) leads to

$$\frac{\mathrm{d}\hat{H}_\alpha}{\mathrm{d}\alpha} = -\hat{U}_\alpha^\dagger \frac{\mathrm{d}\hat{U}_\alpha}{\mathrm{d}\alpha}\hat{U}_\alpha^\dagger \hat{H}_0 \hat{U}_\alpha + \hat{U}_\alpha^\dagger \hat{H}_0 \hat{U}_\alpha \hat{U}_\alpha^\dagger \frac{\mathrm{d}\hat{U}_\alpha}{\mathrm{d}\alpha} \tag{2.7}$$

$$= -\hat{U}_\alpha^\dagger \frac{\mathrm{d}\hat{U}_\alpha}{\mathrm{d}\alpha}\hat{H}_\alpha + \hat{H}_\alpha \hat{U}_\alpha^\dagger \frac{\mathrm{d}\hat{U}_\alpha}{\mathrm{d}\alpha} \tag{2.8}$$

$$= [\hat{H}_\alpha, \hat{U}_\alpha^\dagger \frac{\mathrm{d}\hat{U}_\alpha}{\mathrm{d}\alpha}] \equiv [\hat{H}_\alpha, -\hat{\eta}_\alpha] = [\hat{\eta}_\alpha, \hat{H}_\alpha]. \tag{2.9}$$

Summarizing, this yields the so-called *flow equation*

$$\frac{\mathrm{d}\hat{H}_\alpha}{\mathrm{d}\alpha} = [\hat{\eta}_\alpha, \hat{H}_\alpha], \tag{2.10}$$

where the *generator* $\hat{\eta}_\alpha$ of the flow equation has been defined as follows

$$\hat{\eta}_\alpha \equiv -\hat{U}_\alpha^\dagger \frac{\mathrm{d}\hat{U}_\alpha}{\mathrm{d}\alpha}. \tag{2.11}$$

This generator η_α is anti-Hermitian, as can be shown easily with use of (2.6)

$$\hat{\eta}_\alpha^\dagger = -\frac{\mathrm{d}\hat{U}_\alpha^\dagger}{\mathrm{d}\alpha}\hat{U}_\alpha = \hat{U}_\alpha^\dagger \frac{\mathrm{d}\hat{U}_\alpha}{\mathrm{d}\alpha}\hat{U}_\alpha^\dagger \hat{U}_\alpha = \hat{U}_\alpha^\dagger \frac{\mathrm{d}\hat{U}_\alpha}{\mathrm{d}\alpha} = -\hat{\eta}_\alpha. \tag{2.12}$$

The parameter α characterizing the transformation is called the *flow parameter*. The flow evolution of the Hamiltonian starts at $\alpha = 0$, for which, by definition, we get $\hat{H}_{\alpha=0} = \hat{H}_0$ and $\hat{U}_\alpha^\dagger = \hat{U}_\alpha = \hat{\mathbb{1}}$.

Looking at relation (2.10) we see that the derivative, i.e. the modifications made to $\hat{H}$, depend on two quantities: The current Hamiltonian $\hat{H}_\alpha$ and the current generator η_α. The specific form of the evolution will, therefore, be given by the initial generator η and the way this generator

itself transforms during the flow. In principle any generic anti-Hermitian generator could be used as input to the transformation. The choice of the this generator is ours to make and will determine the nature of the transformation. Being able to choose the exact form of the generator for the SRG provides us with a great flexibility.

Let us try to interpret this generator. If we choose the generator to be of the form $\hat{\eta}_\alpha = [\hat{G}_\alpha, \hat{H}_\alpha]$ it already contains the evolved Hamiltonian, and it satisfies the anti-Hermiticity relation (2.12) as long as $\hat{G}_\alpha$ is Hermitian. An obvious choice for $\hat{G}_\alpha$ would be

$$\hat{G}_\alpha = \hat{H}_\alpha^{\mathrm{diag}} = \sum_i \langle i| \hat{H}_\alpha |i\rangle \ |i\rangle\langle i| \,, \tag{2.13}$$

i.e. taking only the diagonal matrix elements of $\hat{H}_\alpha$. This form of $\hat{\eta}_\alpha$ has the advantage that the generator $\hat{\eta}_\alpha = [\hat{H}_\alpha^{\mathrm{diag}}, \hat{H}_\alpha]$ would vanish as soon as $\hat{H}_\alpha$ becomes diagonal, thus yielding a fix-point at which the evolution will stop. Such an approach would lead to a diagonalization with respect to the generic basis $\{|i\rangle\}$ in which we choose to represent the Hamiltonian.

Another interesting choice for $\hat{G}_\alpha$ would be the intrinsic kinetic energy $\hat{T}_{\mathrm{int}}$, leading to

$$\hat{\eta}_\alpha = (2\mu)^2[\hat{T}_{\mathrm{int}}, \hat{H}_\alpha], \tag{2.14}$$

with the reduced mass $\mu = \frac{m_N}{2}$. A diagonalization with this generator corresponds to a decoupling of states with high and low momenta [Jur+08] (or energies, respectively), leading to a more band-diagonal structure. Those are just two examples of possible generators.

Without the SRG (or a similar transformation) to improve the convergence behaviour we would not be able to obtain meaningful results since many-body methods employing bare interactions converge far too slowly. A disadvantage of the SRG is the generation of irreducible higher-order forces (cf. e.g. [JNF09]). Keep in mind for the operator ranks we have

$$\mathrm{rk}(\hat{A}\hat{B}) = \mathrm{rk}(\hat{A}) + \mathrm{rk}(\hat{B})$$

and

$$\mathrm{rk}([\hat{A}, \hat{B}]) = \mathrm{rk}(\hat{A}) + \mathrm{rk}(\hat{B}) - 1.$$

From (2.14) and (2.10) we can see that the SRG flow will induce operators of higher rank with each evaluation of the commutators. When performing an SRG transformation for an A-body system, each transformed operator eventually contains up to A-body contributions, as shown schematically below for the Hamiltonian:

$$\hat{H}_\alpha = \hat{H}_\alpha^{1\mathrm{B}} + \hat{H}_\alpha^{2\mathrm{B}} + \hat{H}_\alpha^{3\mathrm{B}} + \ldots + \hat{H}_\alpha^{A\mathrm{B}}. \tag{2.15}$$

As an example, by conducting the SRG evolution for ^{40}Ca we will get operators with a particle-rank as large as 40, even if the initial interaction was only a 2B or 3B operator. This poses a problem because any induced contributions with a particle-rank larger than 3 or maybe 4 cannot be considered in the subsequent calculations and, therefore, have to be discarded. Disregarding those higher-order contributions implies an approximation of the sort

$$\hat{H}_\alpha \approx \hat{H}_\alpha^{1\mathrm{B}} + \hat{H}_\alpha^{2\mathrm{B}} + \hat{H}_\alpha^{3\mathrm{B}}. \tag{2.16}$$

It turns out that the size of the induced many-body terms depends on both the flow parameter α and the generator $\hat{\eta}_\alpha$ that was used for the SRG transformation. Based on empirical findings, it seems that, for a rank i operator, the main contribution of the induced higher-order operators comes from the rank $i+1$, while an inclusion of the remaining operators with rank $j > i+1$ cause only small changes in the results. One way to monitor the higher-order contributions from

the SRG evolution is to perform a series of computations with different α values and observe the α dependence of the results. A dependence of our results on the flow parameter, as such, highlights the loss of unitarity that is owed to the truncation performed in (2.16). Nevertheless, since we usually do not know the (true) results of the completely unevolved interaction, a lack of α dependence does not necessarily indicate that the SRG evolution produces the same results as the original one, since there can still be a constant offset to the true values. Thus, going to very large α values would, ultimately, indeed yield a diagonalized Hamiltonian but, at the same time, forcing the basis structure of our generator onto the Hamiltonian causes the contributions of higher particle-ranks to increase strongly. Given that we have to truncate the induced higher-order terms, this makes the limit $\alpha \to \infty$ undesirable. Instead, a reasonable tradeoff between pre-diagonalization and higher-order contributions has to be found.

We note that the generator (2.14) is the most common choice. Recently the exploration of alternative generators yielded suitable results which appear to be comparable in terms of convergence but might induce weaker higher-order forces (cf. [DON14]).

In general, other operators than the Hamiltonian can be transformed as well. In fact, whenever we are using a transformed Hamiltonian, all other operators that are involved in the calculation have to be transformed as well. Not transforming these operators would introduce an inconsistency. We will revisit this issue later on in the context of IM-SRG in section 5.1. The transformation of an arbitrary operator $\hat{O}$ of interest works analogously to (2.9)

$$\frac{\mathrm{d}\hat{O}_\alpha}{\mathrm{d}\alpha} = [\hat{\eta}_\alpha, \hat{O}_\alpha]. \tag{2.17}$$

Note that the generator used in (2.17) for the SRG evolution of other operators $\hat{O}$ is still the same as the one for the evolution of the Hamiltonian (cf. the flow equation (2.10)).

2.3 Normal Ordering

The goal of normal ordering (NO) is to transfer the information contained in a given operator of a certain particle-rank to operators of lower particle-ranks. The advantage of reducing the particle-rank of operators, while — at the same time — preserving most of its information, is twofold: Firstly, if for a specific many-body method we already have the formalism to handle, e.g., 2B interactions we then can, in principle, also include the up-to-2B contributions of operators with particle-ranks higher than 2 (3B, 4B, ...). In other words, NO offers us the possibility to include at least some contributions at a lower particle-rank without having to develop the formalism any further or to derive new equations.

Secondly, concerning the solution of a given problem, higher particle-ranks are usually linked to higher computational effort and, therefore, longer runtimes. Consequently, including higher particle-ranks explicitly (as opposed to via NO) would also tend to make the corresponding calculations unfeasible, especially for heavier nuclei. NO has been successfully applied in a wide variety of applications [Hag$^+$07; Rot$^+$12; Her$^+$13b]. In this section, we will briefly discuss the basic formalism and properties of NO.

Let $\{\hat{a}_i^\dagger\}$ be a set of creation operators and $\{\hat{a}_i\}$ a set of the corresponding annihilation operators defined relative to a certain reference or vacuum state denoted by $|\Psi_0\rangle$, which does not necessarily have to be the particle vacuum $|0\rangle$. The *normal-ordered product* of an arbitrary string $\hat{O}$ of both creation and annihilation operators is defined as

$$\{\hat{O}\} \equiv (-1)^P \cdot (\text{CREATORS} \times \text{ANNIHILATORS}), \tag{2.18}$$

with P being the number of transpositions necessary to sort the string of operators $\hat{O}$ such that all the creation operators are on the left side and all the annihilation operators are on the right side. In this work, the normal-ordered product will be denoted by $\{...\}$, but other notations such as $\mathcal{N}[...]$ or $:...:$ are also common in literature. Technically, we would have to write expressions such as $\{...\}_{|\Psi_0\rangle}$ to indicate the reference state that is being used for the construction of the normal-ordered product. The index $|\Psi_0\rangle$ is often omitted for reasons of brevity, and the particular reference state that is used is clarified prior to the NO calculations.

A convenient property of definition (2.18) is the fact that the reference state expectation value of a normal-ordered product of a string of operators vanishes, i.e.

$$\langle\Psi_0|\{...\}|\Psi_0\rangle = 0. \tag{2.19}$$

The *contraction* of any two creation or annihilation operators $\hat{A}$ and $\hat{B}$ is defined as

$$\overbracket{\hat{A}\hat{B}} \equiv \hat{A}\hat{B} - \{\hat{A}\hat{B}\}, \tag{2.20}$$

and it depends on the reference state $|\Psi_0\rangle$ which is used for the evaluation of the no product. Unlike this definition might suggest, a contraction is in fact a number and not an operator: If the operators are already in NO, then we get

$$\overbracket{\hat{A}\hat{B}} \equiv \hat{A}\hat{B} - \hat{A}\hat{B} \equiv 0. \tag{2.21}$$

If not, we have

$$\overbracket{\hat{A}\hat{B}} \equiv \hat{A}\hat{B} - (-1)\hat{B}\hat{A} = \hat{A}\hat{B} + \hat{B}\hat{A} = [\hat{A}, \hat{B}]_+, \tag{2.22}$$

but this can only be the case with a creator on the right an annihilator on the left, and thus $[\hat{A}, \hat{B}]_+ = \delta_{AB}$. The combination of the concepts of NO and contractions leads to expressions such as

$$\{\overbracket{\hat{A}\hat{B}\hat{C}\hat{D}\hat{E}...\hat{X}\hat{Y}\hat{Z}}\} \equiv (-1)^P \overbracket{\hat{B}\hat{E}}\overbracket{\hat{D}\hat{Y}}\{\hat{A}\hat{C}...\hat{X}\hat{Z}\}, \tag{2.23}$$

with P being the number of transpositions necessary to get all contraction pairs together and to the left of the string of operators. *Wick's theorem* [Wic50] now states

$$\begin{aligned}
\hat{A}\hat{B}\hat{C}\hat{D}\hat{E}... = \quad & \{\hat{A}\hat{B}\hat{C}\hat{D}\hat{E}...\} \\
& + \sum_{1 \text{ contr.}} \{\overbracket{\hat{A}\hat{B}}\hat{C}\hat{D}\hat{E}...\} \\
& + \sum_{2 \text{ contr.}} \{\overbracket{\hat{A}\hat{B}}\overbracket{\hat{C}\hat{D}}\hat{E}...\} \\
& + ... \\
& + \sum_{\text{all contr.}} \{\overbracket{\hat{A}\hat{B}}\overbracket{\hat{C}\hat{D}}\overbracket{\hat{E}...}\},
\end{aligned} \tag{2.24}$$

where e.g. $\sum_{2 \text{ contr.}}$ means the sum over all possible combinations of any two contractions within the given string of operators, the contractions in (2.24) have been inserted as an exemplary illustration. We see that a string of $2n$ operators can be written as the sum over the normal-ordered string of operators with 0 to n contractions. Since the contraction of two operators is simply a constant, each contraction lowers the particle-rank of the string of operators by one.

Detailed introductions on the topic NO can be found, e.g., in [Vob14; Her+16]. For the sake of brevity, we will skip further discussions on NO and continue to an application of NO on a generic 3B operator $\hat{V}_{3\mathrm{N}}$. In standard representation (i.e., vacuum NO), such an operator would look as follows

$$\hat{V}_{3\mathrm{N}} = \frac{1}{36} \sum_{ijk,i'j'k'} v^{3\mathrm{N}}_{ijk,i'j'k'}\, \hat{a}^\dagger_i \hat{a}^\dagger_j \hat{a}^\dagger_k \hat{a}_{k'} \hat{a}_{j'} \hat{a}_{i'}. \tag{2.25}$$

With the help of NO, this operator can be rewritten into

$$\hat{V}_{3\mathrm{N}} = \hat{V}^{\mathrm{N0B}}_{3\mathrm{N}} + \hat{V}^{\mathrm{N1B}}_{3\mathrm{N}} + \hat{V}^{\mathrm{N2B}}_{3\mathrm{N}} + \hat{V}^{\mathrm{N3B}}_{3\mathrm{N}}. \tag{2.26}$$

This holds generally for any chosen reference state $|\Psi_0\rangle$ and is simply an alternative representation, and though looking different, the operator in the new and in the standard form are completely identical. Since we are seeking a way to include effects stemming from 3B interactions into our calculations, without actually expanding the formalism to the level of 3B operators, we discard the last term in (2.26) (which is still a 3B operator) and approximate the normal-ordered operator as follows

$$\hat{V}_{3\mathrm{N}} \cong \hat{V}^{\mathrm{N0B}}_{3\mathrm{N}} + \hat{V}^{\mathrm{N1B}}_{3\mathrm{N}} + \hat{V}^{\mathrm{N2B}}_{3\mathrm{N}}, \tag{2.27}$$

keeping all up-to-2B contributions. This is called the normal-ordered 2B (NO2B) approximation. The operator in (2.27) can be separated into its different particle-ranks. The specific form of the individual operators $\hat{V}^{\mathrm{N}k\mathrm{B}}_{3\mathrm{N}}$ in (2.27) depends on the state $|\Psi_0\rangle$ that was used in the definition of the NO, and hence also the quality of the approximation depends on this state. If we assume the NO to be defined relative to a single Slater-determinant $|\Psi_0\rangle$, we get

$$\hat{V}^{\mathrm{N0B}}_{3\mathrm{N}} = \frac{1}{6} \sum_{ijk}^{\mathrm{occ.}} v^{3\mathrm{N}}_{ijk,ijk} \equiv \frac{1}{6} f \tag{2.28}$$

$$\hat{V}^{\mathrm{N1B}}_{3\mathrm{N}} = \frac{1}{2} \sum_{i,i'} \sum_{jk}^{\mathrm{occ.}} v^{3\mathrm{N}}_{ijk,i'jk} \{\hat{a}^\dagger_i \hat{a}_{i'}\} \equiv \frac{1}{2} \sum_{i,i'} f_{i,i'} \{\hat{a}^\dagger_i \hat{a}_{i'}\}, \tag{2.29}$$

$$\hat{V}^{\mathrm{N2B}}_{3\mathrm{N}} = \frac{1}{4} \sum_{ij,i'j'} \sum_{k}^{\mathrm{occ.}} v^{3\mathrm{N}}_{ijk,i'j'k} \{\hat{a}^\dagger_i \hat{a}^\dagger_j \hat{a}_{j'} \hat{a}_{i'}\} \equiv \frac{1}{4} \sum_{ij,i'j'} f_{ij,i'j'} \{\hat{a}^\dagger_i \hat{a}^\dagger_j \hat{a}_{j'} \hat{a}_{i'}\}, \tag{2.30}$$

where the sum $\sum^{\mathrm{occ.}}$ runs only over the occupied states in $|\psi_0\rangle$. These three relations for the normal-ordered 0B to 2B parts of the original operator can be transformed back into normal-ordered form with respect to the particle vacuum $|0\rangle$, yielding the following operators

$$\hat{V}^{\mathrm{0B}}_{3\mathrm{N}} = \frac{1}{6} f, \tag{2.31}$$

$$\hat{V}^{\mathrm{1B}}_{3\mathrm{N}} = -\frac{1}{2} \sum_{kk'} f_{k,k'}\, \hat{a}^\dagger_k \hat{a}_{k'}, \tag{2.32}$$

$$\hat{V}^{\mathrm{2B}}_{3\mathrm{N}} = \frac{1}{4} \sum_{jk,j'k'} f_{jk,j'k'}\, \hat{a}^\dagger_j \hat{a}^\dagger_k \hat{a}_{k'} \hat{a}_{j'}, \tag{2.33}$$

where, in comparison to the normal-ordered versions, we have omitted the upper index “N”.

Chapter 3

Hartree-Fock Random-Phase Approximation

In this chapter we first present the Hartree-Fock method. This will be the starting point from which we drive the first- and second-order RPA formalism.

3.1 Hartree-Fock Method

The Hartree-Fock (HF) method is a so-called mean-field approximation. This means that the Hamiltonian of the nuclear many-body problem with A interacting particles (here the nucleons inside the nucleus) is reduced to an effective 1B operator. It is assumed that each particle moves independently of the other particles and is only affected by the global mean-field potential, determining its eigenenergy and eigenstate. Since the HF method does not account for any residual interaction between the particles there are no correlations between the different particles. Consequently, the many-body state of a HF calculation, $|\mathrm{HF}\rangle$, can be described by a single Slater-determinant (SD). The HF method is, therefore, one of the simplest approximations to the actual ground states of nuclei, and due to its simplicity also a computationally very cheap method. In this section, we will give an overview of the basic HF equations and properties, since these will in parts be used in the RPA formalism (see section 3.2).

In order to calculate the HF energies and states, we first need to take a look at the Hamiltonian under consideration. For a Hamiltonian $\hat{H}$ with a full 3B interaction we can write

$$\hat{H} = \hat{T} + \hat{V} + \hat{V}_{3\mathrm{N}} \tag{3.1}$$

$$= \sum_{i,i'} t_{i,i'}\, \hat{c}_i^\dagger \hat{c}_{i'} + \frac{1}{4} \sum_{ij,i'j'} v_{ij,i'j'}\, \hat{c}_i^\dagger \hat{c}_j^\dagger \hat{c}_{j'} \hat{c}_{i'} + \frac{1}{36} \sum_{ijk,i'j'k'} v^{3\mathrm{N}}_{ijk,i'j'k'}\, \hat{c}_i^\dagger \hat{c}_j^\dagger \hat{c}_k^\dagger \hat{c}_{k'} \hat{c}_{j'} \hat{c}_{i'}, \tag{3.2}$$

Here the quantities $t_{i,i'}$, $v_{ij,i'j'}$ and $v^{3\mathrm{N}}_{ijk,i'j'k'}$ are antisymmetrized matrix elements of the kinetic energy, the 2B as well as the 3B interaction. The summation indices $i, j, k, i', \ldots$ run over the entire single-particle basis. At this point, the single-particle basis can be chosen arbitrarily. For practical applications, this is usually, as in this case, the harmonic oscillator (HO) basis. The HO basis states have several convenient properties which make them a suitable starting point. Taking the expectation value of the Hamiltonian $\hat{H}$ in the HF Slater-determinant $|\mathrm{HF}\rangle$ yields

the corresponding energy E

$$E = \langle \mathrm{HF}| \hat{H} |\mathrm{HF}\rangle = \langle \mathrm{HF}| \hat{T} + \hat{V} + \hat{V}^{3\mathrm{N}} |\mathrm{HF}\rangle \tag{3.3}$$

$$= \sum_{i,i'} t_{i,i'} \langle \mathrm{HF}| \hat{c}_i^\dagger \hat{c}_{i'} |\mathrm{HF}\rangle + \frac{1}{4} \sum_{ij,i'j'} v_{ij,i'j'} \langle \mathrm{HF}| \hat{c}_i^\dagger \hat{c}_j^\dagger \hat{c}_{j'} \hat{c}_{i'} |\mathrm{HF}\rangle + \frac{1}{36} \sum_{ijk,i'j'k'} v^{3\mathrm{N}}_{ijk,i'j'k'} \langle \mathrm{HF}| \hat{c}_i^\dagger \hat{c}_j^\dagger \hat{c}_k^\dagger \hat{c}_{k'} \hat{c}_{j'} \hat{c}_{i'} |\mathrm{HF}\rangle , \tag{3.4}$$

where (3.2) has been inserted. We can now rewrite the expressions for the HF expectation values in (3.4) by introducing the 1B, 2B and 3B density matrices (for more information on density matrices see section 4.1)

$$\varrho_{i',i} = \langle \mathrm{HF}| \hat{c}_i^\dagger \hat{c}_{i'} |\mathrm{HF}\rangle , \tag{3.5}$$

$$\varrho_{i'j',ij} = \langle \mathrm{HF}| \hat{c}_i^\dagger \hat{c}_j^\dagger \hat{c}_{j'} \hat{c}_{i'} |\mathrm{HF}\rangle , \tag{3.6}$$

$$\varrho_{i'j'k',ijk} = \langle \mathrm{HF}| \hat{c}_i^\dagger \hat{c}_j^\dagger \hat{c}_k^\dagger \hat{c}_{k'} \hat{c}_{j'} \hat{c}_{i'} |\mathrm{HF}\rangle , \tag{3.7}$$

which leads to a formula of the HF ground-state energy as functional of the density matrices

$$E[\varrho^1, \varrho^2, \varrho^3] = \sum_{i,i'} t_{i,i'} \varrho_{i',i} + \frac{1}{4} \sum_{ij,i'j'} v_{ij,i'j'} \varrho_{i'j',ij} + \frac{1}{36} \sum_{ijk,i'j'k'} v^{3\mathrm{N}}_{ijk,i'j'k'} \varrho_{i'j'k',ijk}. \tag{3.8}$$

Since the HF ground state $|\mathrm{HF}\rangle$ has the simple form of a single Slater-determinant, we can write the density matrices of higher particle-rank as a product of 1B density matrices (compare equation (4.34)). In combination with the sum and the coefficients from formula (3.4), the expression for the whole 2B term can be simplified as follows

$$\sum_{ij,i'j'} v_{ij,i'j'} \varrho_{i'j',ij} = \sum_{ij,i'j'} v_{ij,i'j'} \left(\varrho_{j',j} \varrho_{i',i} - \varrho_{j',i} \varrho_{i',j} \right) \tag{3.9}$$

$$= \sum_{ij,i'j'} \left(v_{ij,i'j'} \varrho_{j',j} \varrho_{i',i} - v_{ij,i'j'} \varrho_{j',i} \varrho_{i',j} \right) \tag{3.10}$$

$$= \sum_{ij,i'j'} \left(v_{ij,i'j'} \varrho_{j',j} \varrho_{i',i} - v_{ji,i'j'} \varrho_{j',j} \varrho_{i',i} \right) \tag{3.11}$$

$$= \sum_{ij,i'j'} \left(v_{ij,i'j'} \varrho_{j',j} \varrho_{i',i} + v_{ij,i'j'} \varrho_{j',j} \varrho_{i',i} \right) \tag{3.12}$$

$$= 2 \sum_{ij,i'j'} v_{ij,i'j'} \varrho_{j',j} \varrho_{i',i}, \tag{3.13}$$

where the indices i and j have been exchanged in (3.11) and the antisymmetry of $v_{ij,i'j'}$ has been used in (3.12). Analogously, we can simplify the 3B term, the corresponding density matrix then reads

$$\begin{aligned} \varrho_{i'j'k',ijk} = \quad & \varrho_{k',k} \left(\varrho_{i',i} \varrho_{j',j} - \varrho_{i',j} \varrho_{j',i} \right) \\ & + \varrho_{j',k} \left(\varrho_{i',j} \varrho_{k',i} - \varrho_{i',i} \varrho_{k',j} \right) \\ & + \varrho_{i',k} \left(\varrho_{k',j} \varrho_{j',i} - \varrho_{k',i} \varrho_{j',j} \right) . \end{aligned} \tag{3.14}$$

Inserting (3.14) into the 3B part of (3.8) leads to the following expression

$$\sum_{ijk,i'j'k'} v^{3\mathrm{N}}_{ijk,i'j'k'} \varrho_{i'j'k',ijk} = 6 \sum_{ijk,i'j'k'} v^{3\mathrm{N}}_{ijk,i'j'k'} \varrho_{k',k} \varrho_{i',i} \varrho_{j',j}. \tag{3.15}$$

With the above results, the HF ground-state energy E can now be written as a functional of only the 1B density matrix ϱ, as opposed to formula (3.8). For the energy we obtain

$$E[\varrho] = \sum_{i,i'} t_{i,i'}\, \varrho_{i',i} + \frac{1}{2} \sum_{ij,i'j'} v_{ij,i'j'}\, \varrho_{j',j}\, \varrho_{i',i} + \frac{1}{6} \sum_{ijk,i'j'k'} v^{\mathrm{3N}}_{ijk,i'j'k'}\, \varrho_{k',k}\, \varrho_{j',j}\, \varrho_{i',i}. \tag{3.16}$$

We will use the variational principle to determine the stationary point of $E[\varrho]$ with respect to ϱ. Varying the energy as in (3.16) with ϱ as the degree of freedom yields

$$\delta E[\varrho] = E[\varrho + \delta\varrho] - E[\varrho] \tag{3.17}$$

$$= \sum_{i,i'} t_{i,i'}\, \delta\varrho_{i',i} + \sum_{ij,i'j'} v_{ij,i'j'}\, \delta\varrho_{j',j}\, \varrho_{i',i} + \frac{1}{2} \sum_{\substack{ijk \\ i'j'k'}} v^{\mathrm{3N}}_{ijk,i'j'k'}\, \delta\varrho_{k',k}\, \varrho_{j',j}\, \varrho_{i',i}, \tag{3.18}$$

where terms involving higher orders in $\delta\varrho$ have been neglected. We can now factor out the part of expression (3.18) that carries the variation of the density matrix $\delta\varrho$, which yields

$$\delta E[\varrho] = \sum_{i,i'} \left(t_{i,i'} + \sum_{j,j'} v_{ij,i'j'}\, \varrho_{j',j} + \frac{1}{2} \sum_{jk,j'k'} v^{\mathrm{3N}}_{ijk,i'j'k'}\, \varrho_{j',j}\, \varrho_{k',k} \right) \delta\varrho_{i',i} \tag{3.19}$$

$$\equiv \sum_{i,i'} h_{i,i'}[\varrho]\, \delta\varrho_{i',i}. \tag{3.20}$$

The expression in parentheses in (3.19) defines the HF single-particle or mean-field Hamiltonian $\hat{h}[\varrho]$

$$h_{i,i'}[\varrho] \equiv t_{i,i'} + \sum_{j,j'} v_{ij,i'j'}\, \varrho_{j',j} + \frac{1}{2} \sum_{jk,j'k'} v^{\mathrm{3N}}_{ijk,i'j'k'}\, \varrho_{j',j}\, \varrho_{k',k}\,, \tag{3.21}$$

which is a 1B operator. It can be shown (cf. e.g. [RS80]) that the solution of the stationarity condition

$$\delta E[\varrho] = 0 \tag{3.22}$$

is equivalent to the solution of the eigenvalue problem of the mean-field Hamiltonian $\hat{h}[\varrho]$. That means we have to solve the equation

$$\hat{h}[\varrho]\, |i\rangle = \epsilon_i\, |i\rangle\,, \tag{3.23}$$

where, from now on, the $|i\rangle$ denote the single-particle HF basis states and ϵ_i the corresponding single-particle energies. In the following, the associated creation and annihilation operators in HF basis will be labeled $\hat{a}_i^\dagger$ and $\hat{a}_i$, respectively. Again, it has to be stressed that from this point on all the indices refer HF states and not HO states. In the HF basis, the 1B density matrix ϱ is equivalent to the identity matrix for all occupied states and zero otherwise. With that, the mean-field Hamiltonian simplifies even further to

$$h_{i,i'}[\varrho] = t_{i,i'} + \sum_{j}^{\mathrm{occ.}} v_{ij,i'j} + \frac{1}{2} \sum_{jk}^{\mathrm{occ.}} v^{\mathrm{3N}}_{ijk,i'jk}. \tag{3.24}$$

Note that the sums only run over the occupied states (denoted by "occ." above the sum symbol), which is caused by annihilators of unoccupied states acting on the HF vacuum: $\hat{a}_i\, |\mathrm{HF}\rangle = 0$, if $\epsilon_i > \epsilon_\mathrm{F}$, with the *Fermi energy* ϵ_F denoting the energy of the highest, still occupied state. By using (3.23) we obtain a connection between the matrix elements $h_{i,i'}[\varrho]$ of the mean-field Hamiltonian and its eigenenergies ϵ_i

$$h_{i,i'}[\varrho] = \langle i|\, \hat{h}[\varrho]\, |i'\rangle = \langle i|\, \epsilon_{i'}\, |i'\rangle = \epsilon_{i'}\, \langle i|i'\rangle = \epsilon_{i'}\, \delta_{ii'}, \tag{3.25}$$

and consequently an explicit formula for the single-particle energies

$$\epsilon_i = t_{i,i} + \sum_{j}^{\text{occ.}} v_{ij,ij} + \frac{1}{2} \sum_{jk}^{\text{occ.}} v^{\text{3N}}_{ijk,ijk}. \tag{3.26}$$

The ground-state energy in HF basis reads as follows (cf. (3.16), mind the difference of HO and HF basis)

$$E = \sum_{i}^{\text{occ.}} t_{i,i} + \frac{1}{2} \sum_{ij}^{\text{occ.}} v_{ij,ij} + \frac{1}{6} \sum_{ijk}^{\text{occ.}} v^{\text{3N}}_{ijk,ijk}, \tag{3.27}$$

and by using the formula for the single-particle energies (3.26), this can be rewritten into

$$E = \sum_{i}^{\text{occ.}} \epsilon_i - \frac{1}{2} \sum_{ij}^{\text{occ.}} v_{ij,ij} - \frac{1}{3} \sum_{ijk}^{\text{occ.}} v^{\text{3N}}_{ijk,ijk}. \tag{3.28}$$

With (3.28) we now finally have a formula for the total energy of the A-nucleon system, described via a Hamiltonian that contains a full 3B interaction, in HF approximation.

3.2 Random-Phase Approximation

The random-phase approximation (RPA) is a standard tool for the investigation of excited collective states. Its framework is built on the results of a preceding HF calculation, i.e., it uses the single-particle states of such a calculation (HF-RPA). Within the RPA, all excited states are computed via linear combinations of particle-hole (ph) excitations of the RPA ground state. In particular, the RPA ground state already contains correlations and has, therefore, a far more complicated structure than the simple HF Slater-determinant.

3.2.1 Particle-Hole Formalism

It has already been stated that within RPA, the ground state as well as excited states are obtained via ph excitations of the HF state, therefore, the RPA is referred to as a *particle-hole theory*. Since the concept of ph excitations will be essential to all of the following calculations involving the RPA framework, this section is dedicated to a short introduction to the ph formalism that will be needed later on. In the following, all indices $i, j, p, h, ...$ shall denote HF single-particle states.

In second quantization, a ph excitation is described as follows: One particle in a state $|h\rangle$ below the Fermi energy ϵ_{F} is destroyed by application of an annihilation operator $\hat{a}_h$, while at the same time an unoccupied state $|p\rangle$ above the Fermi energy will be populated with a particle by applying a creation operator $\hat{a}_p^\dagger$. Together, this creator-annihilator pair corresponds to an excitation of a particle from the initial state $|h\rangle$ to the final state $|p\rangle$. One such pair defines a 1-particle-1-hole (1p1h) excitation. If two, three or n creator-annihilator pairs act on a state, we analogously call these 2p2h, 3p3h or npnh excitations, respectively. A schematic view of a 1p1h excitation is depicted in Figure 3.1.

Due to the fact that we excite a particle from a state below ϵ_{F} to a state above ϵ_{F}, physically speaking, these ph excitations cost a certain amount of energy, which is given by the difference of the single-particle energies. In the case described above, this would correspond to

$$\epsilon_{ph} \equiv \epsilon_p - \epsilon_h, \tag{3.29}$$

with ϵ_i being the HF single-particle energy of the state $|i\rangle$ (see (3.26)).

So far we have concerned ourselves only with performing ph excitations. In principle the reversed process, which would be a hole-particle (hp) excitation is of course possible as well. Here, we would annihilate a particle in a state above ϵ_{F} and create one in a state below it. Energetically speaking, this corresponds to a de-excitation which frees energy, in magnitude equal to (3.29). Obviously, such a process can only take place if a matching pair of states is (un-)occupied. More specifically, this is *not* the case for any single Slater-determinant, including $|\text{HF}\rangle$. Mind that in contrast to the hp process, the initially discussed ph excitation is always possible on SDs.

The above discussion suggests a rigid partitioning of the HF basis into two categories, since the states above and below the Fermi energy play different roles in (de-)excitations. This consideration leads to the following convention for the HF indices, which shall be used throughout this thesis unless explicitly stated otherwise:

- Single-particle states **below** the Fermi energy, i.e., "hole" states: $h, h', ...$
- Single-particle states **above** the Fermi energy, i.e., "particle" states: $p, p', ...$
- **All** single-particle states: $i, j, ...$

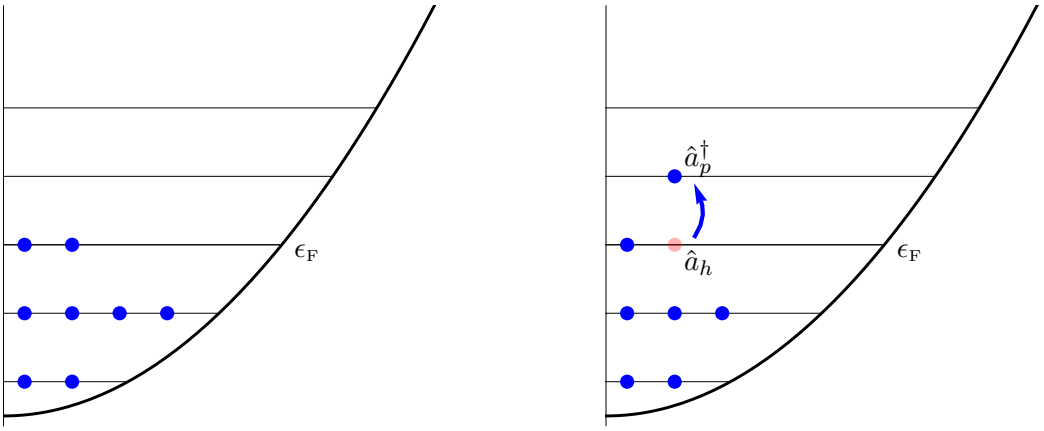

(a) Ground state. (b) Particle-hole excitation.

Figure 3.1: Particle-hole excitation. Figure (a) shows the nucleus in the HF ground state with the Fermi energy ϵ_{F}. In figure (b) we have a similar situation only now with a ph excitation $\hat{a}_p^\dagger \hat{a}_h$ that annihilates a particle in the state $|h\rangle$ below the Fermi energy and creates one in the state $|p\rangle$ above the Fermi energy.

Hence, all (de-)excitations are realized by the application of pairs of fermion operators, either of the sort $\hat{a}_p^\dagger \hat{a}_h$ for excitations or $\hat{a}_h^\dagger \hat{a}_p$ for de-excitations, respectively. Note that this partitioning of our basis is only applicable to nuclei with so-called *subshell closures* where all j orbitals are either completely occupied or entirely unoccupied. If an orbital is partially filled, both excitation and de-excitation operations can be performed and no clear distinction between particle and hole states is possible. In the next section, we will use this ph formalism to derive the basic RPA equations.

3.2.2 Derivation of the basic RPA Equations

In this section the RPA equations shall be derived using the so-called *equations of motion* (EOM) method. The notation and the steps of the derivation are taken from [Suh07]. Within the EOM method the actual calculation of the RPA ground state, which we denote $|\mathrm{RPA}\rangle$, is avoided. For now, this state will only be written implicitly. In order to obtain generic expressions for the ground state $|\mathrm{RPA}\rangle$, we can define *excitation creation operators* (ECO) $\hat{Q}_\omega^\dagger$. These $\hat{Q}_\omega^\dagger$ are intended to create an *excited state* $|\omega\rangle$ when applied to the RPA ground state, i.e.

$$|\omega\rangle \equiv \hat{Q}_\omega^\dagger |\mathrm{RPA}\rangle \,, \tag{3.30}$$

where ω is a short-hand notation for a set of quantum numbers, usually $\omega = (n, J^\pi, M)$, with n being the number of the excited state, J the angular momentum, M the z-projection and π the parity. We usually investigate different angular momenta and parities separately, so when later we write sums over ω this simply implies a sum over n. The corresponding annihilator $\hat{Q}_\omega$ obviously de-excites the associated excited state back to the ground state

$$\hat{Q}_\omega |\omega\rangle = |\mathrm{RPA}\rangle \,. \tag{3.31}$$

When applied to the energetically lowest state, the ground state, further de-excitation is unphysical, thus,

$$\hat{Q}_\omega |\mathrm{RPA}\rangle \equiv 0, \quad \forall\, \omega. \tag{3.32}$$

Expressions (3.30) and (3.32) are the defining relations for the ECOs $\hat{Q}^\dagger_\omega$ as well as for the ground state $|\mathrm{RPA}\rangle$. We stress that the whole set of ECOs $\hat{Q}^\dagger_\omega$ together with the ground state $|\mathrm{RPA}\rangle$ and the excitation energies E^{RPA}_ω define the complete solution to the RPA problem. From these defining relations also the orthogonality of the excited state to the ground state follows:

$$\langle \mathrm{RPA}|\omega\rangle = \langle \mathrm{RPA}|\, \hat{Q}^\dagger_\omega\, |\mathrm{RPA}\rangle = \langle \mathrm{RPA}|\, \hat{Q}_\omega\, |\mathrm{RPA}\rangle^* \equiv 0, \quad \forall\, \omega. \tag{3.33}$$

Formally, the ECOs can be written as $\hat{Q}^\dagger_\omega = |\omega\rangle\langle \mathrm{RPA}|$. However, this is just a generic notation which in itself does not provide any practical assistance for the actual solution of the RPA problem. In fact, the detailed form of the ECOs depends on the type of RPA that is used. Up to this point we have made no restrictions for these operators. In section 3.2.3 we will discuss the most simple form of RPA and its corresponding ECOs.

For the EOM derivation of the RPA equations, it is helpful to first take a look at the stationary Schrödinger equation

$$\hat{H}\, |\mathrm{RPA}\rangle = E_0\, |\mathrm{RPA}\rangle\,, \tag{3.34}$$

$$\hat{H}\, |\omega\rangle = E_\omega\, |\omega\rangle \quad \forall\omega, \tag{3.35}$$

where the RPA ground-state energy has been labeled E_0 and the energies of the excited states E_ω. With the use of (3.30), (3.35) can be rewritten as

$$\hat{H}\hat{Q}^\dagger_\omega\, |\mathrm{RPA}\rangle = E_\omega \hat{Q}^\dagger_\omega\, |\mathrm{RPA}\rangle. \tag{3.36}$$

We can also evaluate the interchanged term on the left-hand side of (3.36), i.e.

$$\hat{Q}^\dagger_\omega \hat{H}\, |\mathrm{RPA}\rangle = \hat{Q}^\dagger_\omega E_0\, |\mathrm{RPA}\rangle = E_0 \hat{Q}^\dagger_\omega\, |\mathrm{RPA}\rangle\,. \tag{3.37}$$

Subtracting (3.37) from (3.36) then yields

$$\hat{H}\hat{Q}^\dagger_\omega\, |\mathrm{RPA}\rangle - \hat{Q}^\dagger_\omega \hat{H}\, |\mathrm{RPA}\rangle = E_\omega \hat{Q}^\dagger_\omega\, |\mathrm{RPA}\rangle - E_0 \hat{Q}^\dagger_\omega\, |\mathrm{RPA}\rangle \tag{3.38}$$

$$\left(\hat{H}\hat{Q}^\dagger_\omega - \hat{Q}^\dagger_\omega \hat{H}\right) |\mathrm{RPA}\rangle = (E_\omega - E_0)\hat{Q}^\dagger_\omega\, |\mathrm{RPA}\rangle \tag{3.39}$$

$$[\hat{H}, \hat{Q}^\dagger_\omega]\, |\mathrm{RPA}\rangle = (E_\omega - E_0)\hat{Q}^\dagger_\omega\, |\mathrm{RPA}\rangle\,, \tag{3.40}$$

where we have introduced the commutator between $\hat{H}$ and $\hat{Q}^\dagger_\omega$. At this point it is convenient to introduce a new quantity, the RPA excitation energy E^{RPA}_ω given by

$$E^{\mathrm{RPA}}_\omega \equiv E_\omega - E_0, \tag{3.41}$$

i.e., the energy of the state $|\omega\rangle$ relative to the ground state $|\mathrm{RPA}\rangle$. With this, (3.40) becomes

$$[\hat{H}, \hat{Q}^\dagger_\omega]\, |\mathrm{RPA}\rangle = E^{\mathrm{RPA}}_\omega \hat{Q}^\dagger_\omega\, |\mathrm{RPA}\rangle\,. \tag{3.42}$$

Relation (3.42) is the so-called *equation of motion* for the excitation creation operators $\hat{Q}^\dagger_\omega$. As mentioned before, in order to actually determine a solution for the operators $\hat{Q}^\dagger_\omega$, we first need to make an ansatz for their structure. The different types of ECOs will be the topic of the next section. Afterwards, we will proceed by solving (3.42) with the help of the variational method.

3.2.3 First-Order ECOs

As already stated in section 3.2.2, the detailed form for the ECOs depends on the type of RPA that is used for the calculations. As a start, we will deal with the *standard* or *first-order* RPA. The first-order RPA is defined by the fact that its ECOs perform only 1p1h (de-)excitations on the ground state $|\mathrm{RPA}\rangle$. So, in summary, the first-order ECOs should

- allow for 1p1h excitations ($\hat{a}_p^\dagger \hat{a}_h$),
- allow for 1p1h de-excitations ($\hat{a}_h^\dagger \hat{a}_p$),
- provide the correct quantum numbers.

Higher-order excitations (2p2h, ...) will of course yield a better description of the system since they allow for more degrees of freedom, but at the same time they are connected to a more complicated formalism. For now we will stick to 1p1h excitations, the natural extension to 2p2h contributions will be discussed in section 3.3.

Earlier we defined ω to be $\omega = (n, J^\pi, M)$. It is convenient to ensure that the pair of fermion operators for (de-)excitations is coupled to the correct angular momentum J with z-component M. This is why, usually, the ECOs do not contain uncoupled pairs of fermion operators but rather the coupled versions. When coupling two single angular momenta to a total angular momentum, this corresponds to a replacement of the two quantum numbers for the single z-components, m_1 and m_2, with the total angular momentum J and its (total) z-component M. In order to express this in the formulae, we introduce a new notation, dividing the quantum numbers which characterize a single-particle state i into one part containing only its z-component, m_i, and one part containing all the remaining "m-less" quantum numbers $\bar{i}$:

$$i \equiv (\bar{i}, m_i). \tag{3.43}$$

We define the coupled product of a pair of fermion operators $\hat{a}_{\bar{p}}^\dagger$ and $\hat{\tilde{a}}_{\bar{h}}$ (see below) as

$$\hat{\mathcal{A}}_{\bar{p}\bar{h}}^\dagger(JM) \equiv [\hat{a}_{\bar{p}}^\dagger \hat{\tilde{a}}_{\bar{h}}]_{JM}, \tag{3.44}$$

where the *tensor product* of two spherical tensors $\boldsymbol{T}_{j_1}$ and $\boldsymbol{T}_{j_2}$ of rank j_1 and j_2 and with components T_{j_1,m_1} and T_{j_2,m_2}, respectively, is given by

$$T_{JM} = [\boldsymbol{T}_{j_1} \boldsymbol{T}_{j_2}]_{JM} = \sum_{m_1,m_2} C(j_1 m_1, j_2 m_2 | JM) T_{j_1 m_1} T_{j_2 m_2}, \tag{3.45}$$

yielding the $2M+1$ components T_{JM} of a new spherical tensor $\boldsymbol{T}_J$ of rank J, with the quantity $C(j_1 m_1, j_2 m_2 | JM)$ denoting a Clebsch-Gordan coefficient. The use of the "tilde" operator $\hat{\tilde{a}}_i$ in (3.44) defined via

$$\hat{\tilde{a}}_i \equiv (-1)^{j_i + m_i}\, \hat{a}_{\bar{i},-m_i}, \tag{3.46}$$

is necessary, because the regular annihilation operator $\hat{a}_i$ is not a spherical tensor operator, and hence it cannot be used for the tensor product. Including the factor $(-1)^{j_i+m_i}$ and changing the sign of the z-component of the operator yields the spherical tensor operator $\hat{\tilde{a}}_i$, as required by (3.45). A more detailed discussion of spherical tensor operators can be found in Appendix A. Following this, the expression $[\hat{a}_{\bar{p}}^\dagger \hat{\tilde{a}}_{\bar{h}}]_{JM}$ is the tensor product of two spherical tensors $\hat{a}_{\bar{p}}^\dagger$ and $\hat{\tilde{a}}_{\bar{h}}$ of rank j_p and j_h, respectively. With the help of (3.45) we can write the new coupled excitation

operator (3.44) as

$$\hat{\mathcal{A}}^\dagger_{\bar{p}\bar{h}}(JM) = [\hat{a}^\dagger_{\bar{p}}\hat{\tilde{a}}_{\bar{h}}]_{JM} \tag{3.47}$$

$$= \sum_{m_p,m_h} (-1)^{j_h+m_h}\, C(j_p m_p, j_h m_h|JM)\, \hat{a}^\dagger_{\bar{p},m_p}\hat{a}_{\bar{h},\text{-}m_h} \tag{3.48}$$

$$= \sum_{m_p,m_h} (-1)^{j_h-m_h}\, C(j_p m_p, j_h \text{-}m_h|JM)\, \hat{a}^\dagger_{\bar{p},m_p}\hat{a}_{\bar{h},m_h} \tag{3.49}$$

$$= \sum_{m_p,m_h} (-1)^{j_h-m_h}\, C(j_p m_p, j_h \text{-}m_h|JM)\, \hat{\mathcal{A}}^\dagger_{ph}, \tag{3.50}$$

where we introduced the uncoupled ph creation operator $\hat{\mathcal{A}}^\dagger_{ph} = \hat{a}^\dagger_p\hat{a}_h$. Note that the Hermitian conjugate of the coupled ph operator, $\hat{\mathcal{A}}_{\bar{p}\bar{h}}(JM)$, is not a spherical tensor operator, but analogously to the case of the simple particle creators and annihilators we can construct a coupled annihilator, which then is a spherical tensor operator, as follows

$$\hat{\tilde{\mathcal{A}}}_{\bar{p}\bar{h}}(JM) \equiv (-1)^{J+M}\hat{\mathcal{A}}_{\bar{p}\bar{h}}(J\text{-}M), \tag{3.51}$$

which shows the exact same modifications as (3.46). Owing to spherical symmetry, in practical applications it suffices to calculate only one of the $\hat{\mathcal{A}}_{\bar{p}\bar{h}}(JM)$. Choosing $M = 0$ yields the convenient property that the spherical, "tilde" annihilators relate directly to their non-spherical counterparts:

$$\hat{\tilde{\mathcal{A}}}_{\bar{p}\bar{h}}(J0) = (-1)^J\hat{\mathcal{A}}_{\bar{p}\bar{h}}(J0). \tag{3.52}$$

With (3.44) and (3.51), we can write the most general form for the *coupled* first-order ECO as

$$\hat{Q}^\dagger_\omega = \sum_{\bar{p},\bar{h}} \left(X^\omega_{\bar{p}\bar{h}}\, \hat{\mathcal{A}}^\dagger_{\bar{p}\bar{h}}(JM) - Y^\omega_{\bar{p}\bar{h}}\, \hat{\tilde{\mathcal{A}}}_{\bar{p}\bar{h}}(JM) \right), \tag{3.53}$$

where the sums run over all occupied states (h) and all unoccupied states (p), respectively. The term $\hat{\mathcal{A}}^\dagger_{\bar{p}\bar{h}}(JM)$ describes a single ph excitation process, while the term $\hat{\tilde{\mathcal{A}}}_{\bar{p}\bar{h}}(JM)$ accomplishes the inverse process, which means a *hp excitation* or *de-excitation* (cf. section 3.2.1). Both these processes can occur and contribute to a certain degree to the excited state $|\omega\rangle$ which is given by the corresponding coefficients ($X^\omega_{\bar{p}\bar{h}}$, $Y^\omega_{\bar{p}\bar{h}}$). These coefficients are usually referred to as *RPA amplitudes*. The uncoupled analogon of (3.53) reads

$$\hat{Q}^\dagger_\omega = \sum_{p,h} \left(X^\omega_{ph}\, \hat{\mathcal{A}}^\dagger_{ph} - Y^\omega_{ph}\, \hat{\mathcal{A}}_{ph} \right). \tag{3.54}$$

Note that the amplitudes in (3.53) and (3.54) are, strictly speaking, not identical, since the first ones refer to the contributions from coupled ph excitations, the latter ones to contributions from the uncoupled excitations. We choose not to introduce a separate notation for the forward (X^ω) and backward (Y^ω) amplitudes of coupled and uncoupled ECOs, since their physical meaning remains the same. The question of coupling is addressed via their index notations, i.e., compare $X^\omega_{\bar{p}\bar{h}}$ to X^ω_{ph}. The uncoupled variant greatly helps in keeping equations lucid. The following discussion is therefore given in an uncoupled formulation. The conversion to coupled expressions will be done only for our final results (see section 3.2.9).

At this point, a remark on the form of the ECO as in (3.54) seems suitable. As stated earlier, the second term allows for hp excitations (or de-excitations). This degree of freedom is directly responsible for the fact that, in general, the RPA ground state $|\text{RPA}\rangle$ is not the simple HF

ground state $|\mathrm{HF}\rangle$. To see this, we could assume that the RPA ground state was indeed $|\mathrm{HF}\rangle$. The application of the annihilator $\hat{Q}_\omega$ on $|\mathrm{HF}\rangle$ would then yield

$$\hat{Q}_\omega |\mathrm{HF}\rangle = \sum_{p,h} \left(X_{ph}^{\omega\,*}\, \hat{a}_h^\dagger \hat{a}_p - Y_{ph}^{\omega\,*}\, \hat{a}_p^\dagger \hat{a}_h \right) |\mathrm{HF}\rangle \tag{3.55}$$

$$= \sum_{p,h} \Big(X_{ph}^{\omega\,*}\, \underbrace{\hat{a}_h^\dagger \hat{a}_p |\mathrm{HF}\rangle}_{=0} - Y_{ph}^{\omega\,*}\, \hat{a}_p^\dagger \hat{a}_h |\mathrm{HF}\rangle \Big) \tag{3.56}$$

$$= -\sum_{p,h} Y_{ph}^{\omega\,*}\, \hat{a}_p^\dagger \hat{a}_h |\mathrm{HF}\rangle\,, \tag{3.57}$$

which generally evaluates to a non-zero value (except for the trivial case that all Y_{ph}^ω are zero). This is in contradiction to the defining relation (3.32), and consequently we find $|\mathrm{HF}\rangle \neq |\mathrm{RPA}\rangle$ for all non-trivial cases. In fact, a model exists where there are no amplitudes Y_{ph}^ω within the ECOs. It is called the Tamm-Dancoff Approximation, which we will briefly discuss in section 3.2.6.

3.2.4 Variational Principle and Quasi-Boson Approximation

Since all excited states $|\omega\rangle$ are orthogonal to the ground state (cf. (3.33)), let us consider a variation $\delta\hat{Q}^\dagger$ of the ECOs $\hat{Q}_\omega^\dagger$. This variation is supposed to span the full model space, with the condition that it still has to be orthogonal to the ground state, i.e.

$$\delta\hat{Q} |\mathrm{RPA}\rangle = 0. \tag{3.58}$$

For first-order RPA this variation can be written as

$$\delta\hat{Q} = \sum_{p,h} \left(\delta X_{ph}^*\, \hat{a}_h^\dagger \hat{a}_p - \delta Y_{ph}^*\, \hat{a}_p^\dagger \hat{a}_h \right). \tag{3.59}$$

We can calculate the overlap of $\langle \delta Q|$ with the EOM expression (3.42), which yields

$$\langle \mathrm{RPA}| \,\delta\hat{Q}[\hat{H}, \hat{Q}_\omega^\dagger] |\mathrm{RPA}\rangle = E_\omega^{\mathrm{RPA}} \langle \mathrm{RPA}| \,\delta\hat{Q}\hat{Q}_\omega^\dagger |\mathrm{RPA}\rangle\,. \tag{3.60}$$

A commutator can be introduced by use of the orthogonality relation (3.58) between the variation and the ground state, leading to

$$\langle \mathrm{RPA}| \,[\delta\hat{Q}, [\hat{H}, \hat{Q}_\omega^\dagger]] |\mathrm{RPA}\rangle = E_\omega^{\mathrm{RPA}} \langle \mathrm{RPA}| \,[\delta\hat{Q}, \hat{Q}_\omega^\dagger] |\mathrm{RPA}\rangle\,, \tag{3.61}$$

which is the general form for the equation of motion. The advantage of (3.61) is that systematically improved extensions for the ECOs can be introduced. We will revisit the above equation later when dealing with second-order RPA. For now we proceed with the first-order ECOs and insert $\delta\hat{Q}$ and $\hat{Q}_\omega^\dagger$ into (3.61). This equation holds for arbitrary variations δQ. We bring to mind that the ph excitations are linearly independent from each other and of course also from the hp excitations. The variational ansatz of (3.61), therefore, leads to a number of separate identities, one for each ph excitation and one for each de-excitation. With this, we get two different sets of equations for each ω, p, h:

$$\delta X_{ph}: \quad \langle \mathrm{RPA}| \,[\hat{a}_h^\dagger \hat{a}_p, [\hat{H}, \hat{Q}_\omega^\dagger]] |\mathrm{RPA}\rangle = E_\omega^{\mathrm{RPA}} \langle \mathrm{RPA}| \,[\hat{a}_h^\dagger \hat{a}_p, \hat{Q}_\omega^\dagger] |\mathrm{RPA}\rangle\,, \tag{3.62}$$

$$\delta Y_{ph}: \quad \langle \mathrm{RPA}| \,[\hat{a}_p^\dagger \hat{a}_h, [\hat{H}, \hat{Q}_\omega^\dagger]] |\mathrm{RPA}\rangle = E_\omega^{\mathrm{RPA}} \langle \mathrm{RPA}| \,[\hat{a}_p^\dagger \hat{a}_h, \hat{Q}_\omega^\dagger] |\mathrm{RPA}\rangle\,. \tag{3.63}$$

The first set (3.62) results from the term carrying the δX amplitudes. Analogously, the second set (3.63) comes from the δY amplitudes.

At this point, we have reached the end of the exact, analytical derivation of the EOMs. The reason for this is the fact that all the ECOs $\hat{Q}^\dagger_\omega$ as well as the ground state $|\mathrm{RPA}\rangle$ depend on each other (cf. section 3.2.2). As a consequence, we are not able to answer, a priori, the question what the application of, e.g., $\hat{a}^\dagger_i$ on $|\mathrm{RPA}\rangle$ will yield. Therefore, the only possibility to solve the above equations would be via an *iterative scheme*: We would have to guess a solution, plug it into the corresponding equations, and from that obtain a new solution. This would have to be done until we achieve a solution which is self-consistent (to a chosen accuracy). Usually, one will not undergo the trouble of self-consistency to solve the RPA equations, this procedure is chosen only in the so-called *self-consistent RPA* [Cat+96].

In order to be able to simplify these equations further, we introduce the *quasi-boson approximation* (QBA). Since we always have pairs (even numbers) of fermion operators in the RPA equations, we can naively assume them to behave at least roughly as *Bose-like* operators. An odd number of fermion operators on the other hand could be considered to behave roughly as *Fermi-like* operators. We can evaluate the commutator of two Bose-like fermion pairs with the help of the basic commutator relations for fermions. This gives us

$$[\hat{a}^\dagger_p\hat{a}_h, \hat{a}^\dagger_{h'}\hat{a}_{p'}] = \delta_{hh'}\,\hat{a}^\dagger_p\hat{a}_{p'} - \delta_{pp'}\,\hat{a}^\dagger_{h'}\hat{a}_h, \tag{3.64}$$

which is an exact operator identity. Within the QBA, the simplification is made that expectation values of commutators of this sort are replaced by their HF expectation value, i.e.

$$\begin{aligned}
\langle\mathrm{RPA}|\,[\hat{a}^\dagger_p\hat{a}_h, \hat{a}^\dagger_{h'}\hat{a}_{p'}]\,|\mathrm{RPA}\rangle &\overset{\mathrm{QBA}}{\approx} \langle\mathrm{HF}|\,[\hat{a}^\dagger_p\hat{a}_h, \hat{a}^\dagger_{h'}\hat{a}_{p'}]\,|\mathrm{HF}\rangle &(3.65)\\
&= \langle\mathrm{HF}|\,\delta_{hh'}\,\hat{a}^\dagger_p\hat{a}_{p'} - \delta_{pp'}\,\hat{a}^\dagger_{h'}\hat{a}_h\,|\mathrm{HF}\rangle &(3.66)\\
&= -\delta_{pp'}\delta_{hh'}. &(3.67)
\end{aligned}$$

Interestingly, this looks just like the basic commutator relation between two bosonic operators $\hat{b}^\dagger_j$ and $\hat{b}_i$, given by

$$[\hat{b}_i, \hat{b}^\dagger_j] = \delta_{ij}, \tag{3.68}$$

which can be seen by defining new operators for the Bose-like terms, i.e.

$$\begin{aligned}
B_i &\equiv \hat{a}^\dagger_{h'}\hat{a}_{p'}, \quad i = (h', p'), &(3.69)\\
B^\dagger_j &= \hat{a}^\dagger_p\hat{a}_h, \quad j = (h, p), &(3.70)
\end{aligned}$$

with the matching orthogonality relation $\delta_{ij} = \delta_{hh'}\,\delta_{pp'}$. We see that replacing expectation values of the sort (3.64) by their HF expectation values leads to expressions which look like the result of the commutator between two bosonic operators, hence the name quasi-boson approximation. In summary, the QBA can be considered as the approximation

$$\langle\mathrm{RPA}|\,\hat{O}_{\text{Bose-like}}\,|\mathrm{RPA}\rangle \approx \langle\mathrm{HF}|\,\hat{O}_{\text{Bose-like}}\,|\mathrm{HF}\rangle\,.$$

The replacement of the expectation value $\langle\mathrm{RPA}|\ldots|\mathrm{RPA}\rangle$ with its $|\mathrm{HF}\rangle$ pendant is justified by the assumption that pairs of fermion operators behave similar to the way bosonic operators would do. However, by performing this replacement we are neglecting some of the operator terms, and, therefore, it remains to be seen whether or not this assumption is a reasonable one.

In order to get a better understanding of the QBA, we will consider the $|\mathrm{RPA}\rangle$ expectation value of the right-hand side of (3.62). Inserting definition (3.54) for the ECO yields

$$\langle \mathrm{RPA}| \left[\hat{a}_h^\dagger \hat{a}_p, \hat{Q}_\omega^\dagger\right] |\mathrm{RPA}\rangle = \sum_{p'h'} X_{p'h'}^\omega \langle \mathrm{RPA}| \left[\hat{a}_h^\dagger \hat{a}_p, \hat{a}_{p'}^\dagger \hat{a}_{h'}\right] |\mathrm{RPA}\rangle + 0 \tag{3.71}$$

$$= \sum_{p'h'} X_{p'h'}^\omega \Big(\delta_{p,p'}\delta_{h,h'} - \delta_{p,p'} \langle \mathrm{RPA}| \hat{a}_{h'} \hat{a}_h^\dagger |\mathrm{RPA}\rangle - \delta_{h,h'} \langle \mathrm{RPA}| \hat{a}_{p'}^\dagger \hat{a}_p |\mathrm{RPA}\rangle \Big) \tag{3.72}$$

$$= X_{ph}^\omega - \sum_{h'} X_{ph'}^\omega \langle \mathrm{RPA}| \hat{a}_{h'} \hat{a}_h^\dagger |\mathrm{RPA}\rangle - \sum_{p'} X_{p'h}^\omega \langle \mathrm{RPA}| \hat{a}_{p'}^\dagger \hat{a}_p |\mathrm{RPA}\rangle . \tag{3.73}$$

If there are no phase correlations between the expectation values and the amplitudes, the last two terms in (3.73) can be expected to be small. Hence the name *random*-phase approximation. Generally, we can assume the QBA to be a reasonable approximation if the RPA ground state $|\mathrm{RPA}\rangle$ does not differ too much from the HF ground state $|\mathrm{HF}\rangle$, i.e., if the ground-state correlations are relatively weak.

3.2.5 RPA Equations

Applying the QBA to (3.62) and (3.63) yields

$$\langle \mathrm{HF}| \left[\hat{a}_h^\dagger \hat{a}_p, [\hat{H}, \hat{Q}_\omega^\dagger]\right] |\mathrm{HF}\rangle = E_\omega^{\mathrm{RPA}} \langle \mathrm{HF}| \left[\hat{a}_h^\dagger \hat{a}_p, \hat{Q}_\omega^\dagger\right] |\mathrm{HF}\rangle , \tag{3.74}$$

$$\langle \mathrm{HF}| \left[\hat{a}_p^\dagger \hat{a}_h, [\hat{H}, \hat{Q}_\omega^\dagger]\right] |\mathrm{HF}\rangle = E_\omega^{\mathrm{RPA}} \langle \mathrm{HF}| \left[\hat{a}_p^\dagger \hat{a}_h, \hat{Q}_\omega^\dagger\right] |\mathrm{HF}\rangle . \tag{3.75}$$

The advantage of this is that we now know exactly what the application of each of the fermion operators to the HF state $|\mathrm{HF}\rangle$ will yield. Therefore, with the help of the QBA, a number simplifications are possible. Taking a look at the right-hand side of (3.74) shows that the second term of the commutator vanishes, since $\hat{a}_p |\mathrm{HF}\rangle = 0$. Similarly, the first term of the commutator on the right-hand side of (3.75) vanishes due to the fact that $\langle \mathrm{HF}| \hat{a}_p^\dagger = 0$. The same, of course, holds true for both of the outer commutators on the left-hand sides of (3.74) and (3.75), respectively. For the moment we are left with the following sets of equations

$$\langle \mathrm{HF}| \hat{a}_h^\dagger \hat{a}_p [\hat{H}, \hat{Q}_\omega^\dagger] |\mathrm{HF}\rangle = E_\omega^{\mathrm{RPA}} \langle \mathrm{HF}| \hat{a}_h^\dagger \hat{a}_p \hat{Q}_\omega^\dagger |\mathrm{HF}\rangle , \tag{3.76}$$

$$\langle \mathrm{HF}| [\hat{H}, \hat{Q}_\omega^\dagger] \hat{a}_p^\dagger \hat{a}_h |\mathrm{HF}\rangle = E_\omega^{\mathrm{RPA}} \langle \mathrm{HF}| \hat{Q}_\omega^\dagger \hat{a}_p^\dagger \hat{a}_h |\mathrm{HF}\rangle . \tag{3.77}$$

We can now insert our choice for the ECOs as in (3.54) into the above equations. Doing this for the matrix element on the right-hand side of (3.76) yields

$$\langle \mathrm{HF}| \hat{a}_h^\dagger \hat{a}_p \hat{Q}_\omega^\dagger |\mathrm{HF}\rangle = \sum_{p'h'} \left(X_{p'h'}^\omega \langle \mathrm{HF}| \hat{a}_h^\dagger \hat{a}_p \hat{a}_{p'}^\dagger \hat{a}_{h'} |\mathrm{HF}\rangle - Y_{p'h'}^\omega \langle \mathrm{HF}| \hat{a}_h^\dagger \hat{a}_p \hat{a}_{h'}^\dagger \hat{a}_{p'} |\mathrm{HF}\rangle \right) \tag{3.78}$$

$$= \sum_{p'h'} \left(X_{p'h'}^\omega \cdot \delta_{hh'}\delta_{pp'} - Y_{p'h'}^\omega \cdot 0 \right) \tag{3.79}$$

$$= X_{ph}^\omega , \tag{3.80}$$

Similarly, for the matrix element on the right-hand side of (3.77) we obtain

$$\langle \mathrm{HF}| \hat{Q}^\dagger_\omega \, \hat{a}^\dagger_p \hat{a}_h \, |\mathrm{HF}\rangle = \sum_{p'h'} \Big(X^\omega_{p'h'} \, \langle \mathrm{HF}| \, \hat{a}^\dagger_{p'} \hat{a}_{h'} \hat{a}^\dagger_p \hat{a}_h \, |\mathrm{HF}\rangle - Y^\omega_{p'h'} \, \langle \mathrm{HF}| \, \hat{a}^\dagger_{h'} \hat{a}_{p'} \hat{a}^\dagger_p \hat{a}_h \, |\mathrm{HF}\rangle \Big) \tag{3.81}$$

$$= \sum_{p'h'} \Big(X^\omega_{p'h'} \cdot 0 - Y^\omega_{p'h'} \cdot \delta_{hh'} \delta_{pp'} \Big) \tag{3.82}$$

$$= -Y^\omega_{ph}. \tag{3.83}$$

As an intermediate result, we end up with

$$\langle \mathrm{HF}| \, \hat{a}^\dagger_h \hat{a}_p [\hat{H}, \hat{Q}^\dagger_\omega] \, |\mathrm{HF}\rangle = \quad E^{\mathrm{RPA}}_\omega X^\omega_{ph}, \tag{3.84}$$

$$\langle \mathrm{HF}| \, [\hat{H}, \hat{Q}^\dagger_\omega] \hat{a}^\dagger_p \hat{a}_h \, |\mathrm{HF}\rangle = -E^{\mathrm{RPA}}_\omega Y^\omega_{ph}. \tag{3.85}$$

The second of the above equations can be rewritten into

$$\langle \mathrm{HF}| \, \hat{a}^\dagger_h \hat{a}_p [\hat{H}, \hat{Q}_\omega] \, |\mathrm{HF}\rangle^* = E^{\mathrm{RPA}}_\omega Y^\omega_{ph}. \tag{3.86}$$

Summarizing, we end up with

$$\langle \mathrm{HF}| \, \hat{a}^\dagger_h \hat{a}_p [\hat{H}, \hat{Q}^\dagger_\omega] \, |\mathrm{HF}\rangle \quad = E^{\mathrm{RPA}}_\omega X^\omega_{ph}, \tag{3.87}$$

$$\langle \mathrm{HF}| \, \hat{a}^\dagger_h \hat{a}_p [\hat{H}, \hat{Q}_\omega] \, |\mathrm{HF}\rangle^* = E^{\mathrm{RPA}}_\omega Y^\omega_{ph}. \tag{3.88}$$

Inserting the definition of the ECO (3.54) into the left-hand sides of the above equations leads to

$$\sum_{p'h'} \Big(X^\omega_{p'h'} \underbrace{\langle \mathrm{HF}| \, \hat{a}^\dagger_h \hat{a}_p [\hat{H}, \hat{a}^\dagger_{p'} \hat{a}_{h'}] \, |\mathrm{HF}\rangle}_{\equiv A_{ph,p'h'}} - Y^\omega_{p'h'} \underbrace{\langle \mathrm{HF}| \, \hat{a}^\dagger_h \hat{a}_p [\hat{H}, \hat{a}^\dagger_{h'} \hat{a}_{p'}] \, |\mathrm{HF}\rangle}_{\equiv -B_{ph,p'h'}} \Big) \quad = E^{\mathrm{RPA}}_\omega X^\omega_{ph}, \tag{3.89}$$

$$\sum_{p'h'} \Big(X^\omega_{p'h'}{}^* \underbrace{\langle \mathrm{HF}| \, \hat{a}^\dagger_h \hat{a}_p [\hat{H}, \hat{a}^\dagger_{h'} \hat{a}_{p'}] \, |\mathrm{HF}\rangle}_{= -B_{ph,p'h'}} - Y^\omega_{p'h'}{}^* \underbrace{\langle \mathrm{HF}| \, \hat{a}^\dagger_h \hat{a}_p [\hat{H}, \hat{a}^\dagger_{p'} \hat{a}_{h'}] \, |\mathrm{HF}\rangle}_{= A_{ph,p'h'}} \Big)^* = E^{\mathrm{RPA}}_\omega Y^\omega_{ph}, \tag{3.90}$$

or in short notation

$$\sum_{p'h'} \Big(\quad X^\omega_{p'h'} \, A_{ph,p'h'} + Y^\omega_{p'h'} \, B_{ph,p'h'} \Big) = E^{\mathrm{RPA}}_\omega X^\omega_{ph}, \tag{3.91}$$

$$\sum_{p'h'} \Big(-X^\omega_{p'h'} \, B^*_{ph,p'h'} - Y^\omega_{p'h'} \, A^*_{ph,p'h'} \Big) = E^{\mathrm{RPA}}_\omega Y^\omega_{ph}. \tag{3.92}$$

In (3.89) we have introduced two new matrices, A and B, with their matrix elements defined via

$$\boxed{A_{ph,p'h'} = \quad \langle \mathrm{HF}| \, \hat{a}^\dagger_h \hat{a}_p [\hat{H}, \hat{a}^\dagger_{p'} \hat{a}_{h'}] \, |\mathrm{HF}\rangle \, ,} \tag{3.93}$$

$$\boxed{B_{ph,p'h'} = -\langle \mathrm{HF}| \, \hat{a}^\dagger_h \hat{a}_p [\hat{H}, \hat{a}^\dagger_{h'} \hat{a}_{p'}] \, |\mathrm{HF}\rangle \, .} \tag{3.94}$$

This notation, in which we explicitly denote the individual particle (p, p') and hole (h, h') indices, is somewhat lengthy. To make things more tractable, we introduce a matrix-notation with collective-indices $i = (ph)$ and $j = (p'h')$. With this the above equations read

$$\sum_j \Big(\quad A_{i,j} X^\omega_j + B_{i,j} Y^\omega_j \Big) = E^{\mathrm{RPA}}_\omega X^\omega_i, \tag{3.95}$$

$$\sum_j \Big(-B^*_{i,j} X^\omega_j - A^*_{i,j} Y^\omega_j \Big) = E^{\mathrm{RPA}}_\omega Y^\omega_i. \tag{3.96}$$

We see that the RPA equations (3.89) and (3.90) can be written into matrix form:

$$\boxed{\begin{pmatrix} A & B \\ -B^* & -A^* \end{pmatrix} \begin{pmatrix} X^\omega \\ Y^\omega \end{pmatrix} = E_\omega^{\mathrm{RPA}} \begin{pmatrix} X^\omega \\ Y^\omega \end{pmatrix}.} \tag{3.97}$$

Equation (3.97) is called the *RPA matrix equation*. Relation (3.97) reduces the RPA problem to an eigenvalue problem, and its solution yields the RPA eigenenergies E_ω^{RPA} as well as the RPA amplitudes X_{ph}^ω and Y_{ph}^ω. It can be shown that the matrix A is Hermitian and B is symmetric, and, therefore, the so-called *RPA supermatrix*

$$R = \begin{pmatrix} A & B \\ -B^* & -A^* \end{pmatrix} \tag{3.98}$$

is non-Hermitian. A discussion regarding the ramifications of this is given in section 3.2.7.

3.2.6 Tamm-Dancoff Approximation

The Tamm-Dancoff Approximation (TDA) is, as already mentioned, a simpler ph theory than the RPA. Within the framework of the TDA, there are ph excitations, but no hp excitations. The lack of hp excitations is the defining difference between the two theories. The ECO of the TDA consequently has the following structure

$$\hat{Q}_\omega^\dagger \overset{\mathrm{TDA}}{=} \sum_{ph} X_{ph}^\omega \, \hat{a}_p^\dagger \hat{a}_h, \tag{3.99}$$

where in comparison to the ECO of the RPA (cf. (3.54)) the second term describing the hp excitations has been omitted. The disregard of the possibility of hp excitations leads to a significant simplification of the TDA as compared to the RPA: The TDA ground state, $|\mathrm{TDA}\rangle$, has to fulfill a similar condition as the RPA ground state, namely

$$\hat{Q}_\omega \, |\mathrm{TDA}\rangle = 0 \quad \forall \omega, \tag{3.100}$$

but with the difference that now (3.100) can basically be understood as $\hat{a}_h^\dagger \hat{a}_p \, |\mathrm{TDA}\rangle = 0$. However, since $\hat{a}_p \, |\mathrm{HF}\rangle = 0 \; \forall p$, we have already found a state that obeys (3.100), and ergo we have

$$|\mathrm{TDA}\rangle = |\mathrm{HF}\rangle \, . \tag{3.101}$$

Furthermore, the TDA can be recovered from the RPA. Since there are no hp excitations (cf. (3.99)), there is no need for the Y_{ph}^ω amplitudes. Additionally, there is no B matrix, which originated from the hp part of the RPA excitation creation operator (cf. (3.62) and (3.63)). Apart from these modifications, the derivation of the TDA equations is very similar to the case of the RPA, and the TDA eigenvalue problem reads

$$AX^\omega = E_\omega^{\mathrm{TDA}} X^\omega. \tag{3.102}$$

3.2.7 Properties of the RPA equations

In section 3.2.4, we used the variational principle to derive the RPA eigenvalue problem (3.97). In this section, we will discuss some of the properties of the solutions to the RPA problem. As stated earlier, the solution of the RPA problem yields a set of quantities, namely $(E_\omega^{\mathrm{RPA}}, X_{ph}^\omega, Y_{ph}^\omega)$.

However, from a given solution we can always construct a second one by performing the following transformation

$$\begin{pmatrix} E_\omega^{\mathrm{RPA}} \\ X^\omega \\ Y^\omega \end{pmatrix} \rightarrow \begin{pmatrix} -E_\omega^{\mathrm{RPA}*} \\ Y^{\omega *} \\ X^{\omega *} \end{pmatrix}. \tag{3.103}$$

In order to confirm that the transformation (3.103) indeed gives another solution to the RPA problem we just need to plug this new set into (3.97). This yields the following transformation of the RPA equations:

$$\begin{aligned} AX^\omega + BY^\omega &= E_\omega^{\mathrm{RPA}} X^\omega \\ -B^* X^\omega - A^* Y^\omega &= E_\omega^{\mathrm{RPA}} Y^\omega \end{aligned} \quad \rightarrow \quad \begin{aligned} AY^{\omega *} + BX^{\omega *} &= -E_\omega^{\mathrm{RPA}*} Y^{\omega *} \\ -B^* Y^{\omega *} - A^* X^{\omega *} &= -E_\omega^{\mathrm{RPA}*} X^{\omega *} \end{aligned} \tag{3.104}$$

From (3.104) we see that the first transformed equation is simply the complex conjugate of the second untransformed equation. Similarly, the second transformed equation relates to the first untransformed equation. However, if we assume the original solution to have a positive energy ($E_\omega^{\mathrm{RPA}} > 0$), the new, transformed solution from (3.103) is unphysical due to the negative excitation energy ($E_\omega^{\mathrm{RPA}\prime} = -E_\omega^{\mathrm{RPA}} < 0$). Considering the form of (3.97), it is not astonishing that we get redundant solutions. We see that the RPA matrix has a block structure consisting of A and B. If n is the number of ph excitations, then both these matrices are $n \times n$ matrices and the supermatrix R is of dimension $(2n) \times (2n)$. Nevertheless, the block structure of R implies that, since no "new" information enters this matrix in the second row, some of the eigenvalues might be redundant. Under certain conditions, a reduction of the RPA eigenvalue problem to dimension n is possible [Pap07; UR71; Ull72].

In section 3.2.4 it was stated that the RPA supermatrix R is non-Hermitian. The lack of Hermiticity, of course, also allows for unphysical, complex eigenvalues. It can be shown [Tho60] that the occurrence of complex eigenvalues results from the failure of the approximate ground state to minimize the energy. In these cases, according to Thouless, the HF state is too far removed from the true ground state to be an adequate approximation. If a nucleus possesses strong ground-state deformations, which cannot be represented by Slater-determinants, then calculating excitations associated with deformations, such as quadrupole states, enlarges the model space towards deformations and suddenly the stationary condition of the variational principle is met rather by a saddle point or even a maximum than by the energy minimum, and ergo the HF state becomes unstable.

Another issue concerning the solutions of the RPA eigenvalue problem are spurious center-of-mass (CM) excitations. As long as we are dealing with closed-subshell nuclei, there is only one non-degenerate ground state, and consequently excitations with zero excitation energy should not occur. This should at least hold true in the case that the Hamiltonian is translationally invariant. Due to the fact that the calculations are always carried out with some sort of localized wave function, the conservation of the CM momentum, and with it the translational invariance, is lost. Nevertheless, it has been shown [Row70; Tho61] that the first-order RPA, when performed consistently, i.e., using the same Hamiltonian as for the HF calculation, eliminates those spurious CM excitations with exactly zero energy.

Finally, we want to give a brief remark on the RPA ground state. It can be written as (cf. [RS80])

$$|\mathrm{RPA}\rangle = N_0 \exp\left(\frac{1}{2} \sum_{ph,p'h'} Z_{ph,p'h'}\, \hat{a}_p^\dagger \hat{a}_h \hat{a}_{p'}^\dagger \hat{a}_{h'} \right) |\mathrm{HF}\rangle\,, \tag{3.105}$$

with

$$\sum_{ph} X^{\omega *}_{ph} Z_{ph,p'h'} = Y^{\omega *}_{p'h'}, \quad \forall \omega. \tag{3.106}$$

From (3.105) and (3.106) we can see that $|\mathrm{RPA}\rangle$ indeed depends on the ECOs via their amplitudes X^{ω}_{ph} and Y^{ω}_{ph}, as was stated in section 3.2.2. In matrix notation this reads

$$\sum_{i} X^{\omega *}_{i} Z_{i,j} = Y^{\omega *}_{j}, \tag{3.107}$$

which is the matrix-vector product $X^{\omega *} Z = Y^{\omega *}$. Using the entire set of vectors X^{ω} and Y^{ω} we can build matrices X and Y with the single vectors as column entries. The amplitudes Z can then be obtained as $Z = (Y X^{-1})^*$.

We can see that $|\mathrm{RPA}\rangle$ has a complicated structure, but fortunately there is no need for an actual calculation of $|\mathrm{RPA}\rangle$, since we are using the EOM approach to the RPA.

3.2.8 RPA with explicit 3B Interaction

In this section the RPA equations (3.93) and (3.94) will be evaluated for a Hamiltonian with explicit 3B forces. We will see that equations resulting from explicit 3B forces are identical to the corresponding equations within an NO2B approximation, cf. section 3.2.10. We first need the Hamiltonian $\hat{H}$ for the system under consideration. In this case, a Hamiltonian with a kinetic energy $\hat{T}$, a 2B interaction $\hat{V}$ and a 3B interaction $\hat{V}_{3\mathrm{N}}$ will be examined,

$$\hat{H} = \hat{T} + \hat{V} + \hat{V}_{3\mathrm{N}} \tag{3.108}$$

$$= \sum_{i,i'} t_{i,i'}\, \hat{a}^\dagger_i \hat{a}_{i'} + \frac{1}{4} \sum_{ij,i'j'} v_{ij,i'j'}\, \hat{a}^\dagger_i \hat{a}^\dagger_j \hat{a}_{j'} \hat{a}_{i'} + \frac{1}{36} \sum_{ijk,i'j'k'} v^{3\mathrm{N}}_{ijk,i'j'k'}\, \hat{a}^\dagger_i \hat{a}^\dagger_j \hat{a}^\dagger_k \hat{a}_{k'} \hat{a}_{j'} \hat{a}_{i'}. \tag{3.109}$$

In order to compute the A and B matrices, we first need to evaluate the commutator of the Hamiltonian $\hat{H}$ and pairs of creation and annihilation operators (c.f. (3.93), (3.94)), i.e., terms of the sort $[\hat{H}, \hat{a}^\dagger_{p'} \hat{a}_{h'}]$. Since

$$[\hat{H}, \hat{a}^\dagger_{p'} \hat{a}_{h'}] = [\hat{T} + \hat{V} + \hat{V}_{3\mathrm{N}}, \hat{a}^\dagger_{p'} \hat{a}_{h'}] \tag{3.110}$$

$$= [\hat{T}, \hat{a}^\dagger_{p'} \hat{a}_{h'}] + [\hat{V}, \hat{a}^\dagger_{p'} \hat{a}_{h'}] + [\hat{V}_{3\mathrm{N}}, \hat{a}^\dagger_{p'} \hat{a}_{h'}], \tag{3.111}$$

one first needs to calculate the commutators of $\hat{T}$, $\hat{V}$ and $\hat{V}_{3\mathrm{N}}$ with the term $\hat{a}^\dagger_{p'} \hat{a}_{h'}$. It is helpful to first evaluate all the basic commutators $[\hat{a}^\dagger_i, \hat{a}_j]$ that will be needed during the calculation of the above commutators. With this, we can start the actual task by evaluating the commutator involving $\hat{T}$

$$[\hat{T}, \hat{a}^\dagger_{p'} \hat{a}_{h'}] = \sum_{i,i'} t_{i,i'} [\hat{a}^\dagger_i \hat{a}_{i'}, \hat{a}^\dagger_{p'} \hat{a}_{h'}] \tag{3.112}$$

$$= \sum_{i,i'} t_{i,i'} \left(\hat{a}^\dagger_i [\hat{a}_{i'}, \hat{a}^\dagger_{p'} \hat{a}_{h'}] + [\hat{a}^\dagger_i, \hat{a}^\dagger_{p'} \hat{a}_{h'}] \hat{a}_{i'} \right) \tag{3.113}$$

$$= \sum_{i,i'} t_{i,i'} \left(\hat{a}^\dagger_i \hat{a}^\dagger_{p'} [\hat{a}_{i'}, \hat{a}_{h'}] + \hat{a}^\dagger_i [\hat{a}_{i'}, \hat{a}^\dagger_{p'}] \hat{a}_{h'} + \hat{a}^\dagger_{p'} [\hat{a}^\dagger_i, \hat{a}_{h'}] \hat{a}_{i'} + [\hat{a}^\dagger_i, \hat{a}^\dagger_{p'}] \hat{a}_{h'} \hat{a}_{i'} \right) \tag{3.114}$$

$$= \sum_{i} \left(t_{i,p'}\, \hat{a}^\dagger_i \hat{a}_{h'} - t_{h',i}\, \hat{a}^\dagger_{p'} \hat{a}_i \right). \tag{3.115}$$

Here we made use of the fact that the first and the fourth term cancel, and in the third term the indices i and i' were exchanged. The two remaining commutators of $\hat{V}$ and $\hat{V}_{3\mathrm{N}}$ are evaluated in the same way, for $\hat{V}$ we get

$$[\hat{V}, \hat{a}^\dagger_{p'}\hat{a}_{h'}] = \frac{1}{4}\sum_{ij,i'j'} v_{ij,i'j'}[\hat{a}^\dagger_i\hat{a}^\dagger_j\hat{a}_{j'}\hat{a}_{i'}, \hat{a}^\dagger_{p'}\hat{a}_{h'}] \tag{3.116}$$

$$= \frac{1}{2}\sum_{ij,j'} v_{ij,p'j'}\,\hat{a}^\dagger_i\hat{a}^\dagger_j\hat{a}_{j'}\hat{a}_{h'} - \frac{1}{2}\sum_{j,i'j'} v_{h'j,i'j'}\,\hat{a}^\dagger_{p'}\hat{a}^\dagger_j\hat{a}_{j'}\hat{a}_{i'}. \tag{3.117}$$

The last commutator for $\hat{V}_{3\mathrm{N}}$ yields

$$[\hat{V}_{3\mathrm{N}}, \hat{a}^\dagger_{p'}\hat{a}_{h'}] = \frac{1}{36}\sum_{ijk,i'j'k'} v^{3\mathrm{N}}_{ijk,i'j'k'}[\hat{a}^\dagger_i\hat{a}^\dagger_j\hat{a}^\dagger_k\hat{a}_{k'}\hat{a}_{j'}\hat{a}_{i'}, \hat{a}^\dagger_{p'}\hat{a}_{h'}] \tag{3.118}$$

$$= \frac{1}{12}\sum_{ijk,j'k'} v^{3\mathrm{N}}_{ijk,p'j'k'}\,\hat{a}^\dagger_i\hat{a}^\dagger_j\hat{a}^\dagger_k\hat{a}_{k'}\hat{a}_{j'}\hat{a}_{h'} - \frac{1}{12}\sum_{jk,i'j'k'} v^{3\mathrm{N}}_{h'jk,i'j'k'}\,\hat{a}^\dagger_{p'}\hat{a}^\dagger_j\hat{a}^\dagger_k\hat{a}_{k'}\hat{a}_{j'}\hat{a}_{i'}. \tag{3.119}$$

With these results, we can formulate the matrix elements of the two matrices A and B as given in (3.93) and (3.94), respectively. For the matrix A, we find

$$\begin{aligned}\langle \mathrm{HF}|\, \hat{a}^\dagger_h\hat{a}_p[\hat{H}, \hat{a}^\dagger_{p'}\hat{a}_{h'}]\,|\mathrm{HF}\rangle = &\sum_i \Big(t_{i,p'}\,\langle \mathrm{HF}|\, \hat{a}^\dagger_h\hat{a}_p\,\hat{a}^\dagger_i\hat{a}_{h'}\,|\mathrm{HF}\rangle - t_{h',i}\,\langle \mathrm{HF}|\, \hat{a}^\dagger_h\hat{a}_p\,\hat{a}^\dagger_{p'}\hat{a}_i\,|\mathrm{HF}\rangle\Big)\\ &+ \frac{1}{2}\sum_{ij,j'} v_{ij,p'j'}\,\langle \mathrm{HF}|\, \hat{a}^\dagger_h\hat{a}_p\,\hat{a}^\dagger_i\hat{a}^\dagger_j\hat{a}_{j'}\hat{a}_{h'}\,|\mathrm{HF}\rangle\\ &- \frac{1}{2}\sum_{j,i'j'} v_{h'j,i'j'}\,\langle \mathrm{HF}|\, \hat{a}^\dagger_h\hat{a}_p\,\hat{a}^\dagger_{p'}\hat{a}^\dagger_j\hat{a}_{j'}\hat{a}_{i'}\,|\mathrm{HF}\rangle\\ &+ \frac{1}{12}\sum_{ijk,j'k'} v^{3\mathrm{N}}_{ijk,p'j'k'}\,\langle \mathrm{HF}|\, \hat{a}^\dagger_h\hat{a}_p\,\hat{a}^\dagger_i\hat{a}^\dagger_j\hat{a}^\dagger_k\hat{a}_{k'}\hat{a}_{j'}\hat{a}_{h'}\,|\mathrm{HF}\rangle\\ &- \frac{1}{12}\sum_{jk,i'j'k'} v^{3\mathrm{N}}_{h'jk,i'j'k'}\,\langle \mathrm{HF}|\, \hat{a}^\dagger_h\hat{a}_p\,\hat{a}^\dagger_{p'}\hat{a}^\dagger_j\hat{a}^\dagger_k\hat{a}_{k'}\hat{a}_{j'}\hat{a}_{i'}\,|\mathrm{HF}\rangle\,.\end{aligned} \tag{3.120}$$

Since the operators in (3.120) are evaluated in an expectation value of the HF state, each respective operator string must not change the resulting state, because otherwise the resulting scalar product would vanish. Ergo, we need to have pairs of creation and annihilation operators of the sort $\hat{a}^\dagger_i\hat{a}_j$ or $\hat{a}_i\hat{a}^\dagger_j$ which, if brought together, will evaluate to either δ_{ij} or directly zero (if $\hat{a}_j$ is unoccupied or $\hat{a}^\dagger_j$ is already occupied). For example

$$\langle \mathrm{HF}|\, \hat{a}^\dagger_h\hat{a}_p\,\hat{a}^\dagger_i\hat{a}_{h'}\,|\mathrm{HF}\rangle = \delta_{hp}\delta_{ih'} + \delta_{hh'}\delta_{pi} \tag{3.121}$$

$$= \delta_{hh'}\delta_{pi}, \tag{3.122}$$

where the δ_{hp}-term vanishes since h and p are disjoint indices. Skipping the details, the final results read

$$\begin{aligned}\langle \mathrm{HF}|\, \hat{a}^\dagger_h\hat{a}_p[\hat{H}, \hat{a}^\dagger_{p'}\hat{a}_{h'}]\,|\mathrm{HF}\rangle = \quad &t_{p,p'}\,\delta_{hh'} - t_{h',h}\,\delta_{pp'}\\ &+ v_{ph',hp'} + \delta_{hh'}\sum_i^{\mathrm{occ.}} v_{pi,p'i} - \delta_{pp'}\sum_i^{\mathrm{occ.}} v_{h'i,hi}\\ &+ \sum_i^{\mathrm{occ.}} v^{3\mathrm{N}}_{ph'i,hp'i} + \frac{1}{2}\delta_{hh'}\sum_{i,j}^{\mathrm{occ.}} v^{3\mathrm{N}}_{pij,p'ij} - \frac{1}{2}\delta_{pp'}\sum_{i,j}^{\mathrm{occ.}} v^{3\mathrm{N}}_{h'ij,hij}.\end{aligned} \tag{3.123}$$

With expression (3.26) for the single-particle energies ϵ_i, this can be written as:

$$\boxed{\begin{aligned} A_{ph,p'h'} &\equiv \langle \mathrm{HF}| \hat{a}_h^\dagger \hat{a}_p [\hat{H}, \hat{a}_{p'}^\dagger \hat{a}_{h'}] |\mathrm{HF}\rangle \\ &= (\epsilon_p - \epsilon_h)\delta_{pp'}\delta_{hh'} + v_{ph',hp'} + \sum_i^{\text{occ.}} v^{\text{3N}}_{ph'i,hp'i}. \end{aligned}} \tag{3.124}$$

For the B matrix, we would have to conduct an analogous calculation, but this time with the commutator $[\hat{H}, \hat{a}_{h'}^\dagger \hat{a}_{p'}]$. Up to (3.120), everything was generic, i.e., the calculations were performed on the level of operators and, therefore, hold true for arbitrary indices p' and h'. This means that in order to obtain the corresponding equations for the B matrix we just have to rename the indices $p' \leftrightarrow h'$. Subsequent to (3.120) the calculations start to differ more strongly because from there on up we used the specific nature (particle/hole) of the operators in order to be able to evaluate the HF expectation value correctly. The principle remains the same though. The result is presented below:

$$\boxed{\begin{aligned} B_{ph,p'h'} &\equiv -\langle \mathrm{HF}| \hat{a}_h^\dagger \hat{a}_p [\hat{H}, \hat{a}_{h'}^\dagger \hat{a}_{p'}] |\mathrm{HF}\rangle \\ &= v_{pp',hh'} + \sum_i^{\text{occ.}} v^{\text{3N}}_{pp'i,hh'i}. \end{aligned}} \tag{3.125}$$

In the case of a 2B Hamiltonian $\hat{H} = \hat{T} + \hat{V}$, these equations would simply read

$$A^{\text{2B}}_{ph,p'h'} = (\epsilon_p^{\text{2B}} - \epsilon_h^{\text{2B}})\delta_{pp'}\delta_{hh'} + v_{ph',hp'}, \tag{3.126}$$

$$B^{\text{2B}}_{ph,p'h'} = v_{pp',hh'}, \tag{3.127}$$

with

$$\epsilon_i^{\text{2B}} = t_{i,i} + \sum_j^{\text{occ.}} v_{ij,ij}. \tag{3.128}$$

The difference between the 2B and the 3B case are the one- and two-fold summations over the matrix elements of the 3B interaction, $v^{\text{3N}}_{ijk,i'j'k'}$, in the expressions for the HF single-particle energies and the RPA matrices.

3.2.9 Coupled RPA Matrices

As mentioned before, the uncoupled formulation of the RPA equations is convenient to keep the equations lucid. For practical applications, however, the spherical, coupled formulation is much more efficient. The coupled versions of (3.124) and (3.125) can be obtained by applying (3.47), which defines the relation between coupled and uncoupled formulation. With a few simplifications, this leads to the following coupled A and B matrices [PR10]

$$\begin{aligned} A_{\bar{p}\bar{h},\bar{p}'\bar{h}'} =& (\epsilon_{\bar{p}} - \epsilon_{\bar{h}})\delta_{\bar{p}\bar{p}'}\delta_{\bar{h}\bar{h}'} \\ &+ \sum_{J_1} (-1)^{j_h + j_{p'} - J_1} (2J_1+1) \begin{Bmatrix} j_p & j_{h'} & J_1 \\ j_{p'} & j_h & J \end{Bmatrix} \langle \bar{p}\bar{h}'; J_1 | \hat{H} | \bar{h}\bar{p}'; J_1 \rangle \,, \end{aligned} \tag{3.129}$$

$$\begin{aligned} B_{\bar{p}\bar{h},\bar{p}'\bar{h}'} =& \sum_{J_1} (-1)^{j_h + j_{p'} + J - J_1} (2J_1+1) \begin{Bmatrix} j_p & j_{p'} & J_1 \\ j_h & j_{h'} & J \end{Bmatrix} \langle \bar{p}\bar{p}'; J_1 | \hat{H} | \bar{h}\bar{h}'; J_1 \rangle \\ &\times (1 + \delta_{\bar{p}\bar{p}'})^{1/2} (1 + \delta_{\bar{h}\bar{h}'})^{1/2}. \end{aligned} \tag{3.130}$$

3.2.10 RPA with Normal-Ordered 3B Interaction

In the following we will show that, for first-order RPA, the use of a normal-ordered interaction is identical to the use of the explicit 3B interaction. In other words, for this particular case the NO2B approximation as introduced in section 2.3 is not an approximation.

We start by showing that the single-particle energies do not change. For the case of an explicit 3B interaction we have

$$\epsilon_i = t_{i,i} + \sum_j^{\text{occ.}} v_{ij,ij} + \frac{1}{2}\sum_{jk}^{\text{occ.}} v^{\text{3N}}_{ijk,ijk}\,, \tag{3.131}$$

and the sole contribution from the 3B interaction is

$$\frac{1}{2}\sum_{jk}^{\text{occ.}} v^{\text{3N}}_{ijk,ijk} = \frac{1}{2} f_{i,i}\,, \tag{3.132}$$

where we used the definition of $f_{i,i}$ as in (2.32). The contributions from the normal-ordered 1B and 2B parts can be identified by means of correspondence. For the usual 1B and 2B operators as in (3.109) we got the contributions t_{ii} and $\sum_j^{\text{occ.}} v_{ij,ij}$ for the single-particle energies. With the 1B and 2B parts of the normal-ordered 3B interaction as in (2.32) and (2.33) we can immediately infer that the contributions are $-\frac{1}{2} f_{i,i}$ and $\sum_j^{\text{occ.}} f_{ij,ij}$, respectively. We see that this is, in sum, identical to the contribution of the explicit 3B interaction (see above)

$$-\frac{1}{2} f_{i,i} + \sum_j^{\text{occ.}} f_{ij,ij} = -\frac{1}{2} f_{i,i} + f_{i,i} = \frac{1}{2} f_{i,i}. \tag{3.133}$$

Finally, again using correspondence, we see that also the contribution to the 2B interaction that is not absorbed by the single-particle energies is identical. For example, the matrix element $v_{ph',hp'}$ corresponds to the NO2B contribution $f_{ph',hp'}$. Reinserting the definition of f gives

$$f_{ph',hp'} = \sum_i^{\text{occ.}} v^{\text{3N}}_{ph'i,hp'i}, \tag{3.134}$$

which is indeed identical to (3.124).

3.3 Second-order RPA (SRPA)

As a particle-hole theory RPA would, untruncated, include up to ApAh excitations, which is obviously unfeasible for nuclei in the medium mass region. First-order RPA results from cutting all but the 1p1h excitations from the model space. In this chapter we will discuss the Second RPA (SRPA), which includes additional 2p2h excitations, as an extension to standard RPA. It represents the natural extension of RPA by going to the next higher order, i.e., neglecting a smaller part of the hypothetical full model space (all but 1p1h and 2p2h terms). Such systematical improvements of a model generally lead to a better description of the systems. This procedure is similar to many other theories such as coupled-cluster theory where either "Singles" or "Singles and Doubles" can be included into the model space (cf. section 4.2).

The corresponding SRPA ECO is written as follows

$$\begin{aligned}\hat{Q}^\dagger_\omega \equiv & \sum_{p_1,h_1} \left(X^\omega_{p_1h_1}\, \hat{a}^\dagger_{p_1}\hat{a}_{h_1} - Y^\omega_{p_1h_1}\, \hat{a}^\dagger_{h_1}\hat{a}_{p_1} \right) \\ & + \sum_{p_1h_1,p_2h_2} \left(X^\omega_{p_1h_1,p_2h_2}\, \hat{a}^\dagger_{p_1}\hat{a}_{h_1}\hat{a}^\dagger_{p_2}\hat{a}_{h_2} - Y^\omega_{p_1h_1,p_2h_2}\, \hat{a}^\dagger_{h_1}\hat{a}_{p_1}\hat{a}^\dagger_{h_2}\hat{a}_{p_2} \right). \end{aligned} \tag{3.135}$$

The first term of (3.135) is equal to (3.53) and is responsible for the 1p1h excitations. Similarly, the second term of (3.135) contains a new set of coefficients ($X^\omega_{p_1h_1,p_2h_2}$, $Y^\omega_{p_1h_1,p_2h_2}$) as well as the 2p2h (de-)excitation operators. Usually the original amplitude vector is considered extended by the additional SRPA entries, since they describe the same processes, only at different order. With this, for X^ω we can write

$$X^\omega = \begin{pmatrix} X^\omega_{ph} \\ X^\omega_{p_1h_1,p_2h_2} \end{pmatrix} \equiv \begin{pmatrix} X^\omega_1 \\ X^\omega_2 \end{pmatrix}. \tag{3.136}$$

In (3.135) we chose to denote the SRPA equations in uncoupled form for reasons of brevity. Coupling will however be a necessity for all practical applications, the details of this are discussed below.

3.3.1 Construction of Pair Creators and Annihilators

For first-order RPA we constructed ph creators and annihilators of the sort

$$\hat{\mathcal{A}}^\dagger{}_{\bar{p}\bar{h}}(JM) = [\hat{a}^\dagger_{\bar{p}}\hat{a}_{\bar{h}}]_{JM}. \tag{3.137}$$

This describes the coupling of one basic creator with one annihilator. For SRPA we now have to construct coupled creators and annihilators for twofold excitations and de-excitations. This could be done by simply concatenating two of the ph-operators known from first-order RPA. We will choose a different approach in which we combine a twofold excitation of two particle states, coupled to a total particle excitation, with the equal counterpart of a total hole de-excitation stemming from a twofold hole de-excitation. The operator for the first, the so-called *pair creator* or pp creator, can be written as [Suh07]

$$\hat{K}^\dagger_{\bar{p}_1,\bar{p}_2}(JM) \equiv N_{\bar{p}_1,\bar{p}_2}\,[\hat{a}^\dagger_{\bar{p}_1}\hat{a}^\dagger_{\bar{p}_2}]_{JM} = N_{\bar{p}_1,\bar{p}_2} \sum_{m_{p_1},m_{p_2}} C(j_{p_1}m_{p_1}, j_{p_2}m_{p_2}|JM)\, \hat{a}^\dagger_{\bar{p}_1,m_{p_1}}\hat{a}^\dagger_{\bar{p}_2,m_{p_2}} \tag{3.138}$$

$$\text{with:} \qquad N_{\bar{p}_1,\bar{p}_2} = N_{\bar{p}_2,\bar{p}_1} = \frac{1}{\sqrt{1+\delta_{j_{p_2},j_{p_1}}}}. \tag{3.139}$$

The normalization factor $N_{\bar{p}_1,\bar{p}_2}$ guarantees the correct normalization in case the two states in the pair creator are the same. To be more precise, this normalization factor is often defined somewhat differently as

$$N_{\bar{p}_1,\bar{p}_2} = \frac{\sqrt{1+\delta_{j_{p_2},j_{p_1}}(-1)^J}}{1+\delta_{j_{p_2},j_{p_1}}}, \tag{3.140}$$

which yields zero in case of $j_{p_2} = j_{p_1}$ and odd J (see section B.1). We directly omit all such combinations of states in our basis and, therefore, use the shorter version of $N_{\bar{p}_1,\bar{p}_2}$. We want to remark that (3.138) is a valid spherical tensor operator. In comparison to the RPA case, the pp creator carries no additional phase factor because, unlike the RPA ph-creator, the pp creator has no annihilation operator from which this phase originated (compare (3.47)). Concerning phases, we will see shortly that the pair-annihilator consequently will carry a phase factor. We also note that in RPA the above normalization factor is not necessary, since particle and hole states are disjoint.

Let us take a look at the symmetry properties of the pair creator:

$$\begin{aligned}
\hat{K}^\dagger_{\bar{p}_1,\bar{p}_2}(JM) &= N_{\bar{p}_1,\bar{p}_2}\,[\hat{a}^\dagger_{\bar{p}_1}\hat{a}^\dagger_{\bar{p}_2}]_{JM} && (3.141)\\
&= N_{\bar{p}_1,\bar{p}_2}\sum_{m_{p_1},m_{p_2}} C(j_{p_1}m_{p_1},j_{p_2}m_{p_2}|JM)\,\hat{a}^\dagger_{\bar{p}_1,m_{p_1}}\hat{a}^\dagger_{\bar{p}_2,m_{p_2}} && (3.142)\\
&= N_{\bar{p}_1,\bar{p}_2}\sum_{m_{p_1},m_{p_2}} (-1)^{j_{p_1}+j_{p_2}-J} C(j_{p_2}m_{p_2},j_{p_1}m_{p_1}|JM)\,\hat{a}^\dagger_{\bar{p}_1,m_{p_1}}\hat{a}^\dagger_{\bar{p}_2,m_{p_2}} && (3.143)\\
&= N_{\bar{p}_1,\bar{p}_2}\sum_{m_{p_1},m_{p_2}} (-1)^{j_{p_1}+j_{p_2}-J+1} C(j_{p_2}m_{p_2},j_{p_1}m_{p_1}|JM)\,\hat{a}^\dagger_{\bar{p}_2,m_{p_2}}\hat{a}^\dagger_{\bar{p}_1,m_{p_1}} && (3.144)\\
&= (-1)^{j_{p_1}+j_{p_2}-J+1} N_{\bar{p}_1,\bar{p}_2}\sum_{m_{p_1},m_{p_2}} C(j_{p_2}m_{p_2},j_{p_1}m_{p_1}|JM)\,\hat{a}^\dagger_{\bar{p}_2,m_{p_2}}\hat{a}^\dagger_{\bar{p}_1,m_{p_1}} && (3.145)\\
&= (-1)^{j_{p_1}+j_{p_2}-J+1} N_{\bar{p}_1,\bar{p}_2}\,[\hat{a}^\dagger_{\bar{p}_2}\hat{a}^\dagger_{\bar{p}_1}]_{JM} && (3.146)\\
&= (-1)^{j_{p_1}+j_{p_2}-J+1} \hat{K}^\dagger_{\bar{p}_2,\bar{p}_1}(JM). && (3.147)
\end{aligned}$$

We find that the particle indices 1 and 2 can be exchanged yielding a simple phase factor. Since those configurations are linearly dependent, we include only one of them into our basis. We include only the "ordered" creators in the basis, i.e., we require $p_1 \leq p_2$ (or $h_1 \leq h_2$ for the pair annihilator, respectively). This ordering of states is defined in [PR10]. The pair annihilator can be calculated by taking the adjoint of the pair creator. This yields

$$\begin{aligned}
\hat{K}_{\bar{p}_1,\bar{p}_2}(JM) =& \hat{K}^\dagger_{\bar{p}_1,\bar{p}_2}(JM)^\dagger && (3.148)\\
=& N_{\bar{p}_1,\bar{p}_2}\sum_{m_{p_1},m_{p_2}} C(j_{p_1}m_{p_1},j_{p_2}m_{p_2}|JM)\,\hat{a}_{\bar{p}_2,m_{p_2}}\hat{a}_{\bar{p}_1,m_{p_1}} && (3.149)\\
=& N_{\bar{p}_1,\bar{p}_2}\sum_{m_{p_1},m_{p_2}} (-1)^{j_{p_1}+j_{p_2}-J} C(j_{p_2}m_{p_2},j_{p_1}m_{p_1}|JM)\,\hat{a}_{\bar{p}_2,m_{p_2}}\hat{a}_{\bar{p}_1,m_{p_1}} && (3.150)\\
=& (-1)^{j_{p_1}+j_{p_2}-J} N_{\bar{p}_2,\bar{p}_1}\sum_{m_{p_1},m_{p_2}} C(j_{p_2}m_{p_2},j_{p_1}m_{p_1}|JM)\,\hat{a}_{\bar{p}_2,m_{p_2}}\hat{a}_{\bar{p}_1,m_{p_1}} && (3.151)\\
=& (-1)^{j_{p_1}+j_{p_2}-J} N_{\bar{p}_2,\bar{p}_1}\,[\hat{a}_{\bar{p}_2}\hat{a}_{\bar{p}_1}]_{JM}. && (3.152)
\end{aligned}$$

Again, the corresponding annihilator $K_{\bar{p}_1,\bar{p}_2}(JM)$ to the creator $K^\dagger_{\bar{p}_1,\bar{p}_2}(JM)$ is not a spherical tensor operator. In order to get a form that is in compliance with the requirements for spherical tensor operators we add another phase factor, similar to what we did for the first-order RPA ph

annihilators $\hat{\tilde{\mathcal{A}}}$. The spherical pair annihilator $\hat{\tilde{K}}$ then reads

$$\hat{\tilde{K}}_{\bar{p_1},\bar{p_2}}(JM) = (-1)^{J-M} K_{\bar{p_1},\bar{p_2}}(J\text{-}M) \tag{3.153}$$

$$= (-1)^{J-M}(-1)^{j_{p_1}+j_{p_2}-J} N_{\bar{p_1},\bar{p_2}} \, [\hat{a}_{\bar{p_2}} \hat{a}_{\bar{p_1}}]_{J\text{-}M} \tag{3.154}$$

$$= (-1)^{j_{p_1}+j_{p_2}-M} N_{\bar{p_1},\bar{p_2}} \, [\hat{a}_{\bar{p_2}} \hat{a}_{\bar{p_1}}]_{J\text{-}M}. \tag{3.155}$$

Note that, alternatively, we could also have started by coupling spherical tensor operators with each other, i.e., start from $[\hat{\tilde{a}}_{\bar{p_2}} \hat{\tilde{a}}_{\bar{p_1}}]_{JM}$. This would then automatically yield a spherical tensor operator where no additional phase has to be added.

3.3.2 2p2h Excitation Operators

We have now laid the necessary ground work for constructing the complete SRPA 2p2h excitation operators. As mentioned before, this is done by combining the pp pair creator (coupled to the intermediate angular momentum J_p) with the hh pair annihilator (coupled to J_h), and again coupling these to the total angular momentum J. Simply inserting all the ingredients yields

$$\hat{\mathcal{A}}^\dagger_{(\bar{p}_1\bar{p}_2)J_p(\bar{h}_1\bar{h}_2)J_h} \equiv [\hat{K}^{\dagger(J_p)}_{\bar{p}_1,\bar{p}_2} \hat{\tilde{K}}^{(J_h)}_{\bar{h}_1,\bar{h}_2}]_{JM} \tag{3.156}$$

$$= \sum_{M_p,M_h} C(J_pM_p, J_hM_h|JM) \, \hat{K}^{\dagger(J_pM_p)}_{\bar{p}_1,\bar{p}_2} \hat{\tilde{K}}^{(J_hM_h)}_{\bar{h}_1,\bar{h}_2} \tag{3.157}$$

$$\begin{aligned} =& N_{\bar{p}_1,\bar{p}_2} \, N_{\bar{h}_1,\bar{h}_2} \sum_{M_p,M_h} C(J_pM_p, J_hM_h|JM) \\ & \times \sum_{m_{p_1},m_{p_2}} C(j_{p_1}m_{p_1}, j_{p_2}m_{p_2}|J_pM_p) \, \hat{a}^\dagger_{\bar{p}_1,m_{p_1}} \hat{a}^\dagger_{\bar{p}_2,m_{p_2}} \\ & \times (-1)^{j_{h_1}+j_{h_2}-M_h} \sum_{m_{h_1},m_{h_2}} C(j_{h_2}m_{h_2}, j_{h_1}m_{h_1}|J_h\text{-}M_h) \, \hat{a}_{\bar{h}_2,m_{h_2}} \hat{a}_{\bar{h}_1,m_{h_1}}. \end{aligned} \tag{3.158}$$

We can modify the last line. Interchanging the coupling order produces a phase according to

$$C(j_{h_2}m_{h_2}, j_{h_1}m_{h_1}|J_h\text{-}M_h) = (-1)^{j_{h_1}+j_{h_2}-J_h} C(j_{h_1}m_{h_1}, j_{h_2}m_{h_2}|J_h\text{-}M_h). \tag{3.159}$$

The single-particle angular momenta j_x are always half-integers, and thus $2j_x$ is always an odd integer. Both the hole angular momenta in sum then yield an even number, the total phase factor can consequently be simplified to $(-1)^{J_h-M_h}$. We can also reorder the M_h sum so that we have a transformation $M_h \to -M_h$. The total result reads

$$\begin{aligned} \hat{\mathcal{A}}^\dagger_{(\bar{p}_1\bar{p}_2)J_p(\bar{h}_1\bar{h}_2)J_h} =& N_{\bar{p}_1,\bar{p}_2} \, N_{\bar{h}_1,\bar{h}_2} \sum_{M_p,M_h} (-1)^{J_h-M_h} C(J_pM_p, J_h\text{-}M_h|JM) \\ & \times \sum_{m_{p_1},m_{p_2}} C(j_{p_1}m_{p_1}, j_{p_2}m_{p_2}|J_pM_p) \\ & \times \sum_{m_{h_1},m_{h_2}} C(j_{h_1}m_{h_1}, j_{h_2}m_{h_2}|J_hM_h) \\ & \times \hat{a}^\dagger_{\bar{p}_1,m_{p_1}} \hat{a}^\dagger_{\bar{p}_2,m_{p_2}} \hat{a}_{\bar{h}_2,m_{h_2}} \hat{a}_{\bar{h}_1,m_{h_1}}, \end{aligned} \tag{3.160}$$

where we put all operators together into one string. With this the coupling of the 2p2h excitations is complete. We note that the operator string in the above equation can be expressed as an uncoupled 2p2h creation operator

$$\hat{\mathcal{A}}^\dagger_{p_1p_2h_1h_2} = \hat{a}^\dagger_{\bar{p}_1,m_{p_1}} \hat{a}^\dagger_{\bar{p}_2,m_{p_2}} \hat{a}_{\bar{h}_2,m_{h_2}} \hat{a}_{\bar{h}_1,m_{h_1}}. \tag{3.161}$$

Mind that, as long as we are dealing with ph pairs, for the m-scheme operator string it does not matter if we group particles and holes together or if we group ph pairs, i.e.

$$\hat{a}^\dagger_{\bar{p}_1,m_{p_1}}\hat{a}^\dagger_{\bar{p}_2,m_{p_2}}\hat{a}_{\bar{h}_2,m_{h_2}}\hat{a}_{\bar{h}_1,m_{h_1}} = \hat{a}^\dagger_{\bar{p}_1,m_{p_1}}\hat{a}_{\bar{h}_1,m_{h_1}}\hat{a}^\dagger_{\bar{p}_2,m_{p_2}}\hat{a}_{\bar{h}_2,m_{h_2}}. \tag{3.162}$$

Before we will move on to the SRPA equations themselves, we will first discuss some basic commutator relations for the excitation operators in the next section.

3.3.3 Commutator Relations for 1p1h and 2p2h Operators

We already derived the expression for 2p2h excitation operators and are now ready to apply them. The notation for the operators $\hat{\mathcal{A}}^\dagger_{(\bar{p}_1\bar{p}_2)J_p(\bar{h}_1\bar{h}_2)J_h}$ that we introduced is quite bulky. In order to shorten terms we abbreviate the detailed particle and hole index structure

$$\hat{\mathcal{A}}^\dagger_{2,\bar{i}} \equiv \hat{\mathcal{A}}^\dagger_{(\bar{p}_1\bar{p}_2)J_p(\bar{h}_1\bar{h}_2)J_h}, \quad \bar{i} \equiv (\bar{p}_1\bar{p}_2)J_p(\bar{h}_1\bar{h}_2)J_h, \tag{3.163}$$

$$\hat{\mathcal{A}}^\dagger_{2,i} \equiv \hat{\mathcal{A}}^\dagger_{p_1p_2h_1h_2}, \qquad i \equiv p_1p_2h_1h_2, \tag{3.164}$$

reducing the notation to a minimum: $\hat{\mathcal{A}}^\dagger_{2,i}$ is an uncoupled two-fold ph creator for a specific particle hole combination i. This is very similar to what we did before with the multi-indices in standard RPA. In fact, when discussing SRPA we will denote $\hat{\mathcal{A}}^\dagger_i$ as $\hat{\mathcal{A}}^\dagger_{1,i}$ to better distinguish between 1p1h and 2p2h excitations. With this, we can use the fact that $\hat{\mathcal{A}}^\dagger_{2,i}$ can be expressed as product of two 1p1h excitations:

$$\hat{\mathcal{A}}^\dagger_{2,i} = \hat{\mathcal{A}}^\dagger_{1,i_1}\hat{\mathcal{A}}^\dagger_{1,i_2}. \tag{3.165}$$

We already hinted at this in (3.162) by reordering the terms. Note that this reduction of the 2p2h creator to two 1p1h creators would not give a strict equality for the coupled versions because the 2p2h operator is coupled in a pp-hh scheme while the 1p1h operators can only couple particles to holes, and a product would thus be coupled in a ph-ph scheme. The following relations will be discussed in m-scheme representation for reasons of brevity. The final, coupled relations will be given later on.

During the derivation of RPA in section 3.2.5 we saw that

$$\langle \mathrm{HF}| [\hat{\mathcal{A}}^\dagger_{1,i}, \hat{\mathcal{A}}^\dagger_{1,j}] |\mathrm{HF}\rangle = 0 \quad \forall i,j. \tag{3.166}$$

Indeed, in section 4.3.1 we will see that this even holds without the surrounding expectation value, i.e., as an operator identity. Using this result, we immediately get the 2p2h analogon:

$$\begin{aligned}
[\hat{\mathcal{A}}^\dagger_{2,i}, \hat{\mathcal{A}}^\dagger_{2,j}] =& [\hat{\mathcal{A}}^\dagger_{1,i_1}\hat{\mathcal{A}}^\dagger_{1,i_2}, \hat{\mathcal{A}}^\dagger_{1,j_1}\hat{\mathcal{A}}^\dagger_{1,j_2}] && (3.167)\\
=& \hat{\mathcal{A}}^\dagger_{1,i_1}\hat{\mathcal{A}}^\dagger_{1,j_1}[\hat{\mathcal{A}}^\dagger_{1,i_2}, \hat{\mathcal{A}}^\dagger_{1,j_2}] + \hat{\mathcal{A}}^\dagger_{1,i_1}[\hat{\mathcal{A}}^\dagger_{1,i_2}, \hat{\mathcal{A}}^\dagger_{1,j_1}]\hat{\mathcal{A}}^\dagger_{1,j_2} \\
&+ \hat{\mathcal{A}}^\dagger_{1,j_1}[\hat{\mathcal{A}}^\dagger_{1,i_1}, \hat{\mathcal{A}}^\dagger_{1,j_2}]\hat{\mathcal{A}}^\dagger_{1,i_2} + [\hat{\mathcal{A}}^\dagger_{1,i_1}, \hat{\mathcal{A}}^\dagger_{1,j_1}]\hat{\mathcal{A}}^\dagger_{1,j_2}\hat{\mathcal{A}}^\dagger_{1,i_2} && (3.168)\\
=& 0 + 0 + 0 + 0. && (3.169)
\end{aligned}$$

The outcome states that the same holds for the additional 2p2h terms of SRPA. Of course we also get $[\hat{\mathcal{A}}_{2,i}, \hat{\mathcal{A}}_{2,j}] = 0$ by taking the adjoint. In the same way we can quickly evaluate the commutator between a first- and a second-order creator

$$\begin{aligned}
[\hat{\mathcal{A}}^\dagger_{1,i}, \hat{\mathcal{A}}^\dagger_{2,j}] =& [\hat{\mathcal{A}}^\dagger_{1,i}, \hat{\mathcal{A}}^\dagger_{1,j_2}\hat{\mathcal{A}}^\dagger_{1,j_1}] && (3.170)\\
=& \hat{\mathcal{A}}^\dagger_{1,j_2}[\hat{\mathcal{A}}^\dagger_{1,i}, \hat{\mathcal{A}}^\dagger_{1,j_1}] + [\hat{\mathcal{A}}^\dagger_{1,i}, \hat{\mathcal{A}}^\dagger_{1,j_2}]\hat{\mathcal{A}}^\dagger_{1,j_1} && (3.171)\\
=& 0 + 0, && (3.172)
\end{aligned}$$

and, likewise, for the annihilator we find $[\hat{\mathcal{A}}_{1,i}, \hat{\mathcal{A}}_{2,j}] = 0$, as well.

If we include the expectation value into our considerations, then obviously the necessary δ-relations for non-zero contributions can only occur between operators of the same order. So while $[\hat{\mathcal{A}}_{1,i}, \hat{\mathcal{A}}^\dagger_{2,j}]$ may yield non-zero values, we do know that its HF expectation value does vanish:

$$\langle \mathrm{HF}| \left[\hat{\mathcal{A}}_{1,i}, \hat{\mathcal{A}}^\dagger_{2,j}\right] |\mathrm{HF}\rangle = 0. \tag{3.173}$$

3.3.4 SRPA Matrix Equation

The derivation of the SRPA equations is in principle identical to the RPA derivation up to the point where we specify the ECO and the variations associated with it. We can start from (3.61), which, after application of the QBA, reads

$$\langle \mathrm{HF}| \left[\delta\hat{Q}, [\hat{H}, \hat{Q}^\dagger_\omega]\right] |\mathrm{HF}\rangle = E^{\mathrm{SRPA}}_\omega \langle \mathrm{HF}| \left[\delta\hat{Q}, \hat{Q}^\dagger_\omega\right] |\mathrm{HF}\rangle . \tag{3.174}$$

Of course we now have to insert the extended ECO for SRPA and also a corresponding variation including 2p2h terms

$$\hat{Q}^\dagger_\omega = \hat{Q}^\dagger_{1,\omega} + \hat{Q}^\dagger_{2,\omega}, \tag{3.175}$$

$$\delta\hat{Q} = \delta\hat{Q}_1 + \delta\hat{Q}_2. \tag{3.176}$$

In first-order RPA we had two sets of equations resulting from two sets of variational amplitudes. Correspondingly, in SRPA we get four sets of equations:

$$\delta X_1: \quad L_{\mathrm{X1}} = \langle \mathrm{HF}| \left[\hat{\mathcal{A}}_{1,i}, [\hat{H}, \hat{Q}^\dagger_\omega]\right] |\mathrm{HF}\rangle = E^{\mathrm{SRPA}}_\omega \langle \mathrm{HF}| \left[\hat{\mathcal{A}}_{1,i}, \hat{Q}^\dagger_\omega\right] |\mathrm{HF}\rangle = R_{\mathrm{X1}} \tag{3.177}$$

$$\delta Y_1: \quad L_{\mathrm{Y1}} = \langle \mathrm{HF}| \left[\hat{\mathcal{A}}^\dagger_{1,i}, [\hat{H}, \hat{Q}^\dagger_\omega]\right] |\mathrm{HF}\rangle = E^{\mathrm{SRPA}}_\omega \langle \mathrm{HF}| \left[\hat{\mathcal{A}}^\dagger_{1,i}, \hat{Q}^\dagger_\omega\right] |\mathrm{HF}\rangle = R_{\mathrm{Y1}} \tag{3.178}$$

$$\delta X_2: \quad L_{\mathrm{X2}} = \langle \mathrm{HF}| \left[\hat{\mathcal{A}}_{2,i}, [\hat{H}, \hat{Q}^\dagger_\omega]\right] |\mathrm{HF}\rangle = E^{\mathrm{SRPA}}_\omega \langle \mathrm{HF}| \left[\hat{\mathcal{A}}_{2,i}, \hat{Q}^\dagger_\omega\right] |\mathrm{HF}\rangle = R_{\mathrm{X2}} \tag{3.179}$$

$$\delta Y_2: \quad L_{\mathrm{Y2}} = \langle \mathrm{HF}| \left[\hat{\mathcal{A}}^\dagger_{2,i}, [\hat{H}, \hat{Q}^\dagger_\omega]\right] |\mathrm{HF}\rangle = E^{\mathrm{SRPA}}_\omega \langle \mathrm{HF}| \left[\hat{\mathcal{A}}^\dagger_{2,i}, \hat{Q}^\dagger_\omega\right] |\mathrm{HF}\rangle = R_{\mathrm{Y2}} \tag{3.180}$$

In the following we will calculate these one by one. The "11"-terms, meaning the 1p1h-1p1h contributions, will be ignored since they have already been computed in first-order RPA and remain unchanged.

Right-Hand Side

We start by calculating the right-hand side. For R_{X1} we find:

$$R_{\mathrm{X1}} = \langle \mathrm{HF}| \left[\hat{\mathcal{A}}_{1,i}, \hat{Q}^\dagger_{1,\omega}\right] |\mathrm{HF}\rangle + \langle \mathrm{HF}| \left[\hat{\mathcal{A}}_{1,i}, \hat{Q}^\dagger_{2,\omega}\right] |\mathrm{HF}\rangle \tag{3.181}$$

$$= \langle \mathrm{HF}| \left[\hat{\mathcal{A}}_{1,i}, \hat{Q}^\dagger_{1,\omega}\right] |\mathrm{HF}\rangle \tag{3.182}$$

$$= X^\omega_i. \tag{3.183}$$

First we used (3.173) to see that the second term vanishes, then we simplified to X_i^ω with what we know from first-order RPA. Analogously, for R_{X2} we get

$$\begin{aligned} R_{\mathrm{X2}} &= \langle \mathrm{HF}| \left[\hat{\mathcal{A}}_{2,i}, \hat{Q}^\dagger_{1,\omega}\right] |\mathrm{HF}\rangle + \langle \mathrm{HF}| \left[\hat{\mathcal{A}}_{2,i}, \hat{Q}^\dagger_{2,\omega}\right] |\mathrm{HF}\rangle && (3.184)\\ &= \sum_j \langle \mathrm{HF}| \left[\hat{\mathcal{A}}_{2,i}, X^\omega_{2,j}\hat{\mathcal{A}}^\dagger_{2,j} - Y^\omega_{2,j}\hat{\mathcal{A}}_{2,j}\right] |\mathrm{HF}\rangle && (3.185)\\ &= \sum_j X^\omega_{2,j} \langle \mathrm{HF}| \left[\hat{\mathcal{A}}_{2,i}, \hat{\mathcal{A}}^\dagger_{2,j}\right] |\mathrm{HF}\rangle - Y^\omega_{2,j} \langle \mathrm{HF}| \left[\hat{\mathcal{A}}_{2,i}, \hat{\mathcal{A}}_{2,j}\right] |\mathrm{HF}\rangle && (3.186)\\ &= \sum_j X^\omega_{2,j} \langle \mathrm{HF}| \left[\hat{\mathcal{A}}_{2,i}, \hat{\mathcal{A}}^\dagger_{2,j}\right] |\mathrm{HF}\rangle + 0 && (3.187)\\ &= \sum_j X^\omega_{2,j}\, \delta_{ij} = X^\omega_{2,i}. && (3.188) \end{aligned}$$

The backward amplitudes can be dealt with just as easily:

$$\begin{aligned} R_{\mathrm{Y1}} &= \langle \mathrm{HF}| \left[\hat{\mathcal{A}}^\dagger_{1,i}, \hat{Q}^\dagger_{1,\omega}\right] |\mathrm{HF}\rangle + \langle \mathrm{HF}| \left[\hat{\mathcal{A}}^\dagger_{1,i}, \hat{Q}^\dagger_{2,\omega}\right] |\mathrm{HF}\rangle && (3.189)\\ &= \langle \mathrm{HF}| \left[\hat{\mathcal{A}}^\dagger_{1,i}, \hat{Q}^\dagger_{1,\omega}\right] |\mathrm{HF}\rangle && (3.190)\\ &= Y^\omega_i, && (3.191) \end{aligned}$$

and

$$\begin{aligned} R_{\mathrm{Y2}} &= \langle \mathrm{HF}| \left[\hat{\mathcal{A}}^\dagger_{2,i}, \hat{Q}^\dagger_{1,\omega}\right] |\mathrm{HF}\rangle + \langle \mathrm{HF}| \left[\hat{\mathcal{A}}^\dagger_{2,i}, \hat{Q}^\dagger_{2,\omega}\right] |\mathrm{HF}\rangle && (3.192)\\ &= \sum_j \langle \mathrm{HF}| \left[\hat{\mathcal{A}}^\dagger_{2,i}, X^\omega_{2,j}\hat{\mathcal{A}}^\dagger_{2,j} - Y^\omega_{2,j}\hat{\mathcal{A}}_{2,j}\right] |\mathrm{HF}\rangle && (3.193)\\ &= \sum_j -Y^\omega_{2,j} \langle \mathrm{HF}| \left[\hat{\mathcal{A}}^\dagger_{2,i}, \hat{\mathcal{A}}^\dagger_{2,j}\right] |\mathrm{HF}\rangle - Y^\omega_{2,j} \langle \mathrm{HF}| \left[\hat{\mathcal{A}}^\dagger_{2,i}, \hat{\mathcal{A}}_{2,j}\right] |\mathrm{HF}\rangle && (3.194)\\ &= \sum_j 0 + -Y^\omega_{2,j} \langle \mathrm{HF}| \left[\hat{\mathcal{A}}^\dagger_{2,i}, \hat{\mathcal{A}}_{2,j}\right] |\mathrm{HF}\rangle && (3.195)\\ &= \sum_j Y^\omega_{2,j}\, \delta_{ij} = Y^\omega_{2,i}. && (3.196) \end{aligned}$$

With this, the right-hand sides are done and we see that the structure of SRPA is more complicated than the RPA version.

Left-Hand Side

Since the left-hand sides involve the 2B Hamiltonian, the computations will be more involved. For example the "12" part will not generally vanish. Our strategy here will be the following: We first identify all terms that are indeed zero. The remaining, non-zero terms will not be computed directly, but later with the help of a diagrammatic approach (cf. section C.1).

In the sense that, when going from RPA to SRPA, we can simply extend our amplitudes, we also have to extend the matrices in the SRPA matrix equation. The A matrix consequently "transforms" according to

$$A = (A_{11}) \longrightarrow A = \begin{pmatrix} A_{11} & A_{12} \\ A_{21} & A_{22} \end{pmatrix}, \tag{3.197}$$

and the same goes for the B matrix. In other words: The same way that we introduced a partitioning to divide the equation into a part concerning the X^ω_{ph} amplitudes and another one

concerning the Y^{ω}_{ph} amplitudes, in SRPA we now also divide the block matrices by their ph rank. To determine the individual submatrices we start with L_{X1} (minus the already known first-order RPA "11" part) and find

$$\begin{aligned}
L_{\mathrm{X1}} - \text{“11”} &= \langle \mathrm{HF}| \left[\hat{\mathcal{A}}_{1,i}, [\hat{H}, \hat{Q}^{\dagger}_{2,\omega}]\right] |\mathrm{HF}\rangle && (3.198)\\
&= \sum_j \langle \mathrm{HF}| \left[\hat{\mathcal{A}}_{1,i}, [\hat{H}, X^{\omega}_{2,j}\hat{\mathcal{A}}^{\dagger}_{2,j} - Y^{\omega}_{2,j}\hat{\mathcal{A}}_{2,j}]\right] |\mathrm{HF}\rangle && (3.199)\\
&= \sum_j X^{\omega}_{2,j} \langle \mathrm{HF}| \left[\hat{\mathcal{A}}_{1,}, [\hat{H}, \hat{\mathcal{A}}^{\dagger}_{2,j}]\right] |\mathrm{HF}\rangle - Y^{\omega}_{2,j} \langle \mathrm{HF}| \left[\hat{\mathcal{A}}_{1,}, [\hat{H}, \hat{\mathcal{A}}_{2,j}]\right] |\mathrm{HF}\rangle && (3.200)\\
&\equiv \sum_j X^{\omega}_{2,j} (A_{12})_{ij} + Y^{\omega}_{2,j} (B_{12})_{ij}. && (3.201)
\end{aligned}$$

We will deal with A_{12} defined as

$$(A_{12})_{ij} = \langle \mathrm{HF}| \left[\hat{\mathcal{A}}_{1,i}, [\hat{H}, \hat{\mathcal{A}}^{\dagger}_{2,j}]\right] |\mathrm{HF}\rangle \tag{3.202}$$

later (see section 3.3.5 and section C.2). The B_{12} matrix can directly be shown to be zero,

$$\begin{aligned}
-(B_{12})_{ij} &= \langle \mathrm{HF}| \left[\hat{\mathcal{A}}_{1,i}, [\hat{H}, \hat{\mathcal{A}}_{2,j}]\right] |\mathrm{HF}\rangle && (3.203)\\
&= \langle \mathrm{HF}| \left[\hat{\mathcal{A}}_{1,i}, [\hat{H}, \hat{\mathcal{A}}_{1,j_1}\hat{\mathcal{A}}_{1,j_2}]\right] |\mathrm{HF}\rangle && (3.204)\\
&= \langle \mathrm{HF}| \left[\hat{\mathcal{A}}_{1,i}, \hat{\mathcal{A}}_{1,j_1}[\hat{H}, \hat{\mathcal{A}}_{1,j_2}]\right] |\mathrm{HF}\rangle \\
&\quad + \langle \mathrm{HF}| \left[\hat{\mathcal{A}}_{1,i}, [\hat{H}, \hat{\mathcal{A}}_{1,j_1}]\hat{\mathcal{A}}_{1,j_2}\right] |\mathrm{HF}\rangle && (3.205)\\
&= 0 + 0, && (3.206)
\end{aligned}$$

where the second term is zero because either $\hat{\mathcal{A}}_{1,j_2}$ or $\hat{\mathcal{A}}_{1,i}$ acts on $|\mathrm{HF}\rangle$. The first term is zero because, in total, $\hat{\mathcal{A}}_{1,i}\hat{\mathcal{A}}_{1,j_1}\ \hat{\mathcal{A}}_{1,j_2}$ is a 3p3h operator, which cannot be compensated by 2B Hamiltonian to yield the necessary δ-relations. For L_{Y1} we find

$$\begin{aligned}
L_{\mathrm{Y1}} - \text{“11”} &= \langle \mathrm{HF}| \left[\hat{\mathcal{A}}^{\dagger}_{1,i}, [\hat{H}, \hat{Q}^{\dagger}_{2,\omega}]\right] |\mathrm{HF}\rangle && (3.207)\\
&= \sum_j \langle \mathrm{HF}| \left[\hat{\mathcal{A}}^{\dagger}_{1,i}, [\hat{H}, X^{\omega}_{2,j}\hat{\mathcal{A}}^{\dagger}_{2,j} - Y^{\omega}_{2,j}\hat{\mathcal{A}}_{2,j}]\right] |\mathrm{HF}\rangle && (3.208)\\
&= \sum_j X^{\omega}_{2,j} \langle \mathrm{HF}| \left[\hat{\mathcal{A}}^{\dagger}_{1,i}, [\hat{H}, \hat{\mathcal{A}}^{\dagger}_{2,j}]\right] |\mathrm{HF}\rangle - Y^{\omega}_{2,j} \langle \mathrm{HF}| \left[\hat{\mathcal{A}}^{\dagger}_{1,i}, [\hat{H}, \hat{\mathcal{A}}_{2,j}]\right] |\mathrm{HF}\rangle , && (3.209)
\end{aligned}$$

with:

$$\begin{aligned}
\langle \mathrm{HF}| \left[\hat{\mathcal{A}}^{\dagger}_{1,i}, [\hat{H}, \hat{\mathcal{A}}^{\dagger}_{2,j}]\right] |\mathrm{HF}\rangle &= \langle \mathrm{HF}| \left[\hat{\mathcal{A}}^{\dagger}_{1,i}, [\hat{H}, \hat{\mathcal{A}}^{\dagger}_{2,j}]\right]^{\dagger} |\mathrm{HF}\rangle^{*} && (3.210)\\
&= - \langle \mathrm{HF}| \left[[\hat{H}, \hat{\mathcal{A}}_{2,j}], \hat{\mathcal{A}}_{1,i}\right] |\mathrm{HF}\rangle^{*} && (3.211)\\
&= \langle \mathrm{HF}| \left[\hat{\mathcal{A}}_{1,i}, [\hat{H}, \hat{\mathcal{A}}_{2,j}]\right] |\mathrm{HF}\rangle^{*} && (3.212)\\
&= - (B_{12})^{*}_{ij}, && (3.213)\\
\langle \mathrm{HF}| \left[\hat{\mathcal{A}}^{\dagger}_{1,i}, [\hat{H}, \hat{\mathcal{A}}_{2,j}]\right] |\mathrm{HF}\rangle &= \langle \mathrm{HF}| \left[\hat{\mathcal{A}}^{\dagger}_{1,i}, [\hat{H}, \hat{\mathcal{A}}_{2,j}]\right]^{\dagger} |\mathrm{HF}\rangle^{*} && (3.214)\\
&= - \langle \mathrm{HF}| \left[[\hat{H}, \hat{\mathcal{A}}^{\dagger}_{2,j}], \hat{\mathcal{A}}_{1,i}\right] |\mathrm{HF}\rangle^{*} && (3.215)\\
&= \langle \mathrm{HF}| \left[\hat{\mathcal{A}}_{1,i}, [\hat{H}, \hat{\mathcal{A}}^{\dagger}_{2,j}]\right] |\mathrm{HF}\rangle^{*} && (3.216)\\
&= (A_{12})^{*}_{ij}. && (3.217)
\end{aligned}$$

We see that this term carries the already identified matrices with the amplitudes exchanged, analog to first-order RPA,

$$L_{\mathrm{Y1}} - \text{“11”} = \sum_j -X^{\omega}_{2,j}(B_{12})^{*}_{ij} - Y^{\omega}_{2,j}(A_{12})^{*}_{ij}. \tag{3.218}$$

We move on to L_{X2}. The A_{12} matrix which we saw in (3.202) can be shown to be identical to the transposed of the A_{21} matrix occurring in L_{X2}. Ignoring this term, we get

$$L_{\mathrm{X2}} - \text{“21”} = \langle \mathrm{HF} | \left[\hat{\mathcal{A}}_{2,i}, [\hat{H}, \hat{Q}^{\dagger}_{2,\omega}] \right] | \mathrm{HF} \rangle \tag{3.219}$$

$$= \sum_j X^{\omega}_{2,j} \langle \mathrm{HF} | \left[\hat{\mathcal{A}}_{2,i}, [\hat{H}, \hat{\mathcal{A}}^{\dagger}_{2,j}] \right] | \mathrm{HF} \rangle - Y^{\omega}_{2,j} \langle \mathrm{HF} | \left[\hat{\mathcal{A}}_{2,i}, [\hat{H}, \hat{\mathcal{A}}_{2,j}] \right] | \mathrm{HF} \rangle \tag{3.220}$$

$$= \sum_j X^{\omega}_{2,j} (A_{22})_{i,j} + Y^{\omega}_{2,j} (B_{22})_{i,j}, \tag{3.221}$$

and similarly to before we will discuss

$$A_{22} = \langle \mathrm{HF} | \left[\hat{\mathcal{A}}_{2,i}, [\hat{H}, \hat{\mathcal{A}}^{\dagger}_{2,j}] \right] | \mathrm{HF} \rangle \tag{3.222}$$

later (see section 3.3.6 and section C.3). The matrix

$$B_{22} = - \langle \mathrm{HF} | \left[\hat{\mathcal{A}}_{2,i}, [\hat{H}, \hat{\mathcal{A}}_{2,j}] \right] | \mathrm{HF} \rangle \tag{3.223}$$

vanishes for the same reason as B_{12} did, except that now we have even one more ph annihilator, so we would need an even higher order Hamiltonian to compensate (cf. above and section 3.3.7). We note that the evaluation of L_{Y2} would yield the complex conjugate versions of the “22” part.

With the above, we now know that the A matrix would indeed look like (3.197), while for B we find no additional terms as long as we are dealing with a 2B Hamiltonian. In the full 1p1h+2p2h space it has the following structure

$$B = \begin{pmatrix} B_{11} & 0 \\ 0 & 0 \end{pmatrix}. \tag{3.224}$$

Summarizing, our SRPA eigenvalue problem now reads

$$\left(\begin{array}{cc|cc} A_{11} & A_{12} & B_{11} & 0 \\ A_{21} & A_{22} & 0 & 0 \\ \hline -B^*_{11} & 0 & -A^*_{11} & -A^*_{12} \\ 0 & 0 & -A^*_{21} & -A^*_{22} \end{array}\right) \begin{pmatrix} X^{\omega}_1 \\ X^{\omega}_2 \\ Y^{\omega}_1 \\ Y^{\omega}_2 \end{pmatrix} = E^{\mathrm{SRPA}}_{\omega} \begin{pmatrix} X^{\omega}_1 \\ X^{\omega}_2 \\ Y^{\omega}_1 \\ Y^{\omega}_2 \end{pmatrix}. \tag{3.225}$$

We will proceed to evaluating the non-zero expressions for A_{12} and A_{22}. The derivation itself for these quantities will be performed by means of diagrammatic notation. The explanation of this formalism, to the required extent, and the derivation of the m-scheme SRPA formulae is given in Appendix C. In the following sections we merely state the m-scheme result and present the corresponding coupled formulae.

3.3.5 A12, Coupled Formula

With the help of diagrams we were able to derive the necessary terms for the A_{12} matrix quite quickly. We found (see (C.24))

$$[A_{12}]_{ph;p_1p_2h_1h_2} = (1 - P(h_1, h_2))\delta_{hh_1} v_{ph_2,p_1p_2} - (1 - P(p_1, p_2))\delta_{pp_1} v_{h_1h_2,hp_2}. \tag{3.226}$$

Those terms are, however, still in m-scheme. A coupled version of this matrix can be found in [PR10] for a pure 2B Hamiltonian. Thankfully, we saw that going from a pure 2B Hamiltonian to a NO Hamiltonian including a 1B term does not change the formula for the A_{12} matrix.

Thus, no new derivation is necessary and we can use the result from [PR10]. In coupled form we get

$$
\begin{aligned}
[A_{12}]_{ph;p_1p_2h_1h_2J_pJ_h} &= \langle ph^{-1};J|\,\hat{H}\,|(p_1p_2;J_p)(h_1h_2;J_h)^{-1};J\rangle \qquad (3.227)\\
&= [1-(-1)^{j_{h_1}+j_{h_2}-J_h}P(h_1,h_2)]\delta_{h_1h}\\
&\quad\times(-1)^{j_p+j_{h_2}+J+J_h}(1+\delta_{h_1h_2})^{-\frac{1}{2}}\hat{J}_p\hat{J}_h\\
&\quad\times\begin{Bmatrix} J_p & J & J_h\\ j_{h_1} & j_{h_2} & j_p\end{Bmatrix}\langle p_1p_2;J_p|\,\hat{H}\,|ph_2;J_p\rangle\\
&\quad-[1-(-1)^{j_{p_1}+j_{p_2}-J_p}P(p_1,p_2)]\delta_{p_1p}\\
&\quad\times(-1)^{j_{p_1}+j_{p_2}+J+J_h}(1+\delta_{p_1p_2})^{-\frac{1}{2}}\hat{J}_p\hat{J}_h\\
&\quad\times\begin{Bmatrix} J_h & J & J_p\\ j_{p_1} & j_{p_2} & j_h\end{Bmatrix}\langle hp_2;J_h|\,\hat{H}\,|h_1h_2;J_h\rangle. \qquad (3.228)
\end{aligned}
$$

We see that the structure of the permutations and the matrix elements, though coupled, is identical to the m-scheme variant. The Clebsch-Gordan coefficients have been simplified to coupled matrix elements of $\hat{H}$ and the $6j$-symbol. Mind that while the coupling terms are somewhat obstructive when identifying the relevant contributions as such, they are absolutely necessary for an efficient, large scale application of SRPA.

3.3.6 A22, Coupled Formula

For the A_{22} matrix of SRPA we saw that the 1B part together with the partially summed part of the 2B operator combined to the HF energies, only this time located on the diagonal of the mean-field Hamiltonian. For the A_{12} off-diagonal SRPA matrix these terms vanished identically. The coupled formula of A_{22} requires, as stated before, a pure 2B Hamiltonian [PR10]. Since all 1B contributions can be absorbed into the HF expressions, the 1B part does not produce any conflicts with this requirement, and again we can still use the formula intended for a pure 2B Hamiltonian. The uncoupled m-scheme formula for A_{22} reads (see (C.57))

$$
\begin{aligned}
[A_{22}]_{p_1p_2h_1h_2;P_1P_2H_1H_2} =&\delta_{H_1h_1}\delta_{P_1p_1}\delta_{P_2p_2}\delta_{h_2,H_2}(\epsilon_{p_1}+\epsilon_{p_2}-\epsilon_{h_1}-\epsilon_{h_2})\\
&-(1-P(P_1,P_2))(1-P(H_1,H_2))\\
&\times(1-P(p_1,p_2))(1-P(h_1,h_2))\\
&\times\delta_{H_1h_1}\delta_{P_1p_1}\,v_{h_2P_2,H_2p_2}\\
&+\delta_{H_1h_1}\delta_{H_2h_2}\,v_{P_2P_1,p_2p_1}\\
&+\delta_{P_2p_2}\delta_{P_1p_1}\,v_{h_1h_2,H_1H_2}. \qquad (3.229)
\end{aligned}
$$

The optimized, coupled variant is

$$
\begin{aligned}
A_{22} \equiv & [A_{22}]_{p_1p_2h_1h_2J_pJ_h;P_1P_2H_1H_2J_PJ_H} && (3.230)\\
= & \delta_{p_1P_1}\delta_{h_1H_1}\delta_{p_2P_2}\delta_{h_2H_2}\delta_{J_pJ_P}\delta_{J_hJ_H}(e_{p_1}+e_{p_2}-e_{h_1}-e_{h_2}) \\
& + \langle (p_1p_2;J_p)(h_1h_2;J_h)^{-1};J)|\,\hat{H}\,|(P_1P_2;J_p)(H_1H_2;J_H)^{-1};J\rangle && (3.231)\\
= & \delta_{p_1P_1}\delta_{h_1H_1}\delta_{p_2P_2}\delta_{h_2H_2}\delta_{J_pJ_P}\delta_{J_hJ_H}(e_{p_1}+e_{p_2}-e_{h_1}-e_{h_2}) \\
& + \delta_{p_1P_1}\delta_{p_2P_2}\delta_{J_pJ_P}\delta_{J_hJ_H}[1+(-1)^{J_p}\delta_{p_1p_2}](1+\delta_{p_1p_2})^{-1} \\
& \times \langle H_1H_2;J_h|\,\hat{H}\,|h_1h_2;J_h\rangle \\
& + \delta_{h_1H_1}\delta_{h_2H_2}\delta_{J_pJ_P}\delta_{J_hJ_H}[1+(-1)^{J_h}\delta_{h_1h_2}](1+\delta_{h_1h_2})^{-1} \\
& \times \langle p_1p_2;J_p|\,\hat{H}\,|P_1P_2;J_p\rangle \\
& + [1-(-1)^{j_{p_1}+j_{p_2}-J_p}P(p_1,p_2)](1+\delta_{p_1p_2})^{-\frac{1}{2}} \\
& \times [1-(-1)^{j_{h_1}+j_{h_2}-J_h}P(h_1,h_2)](1+\delta_{h_1h_2})^{-\frac{1}{2}} \\
& \times [1-(-1)^{j_{P_1}+j_{P_2}-J_p}P(P_1,P_2)](1+\delta_{P_1P_2})^{-\frac{1}{2}} \\
& \times [1-(-1)^{j_{H_1}+j_{H_2}-J_h}P(H_1,H_2)](1+\delta_{H_1H_2})^{-\frac{1}{2}} \\
& \times \delta_{h_2H_2}\delta_{p_2P_2}(-1)^{1+j_{p_1}+j_{p_2}+j_{h_1}+j_{h_2}}\hat{J}_p\hat{J}_P\hat{J}_h\hat{J}_H \\
& \times \sum_L (-1)^{J_h-J_H+J-L}(2L+1)\begin{Bmatrix} J_p & J_P & L \\ J_H & J_h & J\end{Bmatrix} \\
& \times \begin{Bmatrix} J_p & J_P & L \\ j_{P_1} & j_{p_1} & j_{p_2}\end{Bmatrix}\begin{Bmatrix} J_h & J_H & L \\ j_{H_1} & j_{h_1} & j_{h_2}\end{Bmatrix} \\
& \times \sum_{J_1}(-1)^{j_{h_1}+j_{P_1}-J_1}(2J_1+1) \\
& \times \begin{Bmatrix} j_{p_1} & j_{H_1} & J_1 \\ j_{h_1} & j_{P_1} & L\end{Bmatrix}\langle p_1H_1;J_1|\,\hat{H}\,|P_1h_1;J_1\rangle && (3.232)
\end{aligned}
$$

Similar to the A_{12} case, the structure of the coupled expression matches the m-scheme derivation. Aside from the HF terms, we have 2B matrix elements with either four particles or four holes but no permutation terms. Permutations only occur for the "ph-ph" term in (3.232).

3.3.7 SRPA with explicit 3B Forces?

For first-order RPA we derived the A and B matrices for an explicit 3B interaction. However, we see that only the expression for the A matrix changes, while B apparently remains unchanged by the inclusion of explicit 3B terms. In addition, we can show that the NO2B and full 3B case are identical within first-order RPA, see section 3.2.10. In this picture, one could say that RPA can very well *use* explicit 3B contributions, but cannot fully deplete all degrees of freedom associated with a 3B force.

For SRPA, we limited the derivation to up-to 2B Hamiltonians. Nevertheless, using the diagrammatic notation, a derivation of 3B SRPA can be achieved rather easily. We will thus give a brief outlook into the terms that can be expected from a 3B SRPA formalism, showing that SRPA can indeed benefit from those contributions of a 3B interaction that are not included in an NO2B approximation.

For the A_{12} matrix we could additionally construct the following diagram

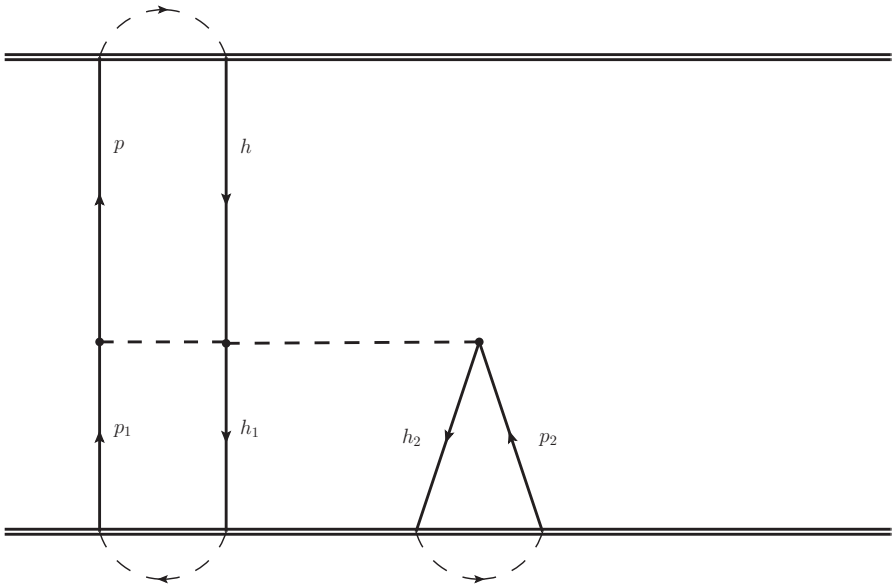

Figure 3.2: A_{12}, 3B part.

Disregarding details, this evaluates to $v_{ph_1h_2,p_1hp_2}$, where no sum over any index pair is present. This gives an additional term to the already present A_{12} matrix.

The A_{22} matrix would be extended by the 3B force as well. One contribution would be

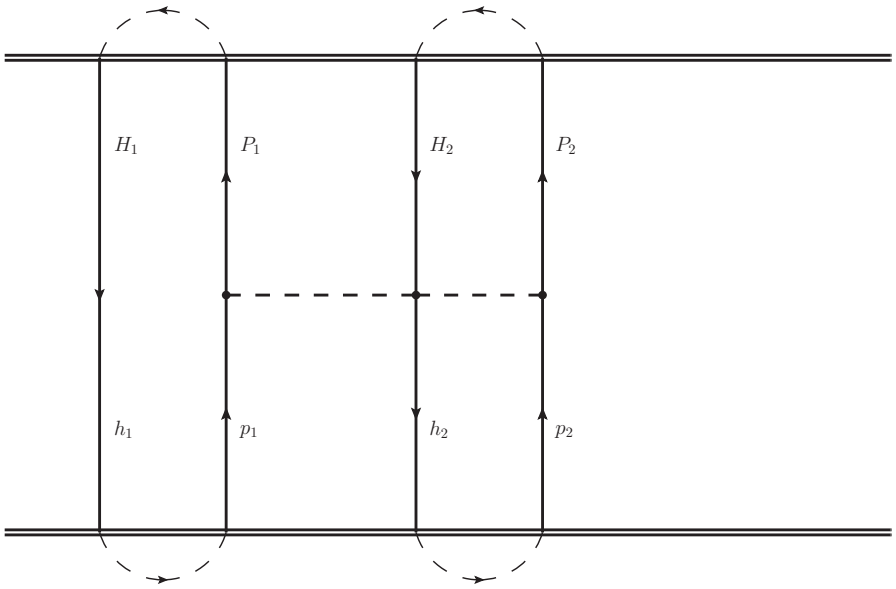

Figure 3.3: A_{22}, 3B part.

This diagram would yield $v_{P_1h_2P_2,p_1H_2p_2}$.

The extension of the SRPA A matrix including non-summed 3B terms alone would warrant further investigation regarding the influence of beyond-NO2B 3B terms. Besides adding terms to the already existing parts of A, employing a full 3B force would even cause the emergence of

the B_{12} matrix, as we have hinted before. Rewriting definition (3.203) we find

$$
\begin{aligned}
(B_{12})_{ij} &= -\langle \mathrm{HF}| [\hat{\mathcal{A}}_{1,i}, [\hat{H}, \hat{\mathcal{A}}_{2,j}]] |\mathrm{HF}\rangle && (3.233)\\
&= -\langle \mathrm{HF}| \hat{\mathcal{A}}_{1,i} [\hat{H}, \hat{\mathcal{A}}_{2,j}] |\mathrm{HF}\rangle && (3.234)\\
&= -\langle \mathrm{HF}| \hat{\mathcal{A}}_{1,i} \hat{H} \hat{\mathcal{A}}_{2,j} |\mathrm{HF}\rangle + \langle \mathrm{HF}| \hat{\mathcal{A}}_{1,i} \hat{\mathcal{A}}_{2,j} \hat{H} |\mathrm{HF}\rangle && (3.235)\\
&= \langle \mathrm{HF}| \hat{\mathcal{A}}_{1,i} \hat{\mathcal{A}}_{2,j} \hat{H} |\mathrm{HF}\rangle && (3.236)\\
&= \langle \mathrm{HF}| \hat{\mathcal{A}}_{1,i} \hat{\mathcal{A}}_{1,j_1} \hat{\mathcal{A}}_{1,j_2} \hat{H} |\mathrm{HF}\rangle . && (3.237)
\end{aligned}
$$

This is represented by the diagram

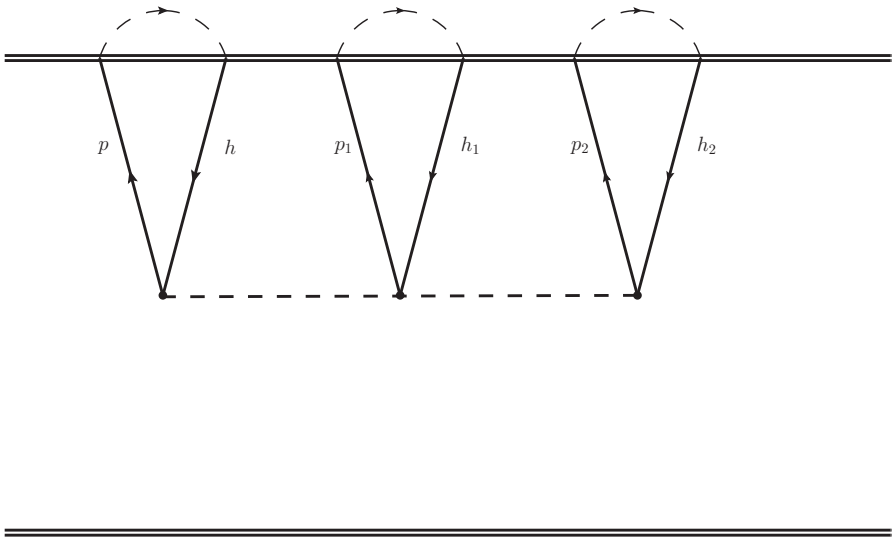

Figure 3.4: B_{12}, 3B part.

Details aside, this evaluates to $v_{pp_1p_2,hh_1h_2}$. Even though these contributions cannot necessarily be expected to be extremely large, the mere existence of another correlation submatrix draws attention to explicit 3B SRPA. Future research on this subject may yield promising results regarding the sensitivity of the RPA formalism with respect to 3B forces.

Chapter 4

Coupled-Cluster RPA

In this chapter we will present the derivation for a correlated RPA formalism. The correlations enter through density matrices of correlated ground states, namely density matrices from coupled-cluster theory. Therefore, we name this theory the coupled-cluster RPA (CC-RPA). Before we get to the discussion of CC-RPA, we first give an introduction to density matrices and coupled-cluster theory itself. We stress that the CC-RPA formalism which we present here is not to be confused with density-functional RPA, see e.g. [GGC10; GGC11]. In addition, it also goes far beyond the renormalized RPA as employed in [Cat$^+$96; Cat$^+$98; GC08].

4.1 Density Matrices

Density matrices both of a single Slater-determinant and of more complex states involving correlations will be important in the upcoming discussions. We will, therefore, give a small introduction to density matrices, their properties and some useful relations.

4.1.1 1B Density Matrix

Density matrices are always given in reference to a certain state whose structure they describe. The 1B density matrix is defined as

$$\varrho_{j,i} = \langle \Phi | \, \hat{a}_i^\dagger \hat{a}_j \, | \Psi \rangle \, . \tag{4.1}$$

From the above definition it is clear that density matrices for different states will yield different results, and it would be appropriate to denote the chosen state within the symbol for the density. In the above case we used different states $|\Phi\rangle$ and $|\Psi\rangle$, so more accurately we should write

$$\varrho \equiv \varrho^{(\Phi,\Psi)}. \tag{4.2}$$

In many cases the reference state, for which the density is calculated, is only defined once in the beginning, it is not explicitly denoted afterwards. For two different states the density will be called a transition density since it describes the overlap of those two states, modified by the operator string in between. Transition densities have different properties (see section 4.1.4 below) than (ground-)state densities, where the bra and ket state are the same. For now we will focus on those densities and omit denoting the reference state. It can easily be shown that the

density matrix is Hermitian:

$$\varrho^*_{j,i} = \langle\Psi|\, \hat{a}^\dagger_i \hat{a}_j \,|\Psi\rangle^* = \langle\Psi|\, \hat{a}^\dagger_j \hat{a}_i \,|\Psi\rangle = \varrho_{i,j} \tag{4.3}$$

$$\Rightarrow \varrho = \varrho^\dagger. \tag{4.4}$$

In particular, real density matrices are symmetric. We will now take a look at the trace of the density matrix. Taking the sum over the diagonal elements immediately yields

$$\mathrm{Tr}(\varrho) = \sum_i \varrho_{ii} = \sum_i \langle\Psi|\, \hat{a}^\dagger_i \hat{a}_i \,|\Psi\rangle = \sum_i \langle\Psi|\, \hat{n}_i \,|\Psi\rangle \tag{4.5}$$

$$= \sum_i n_i = A, \tag{4.6}$$

with n_i being the mean occupation number of the state i. We see that the trace of the 1B density matrix yields the number of particles A in the state $|\Psi\rangle$.

The density matrix is also very useful for the calculation of expectation values. Let $\hat{O}$ be any 1B operator, we then see that the density matrix appears naturally by simply inserting the definition of $\hat{O}$:

$$\langle\Psi|\, \hat{O} \,|\Psi\rangle = \sum_{i,j} o_{i,j} \langle\Psi|\, \hat{a}^\dagger_i \hat{a}_j \,|\Psi\rangle = \sum_{i,j} o_{ij} \varrho_{j,i} = \sum_i (O\varrho)_{i,i} = \mathrm{Tr}(O\varrho). \tag{4.7}$$

In the above equation the matrix product between O and ϱ appears. This matrix product is summed over its diagonal elements, which we write accordingly as the trace of the product matrix $(O\varrho)$. The above relation will be important later for the CC-RPA calculations.

4.1.2 2B Density Matrix

Let us now turn to the 2B case. The analogously defined 2B density matrix is given by

$$\varrho_{i'j',ij} = \langle\Psi|\, \hat{a}^\dagger_i \hat{a}^\dagger_j \hat{a}_{j'} \hat{a}_{i'} \,|\Psi\rangle\,. \tag{4.8}$$

With this definition, a similar connection to the expectation value of 2B operators exists. Inserting yields

$$\langle\Psi|\, \hat{O} \,|\Psi\rangle = \frac{1}{4} \sum_{ij,i'j'} o_{ij,i'j'} \langle\Psi|\, \hat{a}^\dagger_i \hat{a}^\dagger_j \hat{a}_{j'} \hat{a}_{i'} \,|\Psi\rangle = \sum_{ij,i'j'} o_{ij,i'j'} \varrho_{i'j',ij}. \tag{4.9}$$

Summing over one pair of indices, either bra or ket, will give a matrix product between those two quantities. At this point, we have to take the symmetry of our 2B states $|ij\rangle$ into account. Due to symmetry requirements we have $|ij\rangle = -|ji\rangle$. The unrestricted sum over both ij (or $i'j'$) would count every state twice because of this symmetry. To avoid this we can introduce an ordering, we find

$$\langle\Psi|\, \hat{O} \,|\Psi\rangle = \frac{1}{4} \sum_{ij,i'j'} o_{ij,i'j'}\, \varrho_{i'j',ij} = \frac{1}{4}\, 2 \sum_{ij,i'\leq j'} o_{ij,i'j'}\, \varrho_{i'j',ij} = \frac{1}{4} \sum_{ij} (O\varrho)_{ij,ij} \tag{4.10}$$

We already see the structure of a trace. Again, every entry may not be counted more than once. Keeping this in mind, we get

$$\langle\Psi|\, \hat{O} \,|\Psi\rangle = \frac{1}{2} \sum_{ij} (O\varrho)_{ij,ij} = \frac{1}{2}\, 2 \sum_{i\leq j} (O\varrho)_{ij,ij} = \mathrm{Tr}(O\varrho^{\mathrm{2B}}) \tag{4.11}$$

Analogously to the 1B case we can show that 2B densities are also Hermitian (real-symmetric):

$$\varrho_{i'j',ij}{}^{*} = \langle\Psi|\,\hat{a}_i^\dagger\hat{a}_j^\dagger\hat{a}_{j'}\hat{a}_{i'}\,|\Psi\rangle^{*} = \langle\Psi|\,\hat{a}_{i'}^\dagger\hat{a}_{j'}^\dagger\hat{a}_j\hat{a}_i\,|\Psi\rangle = \varrho_{ij,i'j'}. \tag{4.12}$$

The complete trace of the 2B density matrix $\varrho^{\text{2B}} = (\varrho_{ij,i'j'})$ gives

$$\begin{aligned}
\mathrm{Tr}(\varrho^{\text{2B}}) &= \sum_{i\leq j}\varrho_{ij,ij} = \frac{1}{2}\sum_{i,j}\varrho_{ij,ij} && (4.13)\\
&= \frac{1}{2}\sum_{i,j}\langle\Psi|\,\hat{a}_i^\dagger\hat{a}_j^\dagger\hat{a}_j\hat{a}_i\,|\Psi\rangle && (4.14)\\
&= \frac{1}{2}\sum_{i,j}(-1)^2\langle\Psi|\,\hat{a}_j^\dagger\hat{a}_j\hat{a}_i^\dagger\hat{a}_i\,|\Psi\rangle - \delta_{ij}\langle\Psi|\,\hat{a}_j^\dagger\hat{a}_i\,|\Psi\rangle && (4.15)\\
&= \frac{1}{2}\sum_{i,j}\langle\Psi|\,\hat{n}_j\hat{n}_i\,|\Psi\rangle - \frac{1}{2}\sum_i\langle\Psi|\,\hat{n}_i\,|\Psi\rangle && (4.16)\\
&= \frac{1}{2}\sum_{i,j}n_jn_i - \frac{1}{2}\sum_i n_i = \tfrac{1}{2}A^2 - \tfrac{1}{2}A && (4.17)\\
&= \frac{A(A-1)}{2}. && (4.18)
\end{aligned}$$

We can also compute the partial or second trace of the 2B density $\mathrm{Tr}(\varrho^{\text{2B}})_2$, i.e., summing only over the second index. Doing so yields

$$\begin{aligned}
\mathrm{Tr}(\varrho^{\text{2B}})_2 &= \frac{1}{2}\sum_{j}\varrho_{ij,i'j} && (4.19)\\
&= \frac{1}{2}\sum_{j}\langle\Psi|\,\hat{a}_i^\dagger\hat{a}_j^\dagger\hat{a}_j\hat{a}_{i'}\,|\Psi\rangle && (4.20)\\
&= \frac{1}{2}\sum_{j}(-1)^2\langle\Psi|\,\hat{a}_j^\dagger\hat{a}_j\hat{a}_i^\dagger\hat{a}_{i'}\,|\Psi\rangle - \delta_{ij}\langle\Psi|\,\hat{a}_j^\dagger\hat{a}_{i'}\,|\Psi\rangle && (4.21)\\
&= \frac{1}{2}\sum_{j}n_j\langle\Psi|\,\hat{a}_i^\dagger\hat{a}_{i'}\,|\Psi\rangle - \tfrac{1}{2}\langle\Psi|\,\hat{a}_i^\dagger\hat{a}_{i'}\,|\Psi\rangle && (4.22)\\
&= \frac{1}{2}A\langle\Psi|\,\hat{a}_i^\dagger\hat{a}_{i'}\,|\Psi\rangle - \tfrac{1}{2}\langle\Psi|\,\hat{a}_i^\dagger\hat{a}_{i'}\,|\Psi\rangle && (4.23)\\
&= \frac{A-1}{2}\varrho_{i',i}. && (4.24)
\end{aligned}$$

This relation is particularly useful for consistency checks, since it provides a natural hierarchy of densities. Higher ranked densities can always be broken down, via partial sums, to lower rank densities. We note that this works only from higher to lower ranks, the inverse inference does not hold in general, but only for densities of a Slater-determinant (see below).

4.1.3 Densities of a Slater-Determinant

The density of a simple HF Slater-determinant has several special properties. For example regarding the 1B density, only the hole-hole (hh) part is non-zero. This can be seen from

$$\begin{aligned}
\varrho_{hp} = \varrho_{ph} &= \langle\text{HF}|\,\hat{a}_h^\dagger\hat{a}_p\,|\text{HF}\rangle = 0, && (4.25)\\
\varrho_{pp'} &= \langle\text{HF}|\,\hat{a}_p^\dagger\hat{a}_{p'}\,|\text{HF}\rangle = 0. && (4.26)
\end{aligned}$$

Only for $\varrho_{hh'}$ we get

$$\varrho_{hh'} = \langle \mathrm{HF} | \, \hat{a}_h^\dagger \hat{a}_{h'} \, | \mathrm{HF} \rangle = \delta_{hh'} n_h = \delta_{hh'}, \tag{4.27}$$

assuming that the hole states are given in m-scheme indices. In this case the hh part is not only diagonal but each entry is equal to 1. Somewhat more graphically the 1B density matrix, in actual matrix notation, would look as follows

$$\varrho = \begin{pmatrix} \varrho^{\mathrm{hh}} & \varrho^{\mathrm{hp}} \\ \varrho^{\mathrm{ph}} & \varrho^{\mathrm{pp}} \end{pmatrix} = \begin{pmatrix} \varrho^{\mathrm{hh}} & 0 \\ 0 & 0 \end{pmatrix} = \begin{pmatrix} \mathbb{1} & 0 \\ 0 & 0 \end{pmatrix}. \tag{4.28}$$

The above form of the 1B density matrix immediately shows the idempotence of ϱ:

$$\varrho^2 = \varrho. \tag{4.29}$$

For the 2B density matrix we can see via the definition of the matrix elements that

$$\begin{aligned} \varrho_{h_1 h_2, h_1' h_2'} &= \langle \mathrm{HF} | \, \hat{a}_{h_1'}^\dagger \hat{a}_{h_2'}^\dagger \hat{a}_{h_2} \hat{a}_{h_1} \, | \mathrm{HF} \rangle && (4.30) \\ &= (-1)^2 \langle \mathrm{HF} | \, \hat{a}_{h_2'}^\dagger \hat{a}_{h_2} \hat{a}_{h_1'}^\dagger \hat{a}_{h_1} \, | \mathrm{HF} \rangle - \delta_{h_2, h_1'} \langle \mathrm{HF} | \, \hat{a}_{h_2'}^\dagger \hat{a}_{h_1} \, | \mathrm{HF} \rangle && (4.31) \\ &= \langle \mathrm{HF} | \, \hat{a}_{h_2'}^\dagger \hat{a}_{h_2} \hat{a}_{h_1'}^\dagger \hat{a}_{h_1} \, | \mathrm{HF} \rangle - \delta_{h_2, h_1'} \, \delta_{h_1, h_2'} && (4.32) \\ &= \delta_{h_2, h_2'} \, \delta_{h_1, h_1'} - \delta_{h_2, h_1'} \, \delta_{h_1, h_2'}. && (4.33) \end{aligned}$$

The hole indices thus have to be pairwise identical to yield non-zero values. The case that all four hole indices are identical is an exception, here the 2B density vanishes due to antisymmetry. In particular, with (4.27) this could be written as

$$\varrho_{h_1 h_2, h_1' h_2'} = \varrho_{h_2, h_2'} \, \varrho_{h_1, h_1'} - \varrho_{h_2, h_1'} \, \varrho_{h_1, h_2'}. \tag{4.34}$$

From the definition of the 2B density, it also follows immediately that

$$\varrho_{h_1 h_2, h_3 p} = \varrho_{h_1 h_2, p_1 p_2} = \varrho_{h p_1, p_2 p_3} = \varrho_{p_1 p_2, p_3 p_4} = 0, \tag{4.35}$$

i.e., the 2B density vanishes as soon as at least one particle index is present. For SDs the density is thus reduced to the hhhh block. With the above, this result states that in case of Slater-determinants, the entire 2B density can be represented via the 1B density.

4.1.4 Transition Densities

In the above discussion we concerned ourselves with the investigation of ground-state densities. Similar to the previous case, we can also define so-called *transition densities*

$$\varrho_{ij}^{(0\omega)} = \langle \Psi_0 | \, \hat{a}_j^\dagger \hat{a}_i \, | \Psi_\omega \rangle \, . \tag{4.36}$$

These describe the transition between a (ground) state $|\Psi_0\rangle$ and another (excited) state $|\Psi_\omega\rangle$. They represent an off-diagonal matrix element rather than an expectation value, and we can see that this affects the Hermiticity of the transition density matrix

$$\varrho_{j,i}^{(\omega 0)*} \equiv \langle \Psi_\omega | \, \hat{a}_i^\dagger \hat{a}_j \, | \Psi_0 \rangle^* = \langle \Psi_0 | \, \hat{a}_j^\dagger \hat{a}_i \, | \Psi_\omega \rangle = \varrho_{ij}^{(0\omega)}. \tag{4.37}$$

With this we find $\varrho^{(\omega 0)} = \varrho^{(0\omega)\dagger}$.

4.2 Coupled-Cluster Theory

Coupled-Cluster (CC) theory has been employed successfully for many years within quantum chemistry to describe correlation effects of the electrons in atomic and molecular orbitals [Coe58; Číž66; PÍS72]. Given that both nucleons and electrons are fermionic particles, it seems natural that CC is also well suited to describe correlations between the nucleons within a nucleus [CK60]. Recent progress has proven CC to be a very powerful ab initio method [CK60; Hag$^+$10; Bin$^+$13; Bin$^+$14; Bin$^+$16]. This introduction to CC follows the outline of [SB09].

4.2.1 Coupled-Cluster Ground-State

In CC we make an exponential ansatz for the ground state, i.e., we define the correlated state $|\Psi\rangle$ to be given by

$$|\Psi\rangle = e^{\hat{T}} |\Phi\rangle , \quad \hat{T} = \sum_{n=1}^{A} \hat{T}_n, \tag{4.38}$$

where $|\Phi\rangle$ is an uncorrelated reference state, usually chosen to be $|\mathrm{HF}\rangle$, and $\hat{T}$ is the so-called *cluster operator*. This cluster operator is divided into different ranks n that give the ph excitation order. The individual cluster ranks are defined as

$$\hat{T}_1 = \frac{1}{(1!)^2} \sum_{ph} t_h^p \{\hat{a}_p^\dagger \hat{a}_h\}, \tag{4.39}$$

$$\hat{T}_2 = \frac{1}{(2!)^2} \sum_{p_1 p_2 h_1 h_2} t_{h_1 h_2}^{p_1 p_2} \{\hat{a}_{p_1}^\dagger \hat{a}_{p_2}^\dagger \hat{a}_{h_2} \hat{a}_{h_1}\}, \tag{4.40}$$

for the first two ranks, and generally as

$$\hat{T}_m = \frac{1}{(m!)^2} \sum_{\substack{p_1 \ldots p_m \\ h_1 \ldots h_m}} t_{h_1 \ldots h_m}^{p_1 \ldots p_m} \{\hat{a}_{p_1}^\dagger \ldots \hat{a}_{p_m}^\dagger \hat{a}_{h_m} \ldots \hat{a}_{h_1}\}. \tag{4.41}$$

Of course, due to computational costs the cluster operator will have to be truncated, as is the case for every particle hole theory. The 1p1h excitations are referred to as "singles", the 2p2h excitations are called "doubles". As an example, including the $\hat{T}_1$ operator yields the CCS approximation, including only doubles the CCD approximation. Including both gives the singles and doubles truncation CCSD. The particular form of the correlated state, being generated via the exponential ansatz, causes CC results that include singles to be fairly robust against the choice of basis. This can be understood with the help of the *Thouless theorem* [Tho60]. It states that any Slater-determinant $|\Phi'\rangle$ which is not orthogonal to $|\Phi\rangle$ can be rewritten as

$$|\Phi'\rangle = \exp\left(\sum_{ph} C_h^p \hat{a}_p^\dagger \hat{a}_h \right) |\Phi\rangle , \tag{4.42}$$

which is of the form of $\hat{T}_1$ and relates directly the exponential ansatz of (4.38), causing singles, by themselves, to describe a mere change of basis. Furthermore, the exponential structure within CC theory causes the energy to possess a property called *size extensivity*, which ensures the correct scaling of the energy with respect to the particle number [CS00]. In addition, if we choose the HF basis as starting point for our CC calculation, the *Brillouin theorem* [Suh07] causes the $\hat{T}_1$ coefficients, usually referred to as amplitudes, to be small compared to the doubles amplitudes. This seems peculiar since, in the generic sense of a particle-hole hierarchy, we would

expect higher orders to be less important than lower ones. Here the Brillouin theorem offers an explanation, stating that in HF basis the Hamiltonian does not connect the HF state to its 1p1h excitations:

$$\langle\Phi|\,\hat{H}\,|\Phi_h^p\rangle = 0. \tag{4.43}$$

Even though the singles contributions to the ground-state energy may be small, it is still important to include them into the calculations, since they will be relevant for the computation of the 1B densities (see below).

Expanding the exponential function into a Taylor series and inserting $\hat{T}$ gives an expression of the form

$$\begin{aligned} e^{\hat{T}} =& 1 + \hat{T} + \tfrac{1}{2}\hat{T}^2 + \tfrac{1}{3!}\hat{T}^3 + \dots && (4.44)\\ =& 1 + (\hat{T}_1 + \hat{T}_2 + \dots) + \tfrac{1}{2}(\hat{T}_1 + \hat{T}_2 + \dots)^2 + \tfrac{1}{3!}(\hat{T}_1 + \hat{T}_2 + \dots)^3 + \dots . && (4.45)\end{aligned}$$

Terms that carry any of the $\hat{T}_i$ without any powers or products are called *connected-clusters*, while all others, e.g. $\hat{T}_1^2$ or $\hat{T}_1\hat{T}_2$, are called *disconnected-clusters*. So far we have only postulated a particular form for our ground state, but we have not yet determined the amplitudes t of our different cluster operators. This will be done in the next section.

4.2.2 Coupled-Cluster Equations

In order to derive the CC equations for the cluster amplitudes, we partition the ground-state energy into a part without correlations, i.e., the energy of the reference state E_{ref}, and one part containing only the correlations. This correlation energy is called ΔE and we have

$$\Delta E = E - E_{\text{ref}}. \tag{4.46}$$

Transferring this partitioning to the eigenproblem of $\hat{H}$ gives

$$\begin{aligned} \hat{H}\,|\Psi\rangle =& E\,|\Psi\rangle && (4.47)\\ \Rightarrow \hat{H}_N\,|\Psi\rangle =& (E - E_{\text{ref}})\,|\Psi\rangle = \Delta E\,|\Psi\rangle\,, && (4.48)\end{aligned}$$

with $\hat{H}_N = (\hat{H} - E_{\text{ref}})$. Multiplying with $e^{-\hat{T}}$ yields

$$e^{-\hat{T}}\hat{H}_N\,|\Psi\rangle = e^{-\hat{T}}\hat{H}_N e^{\hat{T}}\,|\Phi\rangle \equiv \hat{\mathcal{H}}\,|\Phi\rangle = \Delta E\,|\Phi\rangle\,, \tag{4.49}$$

with the similarity-transformed Hamiltonian $\hat{\mathcal{H}}$ called the *CC effective Hamiltonian*. Two remarks are in order: First, note that $e^{-\hat{T}}e^{\hat{T}} = \hat{\mathbb{1}}$ because the $\hat{T}_i$ commute with each other due to their ph character, the reasoning for this is same as in (3.162). Second, we obviously have $-\hat{T} \neq \hat{T}^\dagger$, since $-\hat{T}$ still describes excitations while $\hat{T}^\dagger$ relates to de-excitations, and thus the transformed Hamiltonian is no longer Hermitian. If we interpret the exponential ansatz as a transformation, then with $\hat{U} = e^{\hat{T}}$ the unitary transformation leading to a new Hermitian Hamiltonian would be

$$\hat{U}^\dagger\hat{H}_N\hat{U}\,|\Phi\rangle = e^{\hat{T}^\dagger}\hat{H}_N e^{\hat{T}}\,|\Phi\rangle = \Delta E\, e^{\hat{T}^\dagger}e^{\hat{T}}\,|\Phi\rangle\,, \tag{4.50}$$

but in this case our right-hand side would be far more complex since the exponentials would not cancel, which is why the unitary ansatz will not be pursued. With $\hat{U}^{-1} = e^{-\hat{T}}$ the effective Hamiltonian $\hat{\mathcal{H}} = \hat{U}^{-1}\hat{H}_N\hat{U}$ represents a similarity transformed version of $\hat{H}_N$ with identical

eigenvalues. We note that for truncated versions of (4.49), CC does not describe a variational problem.

By use of the Baker-Campbell-Hausdorff expansion we can rewrite the effective Hamiltonian into a series of commutators:

$$e^{-\hat{T}}\hat{\mathcal{H}}e^{\hat{T}} = \sum_{n=0}^{\infty} \frac{1}{n!}[\hat{\mathcal{H}}, \hat{T}]_n, \tag{4.51}$$

$$\text{with:} \quad [\hat{\mathcal{H}}, \hat{T}]_n = [[\hat{\mathcal{H}}, \hat{T}]_{n-1}, \hat{T}], \quad [\hat{\mathcal{H}}, \hat{T}]_0 = \hat{\mathcal{H}}. \tag{4.52}$$

If the Hamiltonian is a 2B operator, the in general infinite series truncates at order $n = 4$ due to the fact that $\hat{T}$ describes only excitations.

In order to solve the CC problem, we need to determine the amplitudes of the cluster operators. This can be achieved by projecting (4.49) onto the reference state and its ph excitations:

$$\langle\Phi|\,\hat{\mathcal{H}}\,|\Phi\rangle = \Delta E \tag{4.53}$$

$$\langle\Phi_h^p|\,\hat{\mathcal{H}}\,|\Phi\rangle = 0 \tag{4.54}$$

$$\langle\Phi_{h_1h_2}^{p_1p_2}|\,\hat{\mathcal{H}}\,|\Phi\rangle = 0 \tag{4.55}$$

$$\vdots$$

Using the commutator expansion and inserting it into these relations yields a set of coupled equations for the cluster amplitudes. The evaluation of these relations is usually done within a diagrammatic formalism similar to what we introduced in section C.1 for the SRPA calculations. Details can be found in [SB09].

We also note that nothing would prevent us from constructing the "mirrored" equation of (4.49) by computing its adjoint, i.e.

$$\langle\Phi|\,e^{\hat{T}^\dagger}\hat{H}_N e^{-\hat{T}^\dagger} = \langle\Phi|\,\hat{\mathcal{H}}^\dagger = \langle\Phi|\,\Delta E \tag{4.56}$$

and performing the corresponding projections on this equation. However, due to the lack of Hermiticity, we cannot assume $\hat{\mathcal{H}}^\dagger = \hat{\mathcal{H}}$, and thus the above equation represents a separate eigenvalue problem, which formally leads to two sets of solutions. The consequences of this for CC-RPA will be discussed in section 8.4.1.

4.2.3 Coupled-Cluster Densities

If we want to determine expectation values of operators, we are faced with terms such as

$$\bar{O} = \frac{\langle\Psi|\,\hat{O}\,|\Psi\rangle}{\langle\Psi|\Psi\rangle} = \frac{\langle\Phi|\,e^{\hat{T}^\dagger}\hat{O}e^{\hat{T}}\,|\Phi\rangle}{\langle\Psi|\,e^{\hat{T}^\dagger}e^{\hat{T}}\,|\Psi\rangle}. \tag{4.57}$$

As stated before, the occurrence of $e^{\hat{T}^\dagger}$ allows for de-excitation operations that partially cancel with terms of $\hat{T}$, which leads to more complicated expressions, which do not terminate at finite order. The above equation can, however, be simplified by canceling the entire denominator with certain terms of the numerator [Číž69; SB09]. The remaining term reads

$$\Delta O = \frac{\langle\Phi|\,e^{\hat{T}^\dagger}\hat{O}_N e^{\hat{T}}\,|\Phi\rangle}{\langle\Psi|\,e^{\hat{T}^\dagger}e^{\hat{T}}\,|\Psi\rangle} = \langle\Phi|\,e^{\hat{T}^\dagger}\hat{O}_N e^{\hat{T}}\,|\Phi\rangle_{\mathrm{C}}\,, \tag{4.58}$$

where ΔO is defined analogously to ΔE as $\bar{O} = O_{\text{ref}} + \Delta O$, separating the expectation value into a reference and a correlation part. The index "C" indicates that only connected terms contribute, i.e., those with at least one contraction between $\hat{O}$ and each cluster operator. Since there can only be a limited number of connected terms, for a 2B operator no more than four, this is a tremendous simplification compared to the original form. The now finite number of terms can be translated into diagrams and evaluated accordingly. We already saw that we can use densities to evaluate expectation values of generic operators (see for example section 4.1.1), so within CC we have, e.g.,

$$\varrho_{ji}^{\text{CC}} = \langle \Phi | \, e^{\hat{T}^\dagger} \hat{a}_i^\dagger \hat{a}_j e^{\hat{T}} \, | \Phi \rangle_{\text{C}} \tag{4.59}$$

for the 1B density matrix elements. For CCSD the necessary diagrams have been evaluated in [SB09; Bin14].

4.3 Coupled-Cluster RPA

As the first beyond-HF RPA method we will now discuss the CC-RPA. In past applications of standard RPA, the EOM derivation of the RPA equations was exact up to the point of the evaluation of commutator expressions in RPA expectation values. At this stage the QBA is introduced and the exact, correlated RPA ground state is replaced, in these circumstances, with the uncorrelated HF ground state (cf. section 3.2.4). This QBA has been a source of inconsistency and instability since the beginning of the RPA theory. Within CC-RPA, we evaluate all expectation values, without any truncations, in a completely general correlated state. Since everything is evaluated in expectation values, all we need for the RPA description of an arbitrary ground state are its corresponding density matrices. Thanks to the commutators in our RPA formula, the operator rank of all expressions does not exceed the 2B level (for given 2B Hamiltonian), and for any ground state to be described the knowledge of its 1B and 2B ground-state density (GSD) matrices suffices. We stress that neither 3B RPA nor 2B SRPA can be described this way, since the former would require 3B GSDs and the latter even 3B and 4B GSDs.

A few comments are in order: First, our derivations will not be limited to the CC case. We, therefore, also refer to this framework as "Density-RPA" (D-RPA), since in principle any ground state with 1B and 2B density matrices can be used as input. It should be noted that the terminology of Density-RPA is not be confused with density-functional approaches to RPA [GGC10; GGC11]. Second, the extension of standard RPA to D-RPA is not an abandonment of the QBA. By performing the above generalization, the true RPA ground state as in (3.105) is still not known prior to a calculation. Hence, despite being built on a correlated ground state, D-RPA is still inconsistent and could, in principle, yield unstable solutions. Third, although having correlations in our reference state, we will stick to the rigid, disjoint partitioning of the model space into particle and hole states as given by HF. Conceptionally, the existence of correlations would warrant deserting the particle-hole character altogether within CC-RPA. The excitation operators would then change from $\hat{\mathcal{A}}^\dagger_{ph}$ to $\hat{\mathcal{A}}^\dagger_{ij}$ with indices running over the entire model space. Maintaining the ph partitioning reduces both the formalistic as well as the computational effort. We will revisit this issue in more detail during the discussion of the results in section 8.4.1.

For the derivation of D-RPA we can skip the first few steps in the EOM approach. Up to the point where we apply the QBA, nothing changes. We start with the same set of equations as before (cf. (3.62) and (3.63)):

$$\langle \mathrm{RPA}| [\hat{\mathcal{A}}_{\bar{p}'\bar{h}'}, [\hat{H}, \hat{Q}^\dagger_\omega]] |\mathrm{RPA}\rangle = E^{\mathrm{RPA}}_\omega \langle \mathrm{RPA}| [\hat{\mathcal{A}}_{\bar{p}'\bar{h}'}, \hat{Q}^\dagger_\omega] |\mathrm{RPA}\rangle , \tag{4.60}$$

$$\langle \mathrm{RPA}| [\hat{\bar{\mathcal{A}}}^\dagger_{\bar{p}'\bar{h}'}, [\hat{H}, \hat{Q}^\dagger_\omega]] |\mathrm{RPA}\rangle = E^{\mathrm{RPA}}_\omega \langle \mathrm{RPA}| [\hat{\bar{\mathcal{A}}}^\dagger_{\bar{p}'\bar{h}'}, \hat{Q}^\dagger_\omega] |\mathrm{RPA}\rangle . \tag{4.61}$$

In the following sections, we will calculate the individual terms of the above equations step-by-step, check their consistency with the already known HF relations, and look into their symmetry properties.

4.3.1 Norm-Matrix

We start by looking at the right-hand side of the first equation:

$$\begin{aligned} E^{\mathrm{RPA}}_\omega \langle \mathrm{RPA}| [\hat{\mathcal{A}}_{\bar{p}'\bar{h}'}, \hat{Q}^\dagger_\omega] |\mathrm{RPA}\rangle = E^{\mathrm{RPA}}_\omega \Big(& \langle \mathrm{RPA}| [\hat{\mathcal{A}}_{\bar{p}'\bar{h}'}, \hat{\mathcal{A}}^\dagger{}_{\bar{p}\bar{h}}] |\mathrm{RPA}\rangle X^\omega_{\bar{p}\bar{h}} \\ & - \langle \mathrm{RPA}| [\hat{\mathcal{A}}_{\bar{p}'\bar{h}'}, \hat{\bar{\mathcal{A}}}_{\bar{p}\bar{h}}] |\mathrm{RPA}\rangle Y^\omega_{\bar{p}\bar{h}} \Big). \end{aligned} \tag{4.62}$$

Let us first look at the second term. In standard RPA, this term vanished, cf. (3.78). This time we calculate the commutator directly, without the surrounding expectation value, i.e.

$$\begin{aligned}[\hat{\mathcal{A}}_{\bar{p}'\bar{h}'}, \hat{\tilde{\mathcal{A}}}_{\bar{p}\bar{h}}] = &\sum_{m_{p'},m_{h'}} (-1)^{j_{h'}-m_{h'}}\, C(j_{p'}m_{p'}, j_{h'}\text{-}m_{h'}|J0) \\ &\times \sum_{m_p,m_h} (-1)^{j_p-m_p}\, C(j_p\text{-}m_p, j_h m_h|J0) \\ &\times [\hat{\mathcal{A}}_{p'h'}, \hat{\mathcal{A}}_{ph}]. \end{aligned} \tag{4.63}$$

In the following we will compute the uncoupled operators which is the only crucial component concerning the commutator. For the relevant cases the coupling will be taken into account explicitly, see below. The double commutator can be expanded into

$$[\hat{\mathcal{A}}_{p'h'}, \hat{\mathcal{A}}_{ph}] = [\hat{a}^\dagger_{h'}\hat{a}_{p'}, \hat{a}^\dagger_h\hat{a}_p] \tag{4.64}$$

$$= \hat{a}^\dagger_{h'}\{\hat{a}_{p'}, \hat{a}^\dagger_h\}\hat{a}_p - \hat{a}^\dagger_{h'}\hat{a}^\dagger_h\{\hat{a}_{p'}, \hat{a}_p\} + \{\hat{a}^\dagger_{h'}, \hat{a}^\dagger_h\}\hat{a}_p\hat{a}_{p'} - \hat{a}^\dagger_h\{\hat{a}^\dagger_{h'}, \hat{a}_p\}\hat{a}_{p'}\,, \tag{4.65}$$

where the second and third term vanish, since the anti-commutator of either two creators or two annihilators is zero, giving

$$[\hat{\mathcal{A}}_{p'h'}, \hat{\mathcal{A}}_{ph}] = \hat{a}^\dagger_{h'}\{\hat{a}_{p'}, \hat{a}^\dagger_h\}\hat{a}_p - \hat{a}^\dagger_h\{\hat{a}^\dagger_{h'}, \hat{a}_p\}\hat{a}_{p'} \tag{4.66}$$

$$= \hat{a}^\dagger_{h'}\,\delta_{p',h}\,\hat{a}_p - \hat{a}^\dagger_h\,\delta_{h',p}\,\hat{a}_{p'} \equiv 0. \tag{4.67}$$

The above turns out to be identically zero due to the disjointness of particle and holes, as mentioned at the beginning of our CC-RPA discussion. The expectation value, be it HF or any other state, will not change that. Neither will coupling terms as in (4.63), so we automatically have $[\hat{\mathcal{A}}_{\bar{p}'\bar{h}'}, \hat{\tilde{\mathcal{A}}}_{\bar{p}\bar{h}}] = 0$. Likewise, we can show that

$$[\hat{\mathcal{A}}^\dagger_{p'h'}, \hat{\mathcal{A}}^\dagger_{ph}] \equiv 0 \tag{4.68}$$

by simply taking the adjoint of the entire first equation. Keep in mind that, in these cases, it does not matter if we take the commutator of the spherical version $\tilde{\mathcal{A}}$ of $\mathcal{A}$. We already know that the relation between the "tilde" and "non-tilde" ph-operators is

$$\hat{\tilde{\mathcal{A}}}_{\bar{p}\bar{h}}(J0) = (-1)^J \hat{\mathcal{A}}_{\bar{p}\bar{h}}(J0), \tag{4.69}$$

and we see that the above relations still hold in both cases (spherical and non-spherical). We also note that adding the corresponding terms for the coupling would trigger no significant changes since the anti-commutators responsible for the above result would still yield zero. The right-hand sides of (4.60) and (4.61) now read

$$E^{\mathrm{RPA}}_\omega \langle \mathrm{RPA}| [\hat{\mathcal{A}}_{\bar{p}'\bar{h}'}, \hat{Q}^\dagger_\omega] |\mathrm{RPA}\rangle = E^{\mathrm{RPA}}_\omega \langle \mathrm{RPA}| [\hat{\mathcal{A}}_{\bar{p}'\bar{h}'}, \hat{\mathcal{A}}^\dagger{}_{\bar{p}\bar{h}}] |\mathrm{RPA}\rangle\, X^\omega_{\bar{p}\bar{h}}, \tag{4.70}$$

$$E^{\mathrm{RPA}}_\omega \langle \mathrm{RPA}| [\hat{\tilde{\mathcal{A}}}^\dagger_{\bar{p}'\bar{h}'}, \hat{Q}^\dagger_\omega] |\mathrm{RPA}\rangle = -E^{\mathrm{RPA}}_\omega \langle \mathrm{RPA}| [\hat{\tilde{\mathcal{A}}}^\dagger_{\bar{p}'\bar{h}'}, \hat{\tilde{\mathcal{A}}}_{\bar{p}\bar{h}}] |\mathrm{RPA}\rangle\, Y^\omega_{\bar{p}\bar{h}}. \tag{4.71}$$

For the combination of a ph-creator and a ph-annihilator, this time taking into account the coupling, we get (using the short-hand matrix indices introduced before)

$$
\begin{aligned}
[\hat{\mathcal{A}}_{\bar{j}}, \hat{\mathcal{A}}_{\bar{i}}^\dagger] =& [\hat{\mathcal{A}}_{\bar{p}'\bar{h}'}(J0), \hat{\mathcal{A}}^\dagger{}_{\bar{p}\bar{h}}(J0)] && (4.72)\\
=& \sum_{\substack{m_p' \\ m_p}} (-1)^{j_{h'}-m_{p'}} (-1)^{j_h-m_p}\, C(j_{p'}m_{p'}, j_{h'}\text{-}m_{p'}|J0) C(j_p m_p, j_h\text{-}m_p|J0) \\
& \times [\hat{a}^\dagger_{\bar{h}',m_{p'}} \hat{a}_{\bar{p}',m_{p'}}, \hat{a}^\dagger_{\bar{p},m_p} \hat{a}_{\bar{h},m_p}]. && (4.73)\\
=& (-1)^{j_{h'}+j_h} \sum_{\substack{m_p' \\ m_p}} (-1)^{-m_{p'}-m_p}\, C(j_{p'}m_{p'}, j_{h'}\text{-}m_{p'}|J0) C(j_p m_p, j_h\text{-}m_p|J0) \\
& \times [\hat{a}^\dagger_{\bar{h}',m_{p'}} \hat{a}_{\bar{p}',m_{p'}}, \hat{a}^\dagger_{\bar{p},m_p} \hat{a}_{\bar{h},m_p}]. && (4.74)\\
=& (-1)^{j_{h'}+j_h+1} \sum_{m_p} C(j_{p'}m_p, j_{h'}\text{-}m_p|J0) C(j_p m_p, j_h\text{-}m_p|J0) \\
& \times (\delta_{\bar{p}\bar{p}'}\, \hat{a}^\dagger_{\bar{h}'} \hat{a}_{\bar{h}} - \delta_{\bar{h}\bar{h}'}\, \hat{a}^\dagger_{\bar{p}} \hat{a}_{\bar{p}'}). && (4.75)
\end{aligned}
$$

Taking the expectation value of the above yields

$$
\begin{aligned}
N^{\mathrm{X}}_{\bar{j}\bar{i}} \equiv& \langle \mathrm{RPA}| [\hat{\mathcal{A}}_{\bar{j}}, \hat{\mathcal{A}}^\dagger_{\bar{i}}] |\mathrm{RPA}\rangle , && (4.76)\\
=& (-1)^{j_{h'}+j_h+1} \sum_{m_p} C(j_{p'}m_p, j_{h'}\text{-}m_p|J0) C(j_p m_p, j_h\text{-}m_p|J0) \\
& \times (\delta_{\bar{p}\bar{p}'} \langle \mathrm{RPA}| \hat{a}^\dagger_{\bar{h}'} \hat{a}_{\bar{h}} |\mathrm{RPA}\rangle - \delta_{\bar{h}\bar{h}'} \langle \mathrm{RPA}| \hat{a}^\dagger_{\bar{p}} \hat{a}_{\bar{p}'} |\mathrm{RPA}\rangle) && (4.77)\\
=& (-1)^{j_{h'}+j_h+1} \sum_{m_p} C(j_{p'}m_p, j_{h'}\text{-}m_p|J0) C(j_p m_p, j_h\text{-}m_p|J0) \\
& \times (\delta_{\bar{p}\bar{p}'}\, \varrho_{\bar{h}\bar{h}'} - \delta_{\bar{h}\bar{h}'} \varrho_{\bar{p}'\bar{p}}), && (4.78)
\end{aligned}
$$

where we named this term as matrix N^{X} (with corresponding matrix elements), the reason being that it will occur on the right-hand side and simply "scale" or *normalize* the X-amplitudes, acting as a sort of metric. In standard RPA this term was equal to the identity matrix (i.e. δ_{ij}). Assuming the density is the 1B HF density, we find that

$$
\begin{aligned}
N^{\mathrm{X}}_{\bar{j}\bar{i}} =& (\delta_{\bar{p}\bar{p}'}\, \varrho_{\bar{h}\bar{h}'} - \delta_{\bar{h}\bar{h}'} \varrho_{\bar{p}'\bar{p}}) && (4.79)\\
=& (\delta_{\bar{p}\bar{p}'}\, \delta_{\bar{h}\bar{h}'} - 0) && (4.80)\\
=& \delta_{\bar{i}\bar{j}}. && (4.81)
\end{aligned}
$$

The standard RPA equation, therefore, is the HF special case of the general D-RPA version, as it should be.

Let us take a look at the symmetry properties of the norm-matrix N^{X}. Applying some basic relations to a matrix element of the norm-matrix quickly reveals that this matrix is Hermitian:

$$
\begin{aligned}
N^{\mathrm{X}}_{ij} =& \langle \mathrm{RPA}| [\hat{\mathcal{A}}_i, \hat{\mathcal{A}}^\dagger_j] |\mathrm{RPA}\rangle , && (4.82)\\
=& \langle \mathrm{RPA}| [\hat{\mathcal{A}}_i, \hat{\mathcal{A}}^\dagger_j]^\dagger |\mathrm{RPA}\rangle^* && (4.83)\\
=& \langle \mathrm{RPA}| [\hat{\mathcal{A}}_j, \hat{\mathcal{A}}^\dagger_i] |\mathrm{RPA}\rangle^* && (4.84)\\
=& N^{\mathrm{X}*}_{ji} && (4.85)
\end{aligned}
$$

which already gives us $N^{\mathrm{X}} = N^{\mathrm{X}\dagger}$.

The right-hand term of the second equation is $N^{\mathrm{Y}}_{\bar{j}\bar{i}} \equiv \langle \mathrm{RPA} | \, [\hat{\tilde{\mathcal{A}}}^\dagger_{\bar{p}'\bar{h}'}, \hat{\tilde{\mathcal{A}}}_{\bar{p}\bar{h}}] \, | \mathrm{RPA} \rangle$, which is actually almost identical to the one we just discussed. We just have to express the $\hat{\tilde{\mathcal{A}}}$ in their non-spherical versions and use the Hermiticity we just showed. We then get

$$\begin{aligned} N^{\mathrm{Y}}_{\bar{j}\bar{i}} = \langle \mathrm{RPA} | \, [\hat{\tilde{\mathcal{A}}}^\dagger_{\bar{j}}, \hat{\tilde{\mathcal{A}}}_{\bar{i}}] \, | \mathrm{RPA} \rangle &= (-1)^{2J} \langle \mathrm{RPA} | \, [\hat{\mathcal{A}}^\dagger_{\bar{j}}, \hat{\mathcal{A}}_{\bar{i}}] \, | \mathrm{RPA} \rangle && (4.86) \\ &= \langle \mathrm{RPA} | \, [\hat{\mathcal{A}}^\dagger_{\bar{j}}, \hat{\mathcal{A}}_{\bar{i}}] \, | \mathrm{RPA} \rangle && (4.87) \\ &= \langle \mathrm{RPA} | \, [\hat{\mathcal{A}}^\dagger_{\bar{j}}, \hat{\mathcal{A}}_{\bar{i}}]^\dagger \, | \mathrm{RPA} \rangle^* && (4.88) \\ &= \langle \mathrm{RPA} | \, [\hat{\mathcal{A}}^\dagger_{\bar{i}}, \hat{\mathcal{A}}_{\bar{j}}] \, | \mathrm{RPA} \rangle^* && (4.89) \\ &= - \langle \mathrm{RPA} | \, [\hat{\mathcal{A}}_{\bar{j}}, \hat{\mathcal{A}}^\dagger_{\bar{i}}] \, | \mathrm{RPA} \rangle^* && (4.90) \\ &= - N^{\mathrm{X}*}_{\bar{i}\bar{j}} && (4.91) \\ &= - N^{\mathrm{X}}_{\bar{j}\bar{i}}. && (4.92) \end{aligned}$$

In other words, we find that for these two norm-matrices we have $N \equiv N^{\mathrm{X}} = -N^{\mathrm{Y}}$. The entire right-hand side of (4.60) and (4.61), in matrix notation, thus reads

$$\ldots = E^{\mathrm{RPA}}_\omega \begin{pmatrix} N & 0 \\ 0 & N \end{pmatrix} \begin{pmatrix} X^\omega \\ Y^\omega \end{pmatrix}. \tag{4.93}$$

Mind that $N^{\mathrm{X}} = -N^{\mathrm{Y}}$, but the term N^{Y} appears with a sign in (4.71), so the N in the second row carries no sign.

4.3.2 D-RPA Equations

We now investigate the left-hand sides of (4.60) and (4.61). To make things more tractable, again we use the matrix-notation with collective-indices. Expanding $\hat{Q}^\dagger_\omega$, together with the results for the right-hand side, gives

$$\underbrace{\langle \mathrm{RPA} | \, [\hat{\mathcal{A}}_j, [\hat{H}, \hat{\mathcal{A}}^\dagger_i]] \, | \mathrm{RPA} \rangle}_{A_{ji}} X^\omega_i - \underbrace{\langle \mathrm{RPA} | \, [\hat{\mathcal{A}}_j, [\hat{H}, \hat{\tilde{\mathcal{A}}}_i]] \, | \mathrm{RPA} \rangle}_{-B_{ji}} Y^\omega_i = E^{\mathrm{RPA}}_\omega N_{ji} X^\omega_i, \tag{4.94}$$

$$\underbrace{\langle \mathrm{RPA} | \, [\hat{\tilde{\mathcal{A}}}^\dagger_j, [\hat{H}, \hat{\mathcal{A}}^\dagger_i]] \, | \mathrm{RPA} \rangle}_{-B'_{ji}} X^\omega_i - \underbrace{\langle \mathrm{RPA} | \, [\hat{\tilde{\mathcal{A}}}^\dagger_j, [\hat{H}, \hat{\tilde{\mathcal{A}}}_i]] \, | \mathrm{RPA} \rangle}_{A'_{ji}} Y^\omega_i = -E^{\mathrm{RPA}}_\omega N_{ji} Y^\omega_i. \tag{4.95}$$

Here we introduced similar submatrices as in (3.89) and (3.90), see also below:

$$\begin{aligned} A_{ji} &\equiv \langle \mathrm{RPA} | \, [\hat{\mathcal{A}}_j, [\hat{H}, \hat{\mathcal{A}}^\dagger_i]] \, | \mathrm{RPA} \rangle \, , && (4.96) \\ B_{ji} &\equiv - \langle \mathrm{RPA} | \, [\hat{\mathcal{A}}_j, [\hat{H}, \hat{\tilde{\mathcal{A}}}_i]] \, | \mathrm{RPA} \rangle \, , && (4.97) \\ A'_{ji} &\equiv \langle \mathrm{RPA} | \, [\hat{\tilde{\mathcal{A}}}^\dagger_j, [\hat{H}, \hat{\tilde{\mathcal{A}}}_i]] \, | \mathrm{RPA} \rangle \, , && (4.98) \\ B'_{ji} &\equiv - \langle \mathrm{RPA} | \, [\hat{\tilde{\mathcal{A}}}^\dagger_j, [\hat{H}, \hat{\mathcal{A}}^\dagger_i]] \, | \mathrm{RPA} \rangle \, . && (4.99) \end{aligned}$$

Using basic matrix-element relations, we can show that A' is the complex conjugate of the unprimed matrix, i.e. $A' = A^*$. Likewise, we can show that $B' = B^\dagger$. The matrix equation now reads

$$\begin{pmatrix} A & B \\ -B^\dagger & -A^* \end{pmatrix} \begin{pmatrix} X^\omega \\ Y^\omega \end{pmatrix} = E^{\mathrm{RPA}}_\omega \begin{pmatrix} N & 0 \\ 0 & N \end{pmatrix} \begin{pmatrix} X^\omega \\ Y^\omega \end{pmatrix}. \tag{4.100}$$

Before we start the actual computation of these submatrices, we will first look into their symmetry properties.

4.3.3 Symmetry of the A Matrix

In standard RPA, the matrix A is Hermitian and the matrix B is symmetric. It is important to keep in mind that these properties hold only for those "standard" matrices, i.e. the operators evaluated in the HF state, but not the operators themselves. The symmetry properties of the matrices A and B evaluated within an arbitrary ground state will have to be reexamined. We start with the definition of the A matrix as given in (4.96) and use the basic relation for its Hermitian conjugate

$$\begin{aligned} A_{i,j} &\equiv \langle \mathrm{RPA} | \, [\hat{\mathcal{A}}_i, [\hat{H}, \hat{\mathcal{A}}_j^\dagger]] \, | \mathrm{RPA} \rangle && (4.101) \\ &= \langle \mathrm{RPA} | \, [\hat{\mathcal{A}}_i, [\hat{H}, \hat{\mathcal{A}}_j^\dagger]]^\dagger \, | \mathrm{RPA} \rangle^* && (4.102) \\ &= \langle \mathrm{RPA} | \, [[\hat{H}, \hat{\mathcal{A}}_j^\dagger]^\dagger, \hat{\mathcal{A}}_i^\dagger] \, | \mathrm{RPA} \rangle^* && (4.103) \\ &= \langle \mathrm{RPA} | \, [[\hat{\mathcal{A}}_j, \hat{H}], \hat{\mathcal{A}}_i^\dagger] \, | \mathrm{RPA} \rangle^* . && (4.104) \end{aligned}$$

At this point we can reorder the (inner) commutator using the relation

$$[A, [B, C]] + [B, [C, A]] + [C, [A, B]] = 0. \tag{4.105}$$

This leads us to

$$\begin{aligned} A_{i,j} =& \langle \mathrm{RPA} | \, [\hat{\mathcal{A}}_j, [\hat{H}, \hat{\mathcal{A}}_i^\dagger]] \, | \mathrm{RPA} \rangle^* + \langle \mathrm{RPA} | \, [[\hat{\mathcal{A}}_j, \hat{\mathcal{A}}_i^\dagger], \hat{H}] \, | \mathrm{RPA} \rangle^* && (4.106) \\ =& A_{j,i}^* + \langle \mathrm{RPA} | \, [[\hat{\mathcal{A}}_j, \hat{\mathcal{A}}_i^\dagger], \hat{H}] \, | \mathrm{RPA} \rangle^* . && (4.107) \end{aligned}$$

We, therefore, see that the matrix A is not equal to its Hermitian conjugate, i.e. is non-Hermitian in the most general case. The matrix A would only be Hermitian if the second term in the above equation was zero. Let us assume the state in which we evaluate the expectation value is an eigenstate of the Hamiltonian $\hat{H}$, e.g. the ground state, we would then get the corresponding eigenrelation, i.e.

$$\hat{H} \, | \Psi \rangle = E_0 \, | \Psi \rangle . \tag{4.108}$$

Expanding the outer commutator we would get the above from the first term of the outer commutator and again the same (carrying a minus) from the second term of the commutator. These terms will then cancel as follows

$$\begin{aligned} A_{i,j} =& A_{j,i}^* + \langle \mathrm{RPA} | \, [[\hat{\mathcal{A}}_j, \hat{\mathcal{A}}_i^\dagger], \hat{H}] \, | \mathrm{RPA} \rangle^* && (4.109) \\ =& A_{j,i}^* + \langle \mathrm{RPA} | \, [\hat{\mathcal{A}}_j, \hat{\mathcal{A}}_i^\dagger] \hat{H} \, | \mathrm{RPA} \rangle^* - \langle \mathrm{RPA} | \, \hat{H} [\hat{\mathcal{A}}_j, \hat{\mathcal{A}}_i^\dagger] \, | \mathrm{RPA} \rangle^* && (4.110) \\ =& A_{j,i}^* + \langle \mathrm{RPA} | \, [\hat{\mathcal{A}}_j, \hat{\mathcal{A}}_i^\dagger] \, | \mathrm{RPA} \rangle^* E_0 - E_0 \langle \mathrm{RPA} | \, [\hat{\mathcal{A}}_j, \hat{\mathcal{A}}_i^\dagger] \, | \mathrm{RPA} \rangle^* && (4.111) \\ =& A_{j,i}^*, && (4.112) \end{aligned}$$

and we see that A is, in this case, indeed Hermitian. Since we plan to employ CC GSDs, we cannot assume, per se, that the state described by the GSD (the ϱ-state) is indeed an eigenstate of $\hat{H}$. While the lack of a guaranteed Hermiticity is inconvenient in that we have to compute all matrix elements instead of just one triangle, we stress that this poses no conceptional problem. The entire A-matrix, without truncation of the Hermiticity-breaking terms, can and will be computed in our calculations. Additionally, since the structure of the RPA supermatrix has non-Hermitian character even in HF-RPA (cf. (3.98)), a non-Hermitian A-matrix does not even change the nature of the RPA eigenvalue problem. Nevertheless, we will revisit the issue of symmetry on a numerical basis in section 8.4.1.

Fallback to HF

Again, we want to crosscheck our results with the known ones for the standard RPA case, as we already did for the norm-matrix N. If our ground state was the HF state, we would get

$$A_{i,j} = A^*_{j,i} + \langle \mathrm{HF}| \left[[\hat{\mathcal{A}}_j, \hat{\mathcal{A}}^\dagger_i], \hat{H}\right] |\mathrm{HF}\rangle^* . \tag{4.113}$$

The above argument regarding symmetry does not apply, since the HF state is no eigenstate of the complete Hamiltonian. In this sense, we only know that the HF single-particle states are eigenstates of the 1B mean-field Hamiltonian.

Using our results for the expression $[\hat{\mathcal{A}}_j, \hat{\mathcal{A}}^\dagger_i]$ from section 4.3.1 we can simplify the above further to

$$\langle \mathrm{HF}| \left[[\hat{\mathcal{A}}_j, \hat{\mathcal{A}}^\dagger_i], \hat{H}\right] |\mathrm{HF}\rangle = \delta_{pp'} \langle \mathrm{HF}| \left[\hat{a}^\dagger_{h'} \hat{a}_h, \hat{H}\right] |\mathrm{HF}\rangle - \delta_{hh'} \langle \mathrm{HF}| \left[\hat{a}^\dagger_p \hat{a}_{p'}, \hat{H}\right] |\mathrm{HF}\rangle . \tag{4.114}$$

The second term vanishes in any case due to the particle operators ($\hat{a}_{p'}$ acting on $|\mathrm{HF}\rangle$ to the right, and $\hat{a}^\dagger_p$ to the left). For the first term, the operators $\hat{a}^\dagger_{h'}\hat{a}_h$ can only yield non-zeroes in the case that $h = h'$. If this is the case, we are left with the hole number operator which yields 1 and the commutator $[1, \hat{H}]$ thus vanishes. Both terms vanish in the HF case, yielding

$$A_{i,j} = A^*_{j,i} + 0, \tag{4.115}$$

and we see that A is Hermitian, consistent with the relation from standard RPA.

4.3.4 Symmetry of the B Matrix

For the A matrix (see above) we had to "swap" the index on the ph-creator with the ones on the ph-annihilator in order to arrive at a symmetry relation for this matrix. This is not necessary for the B matrix since we have two ph-annihilators. We can directly rearrange the nested commutators as we did for the A matrix, using the same relation

$$\begin{aligned}
B_{ij} =& - \langle \mathrm{RPA}| \left[\hat{\mathcal{A}}_j, \left[\hat{H}, \hat{\tilde{\mathcal{A}}}_i\right]\right] |\mathrm{RPA}\rangle && (4.116)\\
=& (-1)^{J+1} \langle \mathrm{RPA}| \left[\hat{\mathcal{A}}_i, \left[\hat{H}, \hat{\mathcal{A}}_j\right]\right] |\mathrm{RPA}\rangle , && (4.117)\\
=& (-1)^{J+1} (\langle \mathrm{RPA}| \left[\hat{\mathcal{A}}_j, \left[\hat{H}, \hat{\mathcal{A}}_i\right]\right] |\mathrm{RPA}\rangle - \langle \mathrm{RPA}| \left[\hat{H}, \left[\hat{\mathcal{A}}_j, \hat{\mathcal{A}}_i\right]\right] |\mathrm{RPA}\rangle) && (4.118)\\
=& (-1)^{J+1} \langle \mathrm{RPA}| \left[\hat{\mathcal{A}}_j, \left[\hat{H}, \hat{\mathcal{A}}_i\right]\right] |\mathrm{RPA}\rangle && (4.119)\\
=& B_{ji}. && (4.120)
\end{aligned}$$

The second term in the second line vanishes independently of the state that is used since, as an operator relation, the commutator of two ph-annihilators is zero (compare section 4.3.1). For the A matrix the symmetry properties were not universal but rather depended on the state used for the evaluation of the density matrices. We saw that A is Hermitian whenever the ϱ-state is an eigenstate of the Hamiltonian. For the B matrix, no such distinction is necessary. With this, the B matrix is symmetric just as it is for the case of standard RPA. We note that in total the following relation holds: $B' = B^\dagger = B^*$

4.3.5 Derivation of the A Matrix

We will now derive the terms for the A matrix. In order to make this calculation more tractable we will omit the coupling to a spherical tensor operator. All calculation will be given within the

m-scheme and an explicit coupling of the form

$$A_{i,j} \equiv [\hat{\mathcal{A}}_{\bar{p}'\bar{h}'}, [\hat{H}, \hat{\mathcal{A}}^\dagger_{\bar{p}\bar{h}}]], \tag{4.121}$$

$$= (-1)^{j_h+j_{h'}} \sum_{m,m'} (-1)^{\text{-}m_h\text{-}m_{h'}} C(j_{p'}m', j_{h'}\text{-}m'|J0) C(j_p m, j_h\text{-}m|J0) \tag{4.122}$$

$$\times [\hat{a}^\dagger_{h',m'}\hat{a}_{p',m'}, [\hat{H}, \hat{a}^\dagger_{p,m}\hat{a}_{h,m}]] \tag{4.123}$$

can be applied afterwards. Additionally, we will split the 2B Hamiltonian into a 1B and a 2B part. The former will be denoted as $\hat{T}$ and the later one as $\hat{V}$, owed to the usual form of the 2B Hamiltonian. In case of normal-ordering the 1B and 2B parts of the 3B force can, of course, be dealt with in a completely analogous manner, should one wish to compute these contributions separately. If this is not the case, these could alternatively be added to $\hat{T}$ and $\hat{V}$ silently.

1B Part of A

We will start with the inner commutator for the 1B part. With the help of known commutator relations, this can be evaluated relatively straightforward. Inserting the 1B operator T leads us to the following:

$$[\hat{T}, \hat{a}^\dagger_p\hat{a}_h] = \sum_{i,i'} t_{i,i'} [\hat{a}^\dagger_i\hat{a}_{i'}, \hat{a}^\dagger_p\hat{a}_h]. \tag{4.124}$$

As a brief reminder we state the known commutator relation

$$[AB, CD] = A\{B, C\}D - AC\{B, D\} + \{A, C\}DB - C\{A, D\}B \tag{4.125}$$

and apply this to our creator-annihilator scheme ($\hat{a}^\dagger_1\hat{a}_2$)

$$[\hat{a}^\dagger_1\hat{a}_2, \hat{a}^\dagger_3\hat{a}_4] = \hat{a}^\dagger_1\{\hat{a}_2, \hat{a}^\dagger_3\}\hat{a}_4 - \hat{a}^\dagger_1\hat{a}^\dagger_3\{\hat{a}_2, \hat{a}_4\} + \{\hat{a}^\dagger_1, \hat{a}^\dagger_3\}\hat{a}_4\hat{a}_2 - \hat{a}^\dagger_3\{\hat{a}^\dagger_1, \hat{a}_4\}\hat{a}_2 \tag{4.126}$$

$$= \hat{a}^\dagger_1\{\hat{a}_2, \hat{a}^\dagger_3\}\hat{a}_4 - \hat{a}^\dagger_3\{\hat{a}^\dagger_1, \hat{a}_4\}\hat{a}_2 \tag{4.127}$$

$$= \delta_{2,3}\,\hat{a}^\dagger_1\hat{a}_4 - \delta_{1,4}\,\hat{a}^\dagger_3\hat{a}_2. \tag{4.128}$$

We used the fact the the anti-commutator of two annihilators or two creators, respectively, yields zero for all index combinations. With this, we get

$$[\hat{T}, \hat{a}^\dagger_p\hat{a}_h] = \sum_{i,i'} t_{i,i'} [\hat{a}^\dagger_i\hat{a}_{i'}, \hat{a}^\dagger_p\hat{a}_h] \tag{4.129}$$

$$= \sum_i \left(t_{i,p}\,\hat{a}^\dagger_i\hat{a}_h - t_{h,i}\,\hat{a}^\dagger_p\hat{a}_i \right). \tag{4.130}$$

Now we have to insert this intermediate result into the outer commutator. Again we can apply the above commutator relation and end up with the following

$$[\hat{a}^\dagger_{h'}\hat{a}_{p'}, [\hat{T}, \hat{a}^\dagger_p\hat{a}_h]] = \sum_i \left(t_{i,p}\,[\hat{a}^\dagger_{h'}\hat{a}_{p'}, \hat{a}^\dagger_i\hat{a}_h] - t_{h,i}\,[\hat{a}^\dagger_{h'}\hat{a}_{p'}, \hat{a}^\dagger_p\hat{a}_i] \right) \tag{4.131}$$

$$= \sum_i \Big(t_{i,p}\,(\delta_{p',i}\hat{a}^\dagger_{h'}\hat{a}_h - \delta_{h',h}\hat{a}^\dagger_i\hat{a}_{p'}) - t_{h,i}\,(\delta_{p,p'}\hat{a}^\dagger_{h'}\hat{a}_i - \delta_{i,h'}\hat{a}^\dagger_p\hat{a}_{p'}) \Big) \tag{4.132}$$

$$= -\sum_i (\delta_{h,h'} t_{i,p}\,\hat{a}^\dagger_i\hat{a}_{p'} + \delta_{p,p'} t_{i,h}\,\hat{a}^\dagger_{h'}\hat{a}_i) + t_{p,p'}\,\hat{a}^\dagger_{h'}\hat{a}_h + t_{h,h'}\hat{a}^\dagger_p\hat{a}_{p'}. \tag{4.133}$$

In the last step above we reordered the terms depending on whether the summation remains or not. Since all commutators have been evaluated, we now need to take the expectation value of this expression, introducing the 1B density matrix:

$$\begin{aligned}\langle \mathrm{RPA}| \, [\hat{a}^\dagger_{h'} \hat{a}_{p'}, [\hat{T}, \hat{a}^\dagger_p \hat{a}_h]] \, |\mathrm{RPA}\rangle = &- \sum_i (\delta_{h,h'} t_{i,p} \, \varrho_{i,p'} + \delta_{p,p'} t_{i,h} \, \varrho_{h',i}) \\ &+ t_{p,p'} \, \varrho_{h',h} + t_{h,h'} \varrho_{p,p'}. \end{aligned} \tag{4.134}$$

The above result can be simplified a little further by inspecting the sum terms. For the first one we get

$$\sum_i t_{i,p} \, \varrho_{i,p'} = \sum_i t_{p,i} \, \varrho_{i,p'} = (T\varrho)_{p,p'}. \tag{4.135}$$

We see that those can be written as the matrix product of T with ϱ. We stress that while the matrices of T and ϱ are symmetric, the matrix product $(T\varrho)$ is not symmetric in the most general case. Symmetry of the matrix product requires the individual matrices to commute.

Applying the above to our RPA equation for $\hat{T}$ yields:

$$\boxed{\langle \mathrm{RPA}| \, [\hat{a}^\dagger_{h'} \hat{a}_{p'}, [\hat{T}, \hat{a}^\dagger_p \hat{a}_h]] \, |\mathrm{RPA}\rangle = -\delta_{h,h'} (T\varrho)_{p,p'} - \delta_{p,p'} (T\varrho)_{h,h'} + t_{p,p'} \, \varrho_{h',h} + t_{h,h'} \varrho_{p,p'}.} \tag{4.136}$$

Fallback to HF

In the above section we derived the density-based RPA equations for the 1B part of the Hamiltonian. We will now briefly assume this generic GSD to be the HF density, serving as a crosscheck to validate the consistency of our derivation. Similar considerations will be used for the rest of our formalism. We know that the HF 1B density can be viewed as projector onto the space spanned by the hole states (cf. section 4.1.3). We can, therefore, regard the matrix product of T with ϱ as

$$(T\varrho) = T^{\mathrm{hh}}, \tag{4.137}$$

where we used the same notation for the block structure as in (4.28). With that in mind, it is clear that both $(T\varrho)_{p,p'}$ and $\varrho_{p,p'}$ vanish. We are thus left with

$$\langle \mathrm{HF}| \, [\hat{a}^\dagger_{h'} \hat{a}_{p'}, [\hat{T}, \hat{a}^\dagger_p \hat{a}_h]] \, |\mathrm{HF}\rangle = -\delta_{p,p'} (T\varrho)_{h,h'} + t_{p,p'} \, \varrho_{h',h} \tag{4.138}$$

$$= \delta_{h',h} \, t_{p,p'} - \delta_{p,p'} \, t_{h,h'}, \tag{4.139}$$

which is exactly the contribution that the 1B part of the Hamiltonian yields within standard RPA (cf. (3.123)).

2B Part of A

We will now calculate the contributions from the 2B part of the Hamiltonian. Before we concern ourselves with the actual calculation, we will first derive a few commutator relations that will be helpful later on. For the 1B part we already found that

$$[\hat{a}^\dagger_1 \hat{a}_2, \hat{a}^\dagger_3 \hat{a}_4] = \delta_{2,3} \, \hat{a}^\dagger_1 \hat{a}_4 - \delta_{1,4} \, \hat{a}^\dagger_3 \hat{a}_2. \tag{4.140}$$

This relation was useful because we had to evaluate the commutator of the ph-creator with a 1B operator. Analogously we will now have to consider the commutator of the ph-creator with a 2B

operator. We will consequently encounter terms of the sort $[\hat{a}_i^\dagger \hat{a}_j^\dagger \hat{a}_{j'} \hat{a}_{i'}, \hat{a}_p^\dagger \hat{a}_h]$. The first argument of the commutator can again be split into two: The first half consists of the commutator with both creators $\hat{a}_i^\dagger \hat{a}_j^\dagger$ and the second half of both the annihilators $\hat{a}_{j'} \hat{a}_{i'}$. Expressed schematically using consecutive numbers, this translates to

$$[\hat{a}_1^\dagger \hat{a}_2^\dagger \hat{a}_3 \hat{a}_4, \hat{a}_5^\dagger \hat{a}_6] = \hat{a}_1^\dagger \hat{a}_2^\dagger [\hat{a}_3 \hat{a}_4, \hat{a}_5^\dagger \hat{a}_6] + [\hat{a}_1^\dagger \hat{a}_2^\dagger, \hat{a}_5^\dagger \hat{a}_6] \hat{a}_3 \hat{a}_4. \tag{4.141}$$

The commutator of the first term can then be simplified to

$$[\hat{a}_1^\dagger \hat{a}_2^\dagger, \hat{a}_3^\dagger \hat{a}_4] = -\hat{a}_1^\dagger \hat{a}_3^\dagger \delta_{2,4} + \hat{a}_2^\dagger \hat{a}_3^\dagger \delta_{1,4} = (P(1,2) - 1) \hat{a}_1^\dagger \hat{a}_3^\dagger \delta_{2,4}\,. \tag{4.142}$$

In the last step we reformulated our result using the index-exchange operation $P(i,j)$. This symmetry of the indices 1 and 2 is interesting, because both are carried by creation operators and, in the context of RPA, will have an internal, i.e., a summation index. The structural similarity of both might hint at those terms giving a mere multiplicity instead of two unique terms. We now turn to the second half of the original term, the one carrying both annihilators. Likewise, we find

$$[\hat{a}_1 \hat{a}_2, \hat{a}_3^\dagger \hat{a}_4] = (1 - P(1,2)) \hat{a}_1 \hat{a}_4 \delta_{2,3}\,. \tag{4.143}$$

Again, we see a multiplicity, this time for the two annihilators. Let us now consider this in the context of a 2B operator $\hat{V}$, as we will encounter such terms in RPA. Using our obtained result, this corresponds to

$$\begin{aligned}
\sum_{ij,i'j'} v_{ij,i'j'}\, \hat{a}_i^\dagger \hat{a}_j^\dagger\, [\hat{a}_{j'} \hat{a}_{i'}, \hat{a}_p^\dagger \hat{a}_h] &= \sum_{ij,i'j'} v_{ij,i'j'}\, \hat{a}_i^\dagger \hat{a}_j^\dagger\, (1 - P(j',i')) \hat{a}_{j'} \hat{a}_h \delta_{i',p} && (4.144)\\
&= \sum_{ij,j'} v_{ij,pj'}\, \hat{a}_i^\dagger \hat{a}_j^\dagger\, \hat{a}_{j'} \hat{a}_h \\
&\quad - \sum_{ij,i'} v_{ij,i'p}\, \hat{a}_i^\dagger \hat{a}_j^\dagger\, \hat{a}_{i'} \hat{a}_h && (4.145)\\
&= 2 \sum_{ij,j'} v_{ij,pj'}\, \hat{a}_i^\dagger \hat{a}_j^\dagger\, \hat{a}_{j'} \hat{a}_h\,. && (4.146)
\end{aligned}$$

We see that this involves indeed a multiplicity. Analogously we can transform the second term. The calculation is systematically identical to the one we just performed and, thus, we omit the details. The entire 2B part of the inner commutator necessary for the A matrix can thus be written as

$$\begin{aligned}
[\hat{V}, \hat{a}_p^\dagger \hat{a}_h] &= \frac{1}{4} \sum_{ij,i'j'} v_{ij,i'j'} [\hat{a}_i^\dagger \hat{a}_j^\dagger \hat{a}_{j'} \hat{a}_{i'}, \hat{a}_p^\dagger \hat{a}_h] && (4.147)\\
&= \frac{1}{4} \sum_{ij,i'j'} v_{ij,i'j'} \left(\hat{a}_i^\dagger \hat{a}_j^\dagger [\hat{a}_{j'} \hat{a}_{i'}, \hat{a}_p^\dagger \hat{a}_h] + [\hat{a}_i^\dagger \hat{a}_j^\dagger, \hat{a}_p^\dagger \hat{a}_h] \hat{a}_{j'} \hat{a}_{i'} \right) && (4.148)\\
&= \frac{1}{2} \sum_{ij,j'} v_{ij,pj'}\, \hat{a}_i^\dagger \hat{a}_j^\dagger \hat{a}_{j'} \hat{a}_h - \frac{1}{2} \sum_{j,i'j'} v_{hj,i'j'}\, \hat{a}_p^\dagger \hat{a}_j^\dagger \hat{a}_{j'} \hat{a}_{i'}, && (4.149)
\end{aligned}$$

where we applied the above formulae to the first and second term, respectively. We have now simplified the inner commutator as much as possible and can insert this into the outer commutator:

$$[\hat{a}_{h'}^\dagger \hat{a}_{p'}, [\hat{V}, \hat{a}_p^\dagger \hat{a}_h]] = \frac{1}{2} \sum_{ij,j'} v_{ij,pj'}\, [\hat{a}_{h'}^\dagger \hat{a}_{p'}, \hat{a}_i^\dagger \hat{a}_j^\dagger \hat{a}_{j'} \hat{a}_h] - \frac{1}{2} \sum_{j,i'j'} v_{hj,i'j'}\, [\hat{a}_{h'}^\dagger \hat{a}_{p'}, \hat{a}_p^\dagger \hat{a}_j^\dagger \hat{a}_{j'} \hat{a}_{i'}]\,. \tag{4.150}$$

In principle, we can now repeat the steps given above for the first as well as for the second term. A few changes have to be taken into account. Let us take a look at the first term. Here, the (ij) part can be dealt with exactly as before. On the other side, we see that after the evaluation of the inner commutator, one of the primed indices is already constrained. The inner commutator is responsible for the i' index being replaced by p in the matrix element and by h in the annihilator. The same goes for the second term, only for the non-primed indices: i is replaced by h in the matrix element and by p in the creator. We will treat those terms separately in the following.

First Term

We start by considering the first term. Again we break the commutator down into smaller expressions with either double-creators or double-annihilators. Giving only the non-zero, fully simplified terms, for the first part of (4.150) we get

$$[1] \equiv \frac{1}{2}\sum_{ij,j'} v_{ij,pj'}\,[\hat{a}^\dagger_{h'}\hat{a}_{p'}, \hat{a}^\dagger_i\hat{a}^\dagger_j\hat{a}_{j'}\hat{a}_h] \tag{4.151}$$

$$= \frac{1}{2}\sum_{ij,j'} v_{ij,pj'}\,(\hat{a}^\dagger_i\hat{a}^\dagger_j[\hat{a}^\dagger_{h'}\hat{a}_{p'}, \hat{a}_{j'}\hat{a}_h] + [\hat{a}^\dagger_{h'}\hat{a}_{p'}, \hat{a}^\dagger_i\hat{a}^\dagger_j]\hat{a}_{j'}\hat{a}_h) \tag{4.152}$$

$$\begin{aligned} =& -\delta_{h,h'}\frac{1}{2}\sum_{ij,j'} v_{ij,pj'}\,\hat{a}^\dagger_i\hat{a}^\dagger_j\hat{a}_{j'}\hat{a}_{p'} + \frac{1}{2}\sum_{i,j'} v_{ip',pj'}\,\hat{a}^\dagger_i\hat{a}^\dagger_{h'}\hat{a}_{j'}\hat{a}_h + \frac{1}{2}\sum_{j,j'} v_{p'j,pj'}\,\hat{a}^\dagger_{h'}\hat{a}^\dagger_j\hat{a}_{j'}\hat{a}_h \\ & - \frac{1}{2}\sum_{ij} v_{ij,ph'}\,\hat{a}^\dagger_i\hat{a}^\dagger_j\hat{a}_{p'}\hat{a}_h\,. \end{aligned} \tag{4.153}$$

For further simplification we now consider the second and third term which have a very similar structure. Use of permutations and index renaming gives

$$[2+3] \equiv \frac{1}{2}\sum_{i,j'} v_{ip',pj'}\,\hat{a}^\dagger_i\hat{a}^\dagger_{h'}\hat{a}_{j'}\hat{a}_h + \frac{1}{2}\sum_{j,j'} v_{p'j,pj'}\,\hat{a}^\dagger_{h'}\hat{a}^\dagger_j\hat{a}_{j'}\hat{a}_h \tag{4.154}$$

$$= -\sum_{i,j'} v_{ip',pj'}\,\hat{a}^\dagger_i\hat{a}^\dagger_{h'}\hat{a}_h\hat{a}_{j'}. \tag{4.155}$$

We find that these terms are indeed equal and produce a multiplicity of two, as could be expected. Reinserting this yields

$$[1] = \frac{1}{2}\sum_{ij,j'} v_{ij,pj'}\,[\hat{a}^\dagger_{h'}\hat{a}_{p'}, \hat{a}^\dagger_i\hat{a}^\dagger_j\hat{a}_{j'}\hat{a}_h] \tag{4.156}$$

$$= -\delta_{h,h'}\frac{1}{2}\sum_{ij,j'} v_{ij,pj'}\,\hat{a}^\dagger_i\hat{a}^\dagger_j\hat{a}_{j'}\hat{a}_{p'} - \sum_{i,j'} v_{ip',pj'}\,\hat{a}^\dagger_i\hat{a}^\dagger_{h'}\hat{a}_h\hat{a}_{j'} - \frac{1}{2}\sum_{ij} v_{ij,ph'}\,\hat{a}^\dagger_i\hat{a}^\dagger_j\hat{a}_{p'}\hat{a}_h \tag{4.157}$$

and, since all commutators have been evaluated, we can take the expectation value of our above expression, leaving us with

$$\langle \mathrm{RPA}|\,[1]\,|\mathrm{RPA}\rangle = \frac{1}{2}\sum_{ij,j'} v_{ij,pj'}\,\langle \mathrm{RPA}|\,[\hat{a}^\dagger_{h'}\hat{a}_{p'}, \hat{a}^\dagger_i\hat{a}^\dagger_j\hat{a}_{j'}\hat{a}_h]\,|\mathrm{RPA}\rangle \tag{4.158}$$

$$= -\delta_{h,h'}\frac{1}{2}\sum_{ij,j'} v_{ij,pj'}\,\varrho_{p'j',ij} - \sum_{i,j'} v_{ip',pj'}\,\varrho_{j'h,ih'} - \frac{1}{2}\sum_{ij} v_{ij,ph'}\varrho_{hp',ij}. \tag{4.159}$$

The above equation can be simplified a little further. Let us look at the first term of (4.159). In both matrix elements of the interaction as well as the density, we have the indices ij within

one state (e.g. the ket, mind the symmetries). We, therefore, see that we can apply our matrix-product formula of (4.10) and rewrite this as

$$\sum_{ij,j'} v_{ij,pj'}\, \varrho_{p'j',ij} = 2(V\varrho)_{pj',p'j'}. \tag{4.160}$$

Again we find a matrix product between Hamiltonian and density, as we did for the 1B part. The same goes for the last term of the term [1]. With this we arrive at

$$\langle \mathrm{RPA}|\,[1]\,|\mathrm{RPA}\rangle = -\,\delta_{h,h'} \sum_{j'} (V\varrho)_{pj',p'j'} - \sum_{i,j'} v_{ip',pj'}\, \varrho_{j'h,ih'} - (V\varrho)_{ph',hp'}. \tag{4.161}$$

The first term can again be simplified by using the partial trace introduced in (4.19) as

$$\mathrm{Tr}_2(V\varrho)_{p,p'} \equiv \frac{1}{2} \sum_{j'} (V\varrho)_{pj',p'j'}. \tag{4.162}$$

The complete first term now reads

$$\langle \mathrm{RPA}|\,[1]\,|\mathrm{RPA}\rangle = -\,\delta_{h,h'}\, 2\,\mathrm{Tr}_2(V\varrho)_{p,p'} - \sum_{i,j'} v_{ip',pj'}\, \varrho_{j'h,ih'} + (V\varrho)_{ph',p'h}. \tag{4.163}$$

Note that, in the most general case, ϱ and V do not commute. In this case the matrix product is not symmetric.

Second Term

Similar to what we did for the first term, [1], we will now take a look at the second term of (4.150):

$$[2] \equiv -\frac{1}{2} \sum_{j,i'j'} v_{hj,i'j'}\, [\hat{a}^\dagger_{h'}\hat{a}_{p'}, \hat{a}^\dagger_p \hat{a}^\dagger_j \hat{a}_{j'}\hat{a}_{i'}] \tag{4.164}$$

$$= -\frac{1}{2} \sum_{j,i'j'} v_{hj,i'j'}\, \hat{a}^\dagger_p \hat{a}^\dagger_j [\hat{a}^\dagger_{h'}\hat{a}_{p'}, \hat{a}_{j'}\hat{a}_{i'}] - \frac{1}{2} \sum_{j,i'j'} v_{hj,i'j'}\, [\hat{a}^\dagger_{h'}\hat{a}_{p'}, \hat{a}^\dagger_p \hat{a}^\dagger_j] \hat{a}_{j'}\hat{a}_{i'}. \tag{4.165}$$

We see that in the second term we have a summation in both the interaction and in the string of operators over $i'j'$ which will, again, result in a matrix product. More importantly, the operators carrying those indices are outside of the commutator, ergo no deltas involving either i' or j' will appear. With this we already know that the basic form will be as follows

$$\langle \mathrm{RPA}|\,[2.2]\,|\mathrm{RPA}\rangle \equiv -\frac{1}{2} \sum_{j,i'j'} v_{hj,i'j'}\, \langle \mathrm{RPA}|\,[\hat{a}^\dagger_{h'}\hat{a}_{p'}, \hat{a}^\dagger_p \hat{a}^\dagger_j] \hat{a}_{j'}\hat{a}_{i'}\,|\mathrm{RPA}\rangle \tag{4.166}$$

$$= \ldots = -\sum_j (V\varrho)_{hj,xy} \tag{4.167}$$

where the yet unknown indices denoted by x and y will be determined by the evaluation of the commutator. We apply the previously derived relation

$$[\hat{a}^\dagger_1 \hat{a}^\dagger_2, \hat{a}^\dagger_3 \hat{a}_4] = -\hat{a}^\dagger_1 \hat{a}^\dagger_3 \delta_{2,4} - \hat{a}^\dagger_3 \hat{a}^\dagger_2 \delta_{1,4} \tag{4.168}$$

and get

$$[\hat{a}^\dagger_{h'}\hat{a}_{p'}, \hat{a}^\dagger_p \hat{a}^\dagger_j] = \hat{a}^\dagger_p \hat{a}^\dagger_{h'}\, \delta_{j,p'} + \hat{a}^\dagger_{h'} \hat{a}^\dagger_j\, \delta_{p,p'}. \tag{4.169}$$

This can now be inserted into our schematic xy formula. The entire second term of (4.165) therefore yields

$$\langle \mathrm{RPA}| [2.2] |\mathrm{RPA}\rangle = -\frac{1}{2}\sum_{j,i'j'} v_{hj,i'j'} \langle \mathrm{RPA}| [\hat{a}^\dagger_{h'}\hat{a}_{p'}, \hat{a}^\dagger_p\hat{a}^\dagger_j]\hat{a}_{j'}\hat{a}_{i'} |\mathrm{RPA}\rangle \tag{4.170}$$

$$= -\delta_{p,p'}\sum_j (V\varrho)_{hj,h'j} - (V\varrho)_{hp',ph'} \tag{4.171}$$

$$= -\delta_{p,p'} 2\mathrm{Tr}_2(V\varrho)_{h,h'} - (V\varrho)_{hp',ph'}. \tag{4.172}$$

We will now turn to the first term of (4.165). We can apply the relation

$$[\hat{a}_1\hat{a}_2, \hat{a}^\dagger_3\hat{a}_4] = \hat{a}_1\hat{a}_4\delta_{2,3} + \hat{a}_4\hat{a}_2\delta_{1,3} \tag{4.173}$$

giving

$$[\hat{a}^\dagger_{h'}\hat{a}_{p'}, \hat{a}_{j'}\hat{a}_{i'}] = -\hat{a}_{j'}\hat{a}_{p'}\,\delta_{h',i'} - \hat{a}_{p'}\hat{a}_{i'}\,\delta_{h',j'}. \tag{4.174}$$

Again, from the structure of the commutator, we expect a multiplicity rather than two unique terms. In total, for the first term we get

$$\langle \mathrm{RPA}| [2.1] |\mathrm{RPA}\rangle \equiv -\frac{1}{2}\sum_{j,i'j'} v_{hj,i'j'} \langle \mathrm{RPA}| \hat{a}^\dagger_p\hat{a}^\dagger_j[\hat{a}^\dagger_{h'}\hat{a}_{p'}, \hat{a}_{j'}\hat{a}_{i'}] |\mathrm{RPA}\rangle \tag{4.175}$$

$$= \frac{1}{2}\sum_{j,i'j'} v_{hj,i'j'}\,\varrho_{p'j',pj}\,\delta_{h',i'} + \frac{1}{2}\sum_{j,i'j'} v_{hj,i'j'}\,\varrho_{i'p',pj}\,\delta_{h',j'} \tag{4.176}$$

$$= \sum_{j,j'} v_{jh,h'j'}\,\varrho_{j'p',pj}. \tag{4.177}$$

Finally for the entire term [2] of this section we obtain

$$\langle \mathrm{RPA}| [2] |\mathrm{RPA}\rangle = -\frac{1}{2}\sum_{j,i'j'} v_{hj,i'j'} \langle \mathrm{RPA}| [\hat{a}^\dagger_{h'}\hat{a}_{p'}, \hat{a}^\dagger_p\hat{a}^\dagger_j\hat{a}_{j'}\hat{a}_{i'}] |\mathrm{RPA}\rangle \tag{4.178}$$

$$= \sum_{j,j'} v_{jh,h'j'}\,\varrho_{j'p',pj} - \delta_{p,p'}2\mathrm{Tr}_2(V\varrho)_{h,h'} - (V\varrho)_{hp',ph'}. \tag{4.179}$$

After gathering all terms of the 2B part, we get

$$\boxed{\begin{aligned}\langle \mathrm{RPA}| [\hat{a}^\dagger_{h'}\hat{a}_{p'}, [\hat{V}, \hat{a}^\dagger_p\hat{a}_h]] |\mathrm{RPA}\rangle = &-\delta_{h,h'}2\mathrm{Tr}_2(V\varrho)_{p,p'} + (V\varrho)_{ph',p'h} - \sum_{i,j'} v_{ip',pj'}\,\varrho_{j'h,ih'} \\ &- \delta_{p,p'}2\mathrm{Tr}_2(V\varrho)_{h,h'} - (V\varrho)_{hp',ph'} + \sum_{j,j'} v_{jh,h'j'}\,\varrho_{j'p',pj}\end{aligned}} \tag{4.180}$$

Fallback to HF

As we did before when dealing with the 1B part of A, we now want to perform an analytical crosscheck to see if our results are in agreement with the special case of the ϱ-state being the HF Slater-determinant. We already know that all 2B density matrix terms involving at least one particle state are, within HF, zero (cf. section 4.1.3). This relation already renders three of the four $(V\varrho)$-terms zero. Additionally, the very last term in (4.180) vanishes, too. We are left with

$$\langle \mathrm{HF}| [\hat{a}^\dagger_{h'}\hat{a}_{p'}, [\hat{V}, \hat{a}^\dagger_p\hat{a}_h]] |\mathrm{HF}\rangle = -\delta_{p,p'}2\mathrm{Tr}_2(V\varrho)_{h,h'} - \sum_{i,j'}^{\mathrm{occ.}} v_{ip',pj'}\,\varrho_{j'h,ih'}. \tag{4.181}$$

For further simplifications it is best to reinsert the definition of the matrix product between V and ϱ and use relation (4.33) for the 2B HF density.

$$\langle \mathrm{HF}| [\hat{a}^\dagger_{h'}\hat{a}_{p'}, [\hat{V}, \hat{a}^\dagger_p\hat{a}_h]] |\mathrm{HF}\rangle = -\delta_{p,p'}\tfrac{1}{2}\sum_{ij,j'}^{\mathrm{occ.}} v_{ij,hj'}\varrho_{ij,h'j'} - \sum_{i,j'}^{\mathrm{occ.}} v_{ip',pj'}\,\varrho_{j'h,ih'} \tag{4.182}$$

$$= -\delta_{p,p'}\tfrac{1}{2}\sum_{ij,j'}^{\mathrm{occ.}} v_{ij,hj'}(\delta_{ih'}\delta_{jj'} - \delta_{ij'}\delta_{jh'}) - \sum_{i,j'}^{\mathrm{occ.}} v_{ip',pj'}\,(\delta_{j'i}\delta_{hh'} - \delta_{j'h'}\delta_{ih}) \tag{4.183}$$

$$= -\delta_{p,p'}\tfrac{1}{2}\left(\sum_{j}^{\mathrm{occ.}} v_{h'j,h'j} - \sum_{i}^{\mathrm{occ.}} v_{ih',hi}\right) - \delta_{hh'}\sum_{i}^{\mathrm{occ.}} v_{ip',pi} + v_{hp',ph'} \tag{4.184}$$

$$= -\delta_{p,p'}\sum_{j}^{\mathrm{occ.}} v_{h'j,hj} + \delta_{hh'}\sum_{i}^{\mathrm{occ.}} v_{pi,p'i} + v_{ph',hp'}. \tag{4.185}$$

This is indeed in agreement with the HF version of standard RPA, compare (3.123).

Complete Expression for A in CC-RPA

We now have all 1B and 2B contributions for the A matrix evaluated in a correlated state. In its entirety, it is given by:

$$A_{p'h',ph} = \langle \mathrm{RPA}| [\hat{a}^\dagger_{h'}\hat{a}_{p'}, [\hat{H}, \hat{a}^\dagger_p\hat{a}_h]] |\mathrm{RPA}\rangle \tag{4.186}$$

$$\begin{aligned} &= -\delta_{h,h'}(T\varrho)_{p,p'} - \delta_{p,p'}(T\varrho)_{h,h'} + t_{p,p'}\,\varrho_{h',h} + t_{h,h'}\varrho_{p,p'} \\ &\quad - \delta_{h,h'}2\mathrm{Tr}_2(V\varrho)_{p,p'} + (V\varrho)_{ph',p'h} + \sum_{j,j'} v_{jp',pj'}\,\varrho_{j'h,h'j} \\ &\quad - \delta_{p,p'}2\mathrm{Tr}_2(V\varrho)_{h,h'} + (V\varrho)_{p'h,ph'} + \sum_{j,j'} v_{jh,h'j'}\,\varrho_{j'p',pj} \end{aligned} \tag{4.187}$$

4.3.6 Derivation of the B Matrix

In the previous section we have made several derivations concerning various commutator relations. Those were necessary for evaluating the A matrix on a level of 2B density matrix elements. The increased effort for deriving these formulae is owed to the evaluation of those commutators within the expectation value of a correlated state.

When computing the B matrix, we are faced with similar terms as for the A matrix. The main difference between both is that the inner commutator carries a ph de-excitation operator $\hat{\mathcal{A}}$ instead of ph excitation operator $\hat{\mathcal{A}}^\dagger$ (see (4.96) and (4.97)). Consequently, the indices h and p appear in reversed order in the inner commutator. However, in the entire section 4.3.5 no relations specific to terms of the sort $\hat{a}^\dagger_p\hat{a}_h$ have been used. We solely used the creator-annihilator operator structure of the excitation, i.e. $\hat{a}^\dagger\hat{a}$. The index structure on the other hand did not influence the applied relations.

Since for the B matrix the operator structure stays the same and only the indices change, all we have to do in order to get the CC-RPA expression of B is to exchange the p and h index with each other. The results can then be taken from the expression derived before, i.e. (4.187). This gives

$$\begin{aligned}
B_{p'h',ph} =& -\left[\hat{a}^\dagger_{h'}\hat{a}_{p'},[\hat{H},\hat{a}^\dagger_h\hat{a}_p]\right] && (4.188)\\
=& -\langle\mathrm{RPA}|\left[\hat{a}^\dagger_{h'}\hat{a}_{p'},[\hat{T},\hat{a}^\dagger_h\hat{a}_p]\right]|\mathrm{RPA}\rangle - \langle\mathrm{RPA}|\left[\hat{a}^\dagger_{h'}\hat{a}_{p'},[\hat{V},\hat{a}^\dagger_h\hat{a}_p]\right]|\mathrm{RPA}\rangle && (4.189)\\
=&\delta_{p,h'}(T\varrho)_{h,p'} + \delta_{h,p'}(T\varrho)_{p,h'} - t_{h,p'}\,\varrho_{h',p} - t_{p,h'}\varrho_{h,p'}\\
&+ \delta_{p,h'}2\mathrm{Tr}_2(V\varrho)_{h,p'} - (V\varrho)_{hh',p'p} - \sum_{j,j'} v_{jp',hj'}\,\varrho_{j'p,h'j}\\
&+ \delta_{h,p'}2\mathrm{Tr}_2(V\varrho)_{p,h'} - (V\varrho)_{p'p,hh'} - \sum_{j,j'} v_{jp,h'j'}\,\varrho_{j'p',hj}. && (4.190)
\end{aligned}$$

The δ relations between particles and holes, though not used in section 4.3.5, still yield zero. We, therefore, get

$$\boxed{\begin{aligned}
B_{p'h',ph} =& -\langle\mathrm{RPA}|\left[\hat{a}^\dagger_{h'}\hat{a}_{p'},[\hat{H},\hat{a}^\dagger_h\hat{a}_p]\right]|\mathrm{RPA}\rangle && (4.191)\\
&- t_{h,p'}\,\varrho_{h',p} - t_{p,h'}\varrho_{h,p'}\\
&- (V\varrho)_{hh',p'p} - \sum_{j,j'} v_{jp',hj'}\,\varrho_{j'p,h'j}\\
&- (V\varrho)_{p'p,hh'} - \sum_{j,j'} v_{jp,h'j'}\,\varrho_{j'p',hj}. && (4.192)
\end{aligned}}$$

Fallback to HF

Finally we will perform the HF crosscheck of formula (4.191) for the B matrix. The strategy is the same as for the A matrix. We find

$$\begin{aligned}
B_{p'h',ph} =& \langle\mathrm{HF}|\left[\hat{a}^\dagger_{h'}\hat{a}_{p'},[\hat{V},\hat{a}^\dagger_h\hat{a}_p]\right]|\mathrm{HF}\rangle && (4.193)\\
=& - t_{h,p'}\,\delta_{h',p} - t_{p,h'}\delta_{h,p'}\\
&- (V\varrho)_{hh',p'p} - \sum_{j,j'} v_{jp',hj'}\,\varrho_{j'p,h'j}\\
&- (V\varrho)_{p'p,hh'} - \sum_{j,j'} v_{jp,h'j'}\,\varrho_{j'p',hj} && (4.194)\\
=& - (V\varrho)_{p'p,hh'} && (4.195)\\
=& -\tfrac{1}{2}\sum_{ij}^{\mathrm{occ.}} v_{p'p,ij}\,\varrho_{ij,hh'} = -\tfrac{1}{2}\sum_{ij}^{\mathrm{occ.}} v_{p'p,ij}\,(\delta_{ih}\delta_{jh'} - \delta_{ih'}\delta_{jh}) && (4.196)\\
=& -\tfrac{1}{2}(v_{p'p,hh'} - v_{p'p,h'h}) = v_{pp',hh'}, && (4.197)
\end{aligned}$$

in accordance with (3.125).

4.3.7 Norm of States from CC-RPA

We will now calculate the norm of states from CC-RPA, i.e., the scalar product of $|\omega\rangle$ and $|\omega'\rangle$ which we still require to fulfill orthogonality relations. New terms arising from the evaluation of the expectation value of an arbitrary state instead of the simple HF version will have to be

taken into account. We find

$$\delta_{\omega,\omega'} = \langle\omega|\omega'\rangle = \langle \mathrm{RPA}|\, \hat{Q}_\omega \hat{Q}^\dagger_{\omega'} \,|\mathrm{RPA}\rangle = \langle \mathrm{RPA}|\, [\hat{Q}_\omega, \hat{Q}^\dagger_{\omega'}] \,|\mathrm{RPA}\rangle \tag{4.198}$$

$$= \sum_{ph} X^\omega_{\bar{p}\bar{h}} \langle \mathrm{RPA}|\, [\hat{\mathcal{A}}_{\bar{p}\bar{h}}, \hat{Q}^\dagger_{\omega'}] \,|\mathrm{RPA}\rangle - Y^\omega_{\bar{p}\bar{h}} \langle \mathrm{RPA}|\, [\hat{\tilde{\mathcal{A}}}^\dagger_{\bar{p}\bar{h}}, \hat{Q}^\dagger_{\omega'}] \,|\mathrm{RPA}\rangle \tag{4.199}$$

$$= \sum_{ph}\sum_{p'h'} X^\omega_{\bar{p}\bar{h}} X^{\omega'}_{\bar{p}'\bar{h}'} \langle \mathrm{RPA}|\, [\hat{\mathcal{A}}_{\bar{p}\bar{h}}, \hat{\mathcal{A}}^\dagger{}_{\bar{p}'\bar{h}'}] \,|\mathrm{RPA}\rangle + Y^\omega_{\bar{p}\bar{h}} Y^{\omega'}_{\bar{p}'\bar{h}'} \langle \mathrm{RPA}|\, [\hat{\tilde{\mathcal{A}}}^\dagger_{\bar{p}\bar{h}}, \hat{\tilde{\mathcal{A}}}_{\bar{p}'\bar{h}'}] \,|\mathrm{RPA}\rangle \tag{4.200}$$

$$= \sum_{ph}\sum_{p'h'} X^\omega_{\bar{p}\bar{h}} X^{\omega'}_{\bar{p}'\bar{h}'} \langle \mathrm{RPA}|\, [\hat{\mathcal{A}}_{\bar{p}\bar{h}}, \hat{\mathcal{A}}^\dagger{}_{\bar{p}'\bar{h}'}] \,|\mathrm{RPA}\rangle + Y^\omega_{\bar{p}\bar{h}} Y^{\omega'}_{\bar{p}'\bar{h}'} \langle \mathrm{RPA}|\, [\hat{\mathcal{A}}^\dagger{}_{\bar{p}\bar{h}}, \hat{\mathcal{A}}_{\bar{p}'\bar{h}'}] \,|\mathrm{RPA}\rangle \tag{4.201}$$

$$= \sum_{ph}\sum_{p'h'} X^\omega_{\bar{p}\bar{h}} X^{\omega'}_{\bar{p}'\bar{h}'} N_{\bar{p}\bar{h},\bar{p}'\bar{h}'} - Y^\omega_{\bar{p}\bar{h}} Y^{\omega'}_{\bar{p}'\bar{h}'} \langle \mathrm{RPA}|\, [\hat{\mathcal{A}}_{\bar{p}'\bar{h}'}, \hat{\mathcal{A}}^\dagger{}_{\bar{p}\bar{h}}] \,|\mathrm{RPA}\rangle \tag{4.202}$$

$$= \sum_{ph}\sum_{p'h'} X^\omega_{\bar{p}\bar{h}} X^{\omega'}_{\bar{p}'\bar{h}'} N_{\bar{p}\bar{h},\bar{p}'\bar{h}'} - Y^\omega_{\bar{p}\bar{h}} Y^{\omega'}_{\bar{p}'\bar{h}'} N_{\bar{p}'\bar{h}',\bar{p}\bar{h}}. \tag{4.203}$$

Here we used that $[\hat{\mathcal{A}}_i, \hat{\mathcal{A}}_j] = [\hat{\mathcal{A}}^\dagger_i, \hat{\mathcal{A}}^\dagger_j] \equiv 0$, as shown before. We also inserted the definition of our norm-matrix N, see section 4.3.1. In matrix notation, this can be written (using multi indices) as:

$$\delta_{\omega,\omega'} = \sum_i \sum_j X^\omega_i X^{\omega'}_j N_{ij} - Y^\omega_i Y^{\omega'}_j N_{ji} \tag{4.204}$$

$$= \sum_i \sum_j X^\omega_i N_{ij} X^{\omega'}_j - Y^\omega_i N_{ij} Y^{\omega'}_j \tag{4.205}$$

$$= X^{\omega\,\mathrm{T}} N X^{\omega'} - Y^{\omega\,\mathrm{T}} N Y^{\omega'}. \tag{4.206}$$

In comparison to standard RPA, where the orthogonality relation is simply

$$\delta_{\omega,\omega'} = X^{\omega\,\mathrm{T}} X^{\omega'} - Y^{\omega\,\mathrm{T}} Y^{\omega'}, \tag{4.207}$$

we see that the norm-matrix introduced in section 4.3.1 additionally appears within the scalar product of the forward and backward amplitudes.

4.3.8 Zero-Norm

In RPA, the ECOs are defined to create a certain excited state when applied to the RPA ground state. Likewise, the adjoint of an ECO performs a de-excitation from its excited state to the ground state. Applying the adjoint ECO to the RPA ground state itself would, by definition, "delete" the vacuum and thus yield zero (cf. section 3.2.2). In the EOM derivation of standard RPA, at a certain point we are forced to apply the QBA and continue onward evaluating all expectation values with the HF ground state instead of the true RPA ground state. This imposes an inconsistency to the RPA framework and causes the vacuum-deletion to be inexact due to the fact that ground and excited states are no longer perfectly orthogonal to one another. As mentioned before, the new CC-RPA derived in this thesis employs a correlated ground state instead of the HF Slater-determinant for the evaluation of expectation values, but since this correlated state is from CC and not the true RPA ground state, we still have some degree of inconsistency. In this section we want to define a measure for quantifying this inconsistency. Therefore, instead of using the consistent relation

$$\hat{Q}_\omega \,|\mathrm{RPA}\rangle = 0, \qquad \forall\omega, \tag{4.208}$$

we take into account that the quasi-deletion creates, strictly speaking, a physical state $|\emptyset_\omega\rangle$:

$$\hat{Q}_\omega \,|\mathrm{RPA}\rangle \equiv |\emptyset_\omega\rangle\,. \tag{4.209}$$

This state has a finite norm, which we will call the *zero-norm*, and can be calculated as

$$\langle \emptyset_\omega | \emptyset_\omega \rangle = \langle \mathrm{RPA} | \hat{Q}_\omega^\dagger \hat{Q}_\omega | \mathrm{RPA} \rangle \tag{4.210}$$

$$= \sum_{ph} \left(X_{ph}^\omega \langle \mathrm{RPA} | \hat{\mathcal{A}}_{ph}^\dagger \hat{Q}_\omega | \mathrm{RPA} \rangle - Y_{ph}^\omega \langle \mathrm{RPA} | \hat{\bar{\mathcal{A}}}_{ph} \hat{Q}_\omega | \mathrm{RPA} \rangle \right) \tag{4.211}$$

$$= \sum_{ph} \left(X_{ph}^\omega \langle \mathrm{RPA} | \hat{\mathcal{A}}_{ph}^\dagger \hat{Q}_\omega | \mathrm{RPA} \rangle + (-1)^{J+1} Y_{ph}^\omega \langle \mathrm{RPA} | \hat{\mathcal{A}}_{ph} \hat{Q}_\omega | \mathrm{RPA} \rangle \right) \tag{4.212}$$

$$\begin{aligned} = \sum_{ph} \sum_{p'h'} \Big(& X_{ph}^\omega X_{p'h'}^{\omega *} \langle \mathrm{RPA} | \hat{\mathcal{A}}_{ph}^\dagger \hat{\mathcal{A}}_{p'h'} | \mathrm{RPA} \rangle \\ & + (-1)^{J+1} X_{ph}^\omega Y_{p'h'}^{\omega *} \langle \mathrm{RPA} | \hat{\mathcal{A}}_{ph}^\dagger \hat{\mathcal{A}}^\dagger{}_{p'h'} | \mathrm{RPA} \rangle \\ & + (-1)^{J+1} Y_{ph}^\omega X_{p'h'}^{\omega *} \langle \mathrm{RPA} | \hat{\mathcal{A}}_{ph} \hat{\mathcal{A}}_{p'h'} | \mathrm{RPA} \rangle \\ & + Y_{ph}^\omega Y_{p'h'}^{\omega *} \langle \mathrm{RPA} | \hat{\mathcal{A}}_{ph} \hat{\mathcal{A}}_{p'h'}^\dagger | \mathrm{RPA} \rangle \Big). \end{aligned} \tag{4.213}$$

Here we first expanded the definition of $\hat{Q}_\omega^\dagger$ and then the one of its adjoint. We also used that $(-1)^{2J+2} \equiv 1$ for all integer J. We now take a look at the four individual terms of the above equation. For simplicity, we will stay in an uncoupled formulation. In order to evaluate these expressions as density matrix elements, we have to perform a reordering to bring the creators to the left and the annihilators to the right. Deltas stemming form commutators will be omitted where forbidden by p-h combinations occur. We get

$$\langle \mathrm{RPA} | \hat{\mathcal{A}}_{ph}^\dagger \hat{\mathcal{A}}_{p'h'} | \mathrm{RPA} \rangle = \langle \mathrm{RPA} | \hat{a}_p^\dagger \hat{a}_h \hat{a}_{h'}^\dagger \hat{a}_{p'} | \mathrm{RPA} \rangle = \langle \mathrm{RPA} | \hat{a}_p^\dagger (-\hat{a}_{h'}^\dagger \hat{a}_h + \delta_{hh'}) \hat{a}_{p'} | \mathrm{RPA} \rangle \tag{4.214}$$

$$= - \langle \mathrm{RPA} | \hat{a}_p^\dagger \hat{a}_{h'}^\dagger \hat{a}_h \hat{a}_{p'} | \mathrm{RPA} \rangle + \delta_{hh'} \langle \mathrm{RPA} | \hat{a}_p^\dagger \hat{a}_{p'} | \mathrm{RPA} \rangle \tag{4.215}$$

$$= - \varrho_{p'h,ph'} + \delta_{hh'} \varrho_{p',p}, \tag{4.216}$$

$$\langle \mathrm{RPA} | \hat{\mathcal{A}}_{ph}^\dagger \hat{\mathcal{A}}_{p'h'}^\dagger | \mathrm{RPA} \rangle = \langle \mathrm{RPA} | \hat{a}_p^\dagger \hat{a}_h \hat{a}_{p'}^\dagger \hat{a}_{h'} | \mathrm{RPA} \rangle = - \langle \mathrm{RPA} | \hat{a}_p^\dagger \hat{a}_{p'}^\dagger \hat{a}_h \hat{a}_{h'} | \mathrm{RPA} \rangle \tag{4.217}$$

$$= - \varrho_{h'h,pp'}, \tag{4.218}$$

$$\langle \mathrm{RPA} | \hat{\mathcal{A}}_{ph} \hat{\mathcal{A}}_{p'h'} | \mathrm{RPA} \rangle = \langle \mathrm{RPA} | \hat{a}_h^\dagger \hat{a}_p \hat{a}_{h'}^\dagger \hat{a}_{p'} | \mathrm{RPA} \rangle = - \langle \mathrm{RPA} | \hat{a}_h^\dagger \hat{a}_{h'}^\dagger \hat{a}_p \hat{a}_{p'} | \mathrm{RPA} \rangle \tag{4.219}$$

$$= - \varrho_{p'p,hh'}, \tag{4.220}$$

$$\langle \mathrm{RPA} | \hat{\mathcal{A}}_{ph} \hat{\mathcal{A}}_{p'h'}^\dagger | \mathrm{RPA} \rangle = \langle \mathrm{RPA} | \hat{a}_h^\dagger \hat{a}_p \hat{a}_{p'}^\dagger \hat{a}_{h'} | \mathrm{RPA} \rangle = \langle \mathrm{RPA} | \hat{a}_h^\dagger (-\hat{a}_{p'}^\dagger \hat{a}_p + \delta_{pp'}) \hat{a}_{h'} | \mathrm{RPA} \rangle \tag{4.221}$$

$$= - \langle \mathrm{RPA} | \hat{a}_h^\dagger \hat{a}_{p'}^\dagger \hat{a}_p \hat{a}_{h'} | \mathrm{RPA} \rangle + \delta_{pp'} \langle \mathrm{RPA} | \hat{a}_h^\dagger \hat{a}_{h'} | \mathrm{RPA} \rangle \tag{4.222}$$

$$= - \varrho_{h'p,hp'} + \delta_{pp'} \varrho_{h',h}. \tag{4.223}$$

The first and last term as well as the second and third could of course be obtained from one another by appropriate renaming of particle and hole indices. Reinserting this into the initial equation yields

$$\begin{aligned} \langle \emptyset_\omega | \emptyset_\omega \rangle = \sum_{ph} \sum_{p'h'} \Big(& X_{ph}^\omega X_{p'h'}^\omega (-\varrho_{p'h,ph'} + \delta_{hh'} \varrho_{p',p}) + (-1)^{J+1} X_h^p Y_{p'h'}^\omega (-\varrho_{h'h,pp'}) \\ & + (-1)^{J+1} Y_{ph}^\omega X_{p'h'}^\omega (-\varrho_{p'p,hh'}) + Y_{ph}^\omega Y_{p'h'}^\omega (-\varrho_{h'p,hp'} + \delta_{pp'} \varrho_{h',h}) \Big). \end{aligned} \tag{4.224}$$

We can now use symmetries of the density matrix elements to collect matching terms. This gives

$$\begin{aligned} \langle \emptyset_\omega | \emptyset_\omega \rangle = \sum_{ph} \sum_{p'h'} \Big(& (X_{ph}^\omega X_{p'h'}^\omega + Y_{ph}^\omega Y_{p'h'}^\omega) \varrho_{ph',hp'} \\ & + (-1)^{J+1} \varrho_{hh',pp'} (X_{ph}^\omega Y_{p'h'}^\omega + Y_{ph}^\omega X_{p'h'}^\omega) \\ & + X_{ph}^\omega X_{p'h'}^\omega \delta_{hh'} \varrho_{p,p'} + Y_{ph}^\omega Y_{p'h'}^\omega \delta_{pp'} \varrho_{h,h'} \Big). \end{aligned} \tag{4.225}$$

Fallback to HF Density

We will now take a short look at the situation for the case of an HF density. Using the usual relations for this case, we end up with

$$\langle \emptyset_\omega | \emptyset_\omega \rangle = \sum_{ph} \sum_{p'h'} Y^\omega_{ph} Y^\omega_{p'h'} \delta_{pp'} \varrho_{h,h'} \tag{4.226}$$

$$= \sum_{ph} (Y^\omega_{ph})^2. \tag{4.227}$$

This result is not too surprising. In fact this looks very similar to what we saw in (3.55), where we assumed the RPA ground state to be the HF state. In standard RPA (with QBA), the X amplitudes are unproblematic in the sense that they would vanish anyway in case of an HF ground state (ergo the TDA scenario). The Y amplitudes on the other hand produce the residual terms. Therefore, the stronger the Y amplitudes become, the larger the inconsistency and consequently also the zero-norm should be.

Chapter 5

In-Medium (S)RPA

5.1 In-Medium SRG

In a nutshell, in-medium SRG (IM-SRG) can be considered as a synthesis of the basic concepts used in free-space SRG discussed in chapter 2 and the normal-ordering technique (see section 2.3). The term "in-medium" refers to the fact that the SRG evolution is performed directly for a particular A-body system [TBS11] instead in a generic 2B or 3B space. It has proven to be a numerically efficient method for obtaining ground-state energies [Her$^+$13b]. Recent developments also made it possible to use IM-SRG results as input to shell model calculations [Bog$^+$14; TBS12] and to extent its capabilities to open shell nuclei using a multi-reference (MR) formulation of the normal-ordering, which is called MR-IM-SRG [Her$^+$13a; Her$^+$14; GCR16]. Before we get to the topic of IM-(S)RPA in section 5.2, we first give a brief introduction into the IM-SRG.

5.1.1 Basics

Similar to the free-space SRG, IM-SRG uses a continuous unitary transformation of the form

$$\hat{H}(s) = \hat{U}^\dagger(s)\hat{H}_0\hat{U}(s) \tag{5.1}$$

to evolve the initial Hamiltonian, leading to the same the differential flow-equation as for free-space SRG:

$$\frac{\mathrm{d}\hat{H}(s)}{\mathrm{d}s} = [\hat{\eta}(s), \hat{H}(s)]. \tag{5.2}$$

In free-space SRG the goal of this transformation is to decouple high- from low-momentum states. On the one side, this decoupling is necessary in order to improve convergence. On the other side, we do not desire to decouple these states completely, but only up to a certain point in this pre-diagonalization. We know a priori that evolving too far, i.e. towards a total decoupling would basically yield the momentum eigenstates while at the same time the induced terms that stem from the evaluation of the flow-equation would become unsuitably large, pushing all relevant contributions to higher-order interactions. Thus, the emphasis of SRG is clearly on the *pre*-diagonalization, and in practical applications the "optimal point" in terms of a tradeoff between convergence and induction is not easy to determine.

In IM-SRG, we do not decouple momentum scales, but we decouple the reference state itself from all its ph excitations, which is conceptionally different. Since the IM-SRG uses the same

continuous flow mechanics as free-space SRG it also induces higher-order terms that need to be truncated and whose significance has to be assessed. Within IM-SRG, evolving the flow further and further yields a steadily improved degree of decoupling. This decoupling is favorable, but at the same time the induced terms are expected to increase along the flow. Whether the effects of the decoupling actually outweigh the ones of the induced terms is, initially, unclear. It has been found that, in normal-ordered form, a truncation at the level of 2B operators offers a reasonable approximation since substantial contributions are shifted to lower particle ranks [Her$^+$13b]. This is called IM-SRG(2). Note that free-space SRG is universal in the sense that evolution does not have to be repeated for each nucleus, it is performed on the level of the interactions and does not depend on the A-body system. While this saves some computational effort, it also denies the possibility of applying an NO scheme.

In a particle-hole framework, the Hamiltonian can be pictured as consisting of different blocks with respect to ph excitations, see Figure 5.1. The initial Hamiltonian ($s = 0$) is depicted on the left. For a 2B interaction, according to the Slater-Condon rules [Sla29; Con30] the Hamiltonian cannot connect Slater-determinants that differ by more than two single-particle states. The corresponding ph blocks, for example the 0p0h-3p3h or 1p1h-4p4h blocks, vanish identically (colored white). The remaining blocks, e.g. 0p0h-2p2h, have non-vanishing contributions (gray).

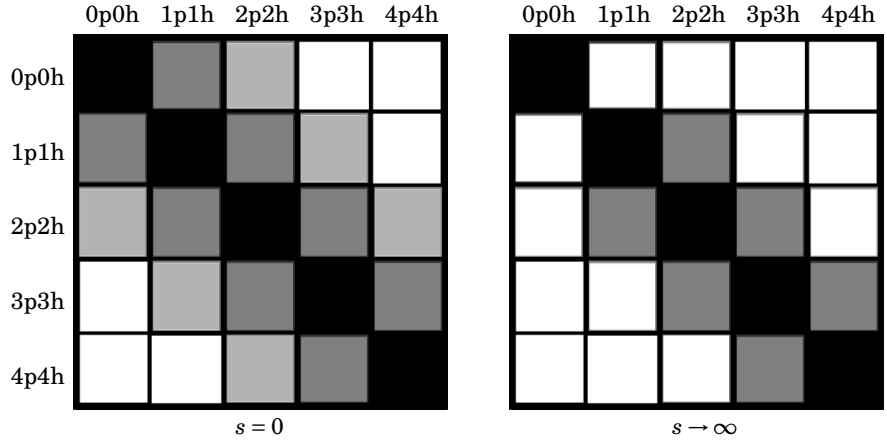

Figure 5.1: IM-SRG Decoupling, figure courtesy of Klaus Vobig.

In order to decouple the reference state we have to suppress all blocks connected to it, so for a 2B Hamiltonian the 0p0h-1p1h and the 0p0h-2p2h blocks which we call the off-diagonal part $\hat{H}^{\mathrm{od}}$. The remaining, diagonal part correspondingly is $\hat{H}^{\mathrm{d}}$ and in total $\hat{H} = \hat{H}^{\mathrm{d}} + \hat{H}^{\mathrm{od}}$. Note that due to the Brillouin theorem, in HF basis the 0p0h-1p1h block given by terms of the sort $\langle\Phi|\,\hat{H}\,|\Phi_h^p\rangle$ would already be zero.

With the Hamiltonian in NO given as

$$\begin{aligned}\hat{H}(s) &= h_0(s) + \hat{h}^1(s) + \hat{h}^2(s) + \hat{h}^3(s) &(5.3)\\ &= E_0(s) + \sum_{i,i'} f_{i,i'}(s)\,\{\hat{a}_i^\dagger \hat{a}_{i'}\} + \frac{1}{4}\sum_{ij,i'j'} \Gamma_{ij,i'j'}(s)\,\{\hat{a}_i^\dagger \hat{a}_j^\dagger \hat{a}_{j'} \hat{a}_{i'}\}\\ &\quad + \frac{1}{36}\sum_{ijk,i'j'k'} W_{ijk,i'j'k'}(s)\,\{\hat{a}_i^\dagger \hat{a}_j^\dagger \hat{a}_k^\dagger \hat{a}_{k'} \hat{a}_{j'} \hat{a}_{i'}\}, &(5.4)\end{aligned}$$

the off-diagonal part can be shown to be [Her$^+$16; Her16]

$$\langle\Phi|\,\hat{H}(s)\,|\Phi_h^p\rangle = f_{h,p}(s), \tag{5.5}$$

$$\langle\Phi|\,\hat{H}(s)\,|\Phi_{h_1h_2}^{p_1p_2}\rangle = \Gamma_{h_1h_2,p_1p_2}(s). \tag{5.6}$$

After the evolution, the Hamiltonian has the form depicted in the right-hand part of Figure 5.1, and the reference state has become the ground state of the evolved Hamiltonian $\hat{H}(\infty)$. In practical applications we will of course stop the evolution at finite s as soon as the off-diagonal part is sufficiently small. For this purpose we can use, e.g., a second order energy correction from perturbation theory [Her$^+$13b; BFS10]. Note that the reason why, e.g., the 1p1h-3p3h vanishes during the evolution is that it consists of the same matrix elements Γ as the 0p0h-2p2h block. To obtain our flow equations, we use the Hamiltonian and our chosen generator and evaluate the commutator using Wick's theorem, giving a set of coupled ordinary differential equations for $E(s), f(s)$ and $\Gamma(s)$.

5.1.2 Generators

Similar to free-space SRG, IM-SRG also exhibits a great flexibility owed to the freedom of choice for the generator of the evolution. Different choices offer alternative approaches to the suppression of the off-diagonal part with varying decoupling behaviour and *decay-scales*, i.e. the amount of steps necessary before the flow sufficiently suppresses those terms. We will briefly remark on three most commonly used generators. For a more detailed discussion on IM-SRG generators see, e.g., [Her$^+$16].

The first is the so-called Wegner generator [Weg94; Weg01] which leads to a monotonic suppression of the off-diagonal part [Weg94]. In terms of numerical efficiency, while showing a rather well-behaved flow, the Wegner generator represents one of the slower choices for $\eta(s)$ [Her$^+$16]. Using this generator, the flow-equations can become quite stiff.

The White generator [Whi02] suppresses all off-diagonal parts equally and produces less stiffness than the Wegner generator. Its computation also requires less computational effort. Unfortunately, due to its definition via a fraction, this generator can become numerically unstable or even undefined.

The imaginary-time generator uses a similar structure as the White generator. The difference to White is that formulation via a fraction is avoided. The imaginary-time generator is not as efficient as the White generator but it also does not suffer from its instabilities [Her$^+$16].

5.1.3 Consistent Evolution of Observables

A severe drawback of IM-SRG in its original formulation (5.2), if we are interested in other quantities than the ground-state energy, lies in the loss of the operator constituting the unitary transformation itself. While in general, other operators can be evolved alongside the Hamiltonian, doing so gives rise to another full set of differential equations analogous to the ones from the Hamiltonian, causing the problem dimension to double [Her$^+$16]. Depending on the generator in use, the numerical errors tend also to accumulate from step to step, making it necessary to use extremely accurate solvers which require vast amounts of memory. Evolving entire sets of operators, as is necessary for a consistent study of various observables, would increase the memory sizes and run times of the IM-SRG transformation accordingly, making this approach rather inapt. Since in RPA are interested not only in the energies of excited states but also in the transition properties of nuclei, the lack of transformed multipole operators poses a problem.

A somewhat different technique to circumvent this problem is the so-called Magnus expansion [Mag54; MPB15; Bla$^+$09]. In short, it utilizes an exponential ansatz $\hat{U}(s) = e^{\hat{\Omega}(s)}$ to obtain the unitary transformation operator. Here the flow equations are formulated and solved for the generator $\hat{\Omega}(s)$ instead of the Hamiltonian. The Hamiltonian itself as well as any other

observables can then be obtained via the application of the Baker-Campbell-Hausdorff formula without increasing the problem size. Work along that path is currently in progress.

5.2 IM-(S)RPA

IM-SRG itself is designed to obtain ground-state energies. Its formalism does not extent to the computation of excited states or transitions directly. The transformed matrix elements that are produced by IM-SRG can, however, be used as the input to second-stage calculations with other methods. As mentioned in the beginning of this chapter, shell model calculations, for example, can benefit from IM-SRG transformed valence-space Hamiltonians [Bog$^+$14; TBS12]. Similarly, IM-SRG could be used as input to RPA in order to address collective excitations.

In the previous sections all RPA calculations, including CC-RPA, have been performed in the HF basis. This has been done for reasons of convergence as well as convenience. In theory though, nothing enforces the use of the HF basis and in principle any basis could be chosen. The HF method offers a basis which is both methodically and computationally relatively easy to obtain. However, HF is a pure mean-field approach to the solution of the many-body problem and, as such, has obvious shortcomings and disadvantages when it comes to precision. For example, it is well known that HF in combination with current chiral interactions produces energies that underbind nuclei considerably, even at the level of 3B forces. At the same time, nuclear radii are still to small, despite the underbinding. These issues directly influence the structure of the HF single-particle spectrum, which in turn has a strong influence on the structure of RPA transition spectra. The basis of IM-SRG transformed matrix elements for example is unknown and, formally, does not have the properties of an HF basis. This is why, in the following, we will briefly revisit the RPA formulae in a generic basis where the matrix elements do not assume a particular form.

5.2.1 Generalization of the Basis

Looking at the derivation of (3.123) for the A matrix, we see that this result would still be valid for any Slater-determinant, even if it is not the HF Slater-determinant. Ergo, we have

$$\begin{aligned}\langle \mathrm{SD}|\, \hat{a}_h^\dagger \hat{a}_p [\hat{H}, \hat{a}_{p'}^\dagger \hat{a}_{h'}]\, |\mathrm{SD}\rangle =& \, t_{p,p'}\, \delta_{hh'} - t_{h',h}\, \delta_{pp'} \\ &+ v_{ph',hp'} + \delta_{hh'} \sum_j^{\text{occ.}} v_{pj,p'j} - \delta_{pp'} \sum_j^{\text{occ.}} v_{h'j,hj} \qquad (5.7)\\ =& \left(t_{p,p'} + \sum_j^{\text{occ.}} v_{pj,p'j} \right) \delta_{hh'} - \left(t_{h',h} + \sum_j^{\text{occ.}} v_{h'j,hj} \right) \delta_{pp'}. \qquad (5.8)\end{aligned}$$

In HF, the terms in parentheses could be abbreviated with the help of the HF single-particle energies

$$\begin{aligned}=& \, \epsilon_p\, \delta_{p,p'} \delta_{hh'} - \epsilon_h\, \delta_{h,h'} \delta_{pp'} \\ &+ v_{ph',hp'}. \qquad (5.9)\end{aligned}$$

If we employ any other basis than HF, the diagonality of the summed 1B terms no longer holds. Of course we can still use a short-hand notation for these terms which simply gives a separate,

non-diagonal 1B quantity:

$$\epsilon_{i,i'} = t_{i,i'} + \sum_{j}^{\text{occ.}} v_{ij,i'j}. \tag{5.10}$$

Note that we use the term *off-diagonal* in the sense of $\hat{H}^{\text{od}}$ for ph terms, whereas we apply the term *non-diagonal* to both pp′ and hh′ terms. The A matrix in a generic basis would thus read:

$$A_{ph,p'h'} = \langle \text{SD}| \hat{a}_h^\dagger \hat{a}_p [\hat{H}, \hat{a}_{p'}^\dagger \hat{a}_{h'}] |\text{SD}\rangle = \epsilon_{p,p'}\, \delta_{hh'} - \epsilon_{h',h}\delta_{pp'} + v_{ph',hp'}. \tag{5.11}$$

We remark that the non-diagonality only appears within the particle and hole blocks, respectively. Off-diagonal terms of the sort $\epsilon_{p,h}$ do not occur, even in a generic basis, as can easily be seen with the help of diagrammatic formalism. We already know that we can obtain the B matrix by interchanging p' with h' in A. This gives

$$B_{ph,p'h'} = \epsilon_{p,h'}\, \delta_{hp'} - \epsilon_{p',h}\delta_{ph'} + v_{pp',hh'} \tag{5.12}$$

$$= v_{pp',hh'}. \tag{5.13}$$

Note that the δ-relations stem from the fact that we still evaluate the RPA terms within a Slater-determinant and have nothing to do the the diagonality of HF.

Extending SRPA to a general basis works analogously. For the A_{22} matrix we simply get non-diagonal contributions, as was the case for A_{11}. Regarding A_{12}, we actually get off-diagonal terms of the sort ϵ_{p_1,h_1}. This can be understood with the help of diagrams, cf. Figure C.1 and Figure C.2. As stated in section C.2, together those diagrams constitute a mean-field term. In HF this term vanished due to the diagonality requirements.

In the following section we will discuss the particular characteristics of the IM-SRG transformed matrix elements and the impact on RPA.

5.2.2 IM-SRG Matrix Elements and Impact on (S)RPA

The specific form of the IM-SRG transformation that suppresses the off-diagonal part of the Hamiltonian leads to some profound consequences for (S)RPA. The chosen decoupling scheme implies in particular that all matrix elements of the sort $v_{pp',hh'}$ are suppressed. These matrix elements are the only ones appearing in the B matrix. Therefore, eliminating those by means of the IM-SRG effectively sets the B matrix to zero. By implication all the Y_{ph}^{ω} amplitudes should vanish and RPA could, therefore, be viewed to be TDA. This is convenient since in TDA there are no de-excitations and thus the ground state does not have to be obtained iteratively, but is equal to the reference state on which the ph excitations are built. Regarding SRPA, the terms ϵ_{p_1,h_1} that would arise in the A_{12} matrix do not contribute because they belong to the off-diagonal part of the Hamiltonian.

The non-diagonal contributions mentioned in the last section actually do appear in RPA calculations after an IM-SRG evolution. This is caused by the fact that IM-SRG enforces only the Brillouin condition, which is a weaker constraint on the 1B structure of the Hamiltonian than HF: Brillouin causes the off-diagonal hp part to disappear, but it does not constrain the hh or pp structure, while HF additionally requires hh and pp diagonality. Therefore, even when starting an IM-SRG calculation in HF basis, the result could have strong off-diagonal mean-field terms. We will see in section 8.4.2 that these HF-breaking contributions tend to be extremely small and do not pose a problem.

Although IM-SRPA represents effectively an IM-STDA, we note that, formally, we will still perform SRPA calculations, but thanks to the small B-terms, we can expect both the energy-weighted and the non-energy-weighted sum rules (cf. section 6.3) to apply. While the changes accompanying the use of IM-SRG transformed matrix elements might seem rather trivial, they actually create a pivotal change: In HF-STDA, we disregard the matrix elements associated with ground-state (de-)excitations. When performing IM-STDA, the same matrix elements are zero anyway, so ignoring them changes nothing. However, it its important to note that their contributions are accounted for implicitly via the IM-SRG transformation. In this sense, IM-SRG is more than a mere, random change of basis. It could be said that the part of the Hamiltonian which HF-STDA neglects is, quite conveniently, made obsolete by the IM-SRG.

Following this line of thought, we also note that STDA is a Hermitian eigenvalue problem and as such cannot have complex eigenvalues, but it can still exhibit unphysical behaviour via the occurrence of negative eigenvalues [PR10]. We will see in section 8.5 that for IM-STDA, and equivalently IM-SRPA, no unphysical solutions are found. Similar to [Pro65], we can find an explanation for this IM-SRG caused stability. The Brillouin's theorem can be derived by means of 1p1h variations against the lowest-energy Slater-determinant. The requirement $\langle\Phi|\,\hat{H}\,|\Phi_h^p\rangle = 0$ results as a necessity for the energy to be stationary. Identically, it follows that if the energy is to be stationary against 2p2h variations, so $\langle\Phi|\,\hat{H}\,|\Phi_{h_1h_2}^{p_1p_2}\rangle = 0$, the corresponding 2p2h matrix elements $v_{p_1p_2,h_1h_2}$ have to be zero.

Chapter 6

Electromagnetic Transitions

We have mentioned before that electromagnetic (EM) transitions are much more sensitive to the detailed form of the wave function than excitation energies. Hence, the calculation and analysis of EM transitions is an excellent instrument for probing the structure of a wave function. In the following, we will address the question of how to compute transitions within the framework of RPA. Our theoretical calculations regarding transitions will be examined and compared to experimental data in chapter 8.

As an introduction, we start with a short review of transitions and standard 1B EM operators. The basic notations and the phase convention we use are in line with the discussion of EM transitions in [Suh07].

6.1 Transition Matrix Elements and Operators

6.1.1 Transition Strengths

The notation for a generic multipole operator is $\hat{T}_{\sigma\lambda}$. Here the quantity σ denotes the transition type (either electric or magnetic) and λ describes its multipolarity. Transition operators are spherical tensors of rank λ with components $\hat{T}_{\sigma\lambda\mu}$, $(\mu = -\lambda \dots \lambda)$. In general, transitions are described via matrix elements in which the corresponding transition operator connects the initial state ω_i with the final state ω_f of the transition, i.e.

$$\langle \omega_f | \, \hat{T}_{\sigma\lambda\mu} \, | \omega_i \rangle. \tag{6.1}$$

Since the angular momentum J of a state is of primary interest for transitions, we introduce a notation where we split the combined quantum numbers of a given state $|\omega_k\rangle$ into two quantum numbers, one being the angular momentum J_k and the other one being a substitute for all the remaining quantum numbers, denoted by ζ_k, i.e. $\omega_k = (\zeta_k, J_k)$.

The *reduced transition probability* or "strength" of a transition from an initial state to a final state is given by

$$B(\sigma\lambda; \zeta_i J_i \to \zeta_f J_f) = \frac{1}{2J_i + 1} |(\zeta_f J_f || \hat{T}_{\sigma\lambda} || \zeta_i J_i)|^2. \tag{6.2}$$

Note that the term probability is somewhat misleading in that B is neither unitsless nor normalized. Here the expression $(\zeta_f J_f || \hat{T}_{\sigma\lambda} || \zeta_i J_i)$ is a so-called *reduced matrix element* which, for

spherical tensor operators such as $\hat{T}_{\sigma\lambda}$, can be defined as

$$(\zeta_f J_f||\hat{T}_{\sigma\lambda}||\zeta_i J_i) = \frac{\sqrt{2J_f+1}}{C(J_i M_i, \lambda\mu|J_f M_f)}\langle\zeta_f J_f M_f|\,\hat{T}_{\sigma\lambda\mu}\,|\zeta_i J_i M_i\rangle \tag{6.3}$$

for arbitrary $M_f = -J_f ... J_f$ and $M_i = -J_i ... J_i$ (as long as $C(J_i M_i, \lambda\mu|J_f M_f) \neq 0$). Relation (6.3) is called the *Wigner-Eckart theorem* (cf. [Eck30; Wig31]). With this and the definition of the tensor product (3.45), we can write the 1B EM operators as

$$\hat{T}_{\sigma\lambda} = \frac{1}{\sqrt{2\lambda+1}}\sum_{jk}(j||\hat{T}_{\sigma\lambda}||k)\,[\hat{a}_j^\dagger\hat{\tilde{a}}_k]_\lambda, \tag{6.4}$$

and its reduced many-body matrix element as

$$(\zeta_f J_f||\hat{T}_{\sigma\lambda}||\zeta_i J_i) = \frac{1}{\sqrt{2\lambda+1}}\sum_{jk}(j||\hat{T}_{\sigma\lambda}||k)(\zeta_f J_f||\,[\hat{a}_j^\dagger\hat{\tilde{a}}_k]_\lambda\,||\zeta_i J_i). \tag{6.5}$$

Note that $(\zeta_f J_f||\hat{T}_{\sigma\lambda}||\zeta_i J_i)$ describes the transition between the many-body states ω_f and ω_i, whereas the expression $(j||\hat{T}_{\sigma\lambda}||k)$ denotes the reduced 1B matrix element between two single-particle states j and k. We note that for the reduced matrix elements of spherical tensor operators the symmetry rule

$$(\zeta J||\hat{T}_J||\zeta' J') = (-1)^{J-J'}(\zeta J'||\hat{T}_J||\zeta J)^* \tag{6.6}$$

applies. For non-scalar tensors, we have both Hermiticity and anti-Hermiticity, depending on the difference of the angular momenta. The case of scalar tensors reduces to the usual Hermiticity rule since $J = J'$ always yields a positive phase factor.

So far we merely stated that the EM operators are 1B quantities. In the next section, we specify the electric and magnetic operator and discuss how to compute reduced transition probabilities for the electromagnetic transition operators.

6.1.2 EM Transition Operators

We already stated that σ denotes the transition type, either electric or magnetic, and commonly in case of an electric transition we also write $\hat{T}_{\mathrm{E}\lambda} \equiv \hat{Q}_\lambda$, analogously for magnetic transitions we denote $\hat{T}_{\mathrm{M}\lambda} \equiv \hat{M}_\lambda$, respectively. They can be written as

$$\hat{Q}_{\lambda\mu} = \sum_{i=1}^{A} e_i \hat{r}_i^\lambda Y_{\lambda\mu}(\hat{\Omega}_i), \tag{6.7}$$

$$\hat{M}_{\lambda\mu} = \frac{\mu_\mathrm{N}}{\hbar c}\sum_{i=1}^{A}\left(\frac{2}{\lambda+1}g_i^l\hat{l}_i + g_i^s\hat{s}_i\right)\cdot\nabla(\hat{r}_i^\lambda Y_{\lambda\mu}(\hat{\Omega}_i)). \tag{6.8}$$

Relation (6.7) and (6.8) are both given in Condon-Shortley phase convention (cf. [Suh07; RS80; HV01]). The sums run over all A particles inside the nucleus, the quantity e_i denotes the charge of the nucleon i. The quantities g_i^l and g_i^s are the *gyromagnetic factors* of the orbital angular momentum $\hat{l}_i$ and spin $\hat{s}_i$, respectively. Note that radial coordinates $\hat{\vec{r}}_i$ are defined relative to the center-of-mass (CM) of the nucleus. In a laboratory frame we can define the CM coordinate of our A-body system to be $\hat{\vec{X}}_\mathrm{CM}$ and the absolute coordinate of the nucleon i to be $\hat{\vec{x}}_i$, thus $\hat{\vec{r}}_i = \hat{\vec{x}}_i - \hat{\vec{X}}_\mathrm{CM}$. With the relative coordinates defined as differences of absolute coordinates, the EM operators are formally translational invariant. We will revisit this issue later on.

From the definition of the electric transition operator and the definition of the reduced transition probability (6.2), we can conclude that the units of the reduced transition probabilities $B(\mathrm{E}\lambda)$ are

$$[B(\mathrm{E}\lambda)] = e^2\,\mathrm{fm}^{2\lambda}, \tag{6.9}$$

And similarly, for the magnetic operator (6.8) we find

$$[B(\mathrm{M}\lambda)] = \left(\tfrac{\mu_\mathrm{N}}{c}\right)^2 \mathrm{fm}^{2(\lambda\,-\,1)}. \tag{6.10}$$

Note that in this thesis, we will only compute electric transitions. The equations for magnetic transitions are given for completeness.

At this point, it is convenient to introduce a new notation. In order to keep the following equations more lucid, we write

$$\hat{\hat{\lambda}} = \sqrt{2\lambda + 1} \tag{6.11}$$

for the square root of the multiplicity. From the above we see that the EM operators carry both a radial and an angular part. With (6.7) for the electric operator, we find (cf. [Suh07])

$$(a||\hat{Q}_\lambda||b) = \frac{e}{\sqrt{4\pi}}(-1)^{j_b+\lambda-\frac{1}{2}}\frac{1+(-1)^{l_a+l_b+\lambda}}{2}\hat{\hat{\lambda}}\hat{\hat{j}}_a\hat{\hat{j}}_b \begin{pmatrix} j_a & j_b & \lambda \\ \frac{1}{2} & -\frac{1}{2} & 0 \end{pmatrix} \mathcal{R}^{(\lambda)}_{ab}, \tag{6.12}$$

with

$$\mathcal{R}^{(\lambda)}_{ab} = \int_0^\infty g_{n_a l_a}(r)\, r^\lambda\, g_{b_b l_b}(r)\, r^2\,\mathrm{d}r. \tag{6.13}$$

The radial wave functions $g_{nl}(r)$ are the harmonic oscillator wave functions. Likewise, for the magnetic operator (6.8) we get

$$\begin{aligned}(a||\hat{M}_\lambda||b) = \frac{\mu_\mathrm{N}}{c\sqrt{4\pi}}(-1)^{j_b+\lambda-\frac{1}{2}}\frac{1-(-1)^{l_a+l_b+\lambda}}{2}\hat{\hat{\lambda}}\hat{\hat{j}}_a\hat{\hat{j}}_b \begin{pmatrix} j_a & j_b & \lambda \\ \frac{1}{2} & -\frac{1}{2} & 0 \end{pmatrix} \\ \times\,(\lambda-\kappa)\left(g_l\left(1+\frac{\kappa}{\lambda+1}\right)-\frac{1}{2}g_s\right)\mathcal{R}^{(\lambda-1)}_{ab},\end{aligned} \tag{6.14}$$

with

$$\kappa = (-1)^{l_a+j_a+\frac{1}{2}}(j_a+\tfrac{1}{2}) + (-1)^{l_b+j_b+\frac{1}{2}}(j_b+\tfrac{1}{2}). \tag{6.15}$$

Again, relation (6.12) and (6.14) are both given in Condon-Shortley phase convention.

It is important to realize that the above 1B expressions are only valid if the multipole operators are indeed 1B quantities. However, with the definition of the relative coordinates as $\hat{\vec{r}}_i = \hat{\vec{x}}_i - \hat{\vec{X}}_\mathrm{CM}$, this is not the case. The reason for this is that the CM coordinate of the nucleus as a whole, $\hat{\vec{X}}_\mathrm{CM}$, enters the equation. The translational invariant formulation of the EM operators, thus, produces an A-body operator. For the moment we postpone any further discussions of this issue and merely state a connection between the above approximation and the topic of isospin decomposition addressed in the next section.

We also note that if we transform the Hamiltonian, e.g. by either SRG or IM-SRG, then for a consistent description of transitions we would have to transform the transition operators, too. Regarding SRG, we first have to transform the operator into the 2B system. This reformulation into Jacobi coordinates can be done quite easily for both the monopole and quadrupole operator,

cf. e.g. [Ste+05; Paa+06]. The changes between bare transition operators and their consistently transformed 2B versions have been found to be small. Therefore, in this thesis we will limit our calculations to 1B transition operators.

We also note that research is underway to include two-body EM currents from χEFT consistently [PSG08; Pas+09; Bar+16].

6.1.3 Isospin Decomposition

It is known that different excitation mechanisms do not randomly excite a nucleus but instead follow specific patterns. Empirically, we find that protons and neutrons tend to perform the same motions, either in phase or out of phase. In order to transfer this structure to our previously defined multiple operators, we will examine their mathematical expression and rewrite the operators so as to represent this feature. We limit ourselves to the discussion of the electric multipole operator, since we will only be calculating electric transition strengths, but in principle similar considerations could be done for the magnetic multipole operator. After the reformulation we will discuss the above-mentioned relation to experiment in more detail.

Taking a closer look at the electric multipole operator as written in (6.7), we see that it can be decomposed into two operators, one containing the contribution of all the protons and the other one containing the contributions of all the neutrons. This partitioning into protonic (π) and neutronic (ν) parts is done by simply splitting the sum accordingly, as can be seen below

$$\hat{Q}_{\lambda\mu} = \sum_{i=1}^{A} e_i \hat{r}_i^\lambda Y_{\lambda\mu}(\hat{\Omega}_i) \tag{6.16}$$

$$= \sum_{\pi=1}^{Z} e_\pi \hat{r}_\pi^\lambda Y_{\lambda\mu}(\hat{\Omega}_\pi) + \sum_{\nu=1}^{N} e_\nu \hat{r}_\nu^\lambda Y_{\lambda\mu}(\hat{\Omega}_\nu) \tag{6.17}$$

$$= \hat{Q}^\pi_{\lambda\mu} + \hat{Q}^\nu_{\lambda\mu}. \tag{6.18}$$

Note that such a decomposition is of course possible for any 1B operator. Since neutrons have no charge ($e_\nu = 0$), the above can be written as

$$\hat{Q}_{\lambda\mu} = \hat{Q}^\pi_{\lambda\mu} = e \sum_{\pi=1}^{Z} \hat{r}_\pi^\lambda Y_{\lambda\mu}(\hat{\Omega}_\pi), \tag{6.19}$$

where we also set $e_\pi = e$. However, we already know that with ensuring translational invariance, the EM operators become A-body operators. The involvement of all particles, including neutrons, motivates the introduction of parameters to correctly capture all contributions. We, therefore, define

$$\hat{Q}^\pi_{\lambda\mu}(e_\nu) = e_\nu \sum_{\nu=1}^{N} \hat{r}_\nu^\lambda Y_{\lambda\mu}(\hat{\Omega}_\nu), \quad \hat{Q}^\nu_{\lambda\mu}(e_\pi) = e_\pi \sum_{\pi=1}^{Z} \hat{r}_\pi^\lambda Y_{\lambda\mu}(\hat{\Omega}_\pi). \tag{6.20}$$

With this, we can rewrite the EM operator as

$$\hat{Q}_{\lambda\mu} = \frac{1}{2}\left(\hat{Q}^\pi_{\lambda\mu}(e_\pi) + \hat{Q}^\nu_{\lambda\mu}(e_\nu)\right) + \frac{1}{2}\left(\hat{Q}^\pi_{\lambda\mu}(e_\pi) - \hat{Q}^\nu_{\lambda\mu}(e_\nu)\right) \equiv \frac{1}{2}\left(\hat{Q}^{\mathrm{IS}}_{\lambda\mu} + \hat{Q}^{\mathrm{IV}}_{\lambda\mu}\right). \tag{6.21}$$

This reformulation gives two electric operators, the first one describes so-called *isoscalar* (IS) transitions and the second one *isovector* (IV) transitions. In the following we will discuss the connection to the physical nature of transitions.

In a macroscopic picture, isoscalar transitions can be viewed as a motion of the nucleus in which the protons and neutrons collectively oscillate in phase. The electric transition operator for an isoscalar transition can hence be written as

$$\hat{Q}^{\mathrm{IS}}_{\lambda\mu} = \hat{Q}^{\pi}_{\lambda\mu}(e_\pi) + \hat{Q}^{\nu}_{\lambda\mu}(e_\nu). \tag{6.22}$$

A prominent example for such a mode is the isoscalar giant monopole resonance (ISGMR or ISM), also called "breathing" or "compressional" mode, in which the protons and neutrons perform a radial oscillation.

From an experimental point of view, in order to excite isoscalar modes, we also need an "isoscalar probe", that is to say a probe that couples to the protons and the neutrons alike. Such a probe is, e.g., given by α-particles [Van$^+$15], since those interact with the nucleus mainly via the strong force and consequently influence both protons and neutrons likewise. In such a case, the charge of the nucleons is hardly relevant. It can further be shown (cf. [Suh07]) that isoscalar modes can only connect states with identical isospin, i.e., $\Delta T_{\mathrm{IS}} = 0$.

Similarly, isovector transitions can be interpreted as modes in which the protons move collectively against the neutrons, i.e., they are oscillating out of phase, which motivates to the following formula for the isovector transition operator:

$$\hat{Q}^{\mathrm{IV}}_{\lambda\mu} = \hat{Q}^{\pi}_{\lambda\mu}(e_\pi) - \hat{Q}^{\nu}_{\lambda\mu}(e_\nu). \tag{6.23}$$

Thus, if we want to examine isovector transitions, we will need a probe that acts differently on protons and on neutrons. An obvious choice would be electrons (cf. e.g. [Str$^+$00]), since those only interact with the protons via the electromagnetic interaction, but not with the uncharged neutrons. Note that it can be shown that isovector transitions connect states with different isospin, i.e., $\Delta T_{\mathrm{IV}} = 1$.

Macroscopic View on Collective Modes

In our upcoming discussion on transitions we will limit ourselves to the cases of the isoscalar monopole (ISM), the isovector dipole (IVD) as well as the isoscalar quadrupole (ISQ) transitions. We note that the calculation of other multipole transitions of electric or magnetic nature would be possible as well. For the mentioned transitions we give a short idea of what they would look like in a macroscopic interpretation. A more detailed description of these and other transitions can be found, e.g., in [HV01].

As already mentioned, the ISM can be pictured as a compressional mode in which protons and neutrons oscillate radially in phase. This mode is of significant importance, since its excitation energy correlates to the incompressibility of nuclear matter (cf. e.g. [Kou$^+$96; YCL99]). Analogously, in the IV monopole mode protons and neutrons contract and expand in an alternating pattern. Note that such a mode does not lead to an overall compression of the nucleus.

The IVD represents a mode in which all the protons move collectively against all the neutrons. As is typical for dipoles, the oscillation is of one-dimensional nature. This causes a separation between the center-of-mass and the center-of-charge within the nucleus [HV01; GT48]. Similar to the ISM, the IS dipole mode is also a compressional mode associated with a density oscillation, which is caused by protons and neutrons oscillating in phase back and forth through the nucleus (cf. e.g. [Dea73; HD81; Miş06]). In contrast to the ISM, the volume of the nucleus stays unchanged.

In the last investigated transition, the ISQ, the neutrons and protons again oscillate in phase. However, in contrast to the ISM, the ISQ is no radial oscillation but rather a quadrupole deformation, i.e., both protons and neutrons deform the nucleus alternately into an oblate and prolate

shape. The IV quadrupole mode would correspond to an out-of-phase quadrupole deformation, so at a certain point when the neutrons assume prolate shape, the protons take oblate shape and vice versa.

We stress that these macroscopic pictures only apply to collective modes were all nucleons are involved. Low-lying excited states usually do not show a collective behaviour.

6.1.4 Translational Invariance and Effective Charges

In short, for the IS transition operator we add the neutronic and protonic parts, while for the IV operators we subtract them to accommodate their phase relations relative to each other. For the IS case we already gave a physical motivation for why neutrons will contribute equally to such transitions, despite carrying no charge.

Regarding IV modes, we already have an idea of their nature from a physical point of view, but so far we did not clarify how neutrons are able to contribute to these modes in the first place. In order to see this, we will use the IVD mode. In this case, when the protons interact with an EM field, they start to move back and forth. Within the CM system, in which our transition operators are defined, the neutrons will automatically assume opposite momenta. This results in a vanishing total momentum of the nucleus, as required by momentum conservation. Complementary, we can argue that if the protons start to move, the center-of-mass changes, and as a consequence the position of all particles in the CM frame changes according to $\hat{\vec{r}}_i = \hat{\vec{x}}_i - \hat{\vec{X}}_{\mathrm{CM}}$. So even if the external probe, e.g. an electron, couples only to the protons we see that, in the CM system, both protons and neutrons are affected.

With this in mind, we conclude that the neutronic contribution does not vanish, in contrast to what (6.7) might naively suggest. However, this becomes evident only if we do not neglect the corresponding CM relations of the A-body system. If we want to avoid this, the canonical alternative is to think of 1B operators with so-called "effective charges" e_{eff} for the neutrons and protons to accommodate the physical properties of the different modes. These effective charges are, therefore, rather meant to reflect the nature of the excitation process. Together with the isoscalar and isovector operators discussed earlier, we define

$$e^{\pi}_{\mathrm{eff}} = e^{\nu}_{\mathrm{eff}} = 1e, \tag{6.24}$$

i.e. we have $e_i = e \ \forall i$.

6.1.5 Special Cases of Transition Operators

Now that we have established the concept of effective charges, we note that there are a few exceptions to the rules. For the monopole transition ($\Delta\lambda = 0$) the electric transition operator as in (6.7) is simply a constant and thus cannot connect two different states. That is why for monopole transitions we will not use the general form of the multipole operator but instead the subleading term of the multipole expansion, given by

$$\hat{Q}_{00} = e \sum_{i}^{A} \hat{r}_i^2 Y_{00}(\hat{\Omega}_i), \tag{6.25}$$

will be used. The corresponding units are $e^2\,\mathrm{fm}^4$ for the reduced matrix elements $B(\mathrm{E0})$.

The second exception are dipole transitions. Although these can, in principle, be described via the general multipole operator (6.7), both IS and IV dipole transitions are often subject to

CM contaminations. In fact, for the 1B form of the operators which we employ, the leading IS dipole operator is even proportional to the CM coordinate, which is why, again, we will use the subleading term. This is in agreement with the macroscopic picture given above: If protons and neutrons move axially and in phase, this is simply a translational motion with no intrinsic component. In order to correct for the remaining spurious CM contributions within the subleading term, we will use the following transition operator (cf. e.g. [Erl12; VS81; HD81; Dea73]) for the isoscalar transition:

$$\hat{Q}^{\mathrm{IS}}_{1\mu} = e\sum_{i}^{A}\left(\hat{r}_i^3 - \tfrac{5}{3}R_{\mathrm{ms}}\hat{r}_i\right)Y_{1\mu}(\hat{\Omega}_i), \tag{6.26}$$

with the mean-square radius R_{ms}. For the IV dipole operator the leading contribution can still be used since it is not purely translational in character. We have, however, to adjust our effective charges to compensate the spurious parts according to [RS80]

$$\hat{Q}^{\mathrm{IV}}_{1\mu} = e\frac{N}{A}\sum_{i}^{Z}\hat{r}_i Y_{1\mu}(\hat{\Omega}_i) - e\frac{Z}{A}\sum_{i}^{N}\hat{r}_i Y_{1\mu}(\hat{\Omega}_i). \tag{6.27}$$

This modification effectively sets the strength of spurious solutions to zero. We note that the above CM spuriosities only occur due to the fact that our basis violates translational symmetry. If our basis would be in accordance with translational invariance, no spurious contributions would arise.

6.2 Transitions in RPA

Within RPA (and its extensions), a general transition matrix element can be written as

$$\begin{aligned} R^{(0\omega)} &= \langle \mathrm{RPA}|\, \hat{T}_{\lambda\mu}\, |\omega\rangle && (6.28)\\ &= \langle \mathrm{RPA}|\, \hat{T}_{\lambda\mu}\, \hat{Q}^{\dagger}_{\omega}\, |\mathrm{RPA}\rangle && (6.29)\\ &= \langle \mathrm{RPA}|\, [\hat{T}_{\lambda\mu}, \hat{Q}^{\dagger}_{\omega}]\, |\mathrm{RPA}\rangle\,, && (6.30) \end{aligned}$$

independently of the transition operator $\hat{T}_{\lambda\mu}$ or the definition of $\hat{Q}^{\dagger}_{\omega}$. Here we have used relation (3.32) introducing a commutator within expectation values, effectively reducing the rank of the operator under consideration and thus the computational as well as formalistic effort, as usual in RPA-related formulae.

In standard RPA, the state for the expectation value has so far been given by the HF state as a consequence of the QBA. When using CC-RPA, we have to employ the CC ground state in order to achieve a consistent description.

We note that for an up-to 2B transition operator in conjunction with SRPA, we would get different types of terms for the transitions. Classifying them by their operator rank and origin, we can call the transition operator 1B part T1 and the 2B part T2. Similarly, the 1B and 2B parts of the excitation operator in SRPA will be denoted by Q1 and Q2, respectively. With this, the standard RPA transition would simply be the T1-Q1 term. For a 1B transition within SRPA, we would thus get the additional T1-Q2 term. Vice versa, the 2B part of the transition operator within RPA produces the term T2-Q1, and finally this same operator within the SRPA extension gives rise to the T2-Q2 term. With the knowledge that the commutator reduces the rank of the operator product by one, we see immediately that for T1-Q1 part a 1B density suffices for the description. Both T1-Q2 and T2-Q1 require a 2B density for a full evaluation

of the resulting expression. Expectably, the last term T2-Q2 can only be fully computed if a 3B density is available. As of today, due to a lack of correlated 3B densities the T2-Q2 term can only be evaluated in HF-SRPA. We also know that the term T1-Q2 cannot yield non-zero contributions within HF-SRPA since this corresponds to a 1B operator connecting the HF state and a 2p2h excitation of the same. This term would contribute, e.g., in CC-SRPA.

We will now compute the transition strengths for a generic state, represented by its density matrices. With the above, we only need to look into the case of a simple 1B transition operator in combination with a 1B excitation operator, i.e., the T1-Q1 case. Using the above basic form for the calculation of transition matrices within RPA, staying in an uncoupled formulation this translates to

$$\begin{aligned} R^{(0\omega)} &= \langle \mathrm{RPA}| \hat{T}_{\lambda\mu} |\omega\rangle && (6.31)\\ &= \sum_{ii'} \langle i| \hat{T}_{\lambda\mu} |i'\rangle \langle \mathrm{RPA}| \hat{a}_i^\dagger \hat{a}_{i'} |\omega\rangle && (6.32)\\ &= \sum_{ii'} t_{ii'}^{\lambda\mu} \langle \mathrm{RPA}| \hat{a}_i^\dagger \hat{a}_{i'} |\omega\rangle && (6.33)\\ &= \sum_{ii'} t_{ii'}^{\lambda\mu} \varrho_{i'i}^{(0\omega)} = \sum_i (T_{\lambda\mu}\varrho)_{ii} = \mathrm{Tr}(T_{\lambda\mu}\varrho^{(0\omega)}), && (6.34) \end{aligned}$$

with the 1B transition density matrix $\varrho^{(0\omega)}$ as introduced in section 4.1.4. The transition density can be calculated with relation (4.126). We find

$$\begin{aligned} \varrho_{i'i}^{(0\omega)} &= \langle \mathrm{RPA}| \hat{a}_i^\dagger \hat{a}_{i'} |\omega\rangle = \langle \mathrm{RPA}| \hat{\mathcal{A}}_{ii'}^\dagger \hat{Q}_{1,\omega}^\dagger |\mathrm{RPA}\rangle && (6.35)\\ &= \langle \mathrm{RPA}| [\hat{\mathcal{A}}_{ii'}^\dagger, \hat{Q}_{1,\omega}^\dagger] |\mathrm{RPA}\rangle && (6.36)\\ &= \sum_{ph} \left(X_{ph}^\omega \langle \mathrm{RPA}| [\hat{\mathcal{A}}_{ii'}^\dagger, \hat{\mathcal{A}}_{ph}^\dagger] |\mathrm{RPA}\rangle - Y_{ph}^\omega \langle \mathrm{RPA}| [\hat{\mathcal{A}}_{ii'}^\dagger, \hat{\mathcal{A}}_{ph}] |\mathrm{RPA}\rangle \right) && (6.37)\\ &= \sum_{ph} \left(X_{ph}^\omega (\delta_{pi'}\varrho_{h,i} - \delta_{hi}\varrho_{p,i'}) - Y_{ph}^\omega (\delta_{hi'}\varrho_{p,i} - \delta_{pi}\varrho_{h,i'}) \right). && (6.38) \end{aligned}$$

We see that in CC-RPA we can use the densities to include correlations both in the Hamiltonian and in the transitions. As mentioned before, IM-RPA relates to a change of basis. The correlations are built into the matrix elements of the Hamiltonian by a unitary transformation. While this provides many advantages such as the simplicity of the IM-RPA formalism, it poses a problem for the description of transitions. In IM-RPA, by construction we do not have a correlated density and, thus, cannot include the correlations as shown above. Instead, similar to the Hamiltonian we will have to transform the EM operators themselves. Since as of today no IM-SRG transformations for tensor operators are available, we are forced to use untransformed operators. This poses an inconsistency in the description of transitions. We will discuss this issue further in section 8.4.2.

6.3 Sum Rules

6.3.1 Energy-Weighted Sum Rule (EWSR)

It can be shown (cf. e.g. [Suh07]) that the RPA obeys the *energy-weighted sum rule* (EWSR). The EWSR for the RPA is given by

$$\sum_\omega E_\omega^{\mathrm{RPA}} |(\omega||\hat{T}_{\sigma\lambda}||\mathrm{RPA})|^2 = \tfrac{1}{2}\hat{\hat{\lambda}}^2 \langle \mathrm{RPA}| [\hat{T}_{\sigma\lambda\mu}^\dagger, \hat{H}, \hat{T}_{\sigma\lambda\mu}] |\mathrm{RPA}\rangle . \quad (6.39)$$

Here we used the symmetrized double commutator, defined as

$$[\hat{A}, \hat{B}, \hat{C}] \equiv \frac{1}{2}\left([\hat{A}, [\hat{B}, \hat{C}]] + [[\hat{A}, \hat{B}], \hat{C}]\right). \tag{6.40}$$

Taking a closer look at the left-hand side of (6.39), we can see that, for a given multipole operator $\hat{T}_{\sigma\lambda}$, it only depends on the RPA results ($|\text{RPA}\rangle$, $|\omega\rangle$, E_ω^{RPA}). Similarly, the right-hand side of (6.39) depends only on quantities which are input to RPA ($|\text{HF}\rangle$, $\hat{H}$). This input vs. output structure allows us to perform a crosscheck of the RPA implementation by evaluating both sides individually and comparing the values from the input-side with the ones from the output-side. If the comparison between the input- and the output-side fails, we know that there has to be a mistake within the RPA calculations. A more useful expression for the actual implementation of the EWSR might be (cf. [Suh07])

$$\sum_\omega E_\omega^{\text{RPA}} |(\omega||\hat{T}_{\sigma\lambda}||\text{RPA})|^2 = {p^\lambda}^{\text{T}} \left(A - (-1)^\lambda B\right) p^\lambda, \tag{6.41}$$

with:

$$p_{ij}^\lambda = (-1)^\lambda (i||\hat{T}_{\sigma\lambda}||j). \tag{6.42}$$

This form of the EWSR is convenient because the evaluation of the double commutator is no longer required. Note that the Hamiltonian enters the input-side via the matrices A and B.

Since the 2B part of $\hat{Q}_\omega^\dagger$ does not contribute any strength when using a 1B transition operator and the HF state, we note that the EWSR is valid in both HF-RPA and HF-SRPA (cf. also [Yan87; AL88]). We call to mind that in SRPA we cannot compute all solutions of the SRPA eigenvalue problem due to the large sizes. Usually we only compute a small fraction of the spectrum. The unknown, high-lying solutions of course also carry a certain amount of the total strength. Therefore, in SRPA the EWSR can additionally be used to determine the fraction of the energy-weighted strength that the known subset of eigenvalues carries. We stress the energy-weighted strength is to be distinguished from the unweighted strength (see also section 6.3.2 below).

Due to its mathematical form the EWSR is sometimes also referred to as the first moment m_1.

6.3.2 Non-Energy-Weighted Sum Rule (NEWSR)

It can be shown [Suh07] that the TDA, and with the same reasoning as before also the STDA, obeys the non-energy-weighted sum rule (NEWSR). It reads

$$\sum_\omega |(\omega||\hat{T}_{\sigma\lambda}||\text{HF})|^2 = \sum_{i,j} |(i||\hat{T}_{\sigma\lambda}||j)|^2. \tag{6.43}$$

Keep in mind that, as pointed out in section 3.2.6, the TDA ground state is given by $|\text{HF}\rangle$. In general the NEWSR does not apply to (S)RPA. However, when discussing IM-SRPA we already stated that the use of an IM-transformed Hamiltonian effectively reduces RPA to TDA calculations. As a consequence, if we formally perform (S)RPA calculations but employ IM-SRG matrix elements both the EWSR and the NEWSR should be valid within reasonable accuracy. The NEWSR has the advantage that in second-order calculations, where we know only a subset of all eigenvalues, it directly corresponds to the strength fraction carried by that subset. We will see that this is quite useful for IM-SRPA. Similar to the case of the EWSR, the NEWSR is also called the m_0-moment.

6.4 Lorentz Curves

As mentioned before, the transition strength that we can compute from the results of an RPA calculation form a discrete distribution, i.e., we get one strength value for each eigenstate $|\omega\rangle$ (cf. (6.31)). We note that experimental data are always continuous distributions. For low-lying, discrete peaks this is due to a limited energy resolution. Regarding higher excitation energies above the neutron separation threshold, the resonances themselves represent a continuum. For an easier comparison it is convenient to build a continuous *strength function* from the discrete theoretical values. This is done by folding the discrete distribution of transition strengths with a *Lorentz curve*. The formula for such a Lorentz function is given by

$$L(E) = \frac{A\Gamma}{((E - E_0)^2 + \Gamma^2)\pi}. \tag{6.44}$$

It describes a peak-like shape centered around E_0 with an amplitude parameter A and a width parameter Γ that has the same units as the energy. However, the maximal height, which is achieved at $E = E_0$, is in fact not A but rather $\frac{A}{\Gamma\pi}$. This is inconvenient when plotting the discrete data points together with the continuous distribution, e.g., for an investigation of the fragmentation. Additionally, the Lorentz curve as in (6.44) changes the units of the discrete data points A, since $[L] = \frac{[A]}{[\Gamma]} = \frac{[A]}{\mathrm{MeV}}$. Therefore, we will always multiply the standard Lorentz curve L as stated above by a factor of $\Gamma\pi$. We will refer to this function

$$\tilde{L}(E) = \frac{A\Gamma^2}{(E - E_0)^2 + \Gamma^2} \tag{6.45}$$

as the modified Lorentz curve. This modified version has the same amplitudes and units as the original, discrete data points. The strength functions which will be shown have been computed with a width parameter of $\Gamma = 1\,\mathrm{MeV}$.

Chapter 7

Ground-State Results

Before we discuss collective excitations in the next chapter, we review certain ground-state properties. We investigate the doubly magic nuclei ^{16}O, ^{24}O, ^{40}Ca, ^{48}Ca, ^{56}Ni, ^{68}Ni and ^{78}Ni, covering three isotopic chains spanning the regime of medium-mass nuclei. We start out with a technical explanation regarding the size of our model space.

7.1 Model Space and Interactions

In this section we will discuss the model space we use and its truncations. It is important to understand these parameters for the discussion of convergence in chapter 8. The naming convention introduced here is consistent with the one used in the code.

- **eMax**: This quantity specifies the maximum value which a single principal quantum number e can take on. It represents a truncation in the SP HO basis and determines the size of the model space. An additional truncation parameter of the SP basis is lMax. It gives the maximum value for the orbital angular momentum l of a SP state. With $e = 2n + l$, where n denotes the radial quantum number, this means that l can get as large as e (for $n = 0$).
- **E3Max**: This quantity limits the total principal quantum number of a 3B matrix element $\langle e_1 e_2 e_3 | \hat{O} | e_1' e_2' e_3' \rangle$ for some operator $\hat{O}$, i.e., $e_1 + e_2 + e_3 \leq$ E3Max has to be fulfilled.

The standard set of parameters that we will use for the calculations is eMax = 12, lMax = 10 and E3Max = 14.

In this thesis we will employ two different chiral interactions. The first interaction is the non-local 2B interaction derived by Entem and Machleidt [EM03] up to the fourth order (N^{3}LO), supplemented by local 3B force at third order (N^{2}LO) [Nav07]. The momentum cutoff for the 2B interaction is 500 MeV and that for the 3B force is 400 MeV, see [Rot$^+$12]. In short we call this interaction the EM400. This interaction has been used in numerous applications with great success. However, it is known to significantly underestimate nuclear charge radii.

The second interaction that we use is the N^{2}LO$_{\text{sat}}$ interaction [Eks$^+$15], which in short we will call SAT. It is consistently derived up to N^{2}LO for both the 2B and the 3B force. Different from the EM400, it is obtained via a simultaneous fitting of the LECs together for the NN and 3N force. In addition, the fit also includes data of heavier nuclei, namely binding energies and charge radii of carbon and oxygen isotopes are employed. The SAT interaction produces similar

results for ground-state energies, but yields substantially larger radii. For the SAT interaction we use a harmonic-oscillator frequency of $\hbar\Omega = 22\,\mathrm{MeV}$ and for the EM400 we use $\hbar\Omega = 24\,\mathrm{MeV}$.

We note that, in the past, for numerical applications of RPA most commonly either phenomenological interactions [PRP07; Pap$^+$12; GPR14] or density-functional theories [TS04; GGC10; Gam$^+$12; Col$^+$13; Tse13] have been employed.

7.2 Ground-State Energies and Charge Radii

Since the RPA calculations are built on different ground-state methods, namely HF, IM-SRG and CCSD, in this section we will investigate how these methods compare on the level of ground-state properties. For this purpose we will examine the ground-state energy E_0 and the charge radius r_{ch}. In Table 7.1 we summarize the experimental values for both quantities, where available.

Nucleus	E_0	r_{ch}
^{16}O	-127.6	2.70
^{24}O	-169.0	
^{40}Ca	-342.0	3.48
^{48}Ca	-416.0	3.48
^{56}Ni	-484.0	
^{68}Ni	-590.4	
^{78}Ni	-641.8	

Table 7.1: Experimental values for the investigated nuclei. The ground-state energies E_0 (given in MeV) are taken from [Wan$^+$12] and the charge radii r_{ch} (given in fm), where available, from [AM13].

7.2.1 Ground-State Energies

We start with a comparison of the ground-state energies. In Table 7.2 we have listed the corresponding values from NN+3N calculations for the SAT interaction with an SRG flow parameter of $\alpha = 0.08\,\mathrm{fm}^4$. For this interaction, both IM-SRG and CCSD tend to slightly overbind the nuclei, though CCSD gives a marginally smaller binding energy for ^{68}Ni and ^{78}Ni as compared to experiment. The overall agreement among these methods and also the experimental values is quite good. The comparison to HF shows a strong underbinding across the investigated nuclei. This is no surprise as HF does not contain correlations, which yield a substantial part of the ground-state energy. By itself, we do not expect HF to give meaningful ground-state energies. However, the HF values are useful as a tool for estimating the fraction of the ground-state energy that, for a given "softness" of the interaction (see below), can be attributed to correlations beyond the HF level.

In Table 7.3 we see the comparison for the same methods as before, but this time with an SRG flow parameter of $\alpha = 0.04\,\mathrm{fm}^4$. This interaction is less "soft", i.e., the SRG flow which determines the progress of the pre-diagonalization is not as far advanced. For all three methods we observe a decrease in binding energy. While the results from IM-SRG and CC decrease only by a few percent, we see that for the HF method the change is quite severe. The correlations within CCSD and IM-SRG can largely compensate this harder interaction. Regarding HF, the lack of correlations prevents this, causing a much slower convergence.

Nucleus	HF	IM-SRG	CCSD	Expt.
^{16}O	-100.5	-136.8	-133.0	-127.6
^{24}O	-135.7	-186.7	-182.5	-169.0
^{40}Ca	-263.5	-366.6	-353.4	-342.0
^{48}Ca	-331.1	-447.5	-436.6	-416.0
^{56}Ni	-372.0	-516.3	-502.4	-484.0
^{68}Ni	-434.9	-595.4	-584.2	-590.4
^{78}Ni	-466.4	-643.2	-631.5	-641.8

Table 7.2: Results for E_0 obtained from the SAT interaction with an SRG flow parameter of $\alpha = 0.08\,\mathrm{fm}^4$ and eMax = 12, E3Max = 14 and $\hbar\Omega = 22\,\mathrm{MeV}$. All values are given in MeV.

Nucleus	HF	IM-SRG	CCSD	Expt.
^{16}O	-81.1	-133.5	-127.7	-127.6
^{24}O	-106.4	-181.3	-173.9	-169.0
^{40}Ca	-208.0	-355.7	-337.2	-342.0
^{48}Ca	-262.6	-434.8	-416.7	-416.0
^{56}Ni	-287.7	-494.6	-476.8	-484.0
^{68}Ni	-333.7	-571.1	-551.8	-590.4
^{78}Ni	-351.7	-613.4	-592.5	-641.8

Table 7.3: Results for E_0 obtained from the SAT interaction with an SRG flow parameter of $\alpha = 0.04\,\mathrm{fm}^4$ and eMax = 12, E3Max = 14 and $\hbar\Omega = 22\,\mathrm{MeV}$. All values are given in MeV.

For the unevolved interaction the HF results show an even worse deficit in E_0. The binding energy of none of the nuclei is significantly larger than 100 MeV. The differences between the IM-SRG results and the experimental values increase, too, but not nearly as strongly as for HF.

The same analysis can be done for the EM400 interaction. The corresponding data are given in Table 7.4 and Table 7.5. We find that heavier nuclei are more strongly bound compared to the SAT interaction. For the HF method, the variations in E_0 for different SRG flow parameters are about the same as for the SAT interaction. Regarding CCSD and especially IM-SRG we see that with the EM400 interaction the ground-state energies are much more stable with respect to the SRG flow parameters as compared the SAT interaction.

Nucleus	HF	IM-SRG	CCSD	Expt.
^{16}O	-101.6	-130.7	-129.0	-127.6
^{24}O	-130.0	-171.0	-168.8	-169.0
^{40}Ca	-300.6	-378.4	-373.4	-342.0
^{48}Ca	-370.3	-462.6	-457.5	-416.0
^{56}Ni	-425.1	-547.5	-539.3	-484.0
^{68}Ni	-539.0	-676.0	-667.8	-590.4
^{78}Ni	-565.9	-724.7	-714.7	-641.8

Table 7.4: Results for E_0 obtained from the EM400 interaction with an SRG flow parameter of $\alpha = 0.08\,\mathrm{fm}^4$ and eMax = 12, E3Max = 14 and $\hbar\Omega = 24\,\mathrm{MeV}$. All values are given in MeV.

Nucleus	HF	IM-SRG	CCSD	Expt.
^{16}O	-81.8	-130.3	-127.0	-127.6
^{24}O	-100.9	-170.4	-165.6	-169.0
^{40}Ca	-240.7	-377.1	-367.1	-342.0
^{48}Ca	-296.7	-462.8	-451.0	-416.0
^{56}Ni	-333.5	-549.4	-531.8	-484.0
^{68}Ni	-429.2	-677.0	-658.5	-590.4
^{78}Ni	-441.1	-725.4	-703.3	-641.8

Table 7.5: Results for E_0 obtained from the EM400 interaction with an SRG flow parameter of $\alpha = 0.04\,\mathrm{fm}^4$ and eMax = 12, E3Max = 14 and $\hbar\Omega = 24\,\mathrm{MeV}$. All values are given in MeV.

7.2.2 Charge Radii

In Table 7.6 we give the charge radii obtained from the three methods that we will employ for RPA calculations. The SAT interaction with an SRG flow parameter of $\alpha = 0.08\,\mathrm{fm}^4$ has been used. Similar to the E_0 case we see that HF yields results that are furthest from the experimental values. Both IM-SRG and CCSD show an improved description with respect to experiment, although the differences between HF and IM-SRG/CCSD are much smaller than for the ground-state energy.

Nucleus	HF	IM-SRG	CCSD	Expt.
^{16}O	2.57	2.61	2.59	2.70
^{24}O	2.59	2.63	2.63	
^{40}Ca	3.30	3.36	3.33	3.48
^{48}Ca	3.30	3.34	3.33	3.48
^{56}Ni	3.51	3.55	3.52	
^{68}Ni	3.63	3.69	3.65	
^{78}Ni	3.67	3.74	3.70	

Table 7.6: Results for r_{ch} obtained from the SAT interaction with an SRG flow parameter of $\alpha = 0.08\,\mathrm{fm}^4$ and eMax = 12, E3Max = 14 and $\hbar\Omega = 22\,\mathrm{MeV}$. All values are given in fm.

The situation for the SAT interaction with $\alpha = 0.04\,\mathrm{fm}^4$ is very similar, see Table 7.7. Overall, the charge radii are slightly larger but still small compared to experiment. We note that the difference between the CCSD results and the experimental value for the charge radius of ^{40}Ca stem from the SRG evolution. For the fit the bare interaction has been used.

Nucleus	HF	IM-SRG	CCSD	Expt.
^{16}O	2.61	2.64	2.62	2.70
^{24}O	2.64	2.67	2.66	
^{40}Ca	3.36	3.39	3.36	3.48
^{48}Ca	3.35	3.38	3.36	3.48
^{56}Ni	3.56	3.58	3.55	
^{68}Ni	3.68	3.72	3.68	
^{78}Ni	3.72	3.76	3.73	

Table 7.7: Results for r_{ch} obtained from the SAT interaction with an SRG flow parameter of $\alpha = 0.04\,\text{fm}^4$ and eMax = 12, E3Max = 14 and $\hbar\Omega = 22\,\text{MeV}$. All values are given in fm.

The corresponding values for the EM400 interaction can be found in Table 7.8 and Table 7.9. We see that the obtained values are notably smaller than the ones from the SAT interaction.

Nucleus	HF	IM-SRG	CCSD	Expt.
^{16}O	2.41	2.47	2.45	2.70
^{24}O	2.42	2.48	2.47	
^{40}Ca	2.98	3.06	3.02	3.48
^{48}Ca	2.96	3.02	2.99	3.48
^{56}Ni	3.15	3.19	3.17	
^{68}Ni	3.22	3.28	3.25	
^{78}Ni	3.26	3.32	3.29	

Table 7.8: Results for r_{ch} obtained from the EM400 interaction with an SRG flow parameter of $\alpha = 0.08\,\text{fm}^4$ and eMax = 12, E3Max = 14 and $\hbar\Omega = 24\,\text{MeV}$. All values are given in fm.

Nucleus	HF	IM-SRG	CCSD	Expt.
^{16}O	2.42	2.46	2.44	2.70
^{24}O	2.42	2.47	2.46	
^{40}Ca	3.00	3.05	3.01	3.48
^{48}Ca	2.97	3.02	2.99	3.48
^{56}Ni	3.18	3.19	3.17	
^{68}Ni	3.25	3.28	3.25	
^{78}Ni	3.29	3.32	3.29	

Table 7.9: Results for r_{ch} obtained from the EM400 interaction with an SRG flow parameter of $\alpha = 0.04\,\text{fm}^4$ and eMax = 12, E3Max = 14 and $\hbar\Omega = 24\,\text{MeV}$. All values are given in fm.

7.3 Single-Particle Spectra

From our RPA formalism we know the SP energies are relevant for the RPA since the ph excitation energies $\epsilon_p - \epsilon_h$ appear on the diagonal of the A matrix. They can be expected to play an important role. We stress that, although SP properties are not observables, their investigation may still yield important insights. We will see later in chapter 8 that the structure

of the SP spectra is indeed helpful for an understanding of the RPA results. Therefore, before we look into RPA calculations we first take a look at the SP spectra.

As discussed in section 5.1, the structure of the IM-SRG transformed matrix elements requires the decoupling of the reference state from all its ph excitations. Formally, this is not identical to the HF basis, but in practice the deviations from the HF condition of mean-field diagonality are extremely small and can safely be neglected. With this, the idea of a mean-field with SP energies can still be applied.

Contrary, we are not able to give SP spectra for CC calculations. As we saw in section 3.1, the mean-field character associated with the SP states is strongly connected to the reducibility of the 2B density. Without this property, the definition of a mean-field, 1B Hamiltonian in the sense of HF is impossible.

In Figure 7.1 we can see the SP energies of ^{40}Ca calculated with the SAT interaction with $\alpha = 0.08\,\mathrm{fm}^4$. We compare the HF SP spectrum (left-hand panels) to one from IM-SRG (right-hand panels). The left-hand figure is for the neutron states, the right-hand one for the proton states. On the horizontal axis we plot the occupancy of the orbitals and on the vertical axis their energies. The quantum numbers are given for all occupied states as well as the first unoccupied state. The unoccupied states are only plotted up to a certain energy and are shown semitransparent to distinguish them from the hole states.

Comparing the SP states of HF versus the ones of IM-SRG, we can see that IM-SRG lowers the occupied levels by a few MeV. With the knowledge that IM-SRG produces significantly lower ground-state energies than HF, the drop in energy for hole states is not surprising. Simultaneously, the unoccupied states are raised in energy, but only by about one MeV. As a consequence, the Fermi gap is significantly widened. The spacing within the particle states as well as within the hole states, however, is almost the same as for HF. Due to its mathematical form, we can expect RPA to depend on the ph excitation energies, i.e., the relative spacing of particle and hole states. Going from HF to IM-SRG, therefore, produces an increase in the ph excitation energies by several MeV while at the same time keeping the ph spectrum otherwise constant. For SRPA, the effect for the increase in 2p2h excitation energies should be twice as large.

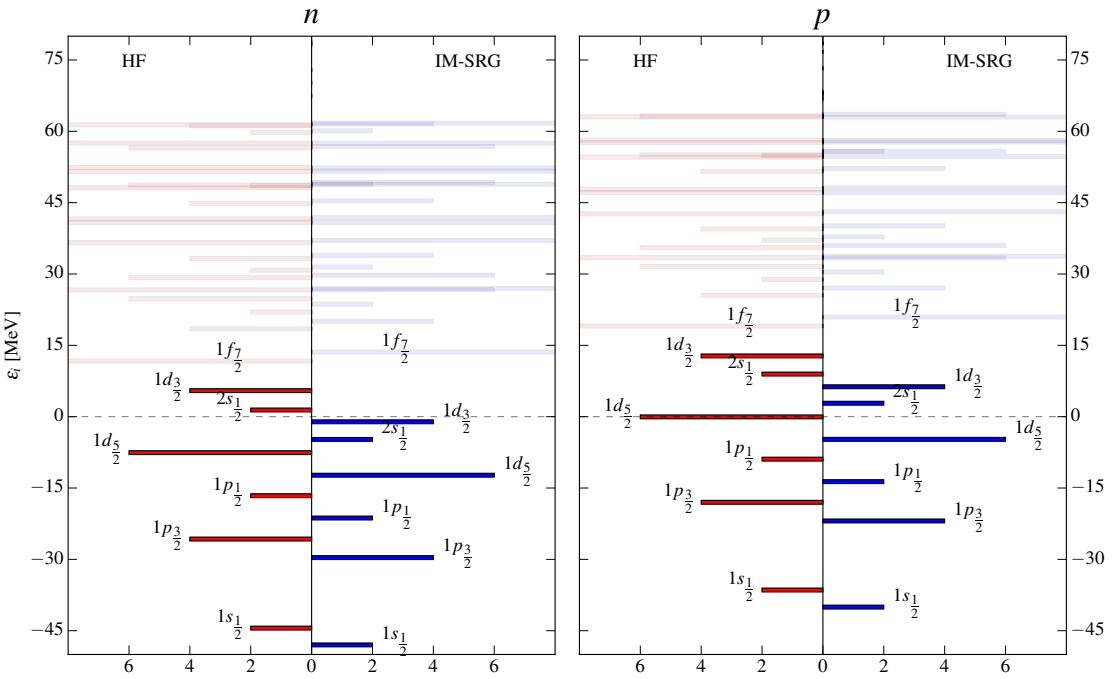

Figure 7.1: Comparison of SP states of ^{40}Ca for HF and IM-SRG matrix elements. For further description see text.

We also note that the charge radius has long been connected to the spread of the single-particle (SP) spectra [Paa+06; HPR11; GPR14]. Therefore, the observed behaviour for the SP states corresponds well to the larger values for r_{ch} that we obtained from IM-SRG in the previous section.

This was exemplarily done for ^{40}Ca but we observe a similar effect when going from HF to IM-SRG for other nuclei, different SRG flow parameters and also for the EM400 interaction.

Chapter 8

Collective Excitations

In this chapter we will discuss the numerical results for different RPA flavors. We start out with the analysis of HF-RPA calculations and move on to the discussion of HF-SRPA. Next we will investigate the impact of GSCs on first-order RPA calculations via both CC-RPA and IM-RPA. Finally, we will turn to the effect of correlations on the level of SRPA by means of IM-SRPA.

Before we discuss our numerical results we first give an overview of the experimental data against which our results will be compared.

8.1 Experimental Data for Transitions

The various values and sources for the experimental data are summarized in Table 8.1. For the ISM and ISQ mode the centroid energies are given, for IVD we use data from the CDFE database [CDF], except for the data from [Ros$^+$13] regarding ^{68}Ni which have kindly been provided via personal communication.

Nucleus	ISM	IVD	ISQ
^{16}O	21.13 [LCY01]	[Ahr$^+$75]	19.76 [LCY01]
^{24}O			
^{40}Ca	19.18 [YLC01]	[Ero$^+$03]	17.84 [YLC01]
^{48}Ca	19.88 [Lui$^+$11]	[Ero$^+$03]	18.61 [Lui$^+$11]
^{56}Ni	19.3 [Mon$^+$08]		16.2 [Mon$^+$08]
^{68}Ni	21.1 [Van$^+$14]	[Ros$^+$13]	15.9 [Van$^+$15]
^{78}Ni			

Table 8.1: Sources and discrete values for experimental transition data. All values are given in MeV.

We stress that, for the comparison of theoretical RPA results to experimental centroid energies, it should be kept in mind that the centroids are given without error estimates. For a single, narrow peak the centroid energy carries all information needed for a reasonable comparison, but for a wide distribution of strength, as often found in giant resonances, the centroid energy alone has limited significance. This is especially true if only a certain part of a wider resonance is measured due to experimental constraints on the energy range that can be probed. We refrain from giving detailed information on this topic and refer to the papers regarding the particular

measurements. Note that there are also other sources for experimental values, for example for the ^{16}O IVD mode [LNH87], for ^{40}Ca IVD [Vey^{+}74] and ISQ [Ber^{+}79] or the IVD of ^{48}Ca [OKe^{+}87]. The values that we show for comparison, however, are those noted in Table 8.1.

8.2 HF RPA

8.2.1 Interaction Ranks: NN-only vs. NN+3N-ind. vs. NN+3N

From many applications we know that for an accurate description of nuclei it is crucial to include 3B forces that arise in χEFT. The RPA is not different in this regard. In Figure 8.1 we show a comparison for the EM400 interaction at the NN-only level (-·-·-), the NN interaction plus its SRG-induced 3N terms, NN+3N-ind. (- - - -), as well as the the former plus initial 3N terms, NN+3N (——). From left to right, the columns show the ISM, IVD and ISQ response, respectively. The rows show the selected isotopes for our investigation from ^{16}O at the top to ^{78}Ni at the bottom. For the ISM and the ISQ mode, the black arrows indicate the positions of the centroid energies, and the experimental distributions for the IVD mode are shown as gray shading. Numerical values and sources for all data are given in Table 8.1.

We observe a large difference between the NN-only and the NN+3N-ind. case. The IVD and ISQ modes appear to be far more sensitive to the inclusion of either induced or initial 3N terms with differences of around 15 MeV. For the ISM we find smaller but still essential changes of about 8 MeV. The observed pattern for the transitions is in accordance with what we expect from the binding energies, which are significantly stronger for the pure NN interaction (cf. [Rot^{+}12]). This overbinding leads to a a substantial stretching of the single-particle spectrum and, thus, a strong increase in unperturbed transition energies. Taking into account the SRG-induced many-body terms captures a large part of the differences to the NN+3N case. However, the NN+3N-ind. case tends to produce some degree of underbinding. The effect of this can be seen for the IVD and ISQ case, where the transitions are at lower energies as compared to the NN+3N situation. Again, the ISM does not show the same degree of sensitivity. While for the light nuclei we see only small differences between the NN+3N-ind. and NN+3N case, the neutron rich isotopes ^{68}Ni and ^{78}Ni show a dependence on the inclusion of initial 3N forces. Contrary to IVD and ISQ, for the ISM mode the inclusion of initial 3N terms leads to slightly more compressed spectra.

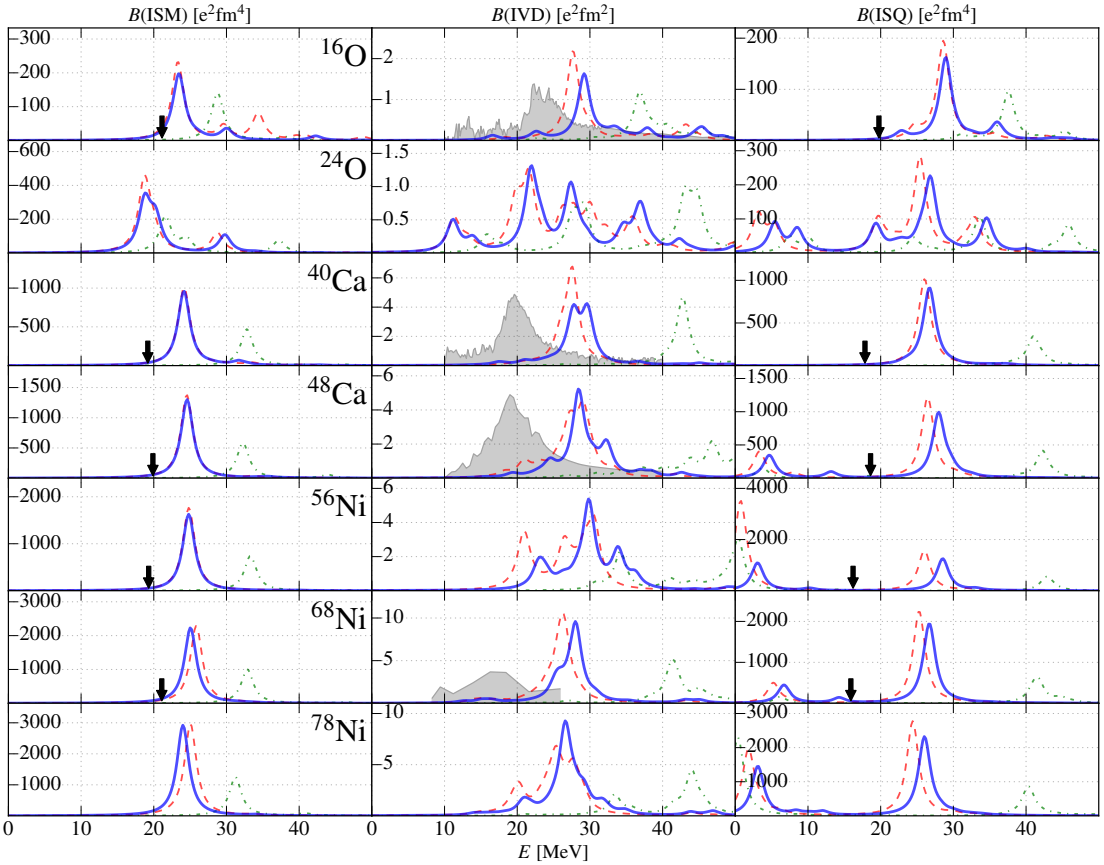

Figure 8.1: HF-RPA results for the EM400 interaction with an SRG flow parameter of $\alpha = 0.08\,\mathrm{fm}^4$. Shown are the transitions obtained for the NN-only (-·-·-), NN+3N-ind. (- - - -) and the NN+3N (——) interaction. Here we use eMax = 12, E3Max = 14 and $\hbar\Omega = 24\,\mathrm{MeV}$.

As expected, we see that the inclusion of 3N terms, which mainly are SRG-induced 3N terms, is crucial for the accurate description of transitions. Therefore, in the following all results will be discussed on the level of NN+3N interactions. In the case of SRPA certain terms are omitted within NO2B compared to a full 3B description, cf. section 3.3.7.

8.2.2 Comparison: HF vs. TDA vs. RPA

In Figure 8.2 we compare the transition strengths obtained from RPA (——), TDA (- - - -) and HF (-·-·-). The TDA has already been introduced as a simplified version of the RPA where the B matrix is zero and, consequently, so are the Y^ω amplitudes. The HF is an even more simplistic response and can be obtained from taking only the diagonal elements of A which correspond directly to the ph excitation energies of HF. We see that the simple HF response produces results that are, both in position and structure of the transitions, far from the RPA and TDA. Only for the IVD mode we observe a notable resemblance. Between TDA and RPA response there are only small differences. The most prominent appear for the ISQ, especially for the low-lying states of the heavier nuclei.

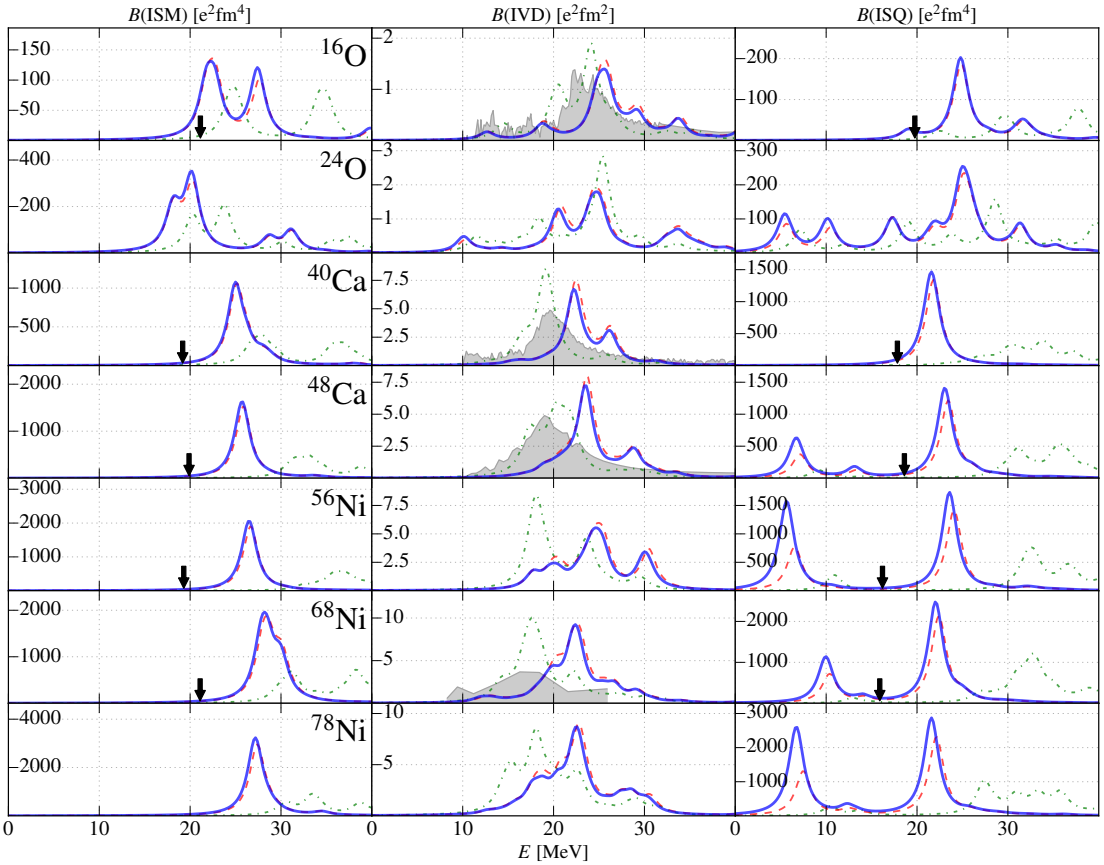

Figure 8.2: Results for the HF (-·-·-), TDA (- - - -) and RPA (——) response. The SAT interaction with an evolution of $\alpha = 0.08\,\mathrm{fm}^4$ is used. Here we use eMax = 12, E3Max = 14 and $\hbar\Omega = 22\,\mathrm{MeV}$.

We stress that the HF response does not require any diagonalization since it consists only of the uncoupled ph excitations. Following this line of thought, these results evidently illustrate the difference between uncoupled and coupled ph excitations. The latter produces the collectivity which cannot exist for the uncoupled case. As can be seen, this collectivity leads to a significant increase in the resonance strength and a strong shift in excitation energies.

We note that the upward shift in energy for the IVD response is in consistence with the findings of RPA calculations using phenomenological interactions, cf. [GPR14].

8.2.3 Interactions: EM400 vs. SAT

In Figure 8.3 we show the comparison of HF-RPA results obtained with the EM400 interaction (- - - -) and the SAT interaction (——). For the ISM we observe that the structure of the transition stays about the same, but for heavier nuclei the SAT interaction tends to predict the ISM at higher energies. IVD transitions with the SAT interaction are shifted towards lower energies. The shift is more pronounced than for the ISM and appears for light nuclei as well as for heavier ones. The strength of the shift stays about the same over the calculated mass range. Regarding the ISQ, we observe a similar shift as for the IVD. At the same time, the low-lying 2^+ states that exist for heavier nuclei are shifted upwards. In total, the SAT interaction yields a more compressed ISQ transition as the EM400 interaction. Overall, both interactions predict the giant resonances at too high energies compared to the experimental values.

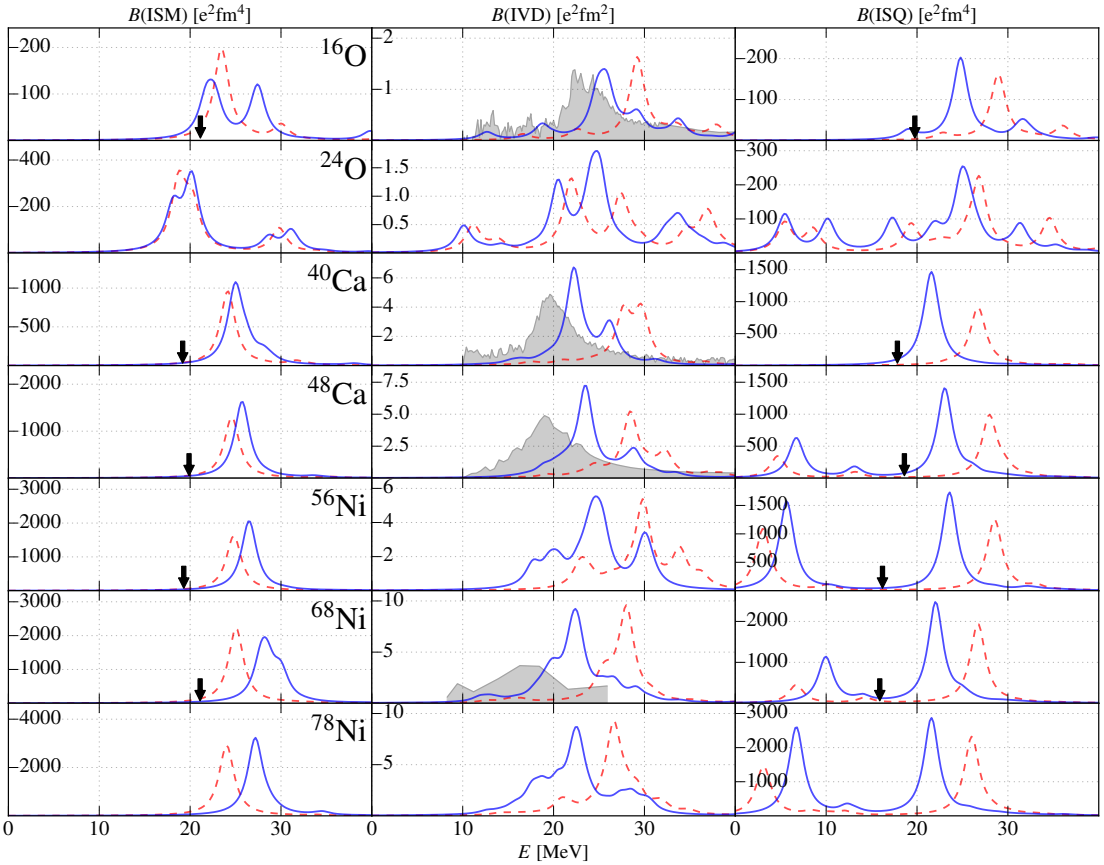

Figure 8.3: HF-RPA results of the EM400 (- - - -) and the SAT interaction (——). Both interactions are shown for an SRG flow parameter of $\alpha = 0.08\,\mathrm{fm}^4$. Here we use eMax = 12, E3Max = 14 and $\hbar\Omega$ as usual for the respective interactions.

We note that, independently of the method, a certain sensitivity of the results with regard to the chiral input is not uncommon, see e.g. [CR16], and that the downward shift in energy for the IVD and ISQ response that we observe using the SAT interaction is in accordance with the the substantially larger charge radii that we found in section 7.2.2.

8.2.4 Model-Space Convergence

We will now test the robustness of our HF-RPA calculations. For that purpose, we calculate the same transitions from the same interactions, but with different model space parameters and truncations. If our results do not change much with respect to these parameters, we can assume our calculations to be converged and the influence of the truncations to be negligible. First we look into the stability with respect to the SRG flow parameter. As mentioned before, for flow parameters there is per se no "right" or "wrong" value, but instead a tradeoff between pre-diagonalization and induced terms has to be found. Next we will investigate the influence of the harmonic oscillator frequency $\hbar\Omega$, where also no clear a priori preference can be given. Only the last parameter that we will look into, eMax, constitutes a truncation for which larger values correspond to larger model spaces and can, thus, be expected to yield better results.

SRG Dependence

We will examine the SRG dependence of HF-RPA results obtained from both SAT and EM400. In Figure 8.4 we show the HF-RPA results of the EM400 interaction for $\alpha = 0.04\,\mathrm{fm}^4$ (- - - -) and $\alpha = 0.08\,\mathrm{fm}^4$ (——). For all cases we observe a shift towards higher energies when going to larger values of α. This can be understood with the help of our previous investigations regarding the SP spectra. The SRG evolution causes the binding energy of nuclei to increase due to the softer nature of the interaction. As a consequence, the SP excitations increase and transitions appear at higher energies. It can also be seen that the low-lying ISQ states are remarkably stable. Those arise from excitations in the immediate vicinity of the Fermi gap that remain almost unchanged by the SRG. We note that the shift is roughly universal with respect to mass and transition type and that it amounts to about 1 to 2 MeV. In particular, the SRG-caused shift is much smaller than the differences we saw from the use of different interactions.

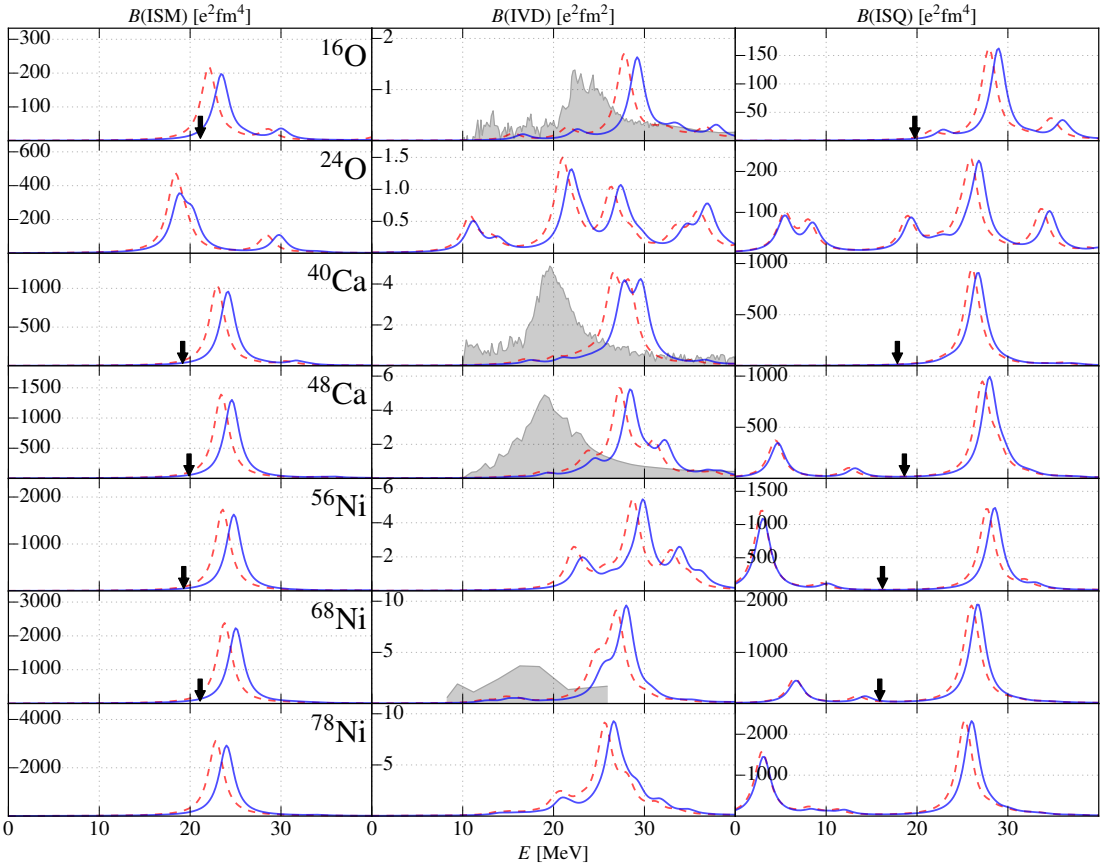

Figure 8.4: HF-RPA results for SRG flow parameters of $\alpha = 0.04\,\mathrm{fm}^4$ (- - - -) and $\alpha = 0.08\,\mathrm{fm}^4$ (——). Here we use the EM400 interaction with eMax = 12, E3Max = 14 and $\hbar\Omega = 24\,\mathrm{MeV}$.

We can investigate the same SRG sensitivity of HF-RPA for the SAT interaction. The corresponding data will not be shown since the systematics of the changes due to the SRG evolution resemble those of the EM400. Again, we observe a small shift to higher energies, and low-lying ISQ states are stable against variations of the SRG flow parameter. The changes for light nuclei, however, appear to be somewhat more pronounced.

Frequency Dependence

In Figure 8.5 we compare the EM400 interaction with an SRG flow parameter of $\alpha = 0.08\,\mathrm{fm}^4$ for two different values of the harmonic oscillator frequency, $\hbar\Omega = 24\,\mathrm{MeV}$ (- - - -) and $\hbar\Omega = 28\,\mathrm{MeV}$ (——). We see that the variations of the RPA results are about the same size as for different SRG flow parameters. Again, the low-lying ISQ states are relatively stable, and overall we see an increase of transition energies for larger frequencies. The differences for the ISM modes, however, are somewhat larger compared to the SRG variations. We also note that the ground-state energies change only marginally for different frequencies. The difference for ^{16}O is far below 1 MeV, for ^{78}Ni it is about 15 MeV. Both are much smaller than the changes that, within HF, arise from different SRG flow parameters, cf. section 7.2.1. We, therefore, see that the lack of changes in the binding energy is not necessarily a sufficient criterion for RPA stability. Instead, the changes in the SP energies are much more significant.

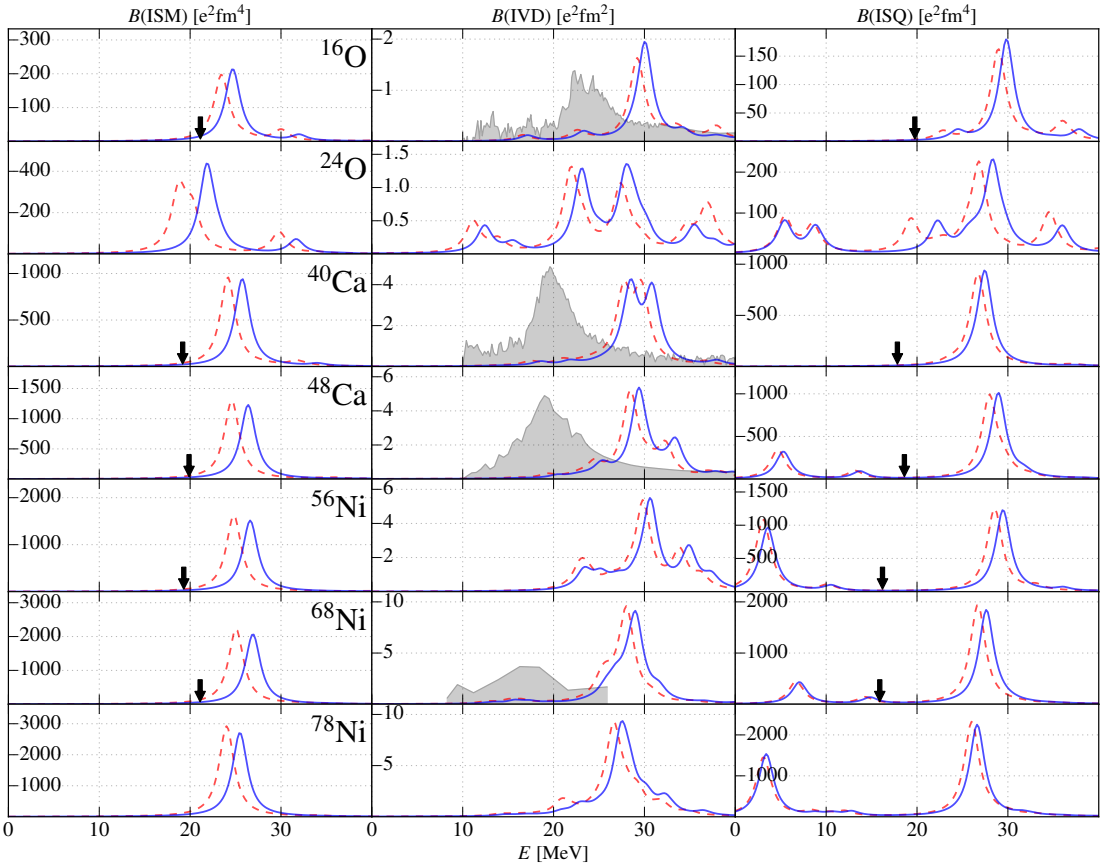

Figure 8.5: HF-RPA results for harmonic oscillator frequencies of $\hbar\Omega = 24\,\mathrm{MeV}$ (- - - -) and $\hbar\Omega = 28\,\mathrm{MeV}$ (——). Here we use the EM400 interaction with an SRG flow parameter of $\alpha = 0.08\,\mathrm{fm}^4$ with eMax = 12, E3Max = 14 and $\hbar\Omega = 24\,\mathrm{MeV}$.

eMax Convergence

In Figure 8.6 we compare different model space sizes, eMax = 12 (- - - -) and eMax = 14 (——). The overall features are similar to the convergence patterns that we already saw. We note that, in particular, the larger model space yields lower excitation energies which are closer to the experimental values. This behaviour can be expected from an increase in the size of the model space. Ideally, we would perform all RPA calculations in the eMax = 14 space, or even larger,

but due to the computational cost in SRPA and the correlated RPA results, for which IM-SRG and CCSD calculations have to be done beforehand, we restrict the large scale calculations to eMax = 12.

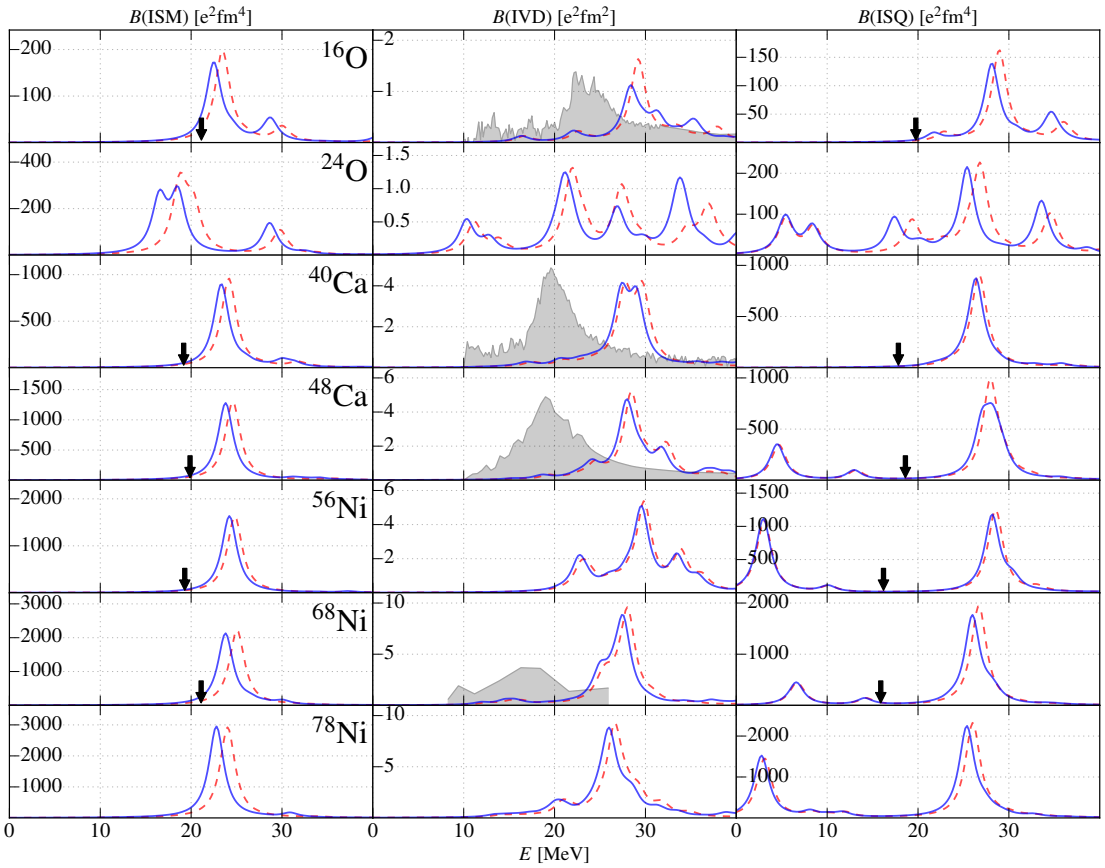

Figure 8.6: HF-RPA results for model-space sizes of eMax = 12 (- - - -) and eMax = 14 (——). Here we use the EM400 with an SRG flow parameter of $\alpha = 0.08\,\mathrm{fm}^4$ with E3Max = 14 and $\hbar\Omega = 24\,\mathrm{MeV}$.

Nevertheless, we conclude that for converged RPA results we need larger model-space sizes. This would solve the issue of eMax convergence, and associated with the insufficient model-space size also the problem of the dependence on the harmonic oscillator frequency. Since the frequency is a mere basis parameter, in sufficiently large model spaces it would have no influence whatsoever on the results. The dependence that we saw is caused by too small spaces, an investigation of this dependence and its weakening with larger spaces can be found in, e.g., [Rot+06]. So, regarding eMax and $\hbar\Omega$ we only need, simply put, more computation power to solve these issues. The SRG dependence is a different matter. We will revisit this in the following sections.

8.3 HF-SRPA

We will now discuss strength distributions on the level of second-order RPA with additional 2p2h excitations. The SRPA formalism has been addressed in section 3.3. It is worth noting that all previous SRPA calculations have been performed using either phenomenological interactions [PR09; Pap14] or are based on density functionals [GGC10; GGC11]. In this thesis we present the first SRPA calculations using interactions derived from χEFT. The calculations will be performed within the NO2B approximation. For first-order RPA, this is exact as shown in section 3.2.10. In SRPA some of the omitted 3B terms would contribute. Due to combinatorics, including the second-order contributions greatly increases the dimension of the eigenvalue problem. The full, untruncated linear dimension of the SRPA 2p2h matrix for medium-mass nuclei in a model space of 13 major shells can reach several millions. For first-order RPA calculations using the same model space, the 1p1h dimension is about a thousand. In the interest of keeping calculations feasible we introduce a new truncation parameter for SRPA. Instead of calculating the entire 2p2h space, we will include only excitations with a total excitation energy up to a certain threshold value $E_{\mathrm{2p2h,max}}$. With the HF energies ϵ_i this condition reads

$$\epsilon_{p_1} - \epsilon_{h_1} + \epsilon_{p_2} - \epsilon_{h_2} \leq E_{\mathrm{2p2h,max}}. \tag{8.1}$$

With the above relation we can limit the size of the SRPA problem. We stress that this restriction only applies to the 2p2h excitations but not to the 1p1h excitations. The regular RPA problem can thus be obtained from SRPA as the special case with $E_{\mathrm{2p2h,max}} = 0\,\mathrm{MeV}$. Going from $E_{\mathrm{2p2h,max}} = 0\,\mathrm{MeV}$ to larger values will gradually transform an RPA into a full SRPA calculation. As the full SRPA space is approached, the results can be expected to converge. We will look into this in the next section. We note that for heavier nuclei there are significantly more 2p2h combinations up to a certain energy than for light nuclei. Additionally, there are also large differences between the different transitions, see Figure 8.7. For example, for the ISM mode we have the constraint that the angular momenta must be able to couple to zero. In terms of the triangular condition for angular momenta j_h and j_p, this means that we have to fulfill

$$|j_h - j_p| \leq 0 \leq j_h + j_p,$$

which is only possible for $j_h = j_p$. For the ISQ the angular momenta may differ by 2.

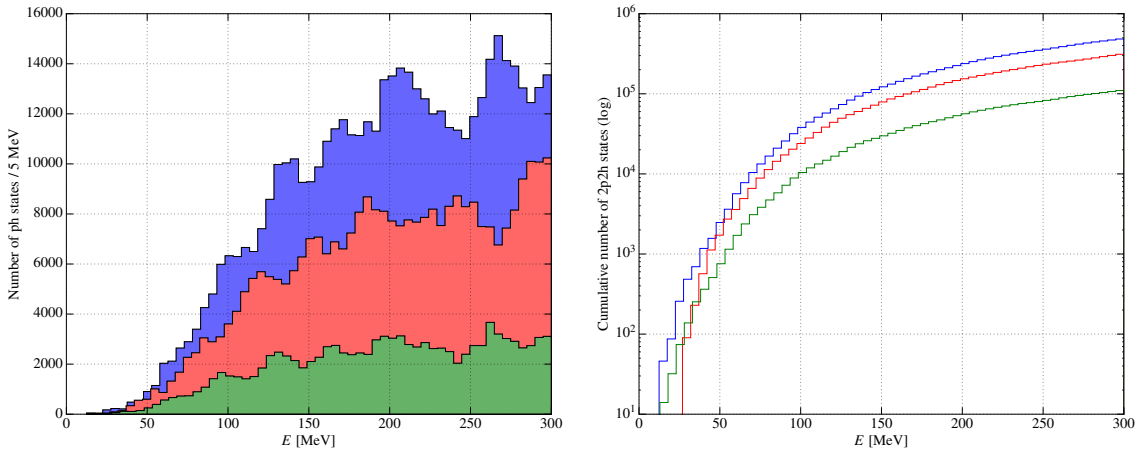

(a) Number of 2p2h states per 5 MeV.

(b) Cumulative number of 2p2h states.

Figure 8.7: Number of 2p2h states in SRPA. Shown are the ISM (——), the IVD (——) and the ISQ (——), exemplarily for ^{40}Ca with the SAT interaction. Here we use an SRG flow parameter of $\alpha = 0.08\,\mathrm{fm}^4$ with eMax = 12, E3Max = 14 and $\hbar\Omega = 22\,\mathrm{MeV}$.

An advantage of this truncation is that we automatically include all states up to the given energy, independently of how many there are. With respect to convergence, through the formulation via an energy threshold we also gain insight into the question of up to which excitation energy we get important contributions. This is relatively independent of the response mode or the isotope.

It should be noted at this point that, with or without truncation, the size of the SRPA problem does not allow to compute all eigenvalues and eigenstates. Usually only a small part of the spectrum, dozens up to a few hundred eigenstates, are calculated. If we do not know the complete spectrum, this obviously has consequences for the sum rules introduced in section 6.3. The connection between input and output is only valid if indeed we sum over all eigenvalues. For now we postpone the discussion of sum rules within SRPA. This issue will be dealt with in the context of IM-SRPA later on.

We now look into the convergence properties of SRPA with respect to $E_{\mathrm{2p2h,max}}$. In Figure 8.8 we show the transition strengths obtained in RPA (·····) and SRPA with an $E_{\mathrm{2p2h,max}}$ of 100 MeV (-·-·-), 200 MeV (- - - -) and 300 MeV (——). We use the SAT interaction with an SRG flow parameter of $\alpha = 0.08\,\mathrm{fm}^4$. Going from RPA to $E_{\mathrm{2p2h,max}} = 100\,\mathrm{MeV}$, we observe a large shift towards lower energies. The next step to $E_{\mathrm{2p2h,max}} = 200\,\mathrm{MeV}$ again yields a similar shift. Any further increase in the truncation threshold does not produce any changes. This holds for all nuclei and transitions, and we can safely assume that for $E_{\mathrm{2p2h,max}}$ above 300 MeV the truncation has no sizable effect on the results, which allows us to reduce to the computational effort without losing any significant contributions. We note that the SRPA convergence looks similar for the EM400 interaction, so the corresponding plot is not shown. Employing smaller SRG flow parameters for either interaction leads to a somewhat slower SRPA convergence, but still this does not pose a problem. With the observed SRPA convergence, if not stated otherwise all SRPA calculations will be performed with $E_{\mathrm{2p2h,max}} = 300\,\mathrm{MeV}$.

In total, the effect of the inclusion of second-order terms within RPA leads to a substantial shift of the main transition strength energies towards lower energies, typically by about 8 MeV. Due to this shift, for the ISM mode the agreement between SRPA and experiment is greatly improved. Furthermore, for the ISM modes of ^{40}Ca and heavier nuclei we see a broadening of the resonance structure in SRPA calculations. The IVD and ISQ modes on the other hand appear to be shifted too low. For both we see that the theoretical predictions tend to be few MeV below the experimental results. We also notice that for the ISQ mode, the low-energy spectra seem different. The strong peaks from low-lying 2^+ states in ^{48}Ca and heavier nuclei, cf. e.g. Figure 8.3, have largely vanished. In short, the loss of these states is a result of the strong SRPA shift, which causes these states to occur at unphysical energies, i.e., either imaginary or complex eigenvalues. This issue will be discussed in the next section.

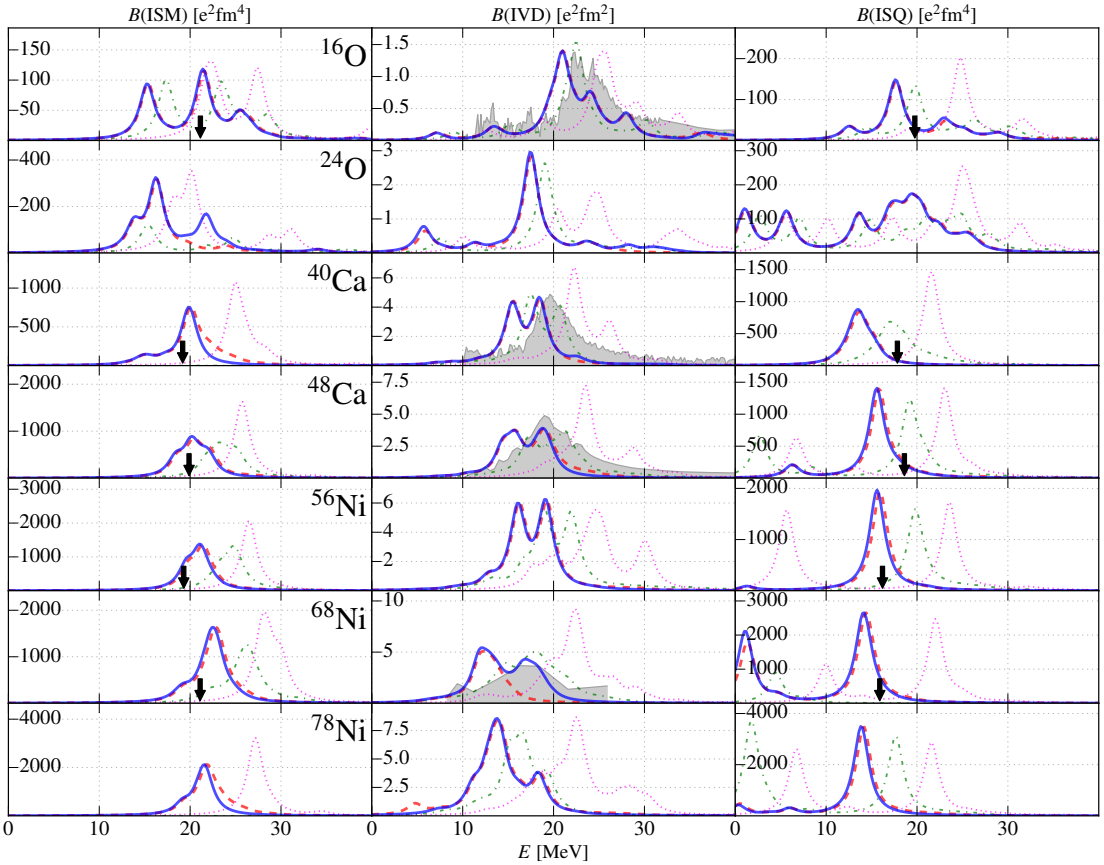

Figure 8.8: SRPA convergence for the SAT interaction. Shown are the transitions for RPA (·····) and SRPA with an $E_{\mathrm{2p2h,max}}$ of 100 MeV (-·-·-), 200 MeV (- - - -) and 300 MeV (——). Here we use an SRG flow parameter of $\alpha = 0.08\,\mathrm{fm}^4$ with eMax = 12, E3Max = 14 and $\hbar\Omega = 22\,\mathrm{MeV}$.

As stated before, for the EM400 interaction the convergence from RPA to SRPA is about the same. From our HF-RPA comparison of EM400 and SAT we know that for the EM400 interaction we started out with a more stretched ISQ spectrum and also higher-lying IVD resonances. Since the shift is roughly identical, this translates directly from RPA to SRPA. The comparison o HF-SRPA results for both interactions is shown in Figure 8.9. In total, for the EM400 the HF-SRPA results are about the same for the ISM, though a little less fragmented. The IVD is a few MeV higher than the experimental values, but since for the SAT interaction it is at roughly equally lower energies, the agreement of either with experiment is virtually the same. Likewise, the ISQ contributions are predicted at too high energies.

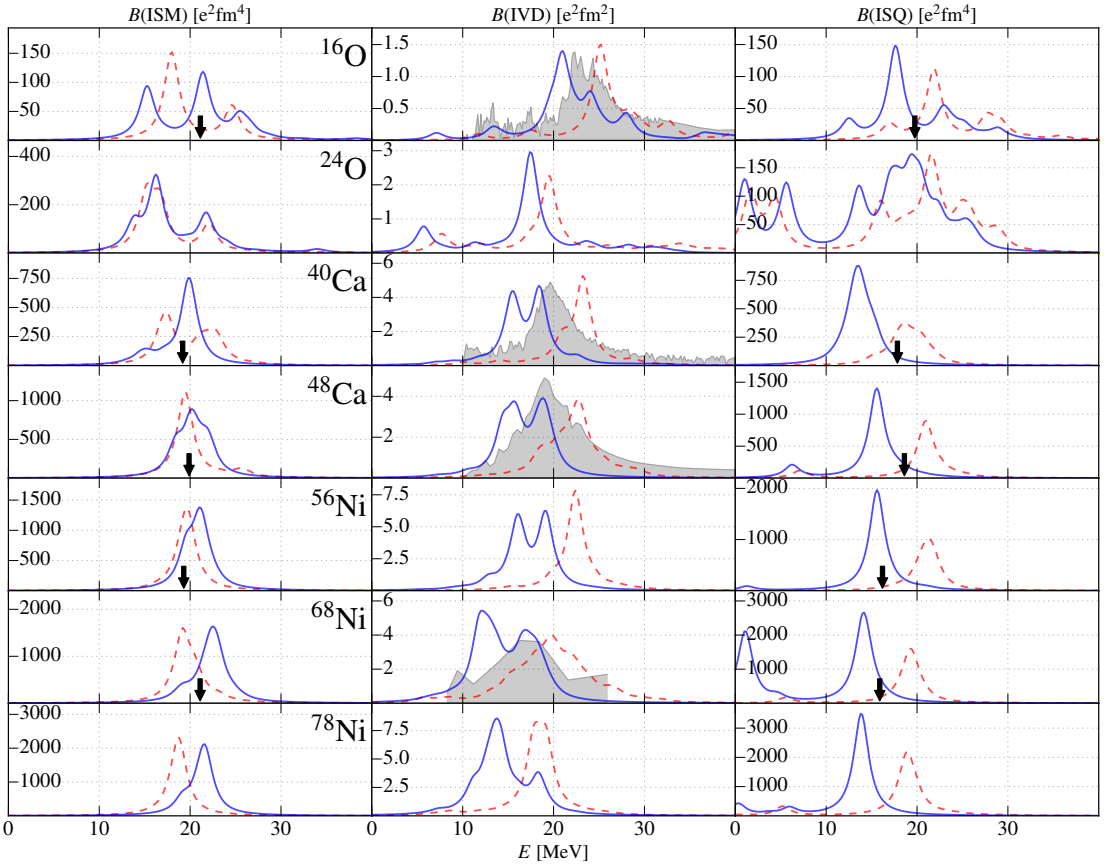

Figure 8.9: HF-SRPA results of the EM400 (- - - -) and the SAT interaction (——). Here we use the an SRG flow parameter of $\alpha = 0.08\,\mathrm{fm}^4$ with eMax = 12, E3Max = 14 and $\hbar\Omega$ as usual for the respective interactions.

8.3.1 SRPA Instabilities

Comparing RPA to SRPA calculations we found a strong shift towards lower energies. For RPA calculations it is known that, even with the inclusion of (normal-ordered) 3B forces, the bulk of the strength distribution still lies at much higher energies as compared to experiment. So on one hand, this shift appears to be necessary in order to achieve at least some degree of agreement with experimental data, see Figure 8.8. It is also not surprising that the inclusion of higher ranks of ph excitations yields more accurate results. In this case particularly, the 2p2h contributions appear to have a pivotal impact on the results. On the other hand, this shift also represents the most severe drawback of SRPA. We observe that roughly the entire strength distribution gets shifted towards lower energies by about the same amount. While this is "desired" for the collective strength, for some nuclei with low-lying states this can become quite problematic: If the energetic shift is larger then the excitation energy itself, the low-lying state gets shifted to negative excitation energies, which is of course an unphysical artifact. When using (S)RPA we are usually interested in the energy region of the giant dipole resonance and not in the low-lying states themselves, but even though it is still worrisome that the low-lying states become unphysical. This is a known issue for SRPA and source of some mistrust towards its results [PR10; GGC11; Gam+12; Pap14], especially regarding the low-lying states but also for the resonances.

Mathematically, the reason why instabilities can occur in HF-SRPA is that the HF ground

state only represents the minimum-energy state with respect to 1p1h variations. In a model space that also includes 2p2h contributions, the HF state is not necessarily stable against such 2p2h variations. Further considerations on this issue via a variational approach can be found in [Pro65]. Physically, this is attributed to the lack of ground-state correlations which we do not take into account in HF-SRPA. For phenomenological interactions a detailed analysis and discussion of this problem can be found in [Pap14]. It should also be stressed that the SRPA instabilities from nucleon-nucleon interactions are not to be confused with double-counting issues that arise within a density functional theory approach, see also [Tse13]. We refrain from an in-depth discussion on instabilities with reference to the situation within IM-SRPA, see section 8.5.

Regarding STDA, as mentioned before, this constitutes a Hermitian problem, so by definition no imaginary of complex eigenvalues can appear. Nonetheless, as the HF state is not the minimum in a model space that includes 2p2h variations, unphysical states with negative energy can still appear. Numerically this is examined, e.g., in [PR10].

Specific to the HF-SRPA calculations shown here, we note that we get no instabilities for the ISM modes. The IVD modes always carry spurious states. For HF-RPA, they appear at exactly zero energy as shown in [Tho61]. In HF-SRPA, they appear at finite, but unphysical energies. For the ISQ mode we find unphysical states for the heavier nuclei with low-lying states.

8.3.2 Model-Space Convergence

We will now turn to the subject of model-space convergence within HF-SRPA and perform the same comparisons as in section 8.2.4.

SRG Dependence

We start with the SRG dependence. In Figure 8.10 we see a comparison of strength distributions obtained from the EM400 interaction for SRG flow parameters of $\alpha = 0.04\,\mathrm{fm}^4$ (- - - -) and $\alpha = 0.08\,\mathrm{fm}^4$ (——). For larger SRG flow parameters we observe higher excitation energies, similar to the situation for HF-RPA that we saw in Figure 8.4. However, we notice an important difference — with up to 4 MeV the differences in HF-SRPA strength distributions are significantly stronger than for HF-RPA. The initial differences that appear in first-order RPA seem to propagate into the second-order excitations and also to worsen. The rather strong dependence on the SRG flow parameter is problematic. As mentioned before, there is no preferred choice for this parameter. Lower values have the advantage to usually give less induced many-body forces. At the same time they also yield harder interactions for which calculations converge slower than for softer ones. The latter tend to have stronger many-body contributions. We usually use a flow parameter of $\alpha = 0.08\,\mathrm{fm}^4$ because it provides a good compromise between convergence and induced many-body terms for a wide range of other many-body methods. With the dependence that we see, it is difficult to say if this choice is better or worse than a lower flow parameter. Again, we refer this issue to the following discussions.

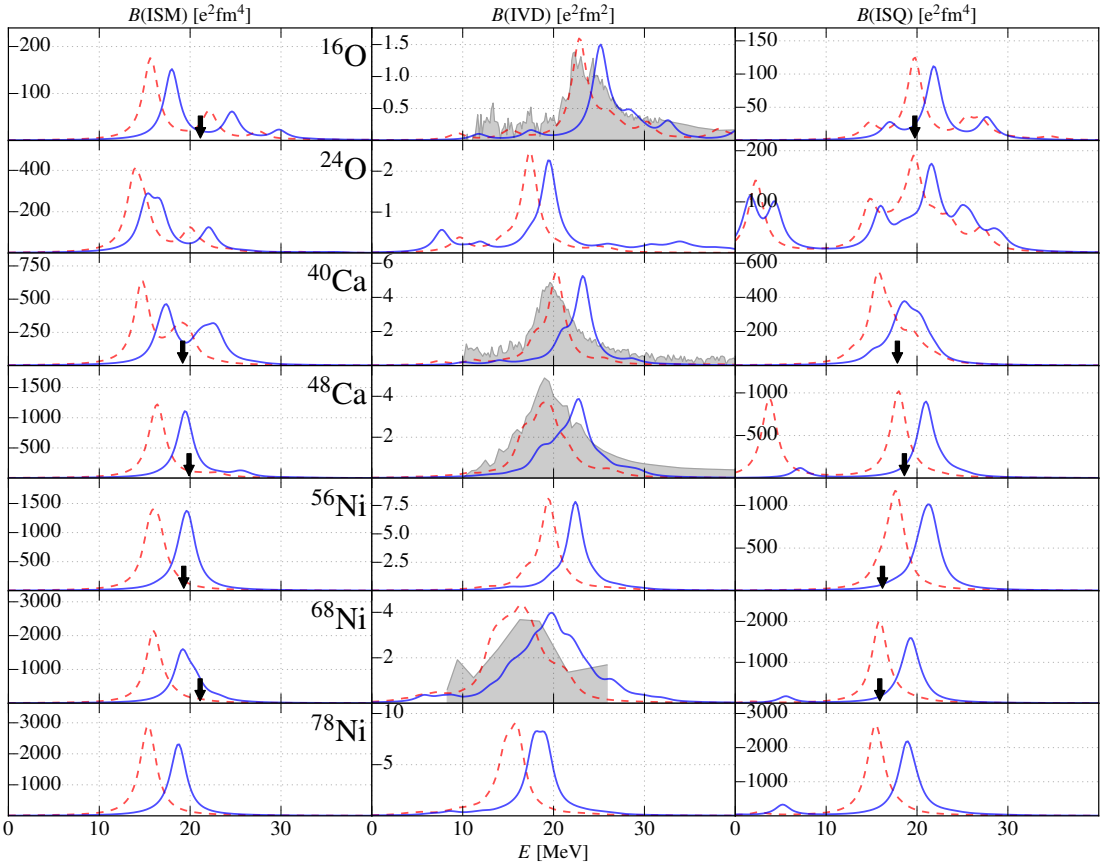

Figure 8.10: HF-SRPA results of the EM400 interaction with SRG flow parameters of $\alpha = 0.04\,\mathrm{fm}^4$ (- - - -) and $\alpha = 0.08\,\mathrm{fm}^4$ (——). Here we use eMax = 12, E3Max = 14 and $\hbar\Omega = 24$.

Frequency Dependence

The frequency dependence of HF-SRPA can be assessed with the help of Figure 8.11, where we show the results of the EM400 interaction ($\alpha = 0.08\,\mathrm{fm}^4$) with HO frequencies of $\hbar\Omega = 24\,\mathrm{MeV}$ (- - - -) and $\hbar\Omega = 28\,\mathrm{MeV}$ (——). Overall we see a very similar pattern for the differences as for first-order RPA examined in Figure 8.5. Interestingly, unlike for the SRG dependence we do not see an increase of the dependence. The discrepancies for different values of $\hbar\Omega$ seem to be about the same for SRPA and for RPA.

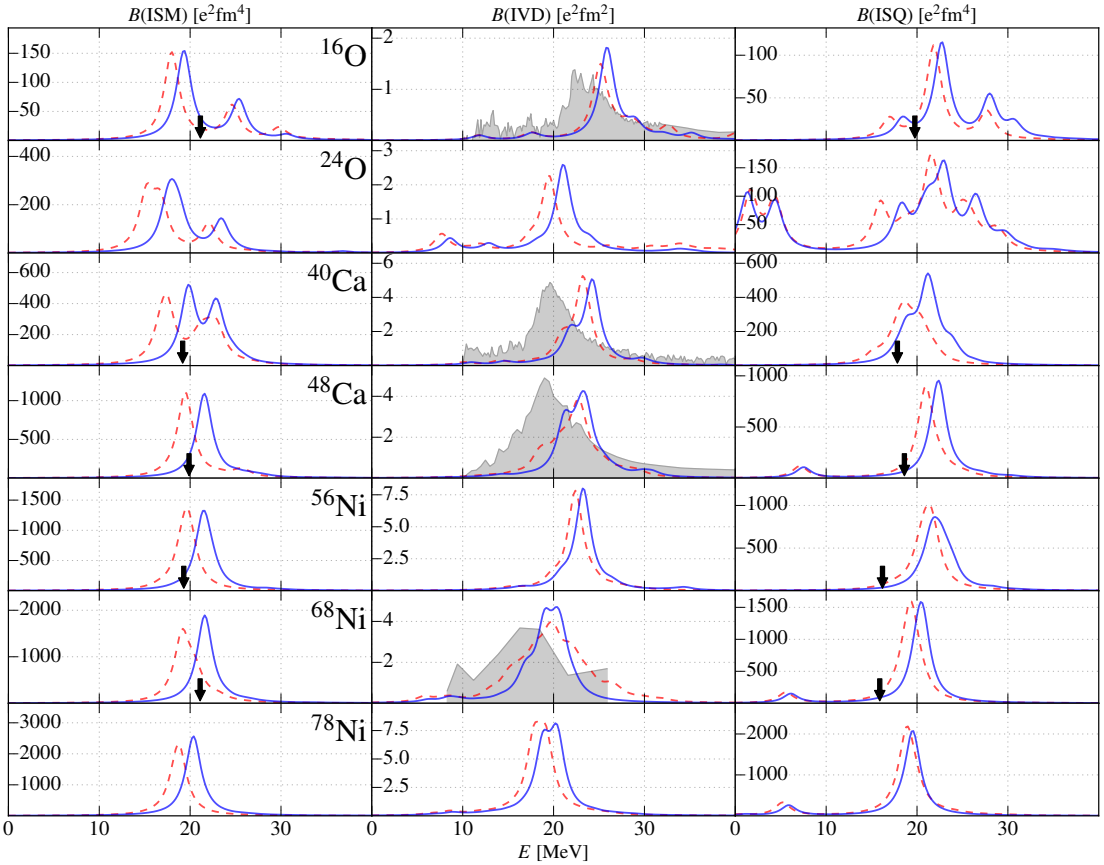

Figure 8.11: HF-SRPA results of the EM400 interaction with HO frequencies of $\hbar\Omega = 24\,\mathrm{MeV}$ (- - - -) and $\hbar\Omega = 28\,\mathrm{MeV}$ (——). Here we use an SRG flow parameter of $\alpha = 0.08\,\mathrm{fm}^4$ with eMax = 12 and E3Max = 14.

eMax Convergence

Finally, we investigate the convergence with respect to the model-space size. In Figure 8.12 we see transitions calculated with the EM400 ($\alpha = 0.08\,\mathrm{fm}^4$) for eMax = 12 (- - - -) and eMax = 14 (——). We note that the SRPA results for the larger model space with eMax = 14 have been obtained using the SRPA diagonal approximation, SRPA0, where all matrix elements of the A_{22} matrix except the diagonal are ignored. This has been shown to be a very good approximation to the results of SRPA including all elements of A_{22} [PR10; Pap14]. In comparison to the situation for RPA in Figure 8.6, the convergence even seems to have improved with the inclusion of second-order terms.

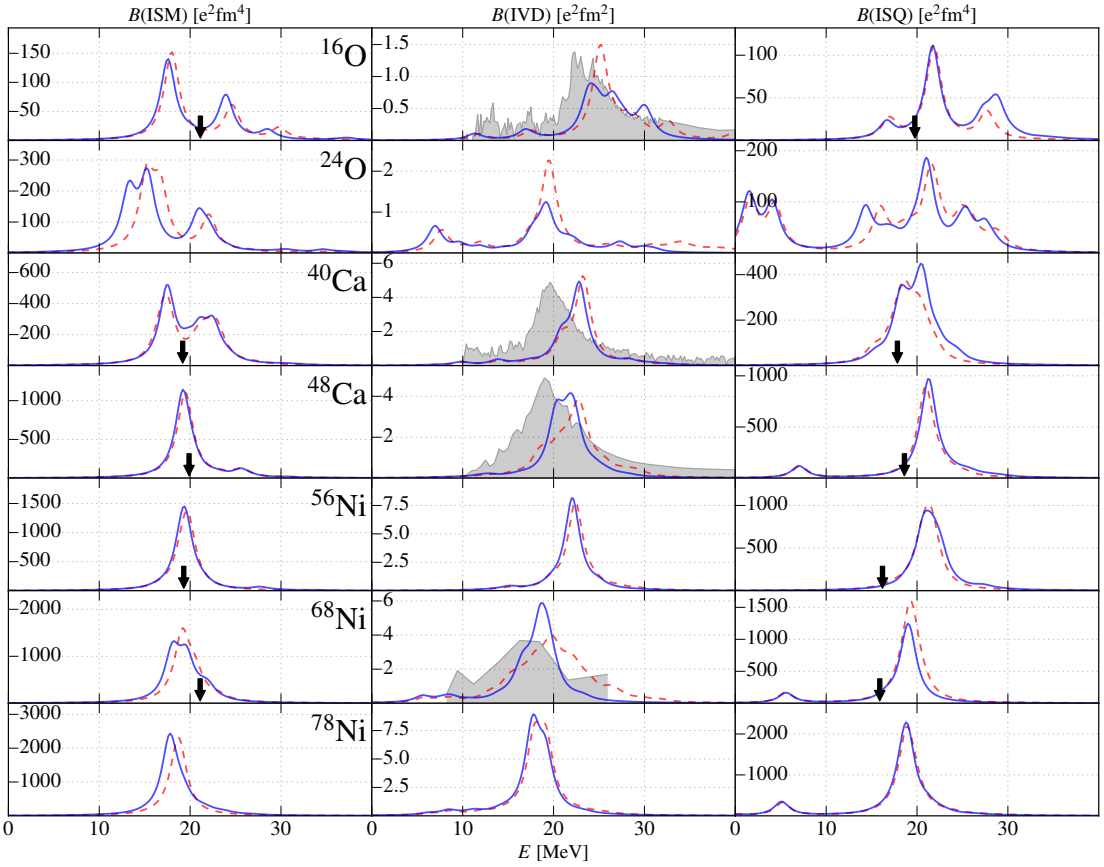

Figure 8.12: HF-SRPA results of the EM400 interaction with eMax = 12 (- - - -) and eMax = 14 (——). Here we use the an SRG flow parameter of $\alpha = 0.08\,\mathrm{fm}^4$ with E3Max = 14 and $\hbar\Omega = 24\,\mathrm{MeV}$.

In conclusion, also for HF-SRPA, the SRG dependence remains the most difficult issue regarding the robustness of the strength distributions. Again, the $\hbar\Omega$ dependence can be expected to decrease for larger model spaces. The improved eMax convergence that we observe shows the necessity of including second-order terms for obtaining converged RPA results. The reason for this is the fact that first-order RPA can only include very specific non-mean-field matrix elements, cf. section 3.2.8. All other contributions of the Hamiltonian are neglected by first-order RPA. SRPA on the other hand can benefit from all contributions of the Hamiltonian, see section 3.3. The good convergence of SRPA with respect to the model-space size relates well to the fact that ground-state energies exhibit good convergence, too.

8.4 Correlated RPA

We will now discuss the different RPA methods for including GSCs into RPA calculations. The results from CC-RPA and IM-RPA will be compared to the already known HF results and to each other. We start with the CC-RPA method introduced in chapter 4.

8.4.1 CC-RPA

Crosschecking the Formalism

Before we discuss the results of CC-RPA we first remark the following: The density-matrix based framework that we use for the CC-RPA calculations is quite different from the standard approach in HF-RPA. We already performed an analytical crosscheck of the CC-RPA formulae when deriving the corresponding equations for the special case of HF 1B and 2B GSDs. In terms of numerically crosschecking this new framework, ideally, we would like to compare RPA with a transformed, "correlated" Hamiltonian but uncorrelated density matrices to RPA with a standard Hamiltonian but correlated densities. So far, for both IM-SRG and CC-RPA we have one side of the coin, but not the other. Obtaining, e.g., GSDs from IM-SRG would yield two advantages: First, it would give us the opportunity for a crosscheck of the matrix element based framework with the results from the far more involved density-matrix calculations. Second, we would be able to compare the GSDs from CC and IM-SRG themselves and of course the transition properties linked to them. We already know that CC and IM-SRG ground-state energies are very similar (cf. section 7.2.1 or [Her$^+$16]), so investigating the similarities of these methods on a deeper, more sensitive level containing transitions would be interesting.

Given that, as of today, for neither method we have both, correlated GSDs and correlated Hamiltonians, we resort to the strategy of using the unitary transformation between HO and HF basis for a numerical crosscheck of the density formalism: In HF basis, we have a diagonal 1B mean-field Hamiltonian as described in section 3.1 and can apply the regular RPA equations. Unfortunately, the HF density is, of course, diagonal in HF basis. Any crosscheck with this diagonal HF density will still miss all terms going beyond the HF level, i.e., only the most trivial terms could be crosschecked. So in order to get a non-trivial density, we simply transform the HF density back to the HO basis. This, in combination with the Hamiltonian, also in HO basis, yields a non-trivial problem in both the matrix elements of $\hat{H}$ as well as the density. The information about the HF state (or, equivalently, the HF basis) is fully contained within the density matrix, independently of the basis in which we choose to represent it. Thus, the results should be exactly the same as the ones from a regular RPA calculation in HF basis.

This numerical crosscheck is straight forward and effectively shows no differences between the calculations with the HF state in either HF or HO basis. We will, therefore, refrain from giving a plot with according data since all deviations of eigenvalues and transition strengths are caused by numerical errors which are on the scale of 10^{-3}. In conclusion, the consistency of the new framework has been verified. It has to be stressed that the above check uses the density of a Slater-determinant. Such a density does not have the same formal properties as the density of a correlated state, even if it is represented in a basis other than its eigenbasis. For ruling out any potential bugs that only affect correlation terms, the need for a complementary set of correlated matrix elements of $\hat{H}$ and correlated densities still persists.

Occupation Numbers

For our CC-RPA we use the densities of a correlated state, and we noted in section 4.3 that GSCs, strictly speaking, contradict the idea of a disjoint partitioning of our model space into particle states on the one side and hole states on the other. We also noted that we chose to stick to the ph partitioning, which reduces both the formal as well as the computational effort. This approximation will be reasonable as long as the neglected terms remain small, which in turn can be expected to be the case when disjointness is approximately given. In order to assess this, we will investigate the occupation numbers that are given by the diagonal elements of the 1B density. This will help us to estimate the "degree" of disjointness between particle and hole states. As a mathematical measure to assess this, we calculate the sum of all occupation probabilities within the particle states. The orbitals and corresponding occupation probabilities for the HF and the CCSD density of ^{40}Ca (SAT, $\alpha = 0.08\,\mathrm{fm}^4$) are plotted in Figure 8.13. Keep in mind that, as argued in section 7.3, we are not able to calculate SP energies when using correlated densities. The energies ϵ_i at which we choose to show the occupation numbers associated with a certain orbital are identical to the HF SP energies.

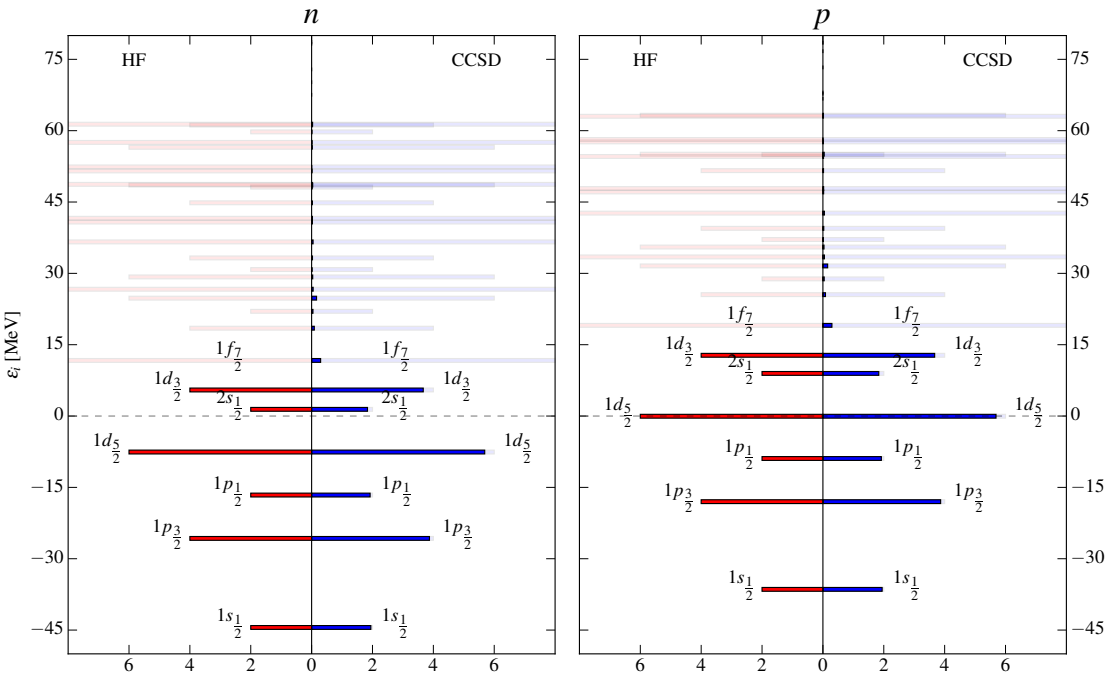

Figure 8.13: Comparison of occupation numbers of ^{40}Ca from HF and CCSD results for the SAT interaction with $\alpha = 0.08\,\mathrm{fm}^4$ and eMax = 12, E3Max = 14 and $\hbar\Omega = 22\,\mathrm{MeV}$.

The structure of the plot is analogous to the one we presented in Figure 7.1. Left-hand panels show the HF occupation numbers, right-hand panels the CCSD values. The left-hand figure shows neutron states, the right-hand proton states. We observe that orbitals which in HF lie at energies right above the Fermi gap carry small occupation probabilities. Orbitals at higher HF energies are almost completely unoccupied. The sum of all occupation probabilities is about 1 for both protons and neutrons. Since for ^{40}Ca we have 20 neutrons and 20 protons, we conclude that roughly 5 % of the occupation probabilities can be attributed to particle states. The situation looks very similar for the other nuclei and also for the use of the EM400 interaction. The analysis of the occupation numbers shows that no cases occur where one or more of the particle states obtain substantial occupation probabilities. Superficially, this justifies the partitioning we use.

It should be stressed, however, that this does not include an assessment of how important the neglected terms are. We will revisit this point in section 8.4.3.

First Results from Correlated CC-RPA

In the previous sections we have investigated the results from both the SAT and the EM400 interaction for uncorrelated HF-RPA calculations. We saw that, for either interaction, first-order RPA yielded transition energies that are too high compared to experimental values.

In Figure 8.14 we compare HF-RPA calculations to CC-RPA for the SAT interaction with $\alpha = 0.08\,\mathrm{fm}^4$. For all nuclei and transition modes, the inclusion of GSCs produces a significant upward shift in energy. The shift is comparable to the one we observed when going from RPA to SRPA, but unlike the shift produced by the second-order terms it increases the transition energies.

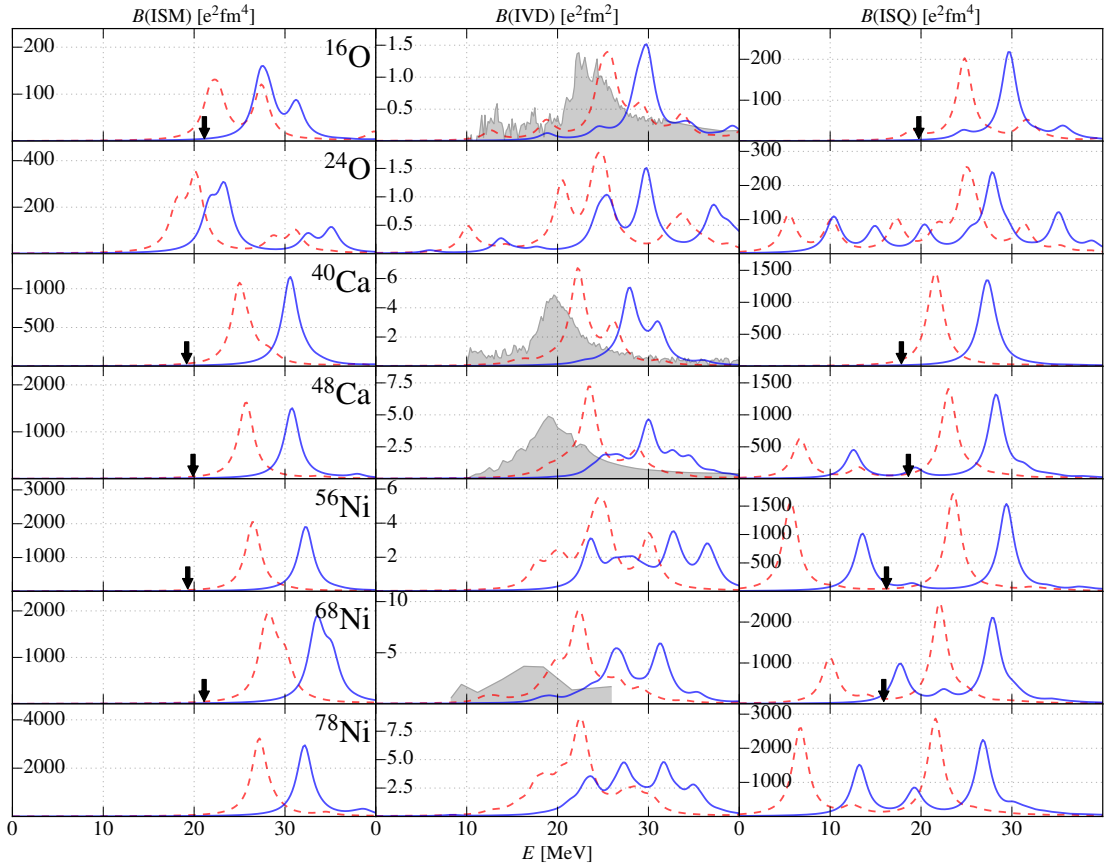

Figure 8.14: Comparison of HF-RPA (- - - -) to CC-RPA (——) results for the SAT interaction. Here we use an SRG flow parameter of $\alpha = 0.08\,\mathrm{fm}^4$ with eMax = 12, E3Max = 14 and $\hbar\Omega = 22\,\mathrm{MeV}$.

Regarding the structure of the correlated transitions, we observe a slight compression of the ISQ mode. The details of the ISM mode remain largely unchanged, and for the IVD mode it appears that the single, strong peaks in the resonance region decrease in strength, yielding an overall more even distribution. Without showing the respective data, we note that the general changes from HF-RPA to correlated CC-RPA are very similar for other SRG flow parameters and also for the EM400 interaction.

The fact that we observe an increase in transition energies is a peculiar result since HF-RPA already yielded energies that are too high. Consequently, including GSCs appears to lead to even larger discrepancies with experiment. In addition, these results strongly contradict the findings of former RPA calculations that tried to include GSCs via occupation numbers yielding a so-called "renormalized" RPA, cf. [Cat$^+$96; Cat$^+$98; GC08; PR10].

From a conceptional point of few, CC-RPA is superior to RPA in that it includes GSCs and produces less inconsistency (see below). For the unexpected result of higher transition energies the most likely explanation is that our calculations are not fully converged. The discussion of HF-based RPA results already showed that the second-order contributions of SRPA have an important impact on the strength distributions. A similar effect can be expected for a CC-based description. This seems especially relevant since we use CCSD densities, where contributions from "doubles" already occur in the calculation of the ground state. Continuing onwards to calculate excited states using only first-order RPA suggests a mismatch.

We want to briefly comment on how CC-RPA performs in terms of consistency. For HF-(S)RPA, the inconsistencies stem from the use of the QBA. While CC-RPA does not employ the true RPA ground state but a (inconsistent) CC state instead, we can still expect the inconsistencies to be smaller than before, although we stress that there is no guarantee for that. We find that within CC-RPA the zero-norm defined in section 4.3.8 is about one order of magnitude smaller in than in HF-RPA. However, this is only the case for the IVD and ISQ modes. Interestingly, for the ISM we see practically no improvement at all when employing the EM400 interaction and the use of the SAT interaction yields only a small reduction of the zero-norm.

Impact of Correlations on Transition Strengths

In Figure 8.14 the first results from CC-RPA were shown. There, we used the ground-state densities both in the construction of the RPA matrix (see section 4.3) as well as for the description of the transitions (see section 6.2). In this sense, the consistent use of GSCs is a two-stage procedure. The use of density matrices in the construction of the RPA matrix influences the eigensystem, and based on the shift we saw that GSCs are important for the transition energies, i.e., the eigenvalues. The structure of the modes, however, which is determined by the eigenvectors, remained largely the same.

In order to assess to what degree the eigenvectors utilize the GSCs within the computation of transitions, we apply GSCs for the first stage, i.e., the construction of the RPA matrix, but not for the second stage, the calculation of transition strengths. The corresponding modes are shown in Figure 8.15.

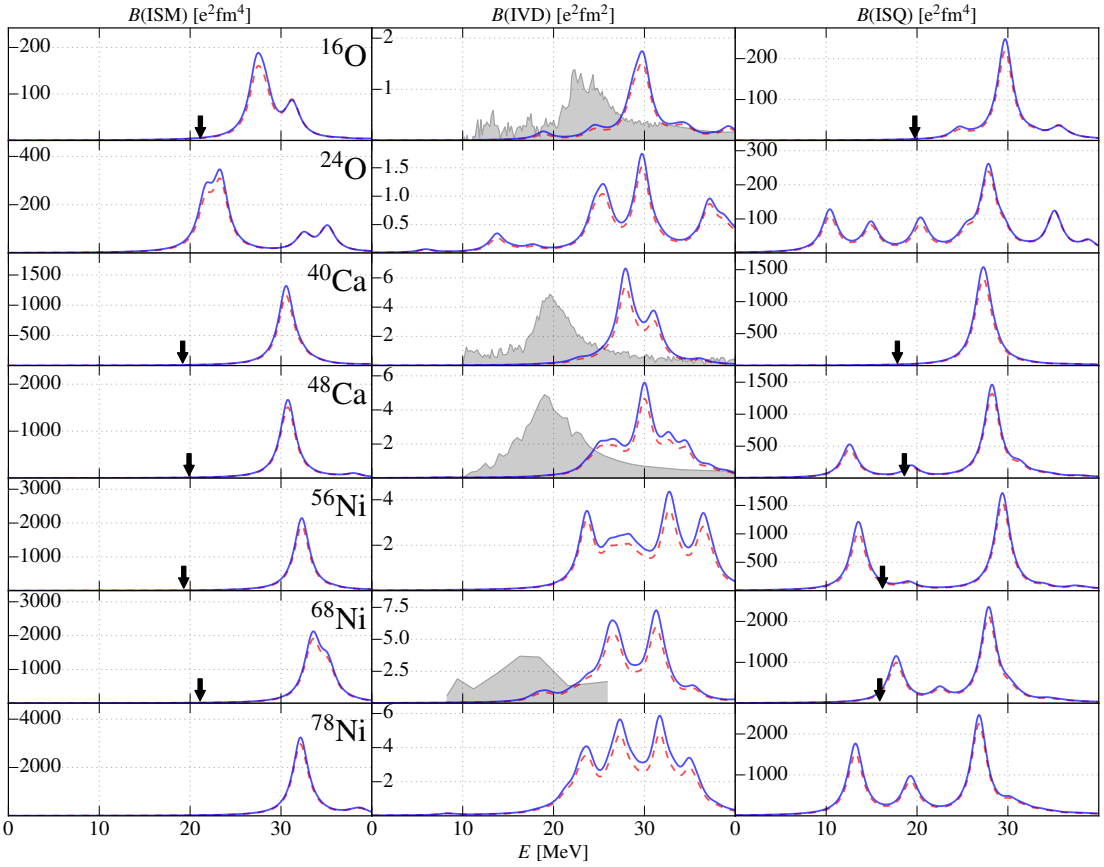

Figure 8.15: CC-RPA results for the SAT interaction, with both uncorrelated (- - - -) and correlated (——) transitions. Here we use an SRG flow parameter of $\alpha = 0.08\,\mathrm{fm}^4$ with eMax = 12, E3Max = 14 and $\hbar\Omega = 22\,\mathrm{MeV}$.

We see that the differences between uncorrelated (- - - -) and correlated (——) transitions are small. In conclusion, we can state that GSCs are important for the RPA matrix and its eigenvalues, but negligible for the description of the transition strengths and the eigenvectors. Of course, we have to stress that this result is obtained on the level of 1B transition operators. Regarding future research, it will be interesting to examine how the use of 2B transition operators, stemming from a consistent evolution or the use of nuclear currents, influences the structure of the strength distributions, both with and without GSCs.

Symmetry of A

In section 4.3.3 we saw that the A matrix of CC-RPA will not necessarily be symmetric due to the fact that the ground state of CCSD is no eigenstate of the Hamiltonian. Numerically, we can probe the degree to which A is asymmetric. For this purpose we calculate the difference $A - A^{\mathrm{T}}$. This filters out all symmetric contributions and yields an anti-symmetric matrix containing all symmetry-breaking terms. The corresponding matrix-plot for the ISM mode of ^{40}Ca with the EM400 interaction ($\alpha = 0.08\,\mathrm{fm}^4$) is given in Figure 8.16. The full A matrix is given for comparison. Note that the diagonal of A exceeds the given color-coding.

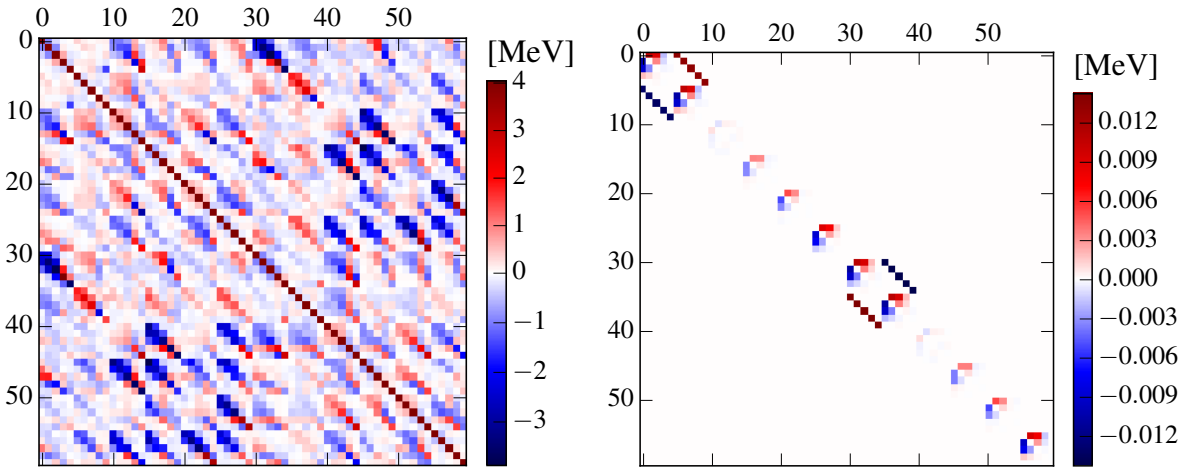

(a) Matrix A (b) Matrix $A - A^{\mathrm{T}}$

Figure 8.16: Asymmetry of the CC-RPA A matrix defined as $A - A^{\mathrm{T}}$ and full A matrix for comparison. Exemplarily shown for the ISM mode of ^{40}Ca with the EM400 interaction. Here we use an SRG flow parameter of $\alpha = 0.08\,\mathrm{fm}^4$ with eMax = 12, E3Max = 14 and $\hbar\Omega = 24\,\mathrm{MeV}$.

We see that the deviations from the symmetric case are of the order of $10^{-2}\,\mathrm{MeV}$, whereas the off-diagonal elements of A are of the order of MeV. Keeping in mind that the A matrix has ph excitation energies as its diagonal entries which are of the order of $10^2\,\mathrm{MeV}$, we can safely assume that the asymmetric parts of A are insignificant. In fact, to further verify this we can substitute A in the RPA eigenvalue problem by its transposed A^{T}. Doing so, we find that the eigensystem of CC-RPA indeed remains almost unchanged. All discrepancies can be neglected. This holds for all nuclei and excitation modes.

At this point we remark on another issue of CC-RPA regarding symmetry. In section 4.2.2 we stated that, as a consequence of the non-Hermiticity of the effective Hamiltonian, CC possesses two eigensystems. Naturally, formally this also produces two sets GSDs. As discussed earlier, such an asymmetric density matrix is unphysical. Hence, as the input to CC-RPA we can only use one of the two sets of densities. We find that the computation of transitions with either set or the arithmetic mean of both always yields the same eigensystem, negligible discrepancies aside. The differences in the energies, for example, are on a scale of $10^{-3}\,\mathrm{MeV}$. We infer that CC-RPA is robust with respect to this formal problem of asymmetry.

Model-Space Convergence

Again, we want to test the degree of convergence of our results, this time from CC-RPA. We will focus on the convergence with respect to the SRG flow parameter. The corresponding plot is shown in Figure 8.17 for the SAT interaction. We find good convergence for light nuclei. For heavier nuclei the degree of convergence decreases to roughly the quality we observed for HF-RPA, cf. Figure 8.4. For the EM400 interaction the SRG dependence is also better for lighter nuclei but overall not quite as good as for the SAT interaction. In contrast to HF-RPA, we see that higher SRG flow parameters lead to lower transition energies. This holds for either interaction.

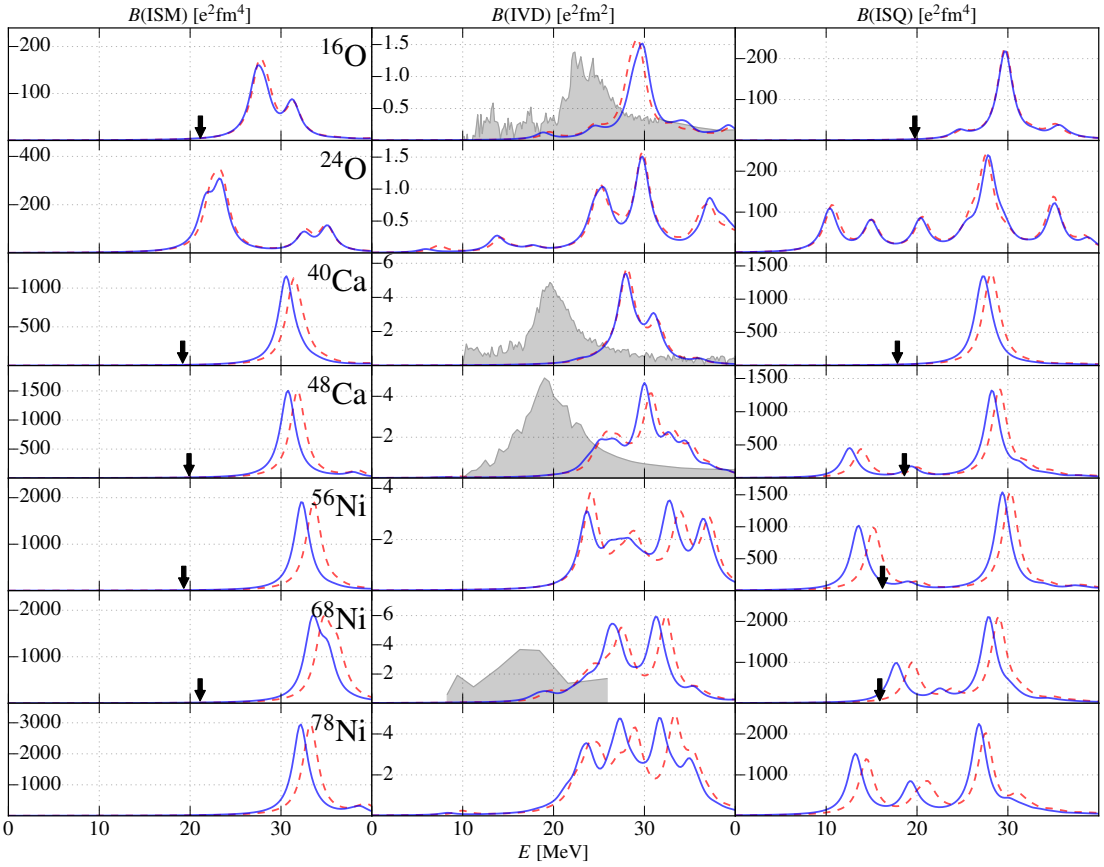

Figure 8.17: Results from CC-RPA for the SAT interaction with SRG flow parameters of $\alpha = 0.04\,\mathrm{fm}^4$ (- - - -) and $\alpha = 0.08\,\mathrm{fm}^4$ (——). Here we use eMax = 12, E3Max = 14 and $\hbar\Omega = 22\,\mathrm{MeV}$.

8.4.2 IM-RPA

In this section we present our second method for obtaining correlated RPA results, the IM-RPA. Again, we emphasize that within IM-RPA, the HF state is the true ground state of the system described by the transformed Hamiltonian. Consequently, we do not have to concern ourselves with non-integer occupation numbers as in section 8.4.1 and the disjoint ph partitioning is exact within IM-RPA.

In section 5.2.2 we stated that IM-SRG does not conserve the diagonality of the mean-field Hamiltonian that we have within HF. We also claimed that these HF-breaking terms are small which now we will confirm numerically. For that purpose, in Figure 8.18 we plot the mean-field Hamiltonian of the IM-transformed Hamiltonian, exemplarily for ^{40}Ca (EM400, $\alpha = 0.08\,\mathrm{fm}^4$).

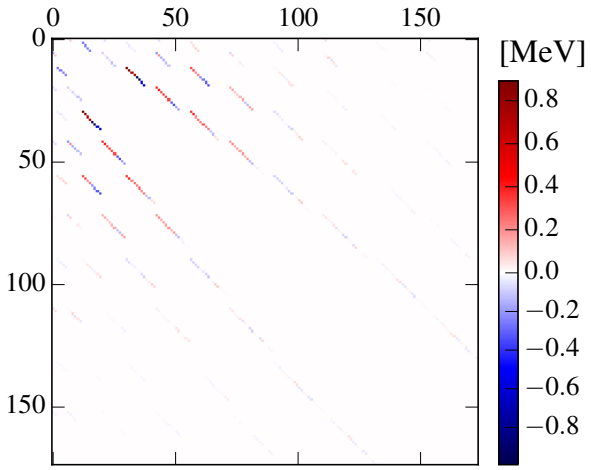

Figure 8.18: Mean-field Hamiltonian of ^{40}Ca for the IM-transformed EM400 interaction. The diagonal has been set to zero for better visibility of the off-diagonal terms. Here we use an SRG flow parameter of $\alpha = 0.08\,\mathrm{fm}^4$ with eMax = 12, E3Max = 14 and $\hbar\Omega = 24\,\mathrm{MeV}$.

Note that the dimension of the mean-field matrix corresponds to the number of single-particle states within the model space, i.e., this is determined by eMax. The ordering in which these states appear in the columns or rows of this matrix follows an internal convention of the code. The diagonal of the mean-field matrix has been set to zero in order to emphasize the off-diagonal terms. It can be seen that none of the absolute values of the off-diagonal terms exceeds 1 MeV. For comparison, since the diagonal consists of the IM-transformed HF energies, its entries range from roughly $-50\,\mathrm{MeV}$ to $200\,\mathrm{MeV}$, cf. Figure 7.1. The situation is qualitatively the same for other nuclei and also for the SAT interaction. Thus, we can conclude that the off-diagonal terms introduced via IM-SRG are sufficiently small to be neglected.

With this, we can readily employ the standard RPA formalism for the computation of IM-RPA. Figure 8.19 shows the results of an IM-RPA calculation for the SAT interaction ($\alpha = 0.08\,\mathrm{fm}^4$). So far, the IM-SRG transformation for non-scalar operators has not been implemented. Hence, we calculate transition strengths from HF matrix elements. This inconsistency concerns the transition strengths but not the transition energies, i.e., the eigenvalues, of IM-RPA. We will revisit this issue in section 8.4.3.

Very similar to the case of CC-RPA, we observe a significant shift to higher energies while the structure of the modes remains almost unchanged.

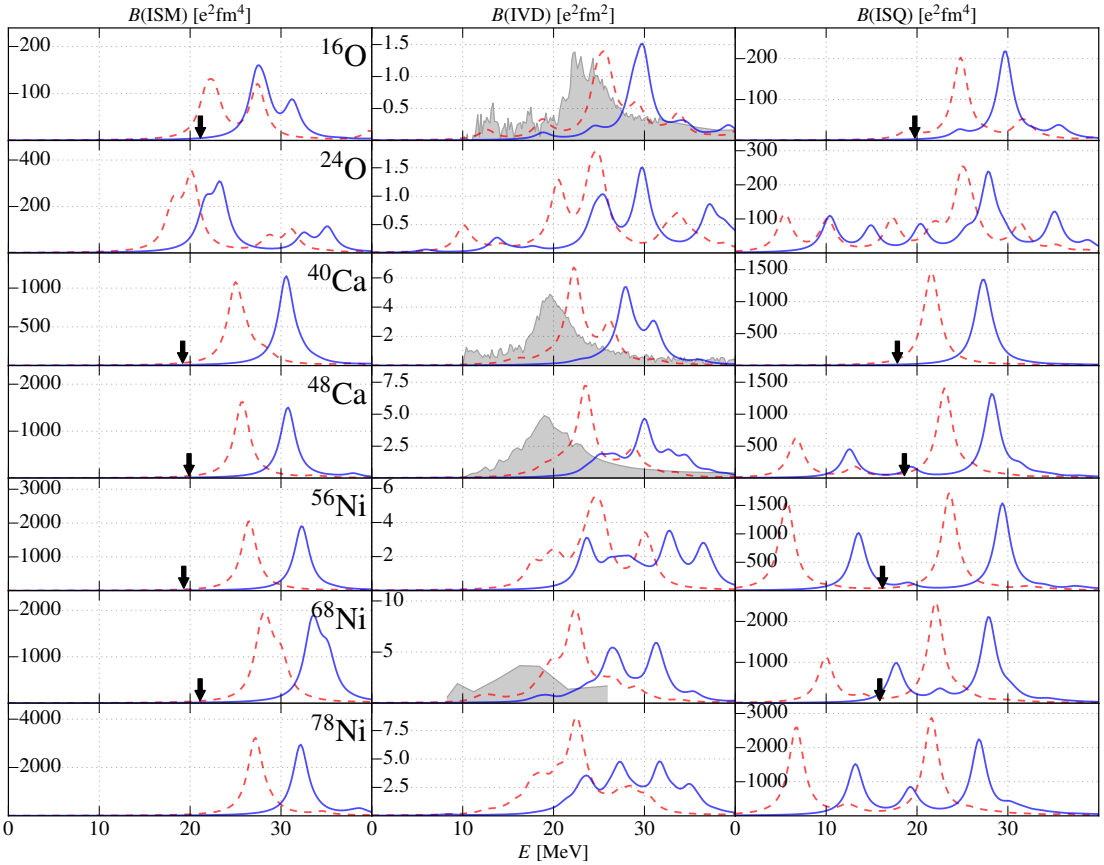

Figure 8.19: Results from RPA (- - - -) and IM-RPA (——). Here we use the SAT interaction ($\alpha = 0.08\,\mathrm{fm}^4$) with eMax = 12, E3Max = 14 and $\hbar\Omega = 22\,\mathrm{MeV}$.

For IM-RPA, there is this a relatively easy mathematical motivation for this effect. In Figure 7.1 we already saw a widening of the Fermi gap when going from HF to IM-SRG. However, this representation makes it difficult to see exactly how much energy the individual ph excitations gain. To facilitate this analysis, in Figure 8.20 we plot the cumulative number of ph excitations over the excitation energy at which they appear, both for HF (——) and IM-SRG (——).

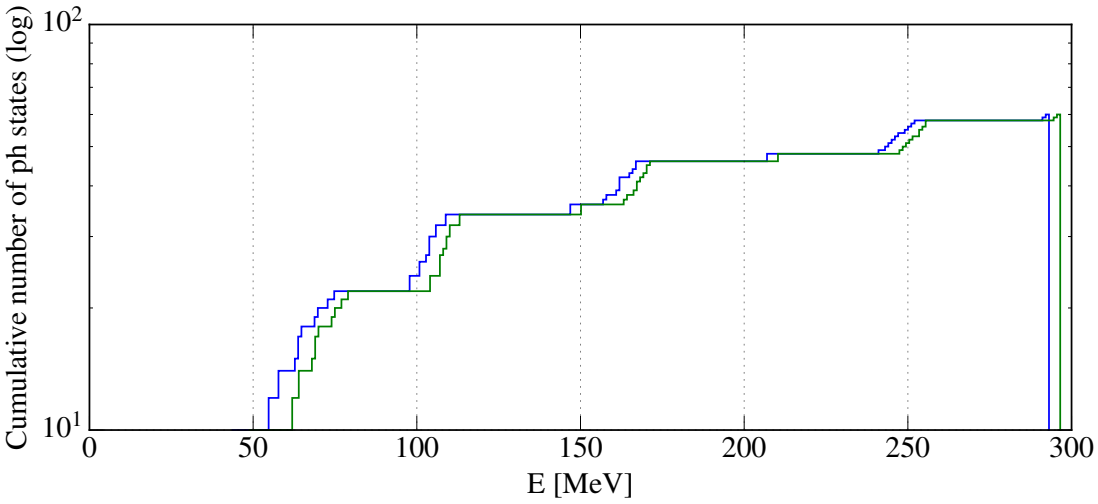

Figure 8.20: Cumulative number of 1p1h excitations of the ISM mode of ^{40}Ca for matrix elements from HF (——) and from IM-SRG (——). Here we use the SAT interaction with an SRG flow parameter of $\alpha = 0.08\,\mathrm{fm}^4$ with eMax = 12, E3Max = 14 and $\hbar\Omega = 22\,\mathrm{MeV}$.

The chosen case is the ISM mode of ^{40}Ca for the SAT interaction with $\alpha = 0.08\,\mathrm{fm}^4$. We can see that for both cases the number of ph excitations and the intervals at which they appear are very similar up to an offset of about 7 MeV. This corresponds well to the observed shift.

IM-SRG Flow and Generator Dependence

A few remarks on the robustness of IM-RPA with respect to its input from IM-SRG are in order. In the process of decoupling the ground state, the IM-SRG flow has to be terminated at some point. For meaningful results we need the IM-RPA calculations to converge with respect to the IM-SRG flow. In order to assess this convergence, we look at strength distributions obtained from different points of the IM-SRG evolution, i.e., Hamiltonians $\hat{H}(s)$ with varying s. Exemplarily, in Figure 8.21 we show the convergence of the ISQ transition of ^{16}O using the SAT interaction ($\alpha = 0.08\,\mathrm{fm}^4$). Plotted are the strength distributions for RPA (·····) and IM-RPA at flow parameters of $s = 0.1$ (-·-·-), $s = 0.5$ (- - - -) and $s = 0.9$ (——). For the IM-SRG evolution the unitless White generator has been employed.

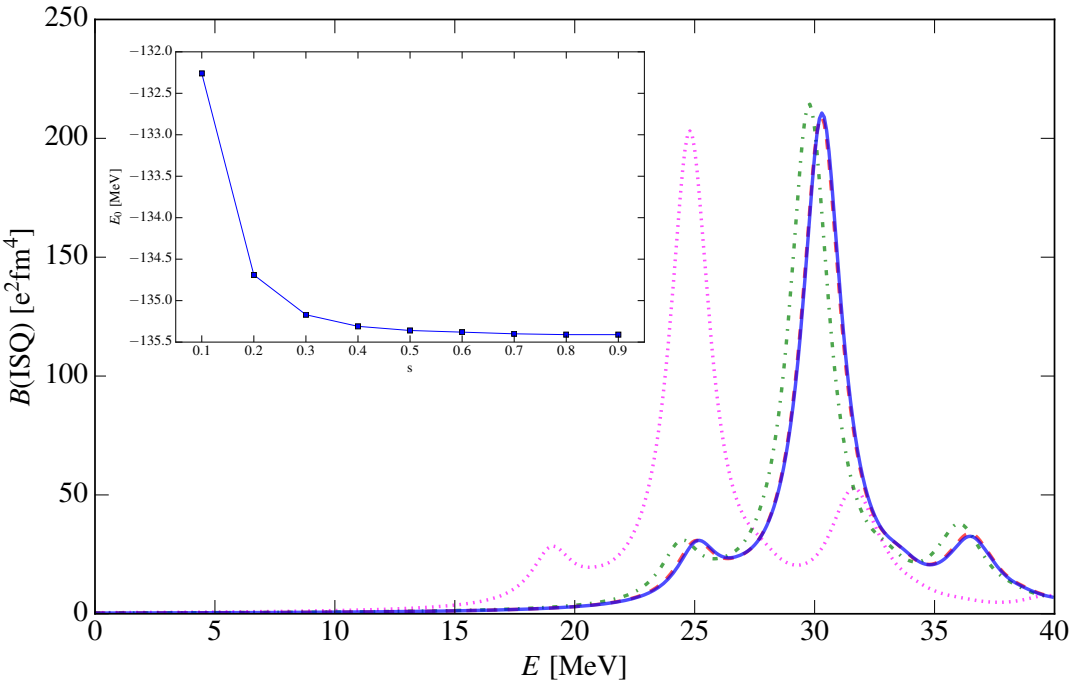

Figure 8.21: ISQ response of ^{16}O for RPA (·····) and IM-RPA at flow parameters of $s = 0.1$ (-·-·-), $s = 0.5$ (- - - -) and $s = 0.9$ (——). For the flow the White generator has been employed. Here we use the SAT interaction ($\alpha = 0.08\,\mathrm{fm}^4$) with eMax = 12, E3Max = 14 and $\hbar\Omega = 22\,\mathrm{MeV}$.

It turns out that IM-RPA calculations converge very rapidly. After the first iteration step, leading to $s = 0.1$, the transition energies are already shifted significantly upward. A small energy shift exists for the next steps up to $s = 0.5$, for further iterations beyond this point almost no change can be found up to $s = 0.9$. For a comparison in terms of the IM-SRG convergence, the inset in Figure 8.21 shows the evolution of the ground-state energy E_0 as a function of the flow parameter s. Here the starting point of $s = 0$, corresponding to the HF case, has been omitted.

We note that, along with the convergence regarding the IM-SRG flow, we also see that IM-RPA is indeed completely identical to IM-TDA, as we can expect for the a sufficiently decoupled ground state. For this aspect no data will be shown.

As stated in section 5.1.2, when performing IM-SRG we have to choose a generator that will characterize the evolution. Ideally, the choice of the generator should make little to no difference and thus different generators would yield the same results. It is known that different IM-SRG generators yield practically identical ground-state energies [TBS11; Her$^+$13b]. Ground-state energies themselves, however, tend to be rather robust against structural details, so this is by far no guarantee that IM-RPA results will be stable against a variation of the generators. For robustness of IM-RPA results we need at least a certain stability of the single-particle spectra. A comparison between SP spectra obtained with the White and the imaginary-time generator can be found in Figure 8.22. Due to computational requirements, we limit this investigation to a model space of eMax = 8 and to the ^{40}Ca isotope with the EM400 interaction ($\alpha = 0.08\,\mathrm{fm}^4$).

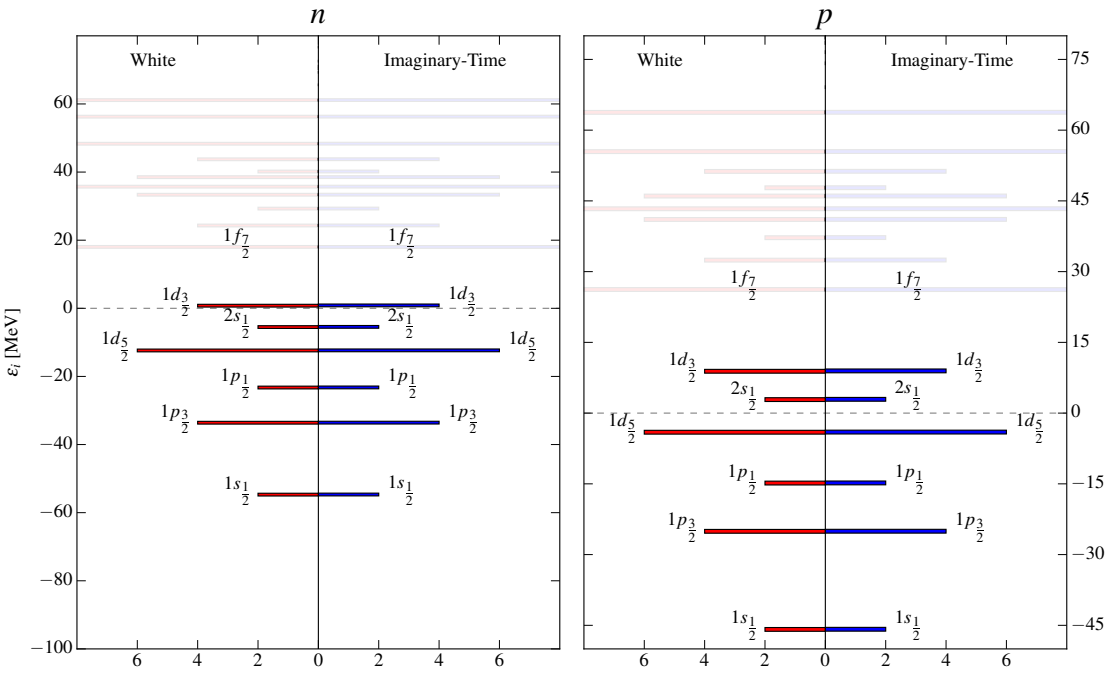

Figure 8.22: Comparison of IM-SRG SP states of ^{40}Ca using the White (left-hand panels) and the imaginary-time (right-hand panels) generator. Here we use the EM400 interaction ($\alpha = 0.08\,\mathrm{fm}^4$) with eMax = 8, E3Max = 14 and $\hbar\Omega = 24\,\mathrm{MeV}$.

We see that the SP spectra are practically identical. The comparison between the White and the Wegner generator can be seen in Figure 8.23. Here the differences are slightly larger but overall still extremely small. As a reminder, the differences between HF and IM-SRG SP spectra, for example, were significantly larger, cf. Figure 7.1.

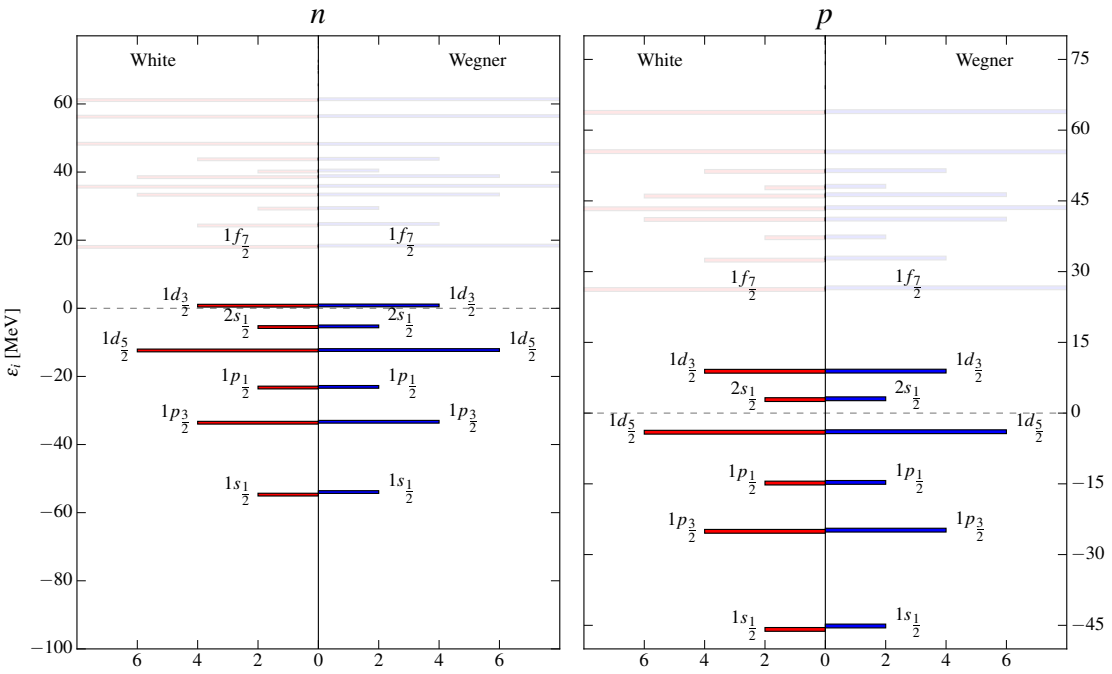

Figure 8.23: Comparison of IM-SRG SP states of ^{40}Ca using the White (left-hand panels) and the Wegner (right-hand panels) generator. Here we use the EM400 interaction ($\alpha = 0.08\,\mathrm{fm}^4$) with eMax = 8, E3Max = 14 and $\hbar\Omega = 24\,\mathrm{MeV}$.

The actual calculation of transition strengths yields a similar picture. The IVD response of ^{40}Ca using all three generators is presented in Figure 8.24. In conclusion, we find that IM-RPA converges both with respect to the IM-SRG flow and also across different generators. From this, we infer that IM-SRG is a robust input to RPA calculations.

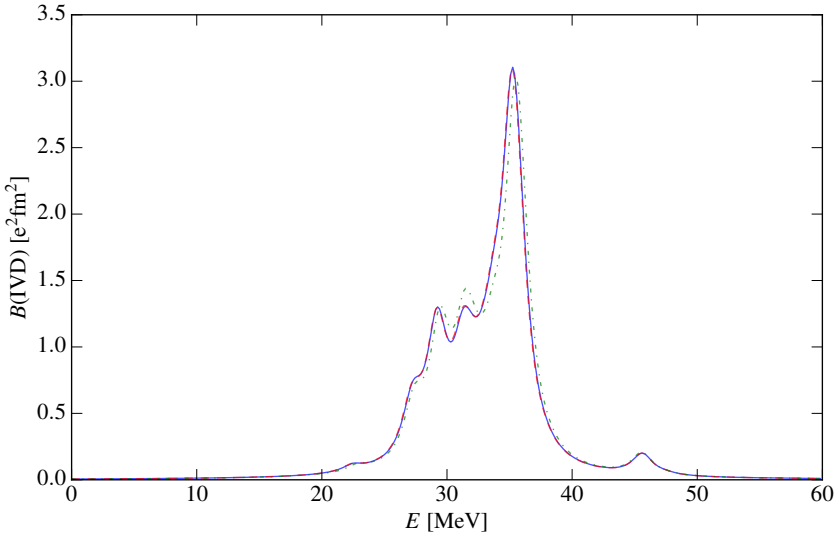

Figure 8.24: IVD response of ^{40}Ca within IM-SRG using the Wegner (·-·-·), the imaginary-time (- - - -) and the White (——) generator. Here we use the EM400 interaction ($\alpha = 0.08\,\mathrm{fm}^4$) with eMax = 8, E3Max = 14 and $\hbar\Omega = 24\,\mathrm{MeV}$.

Model Space Convergence

Similar to the case of CC-RPA, due to computational costs we are limited in the convergence checks that we can perform. We focus on the stability with respect to the SRG flow parameter. The corresponding plot is shown in Figure 8.25 for the SAT interaction. We find that the behaviour is strongly related to the case of CC-RPA SRG stability, cf. Figure 8.17.

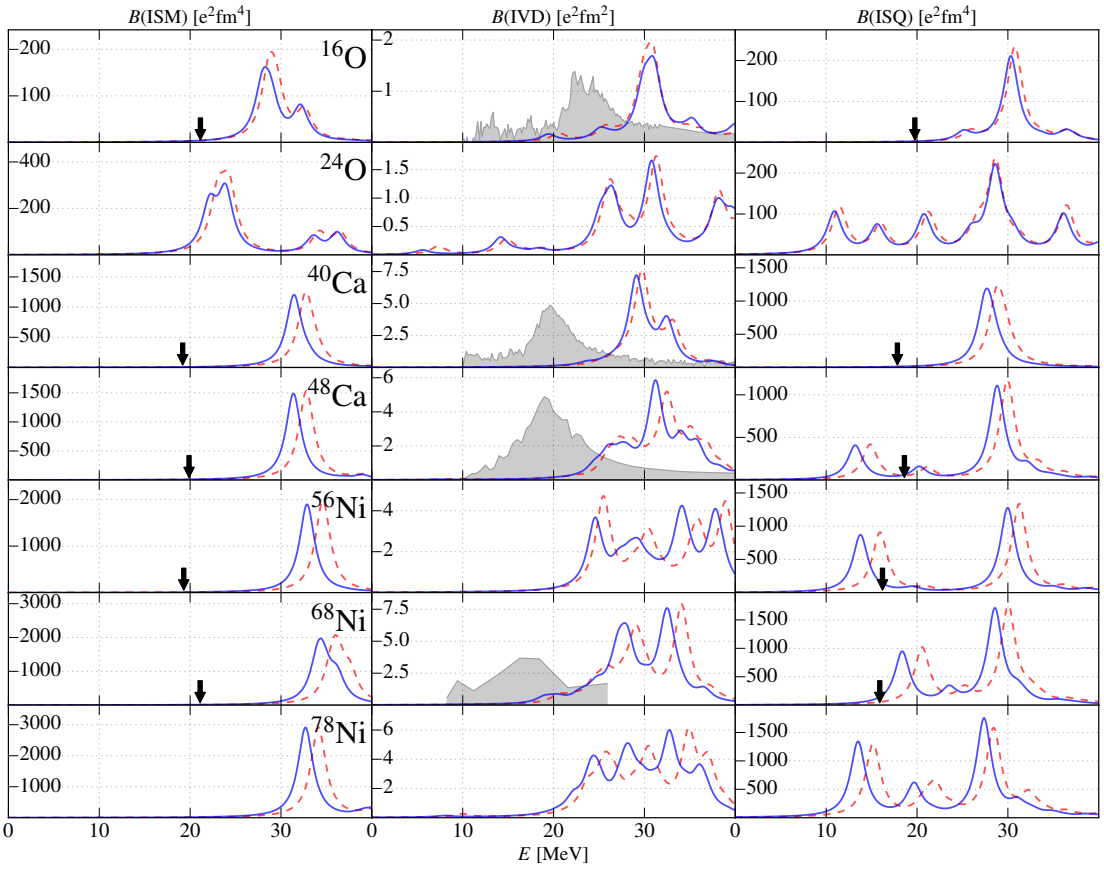

Figure 8.25: IM-RPA results for the IM-SRG transformed SAT interaction with SRG flow parameters of $\alpha = 0.04\,\mathrm{fm}^4$ (- - - -) and $\alpha = 0.08\,\mathrm{fm}^4$ (——). Here we use eMax = 12, E3Max = 14 and $\hbar\Omega = 22\,\mathrm{MeV}$.

Lighter nuclei exhibit a relatively good stability which decreases for heavier systems. In contrast to HF-RPA, we see that larger SRG flow parameters lead to lower transition energies. Thus, the effect that larger flow parameters lead to lower transition energies can be observed for both IM-RPA and CC-RPA. For the EM400 interaction the SRG stability is also better for lighter nuclei, but overall not quite as good as for the SAT interaction, cf. Figure 8.26.

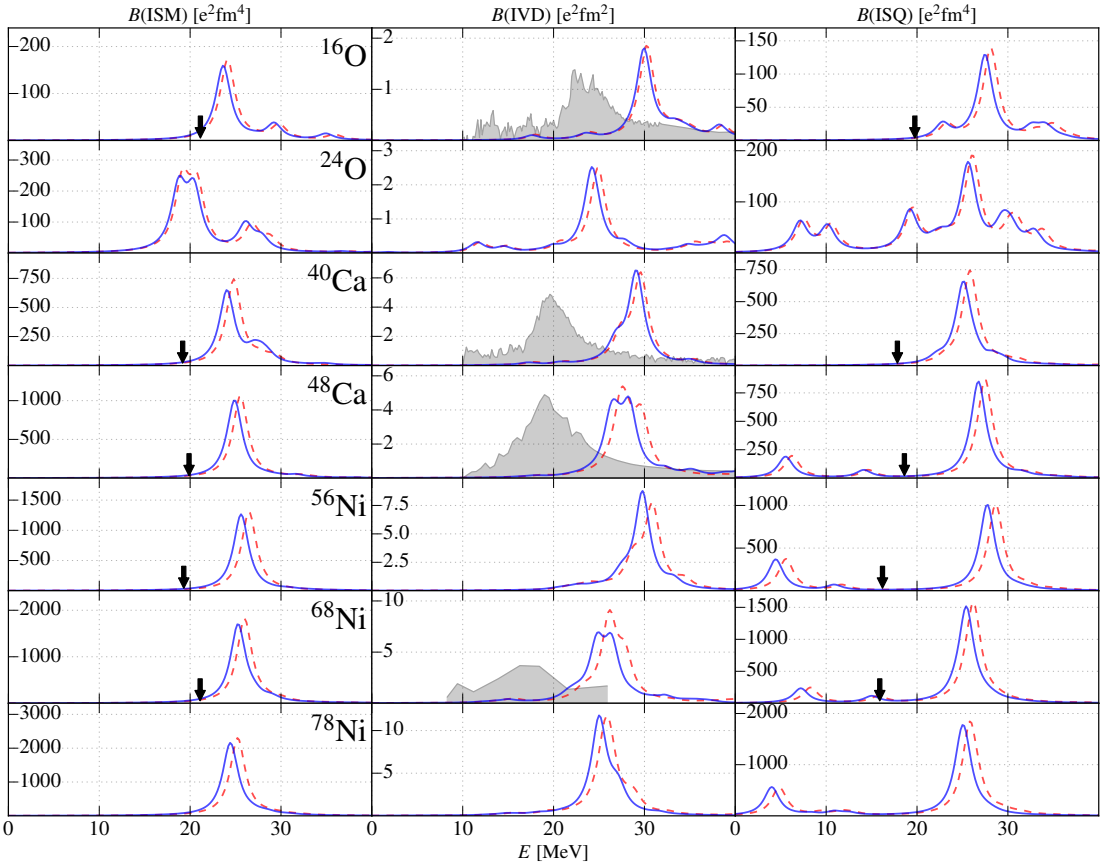

Figure 8.26: IM-RPA results for the IM-SRG transformed EM400 interaction with SRG flow parameters of $\alpha = 0.04\,\mathrm{fm}^4$ (- - - -) and $\alpha = 0.08\,\mathrm{fm}^4$ (——). Here we use eMax = 12, E3Max = 14 and $\hbar\Omega = 24\,\mathrm{MeV}$.

8.4.3 Comparison of HF-RPA, IM-RPA and CC-RPA

In both, CC-RPA and IM-RPA, we saw an upward shift in the transition energies. Both methods include GSCs into the RPA calculations, though in very different ways. A resemblance of the results from these correlated methods is all the more interesting, and on this account we will now compare HF-RPA (-·-·-), CC-RPA (- - - -) and IM-RPA (——) results in Figure 8.27.

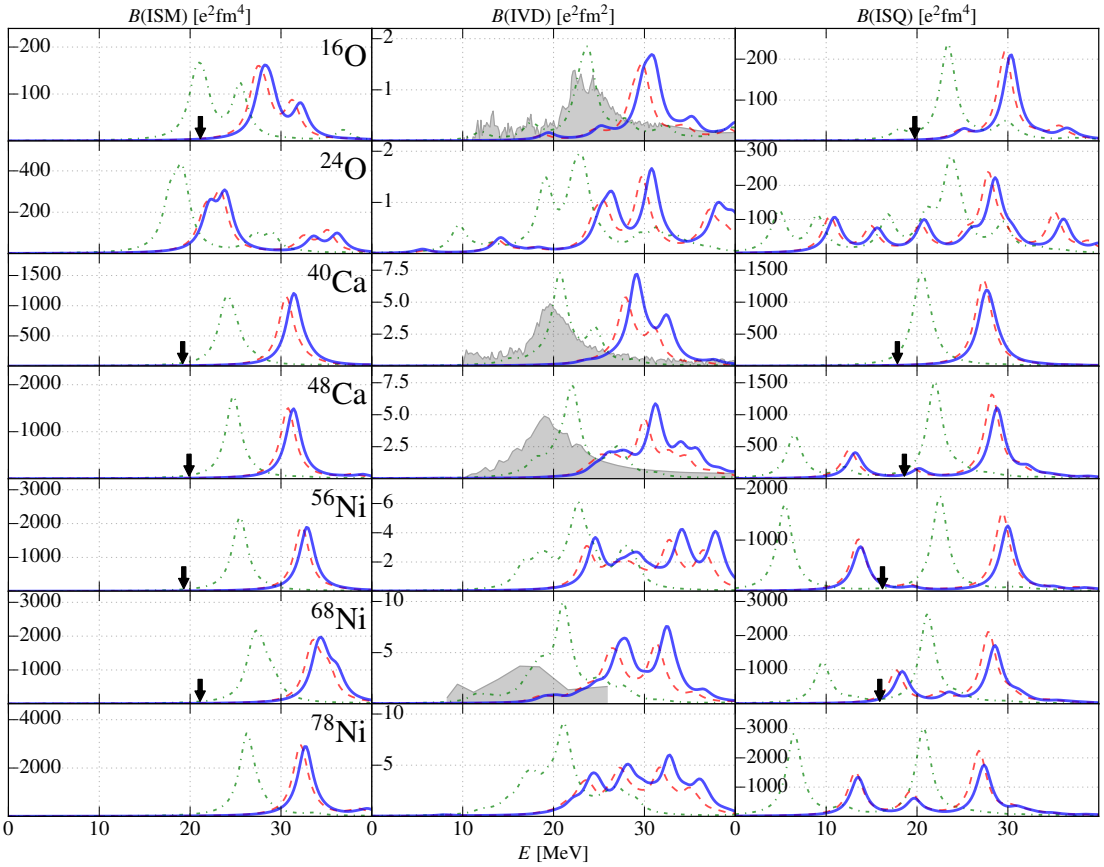

Figure 8.27: Results from HF-RPA (-·-·-), CC-RPA (- - - -), IM-RPA (——). Here we use the SAT interaction ($\alpha = 0.08\,\mathrm{fm}^4$) with eMax = 12, E3Max = 14 and $\hbar\Omega = 22\,\mathrm{MeV}$.

Interestingly, we see that not only is the shift in energy almost identical, we also observe that, for those cases where the structure of the response changes with the inclusion of GSCs, the structures change in a very similar way for CCSD and IM-SRG. The responses obtained from the latter seem to appear at slightly higher energies than CCSD, but given what we know about model space convergence of RPA, these changes are relatively small.

We find a similar pattern for the EM400 interaction, see Figure 8.28. The agreement for the ISM and ISQ response is even better than for the SAT interaction. For the IVD the variations between both methods are about the same.

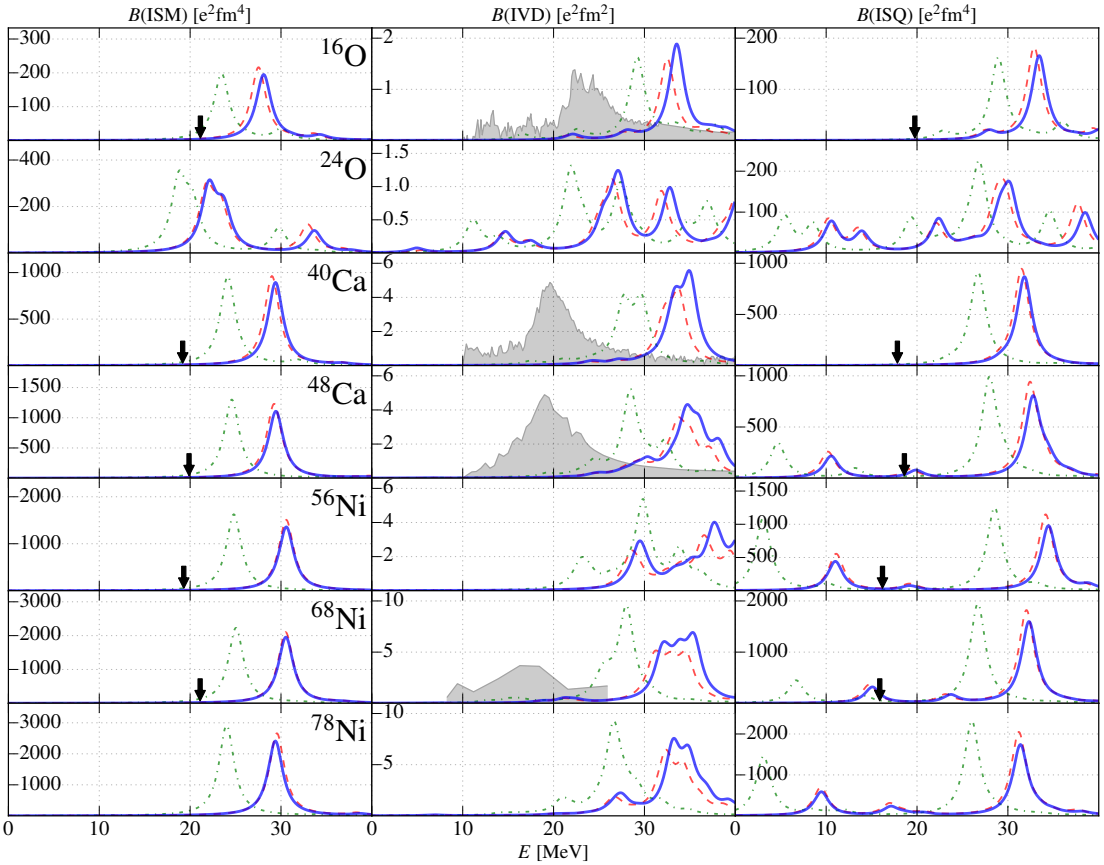

Figure 8.28: Results from HF-RPA (-·-·-), CC-RPA (- - - -), IM-RPA (——). Here we use the EM400 interaction ($\alpha = 0.08\,\mathrm{fm}^4$) with eMax = 12, E3Max = 14 and $\hbar\Omega = 24\,\mathrm{MeV}$.

This similarity is, in many ways, a very important result. Note that there is no formal constraint that would enforce an equality of CCSD and IM-SRG results. It is known that these methods yield very similar ground-state energies, but we stress that, nonetheless, the similarities we find for the transition spectra of IM-SRG and CCSD cannot be expected. With IM-RPA and CC-RPA, we have two correlated methods for the calculation of strength distributions that go beyond the level of HF. IM-RPA is realized via the use of a transformed Hamiltonian while CC-RPA uses an untransformed Hamiltonian in conjunction with densities that describe a correlated state. Therefore, both correlated RPA approaches employ a completely different formalism. We saw that a shortcoming of CC-RPA was the assumption of disjointness in the ph basis despite the use of a correlated state. In IM-RPA, the flow transfers all GSCs into the matrix elements themselves and the HF state is the true ground state for the Hamiltonian. Here, the problem of approximate disjointness does not arise. The responses from IM-RPA employ untransformed, uncorrelated transition operators. CC-RPA, on the other hand, is capable of including correlations into the description of transitions, which allowed us to investigate the importance of correlations regarding transitions. We saw that the changes were relatively small.

Together, this gives us a unique, stereoscopic view on correlated transitions in RPA methods. The unexpected but fortunate similarities that we observe, both in energies and transition strengths, allow us to infer that neither of the above issues has severe consequences for the RPA-based description of transitions.

At this point, the strongest downside of both methods is that they predict the transitions at too high energies which, in fact, the inclusion of GSCs made even worse. We saw for HF-SRPA

in section 8.3 that taking into account second-order ph contributions lowered the transition energies substantially. Therefore, at least with respect to this aspect we can assume that first-order RPA, even based on correlations, does not yield converged results. For the case of CC-RPA the discussion ends here due to the lack of higher-order densities, but we will investigate this issue further for IM-SRPA in the next section.

8.5 Correlated SRPA: IM-SRPA

As the last method for the description of correlated transitions, we discuss the IM-SRPA which is simply the second-order extension of IM-RPA, identical to the case of HF-(S)RPA. We already discussed the robustness of IM-based RPA calculations and note that the input from IM-SRG does not change. The IM-SRG single-particle spectra or the mean-field Hamiltonian as seen in section 8.4.2 are exactly the same, whether we include second-order terms in RPA or not. In fact, if at all we could expect the influence of the non-diagonal mean-field terms, cf. Figure 8.18, to be even less important since the diagonal of A_{22} carries the single-particle energies of 2p2h excitations which are roughly twice as large as those from A_{11}. Therefore, we do not repeat this discussion.

In Figure 8.29 we compare results obtained from IM-RPA (- - - -) and IM-SRPA (——).

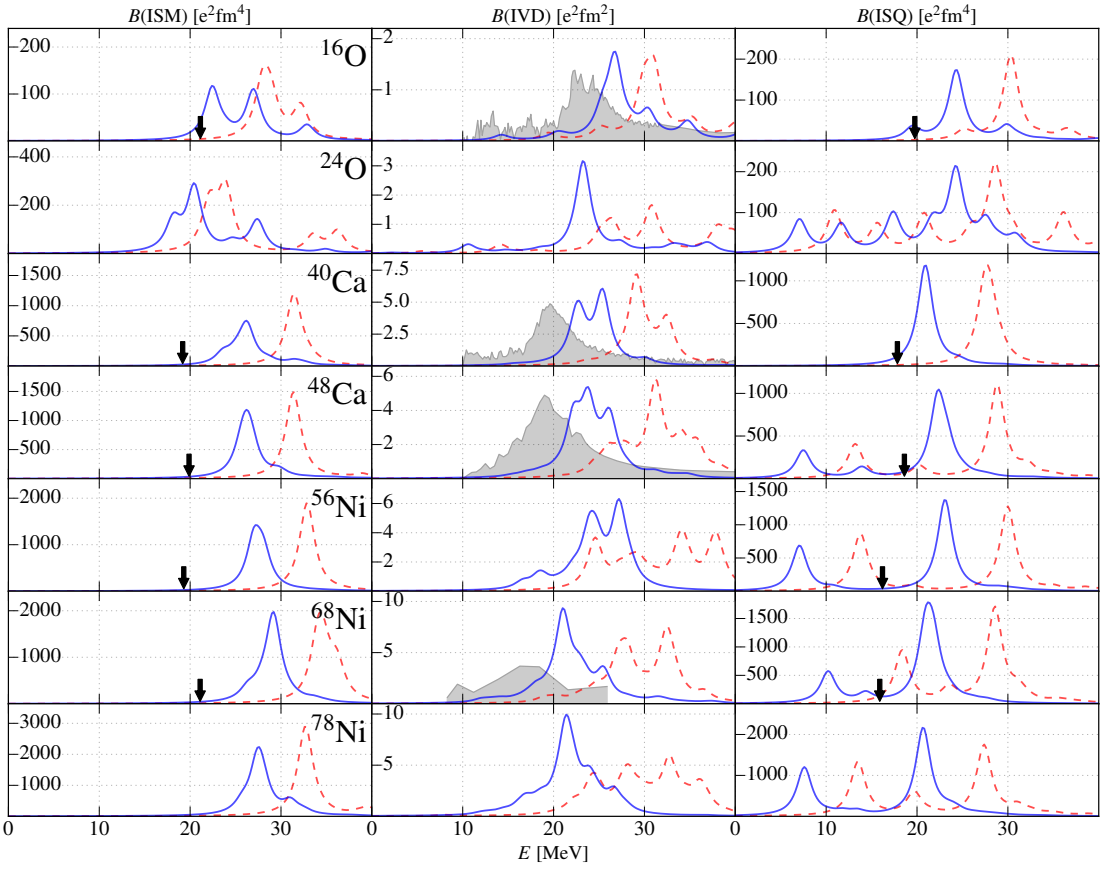

Figure 8.29: Comparison of results from IM-RPA (- - - -) and IM-SRPA (——). Here we use the SAT interaction ($\alpha = 0.08\,\mathrm{fm}^4$) with eMax = 12, E3Max = 14 and $\hbar\Omega = 22\,\mathrm{MeV}$.

Overall, we see a similar pattern as for the HF case. The downward shift in energy is of similar strength for IM as it is for HF. Hence, the upward shift resulting from the use of IM-SRG matrix elements that we saw comparing HF-RPA and IM-RPA can also be seen in SRPA. If the shift associated with the inclusion of second-order terms would have been significantly stronger in IM-based RPA, the use of correlations may have ultimately resulted in very similar excitation energies as we obtain from the uncorrelated variant. The corresponding comparison of HF-SRPA (- - - -) and IM-SRPA (——) is given in Figure 8.30.

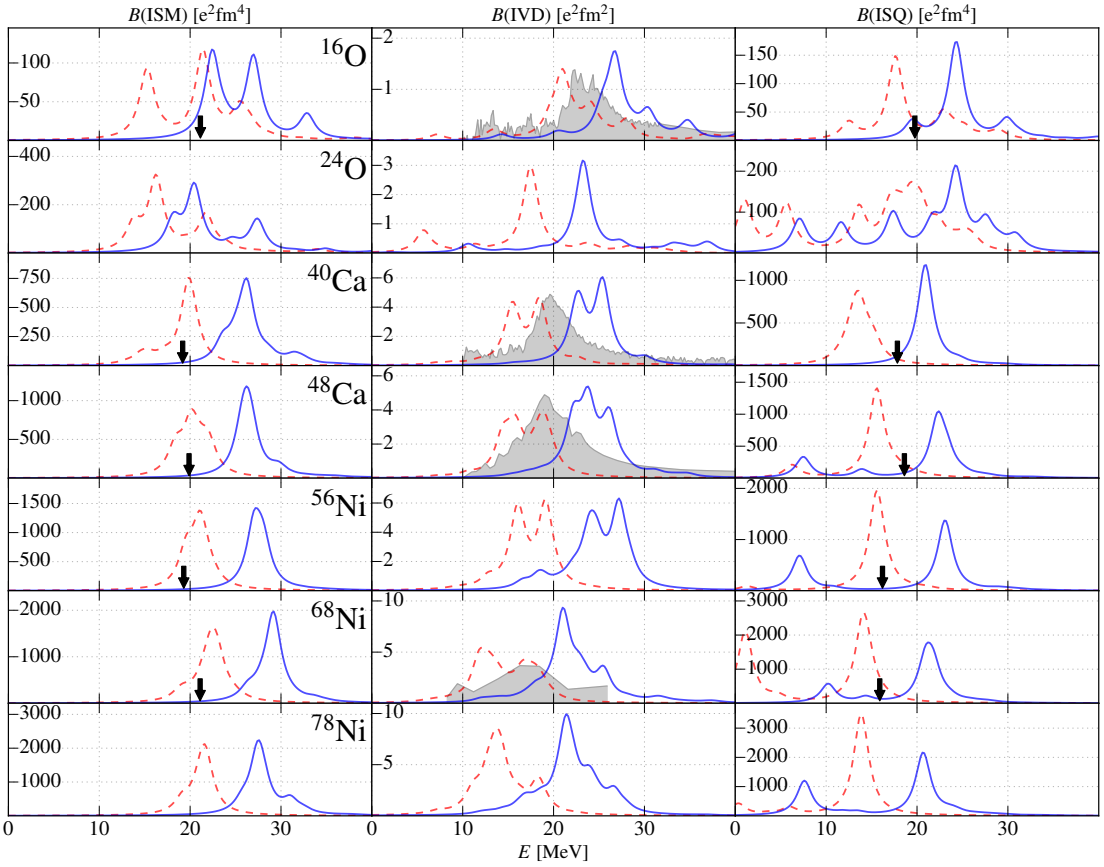

Figure 8.30: Comparison of results from HF-SRPA (- - - -) and IM-SRPA (——). Here we use the SAT interaction ($\alpha = 0.08\,\mathrm{fm}^4$) with eMax = 12, E3Max = 14 and $\hbar\Omega = 22\,\mathrm{MeV}$.

As a consequence, the inclusion of correlations by means of the IM-SRG leads to a prediction of transitions at too high energies. Nonetheless, we stress that, with exception of the ISM mode, the agreement with experiment is not per se worse in IM-SRPA. In many cases the discrepancies for the correlated variant are roughly of the same size as for the uncorrelated version, the calculations simply predict slightly higher instead of slightly lower energies.

We also stress that IM-SRPA does not suffer from the instabilities that we found in HF-SRPA. In fact, independently of the interaction or the SRG flow parameter we do not find a single case with instabilities. For the ISQ this can be seen in the low-energy part of the spectra. The lack of instabilities can be attributed to the fact that the IM-SRG ground state is decoupled from both its 1p1h and 2p2h excitations, though the initial upward shift in energy may play a role in this as well.

In terms of convergence, we stress that larger model spaces, i.e., employing eMax = 14 or higher, can be expected to further reduce the predicted energies. This would improve the agreement of IM-SRPA results with experiment. Other aspects, such as using a full, non-normal-ordered 3B force or an extension to consistently transformed transition operators, may of course influence both position and structure of the responses as well, but these effects cannot easily be anticipated.

8.5.1 Sum Rules

We mentioned before that in converged SRPA calculations, we are not able to obtain the entire spectrum of the SRPA matrix, but only a small fraction. As a consequence, we also only get a certain percentage of the total strength. The question arises how large this fraction is. If we were to obtain only a few percent, our calculations would hardly yield meaningful results.

The total strength is given by the non-energy-weighted sum rule for TDA, and also for IM-based RPA calculations. Again, this is due to the fact that the decoupling of IM-SRG renders the Y amplitudes obsolete, effectively reducing RPA to TDA calculations. For RPA calculations with matrix elements from HF, only the energy-weighted sum rule is valid. More detailed information on this can be found in section 6.3.

In order to test to what degree the obtained subset of eigenvalues exhausts the total strength, we can compare the corresponding values. For IM-SRPA calculations using the SAT interaction ($\alpha = 0.08\,\mathrm{fm}^4$) this is done in Table 8.2 for the non-energy-weighted sum rule. We find that the subset of eigenvalues exhausts roughly 90 % of the total strength. From this we conclude that enough eigenstates have been calculated, since no more than 10 % of the strength are neglected, most of which can be expected at higher energies that do not concern collective excitations.

Nucleus	ISM	IVD	ISQ
^{16}O	88.68	86.19	91.46
^{24}O	91.72	81.31	93.07
^{40}Ca	85.14	87.39	89.98
^{48}Ca	92.65	84.79	93.50
^{56}Ni	90.41	87.67	93.93
^{68}Ni	88.53	85.90	92.37
^{78}Ni	92.19	86.39	94.26

Table 8.2: Results of the non-energy-weighted sum rule from IM-SRPA calculations. Given are the fractions of the total strengths for the obtained subset of eigenvalues. All values are given in percent. Here we use the SAT interaction ($\alpha = 0.08\,\mathrm{fm}^4$) with eMax = 12, E3Max = 14 and $\hbar\Omega = 22\,\mathrm{MeV}$.

At the same time, the energy-weighted sum rule gives values of roughly 70 %. No data will be shown. This emphasizes the difference between both sum rules: Thanks to the non-energy-weighted sum rule, we can be sure to have obtained around 90 % of the total strength. The lower values for the energy-weighted sum rule simply state that we included 70 % of the *energy weighted* sum rule. The difference of 20 % stresses that most of the missing contributions lie at higher energies than the contributions that we found.

For HF-SRPA calculations only the energy-weighted sum rule is valid, so we have no measure for the percentage of the total strength in the sense of the non-energy-weighted sum rule. The energy-weighted sum rule values for this case lie at around 55 %. This might seem insufficient, but with the knowledge that both structure and strength of the results from HF-SRPA calculations are comparable to those from IM-SRPA, we can safely assume that this suffices. In addition, instabilities within HF-SRPA may also cause a fraction of the total strength to become unobtainable.

8.5.2 Model-Space Convergence

Similar to the case of IM-RPA we will look into the model-space convergence of IM-SRPA, and for the same reasons we restrict the discussion to the case of different SRG flow parameters. For first-order IM-RPA we already saw that the use of IM-SRG transformed matrix elements reduced the dependence of the results on the flow parameter, especially for lighter nuclei, cf. Figure 8.25. In Figure 8.31 we compare the results of IM-SRPA calculations of the bare SAT interaction, i.e., $\alpha = 0\,\mathrm{fm}^4$ (-·-·-) and with SRG flow parameters of $\alpha = 0.04\,\mathrm{fm}^4$ (- - - -) and $\alpha = 0.08\,\mathrm{fm}^4$ (——). We find a remarkable stability for all three cases across all nuclei and response modes.

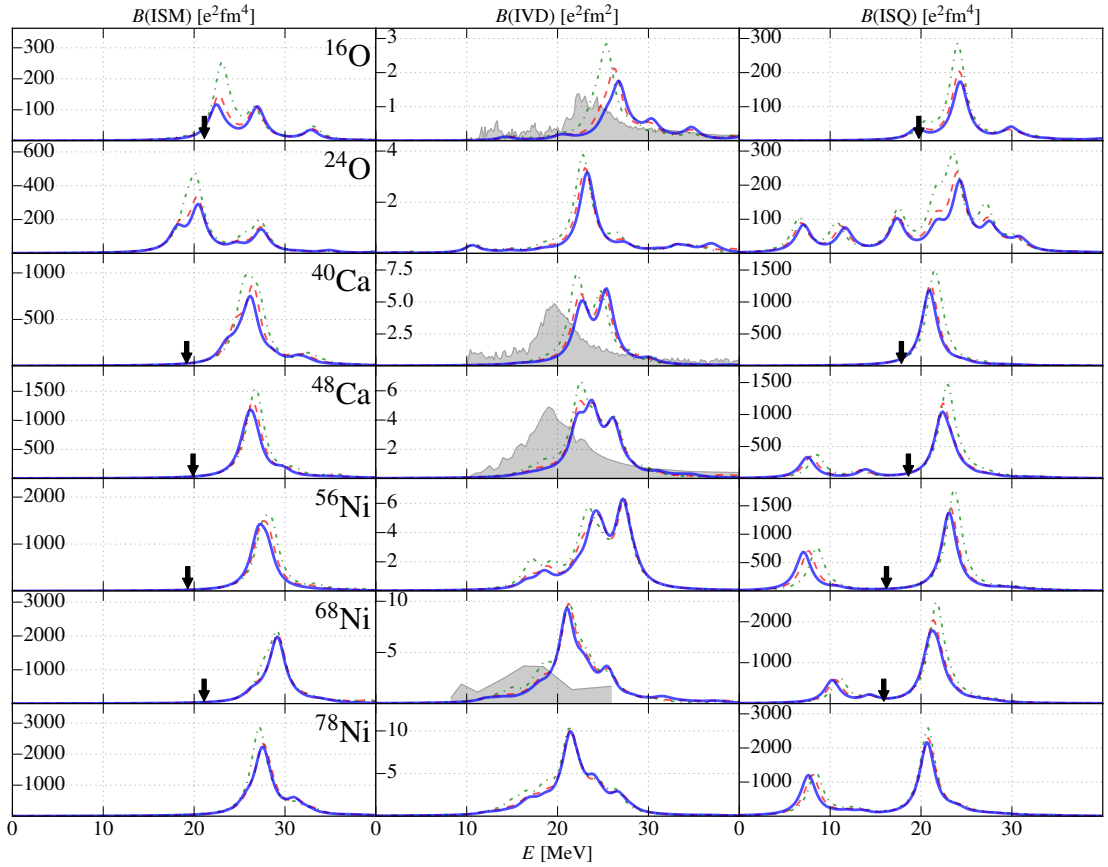

Figure 8.31: Comparison of results from IM-SRPA with the bare interaction $\alpha = 0\,\mathrm{fm}^4$ (-·-·-) and with SRG flow parameters of $\alpha = 0.04\,\mathrm{fm}^4$ (- - - -) and $\alpha = 0.08\,\mathrm{fm}^4$ (——). Here we use the SAT interaction with eMax = 12, E3Max = 14 and $\hbar\Omega = 22\,\mathrm{MeV}$.

Since the results are almost identical for the bare as well as for the SRG evolved versions of the SAT interaction, we can also rule out that induced many-body forces from free-space SRG have any significant impact on the RPA results. This observation of course does not extend to induced forces from IM-SRG, which may still have a relevant effect on the results. In that case, however, we can at least infer that their effect remains largely the same for different SRG flow parameters.

The SRG stability is not quite as good for the EM400 interaction, cf. Figure 8.32, but still better than both IM-RPA and HF-SRPA SRG stabilities, cf. Figure 8.26 and Figure 8.10, respectively.

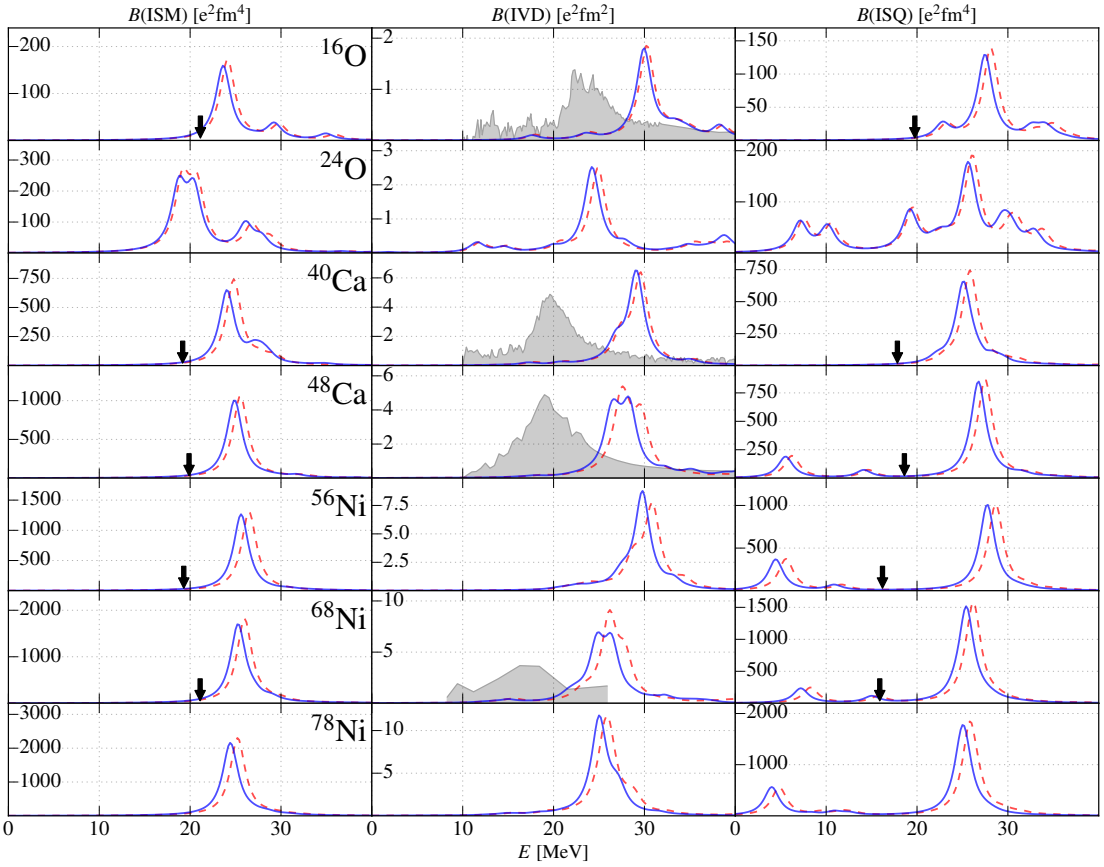

Figure 8.32: Comparison of results from IM-SRPA with SRG flow parameters of $\alpha = 0.04\,\mathrm{fm}^4$ (- - - -) and $\alpha = 0.08\,\mathrm{fm}^4$ (——). Here we use the EM400 interaction with eMax = 12, E3Max = 14 and $\hbar\Omega = 24\,\mathrm{MeV}$.

We conclude that the inclusion of second-order terms within IM-based RPA calculations improves the SRG stability. This is particularly interesting since for the case of HF-SRPA we saw that the extension to SRPA tended to produce larger differences for results obtained with different SRG flow parameters. Hence, even though we observed good SRG stability for light nuclei in IM-RPA calculations, with the knowledge from HF-SRPA we would still expect this stability to deteriorate in IM-SRPA. The fact that the SRG stability improves when going from IM-RPA to IM-SRPA suggests that the inclusion of second-order terms is a necessity for obtaining converged results based on IM-SRG matrix elements. When we describe ground states with 1p1h plus 2p2h correlations, it seems only natural that for a consistent description of excitations we have to include 1p1h and 2p2h excitations as well. Within first-order RPA we omit all terms associated with 2p2h excitations and, consequently, find a certain dependence of the results. This can be attributed to the fact that for different SRG flow parameters the omitted terms carry varying contributions. In SRPA we include all terms, and as a result we find almost completely stable results.

8.6 Polarizability

Another quantity related to transitions is the *electric dipole polarizability* α_{D} (sometimes also α_{E}) [Pie11; Bac$^+$14; Mio$^+$16]. It can be viewed as an "inverse" energy-weighted sum rule and is, discretized, defined as [Pie11]

$$\alpha_{\mathrm{D}} = \frac{8\pi}{9} e^2 \sum_i \frac{B(\mathrm{E1}; 0^+ \to 1^-)}{E_i}, \tag{8.2}$$

with the reduced isovector dipole transition probability $B(\mathrm{E1})$. This definition with the energy appearing in the denominator makes it sensitive to the low-energy behaviour of the dipole strength.

We know that SRPA lowers the strength distribution in comparison to RPA, while at the same time leaving the structure relatively unchanged. With this, we can deduce how α_{D} changes when going from RPA to SRPA. Essentially, this relates to dividing by a smaller denominators, which will of course give a larger value for α_{D}. The instabilities of HF-SRPA, especially in the low-lying part of the spectra, suggest that this theory is unfit for the calculation of a quantity which possesses a strong sensitivity to the low-lying part of the spectrum. We will, therefore, refrain from giving RPA and HF-SRPA results for α_{D}. In Table 8.3 we present polarizabilities calculated with the EM400 as well as with the SAT interaction using the IM-SRPA method, together with experimental values (where available).

Nucleus	EM400	SAT	Expt.
^{16}O	0.39	0.49	0.58 [Ahr$^+$75]
^{24}O	0.75	0.89	
^{40}Ca	1.21	1.79	2.23 [Ahr$^+$75]
^{48}Ca	1.29	1.97	2.07 [Bir$^+$16]
^{56}Ni	1.56	2.35	
^{68}Ni	2.10	3.29	3.40 [Ros$^+$13]
^{78}Ni	2.46	3.63	

Table 8.3: Polarizability α_{D} from IM-SRPA calculations and, where available, experimental data with given sources. All values are given in fm^3. Here we use an SRG flow parameter of $\alpha = 0.08\,\mathrm{fm}^4$ with eMax = 12, E3Max = 14 and $\hbar\Omega$ as usual for the respective interactions.

We can see that both interactions yield comparable results for the oxygen isotopes, but start to differ for heavier nuclei. In this mass-region the SAT interaction yields larger values. In comparison to the experimental values, the predictions from IM-SRPA are somewhat lower. This can be expected, since the IM-SRPA results are at higher energies, i.e., yield larger denominators. We note that if we shift the IM-SRPA results artificially to lower energies, such that the predictions agree with experimental data, the polarizabilities also conincide very well with the experimental values given in Table 8.3. This suggests that IM-SRPA may be well suited for describing polarizabilities.

Chapter 9

Conclusion & Outlook

In the past years, substantial resources have been devoted to an accurate ab initio description of ground-state properties of medium mass nuclei. Many methods have emerged, amongst them CC and IM-SRG, that perform very well in this regard. At the same time, the description of excited states and transitions has scarcely been explored and largely remained the domain of phenomenological methods. The important next step towards a unification for the description of all properties of nuclei, will be to calculate excited states and transitions on an equal foundation.

The goal of this thesis was twofold: Firstly, we aimed for the extension of RPA and SRPA to include normal-ordered chiral 3B interactions. Secondly, we set out to remedy the long standing problem of missing correlations within RPA. The latter has been achieved in two different ways, one is the inclusion of correlations via the use of correlated density matrices from CC, the other is the use of IM-SRG transformed matrix elements. With this we target the gap between the description of ground-state properties and excited states. Along this path, a reduction or possibly elimination of the problem of inconsistencies within RPA theories, that arises from the QBA, can be expected.

In this work we employed two chiral NN+3N interactions. The EM400 interaction, which has been applied in numerous ab initio applications with great success, and the relatively new SAT interaction, which has been designed to give more accurate charge radii for medium-mass nuclei.

Using chiral interactions in conjunction with SRPA showed a similar effect as has been found before, using phenomenological interactions, a strong downward shift in energy that also causes instabilities of low-lying states. While for first-order RPA the use of normal-ordered 3B forces does not introduce an approximation, for SRPA some of the omitted 3B terms would contribute. For future research it will be interesting to investigate the impact of these omitted terms on position and structure of SRPA transitions, as well as on the instabilities.

For the density-based RPA we employed density matrices obtained from CCSD calculations, but in principle density matrices from any other ab initio method can be applied. This offers some degree of flexibility and allows for a comparison of different ab initio methods on the level of collective excitations. In the formulation of CC-RPA we chose to maintain the partitioning of the basis states as given by HF. From an investigation of the CCSD densities, we saw that the occupation numbers for particle states were indeed small, justifying this approach. For CC-RPA we saw that the use of correlated densities yielded a strong increase in excitation energies in comparison to HF-RPA. The structure of the transitions stayed largely the same. We found that the ground-state correlations are important for the RPA eigenvalue problem that gives the excitation energies, the changes due to correlations for the description of transition strength, however, were relatively small. We saw for the other cases that the inclusion of second-order

terms gives important contributions, especially regarding the lowering of excitation energies. Unfortunately, the extension of CC-RPA to CC-SRPA in a straight-forward manner requires higher-order density matrices, which are computationally challenging. For this, an approximate scheme would have to be devised. Without second-order terms the agreement of CC-based RPA with experiment cannot be improved significantly. We argued that the importance of second-order terms can also be attributed to the fact that CC-RPA is limited to singles, while CCSD includes additional doubles contributions.

Regarding IM-RPA we saw a similar, upward shift in energy as for CC-RPA. A comparison of the results obtained from both methods indeed showed a striking resemblance in position as well as structure of the transitions. The extension of IM-RPA to IM-SRPA is straight forward, which is a great advantage of this scheme. With this, we find an agreement with experiment for IM-SRPA that is comparable to that of HF-SRPA. IM-SRPA tends to produce slightly higher resonance energies, while HF-SRPA tends to produce slightly lower energies. The exception was the ISM mode, where the agreement was substantially better for HF-SRPA. We argued that the discrepancies of IM-SRPA could be caused by convergence issues regarding the model space. Furthermore, explicit 3B forces, third-order RPA contributions and the use of consistently transformed 2B operators containing EM currents may also influence the results. Additionally, IM-based RPA represents the superior method which, e.g., manifests in the absence of instabilities for IM-SRPA. Finally, we stress that we cannot be certain that the employed interactions will reproduce the experimental findings. To answer this question, the need for an exact benchmark from, e.g., NCSM calculations arises. For small systems such as ^{16}O this would allow for a comparison to results from different RPA theories.

In terms of future research, to avoid inconsistencies within IM-(S)RPA, the completely consistent evolution of transition operators will be the next important step. The above-mentioned extension to explicit 3B forces will be interesting for both HF- and IM-based SRPA calculations.

Appendix A

Spherical Tensor Operators

In this section, we will discuss the subject of spherical tensor operators (STO) in closer detail (cf. section 3.2.3). When an STO T_{JM} is transformed, it has to obey certain transformation rules. It can be shown [Suh07] that this transformation behaviour is equivalent to fulfilling the following two commutation relations:

$$[J_z, T_{JM}] = M\hbar T_{JM}, \tag{A.1}$$
$$[J_\pm, T_{JM}] = \hbar m_M^\pm T_{J,M\pm1}, \tag{A.2}$$
$$\text{with:} \quad m_M^\pm = \sqrt{(J \pm M + 1)(J \mp M)}. \tag{A.3}$$

The quantities J_z and $J_\pm$ are the usual z-component and ladder operators, respectively, of the angular momentum operator J. They can be written as

$$J_z = \hbar \sum_\beta m_\beta \hat{a}_\beta^\dagger \hat{a}_\beta, \tag{A.4}$$
$$J_\pm = \hbar \sum_\beta m_\beta^\mp \hat{a}_\beta^\dagger \hat{a}_{\beta\mp1}. \tag{A.5}$$

The fulfillment of (A.1) and (A.2) can ergo be used to test whether a particular operator is a spherical tensor or not. For the creation operator $\hat{a}_\alpha^\dagger$ we get for the first relation

$$[J_z, \hat{a}_\alpha^\dagger] = \hbar \sum_\beta m_\beta [\hat{a}_\beta^\dagger \hat{a}_\beta, \hat{a}_\alpha^\dagger] \tag{A.6}$$
$$= \hbar \sum_\beta m_\beta \left([\hat{a}_\beta^\dagger, \hat{a}_\alpha^\dagger] \hat{a}_\beta + \hat{a}_\beta^\dagger [\hat{a}_\beta, \hat{a}_\alpha^\dagger] \right) \tag{A.7}$$
$$= \hbar \sum_\beta m_\beta \left(0 + \delta_{\beta,\alpha}\, \hat{a}_\beta^\dagger \right) \tag{A.8}$$
$$= \hbar m_\alpha \hat{a}_\alpha^\dagger, \tag{A.9}$$

which shows that the creation operator fulfills (A.1). Inserting into the second equation yields

$$[J_\pm, \hat{a}^\dagger_\alpha] = \hbar \sum_\beta m^\mp_\beta [\hat{a}^\dagger_\beta \hat{a}_{\beta\mp1}, \hat{a}^\dagger_\alpha] \tag{A.10}$$

$$= \hbar \sum_\beta m^\mp_\beta \left(\hat{a}^\dagger_\beta [\hat{a}_{\beta\mp1}, \hat{a}^\dagger_\alpha] + [\hat{a}^\dagger_\beta, \hat{a}^\dagger_\alpha] \hat{a}_{\beta\mp1} \right) \tag{A.11}$$

$$= \hbar \sum_\beta m^\mp_\beta \left(\delta_{\beta\mp1,\alpha}\, \hat{a}^\dagger_\beta + 0 \right) \tag{A.12}$$

$$= \hbar m^\mp_{\alpha\pm1} \hat{a}^\dagger_{\alpha\pm1} = \hbar m^\pm_\alpha \hat{a}^\dagger_{\alpha\pm1}. \tag{A.13}$$

As can be seen, the second equation holds true as well, and therefore the creation operator $\hat{a}^\dagger_\alpha$ is a spherical tensor operator. For the annihilation operator we find

$$[J_z, \hat{a}_\alpha] = \hbar \sum_\beta m_\beta [\hat{a}^\dagger_\beta \hat{a}_\beta, \hat{a}_\alpha] \tag{A.14}$$

$$= \hbar \sum_\beta m_\beta \left([\hat{a}^\dagger_\beta, \hat{a}_\alpha] \hat{a}_\beta + \hat{a}^\dagger_\beta [\hat{a}_\beta, \hat{a}_\alpha] \right) \tag{A.15}$$

$$= \hbar \sum_\beta m_\beta \left(-\delta_{\beta,\alpha}\, \hat{a}_\beta + 0 \right) \tag{A.16}$$

$$= -\hbar m_\alpha \hat{a}_\alpha \neq \hbar m_\alpha \hat{a}_\alpha. \tag{A.17}$$

Due to the spare minus sign, (A.1) is not fulfilled and the annihilation operator $\hat{a}_\alpha$ is *no* spherical tensor operator. However, the regular annihilation operator can be used to construct a spherical tensor operator by modifying it accordingly. In (3.46), we proposed the operator $\hat{\tilde{a}}_\alpha = (-1)^{j_a + m_\alpha}\, \hat{a}_{j_a,\text{-}m_\alpha}$ and stated without proof that it was, in contrast to the regular annihilator $\hat{a}_\alpha$, a spherical tensor operator. The test for this operator yields

$$[J_z, \hat{\tilde{a}}_\alpha] = \hbar \sum_\beta m_\beta [\hat{a}^\dagger_\beta \hat{a}_\beta, \hat{\tilde{a}}_\alpha] = \hbar \sum_\beta m_\beta [\hat{a}^\dagger_\beta \hat{a}_\beta, \hat{a}_{\text{-}\alpha}] (-1)^{j_a + m_\alpha} \tag{A.18}$$

$$= \hbar \sum_\beta m_\beta \left([\hat{a}^\dagger_\beta, \hat{a}_{\text{-}\alpha}] \hat{a}_\beta + \hat{a}^\dagger_\beta [\hat{a}_\beta, \hat{a}_{\text{-}\alpha}] \right) (-1)^{j_a + m_\alpha} \tag{A.19}$$

$$= \hbar \sum_\beta m_\beta \left(-\delta_{\beta,\text{-}\alpha} \hat{a}_\beta + 0 \right) (-1)^{j_a + m_\alpha} \tag{A.20}$$

$$= -\hbar m_{\text{-}\alpha} \hat{a}_{\text{-}\alpha} (-1)^{j_a + m_\alpha} = \hbar (-m_{\text{-}\alpha}) \hat{\tilde{a}}_\alpha = \hbar m_\alpha \hat{\tilde{a}}_\alpha \tag{A.21}$$

for the first relation, and

$$[J_\pm, \hat{\tilde{a}}_\alpha] = \hbar \sum_\beta m^\mp_\beta [\hat{a}^\dagger_\beta \hat{a}_{\beta\mp1}, \hat{\tilde{a}}_\alpha] = \hbar \sum_\beta m^\mp_\beta [\hat{a}^\dagger_\beta \hat{a}_{\beta\mp1}, \hat{a}_{\text{-}\alpha}] (-1)^{j_a + m_\alpha} \tag{A.22}$$

$$= \hbar \sum_\beta m^\mp_\beta \left(\hat{a}^\dagger_\beta [\hat{a}_{\beta\mp1}, \hat{a}_{\text{-}\alpha}] + [\hat{a}^\dagger_\beta, \hat{a}_{\text{-}\alpha}] \hat{a}_{\beta\mp1} \right) (-1)^{j_a + m_\alpha} \tag{A.23}$$

$$= \hbar \sum_\beta m^\mp_\beta \left(0 - \delta_{\beta,\text{-}\alpha} \hat{a}_{\beta\mp1} \right) (-1)^{j_a + m_\alpha} \tag{A.24}$$

$$= -\hbar m^\mp_{\text{-}\alpha} \hat{a}_{\text{-}\alpha\mp1} (-1)^{j_a + m_\alpha} = \hbar m^\mp_{\text{-}\alpha} \hat{a}_{\text{-}(\alpha\pm1)} (-1)^{j_a + m_{\alpha\pm1}} \tag{A.25}$$

$$= \hbar m^\mp_{\text{-}\alpha} \hat{\tilde{a}}_{\alpha\pm1} = \hbar m^\pm_\alpha \hat{\tilde{a}}_{\alpha\pm1} \tag{A.26}$$

for the second one. With this, we have shown that $\hat{\tilde{a}}_\alpha$ is indeed a spherical tensor operator.

Appendix B

Symmetries and Norms of Coupled 2B States

Coupled 2B state (without uncoupled quantum numbers):

$$|(j_1 j_2)JM\rangle = \sum_{m_1,m_2} C(j_1 m_1, j_2 m_2|JM)\,|j_1, m_1|j_2, m_2\rangle\,. \tag{B.1}$$

B.1 Norm

Overlap with another coupled state $|(j_{1'} j_{2'})J'M'\rangle$:

$$\begin{aligned}\langle (j_{1'} j_{2'})J'M'|(j_1 j_2)JM\rangle = &\sum_{\substack{m_1,m_2\\ m_{1'},m_{2'}}} C(j_{1'} m_{1'}, j_{2'} m_{2'}|J'M')C(j_1 m_1, j_2 m_2|JM)\\ &\times \langle j_{1'} m_{1'}, j_{2'} m_{2'}|j_1 m_1, j_2 m_2\rangle\,.\end{aligned} \tag{B.2}$$

With

$$\langle j_{1'} m_{1'}, j_{2'} m_{2'}|j_1 m_1, j_2 m_2\rangle \equiv \langle s_{1'} s_{2'}|s_1 s_2\rangle = \delta_{s_1,s_{1'}}\delta_{s_2,s_{2'}} - \delta_{s_1,s_{2'}}\delta_{s_2,s_{1'}} \tag{B.3}$$

we get

$$\begin{aligned}\langle (j_1' j_2')J'M'|(j_1 j_2)JM\rangle = &\sum_{m_1,m_2} C(j_1 m_1, j_2 m_2|J'M')C(j_1 m_1, j_2 m_2|JM)\\ &- C(j_2 m_2, j_1 m_1|J'M')C(j_1 m_1, j_2 m_2|JM).\end{aligned} \tag{B.4}$$

Using orthogonality and symmetry relations of the Clebsch-Gordan coefficients we find

$$\langle (j_{1'} j_{2'})J'M'|(j_1 j_2)JM\rangle = \delta_{J,J'}\delta_{M,M'}\left(\delta_{j_1,j_1'}\delta_{j_2,j_2'} - \delta_{j_1,j_2'}\delta_{j_2,j_1'}(-1)^{j_1+j_2+J}\right). \tag{B.5}$$

The norm then is

$$\langle (j_1 j_2)JM|(j_1 j_2)JM\rangle = \left(1 - \delta_{j_1,j_2}\delta_{j_2,j_1}(-1)^{j_1+j_2+J}\right) = \begin{cases}1, & j_1 \neq j_2\\ (1-(-1)^{j_1+j_2+J}), & \text{else}\end{cases}. \tag{B.6}$$

For the case of $j_1 = j_2$, we know that $j_1 + j_2 = 2j_1$ is always odd for half-integer j_1, and thus we find

$$\langle (j_1 j_1)JM|(j_1 j_1)JM\rangle = (1+(-1)^J) = \begin{cases}2, & \text{if } J \text{ even}\\ 0, & \text{else (forbidden case)}\end{cases}. \tag{B.7}$$

B.2 Symmetry

Uncoupled symmetry:

$$|j_1 m_1, j_2 m_2\rangle = -\,|j_2 m_2, j_1 m_1\rangle \tag{B.8}$$

Coupled (without uncoupled quantum numbers):

$$|(j_1 j_2) JM\rangle = (-1)^{J-j_1-j_2}\,|(j_2 j_1) JM\rangle\,. \tag{B.9}$$

Coupled (with uncoupled quantum numbers):

$$|\xi_1\xi_2, (j_1 j_2) JM\rangle = (-1)^{J-j_1-j_2}\,|\xi_1\xi_2, (j_2 j_1) JM\rangle \tag{B.10}$$

$$= (-1)^{J-j_1-j_2+1}\,|\xi_2\xi_1, (j_2 j_1) JM\rangle\,. \tag{B.11}$$

Appendix C

Diagrammatic SRPA Derivation

C.1 Diagrammatic Formalism

In this section we will briefly introduce the diagrammatic techniques which allow for a more systematic derivation of the SRPA terms. In general, diagrammatic notations aim at facilitating the evaluation of complicated matrix elements. The straight-forward computation of matrix elements is convenient for shorter expressions, but with increasing number of operators the evaluation becomes more and more tedious. For example the matrix element

$$\langle \mathrm{HF}| \hat{a}_1^\dagger \hat{a}_2 \hat{a}_i^\dagger \hat{a}_j^\dagger \hat{a}_{j'} \hat{a}_{i'} \hat{a}_3^\dagger \hat{a}_4 |\mathrm{HF}\rangle \tag{C.1}$$

would usually yield a number of δ-terms, depending on the p-h structure of the indices. Instead of evaluating all terms by the basic rules, diagrammatic notations aims at delivering a more systematic approach and giving regard only to the non-zero terms. The subsequent derivation of the rules for diagrammatic notations follows the strategy of [SB09]. It will only cover the parts necessary for the derivation of the SRPA expressions.

The diagrammatic evaluation of matrix elements as above first requires the definition of a "time" axis. The term time here refers to the order in which we will handle the different states and operators in the given expressions. We use the convention that the bottom represents the ket state and the top the bra state, i.e. the time axis is aligned vertically. The operators inside the matrix elements are placed in between the states, the rightmost directly above the initial state, the next one above that and so on. The HF Slater-determinant is depicted by a thick horizontal (double) line. If we want to represent a ph excitation on the HF state we need to introduce particle and hole operators. Both will be represented by simple vertical lines. The direction of a particle line coming from the bottom HF state is upward, the direction of a hole line downward. Labels denoting the index are simply written next to the corresponding line. A simple excitation $\hat{a}_p^\dagger \hat{a}_h |\mathrm{HF}\rangle$ would thus translate to

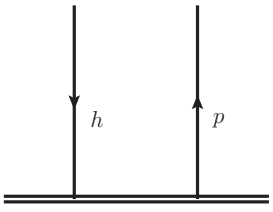

Lines connected to either of the Slater-determinants are called *external lines*. For the evaluation of the diagrams, the horizontal order of the operators is, in this case, irrelevant. A shorthand

notation for the above ph excitation that we will be using is $|\mathrm{HF}_h^p\rangle \equiv \hat{a}_p^\dagger \hat{a}_h \, |\mathrm{HF}\rangle$. If we are dealing with multiple ph excitations, e.g.

$$|\mathrm{HF}_{h_1 h_2}^{p_1 p_2}\rangle \equiv \hat{a}_{p_1}^\dagger \hat{a}_{p_2}^\dagger \hat{a}_{h_2} \hat{a}_{h_1} \, |\mathrm{HF}\rangle \, ,$$

we can choose a horizontal order that seems convenient, but in order to eliminate a phase ambiguity between $|\mathrm{HF}_{h_1 h_2}^{p_1 p_2}\rangle$ and $|\mathrm{HF}_{h_1 h_2}^{p_2 p_1}\rangle = -\,|\mathrm{HF}_{h_1 h_2}^{p_1 p_2}\rangle$ we connect related indices, meaning those that are written above/below the other, via a curved, dashed line running on the outer side. The term $|\mathrm{HF}_{h_1 h_2}^{p_1 p_2}\rangle$ would correspond to

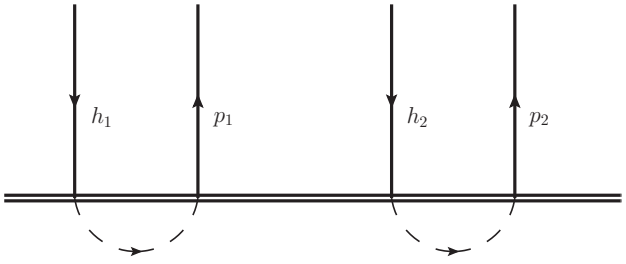

A 1B operator will be denoted by dashed horizontal line connecting the *vertex* (dot), which is the point of operation of the interaction, with a marker (e.g. a hash) to specify the particular 1B operator. At a vertex there always has to be one incoming and one outgoing line, see below.

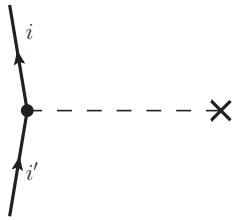

We sum implicitly over the *internal indices* i and i', corresponding to $\sum_{i,i'} t_{i,i'} \, \hat{a}_i^\dagger \hat{a}_{i'}$. Note that the angle at which we draw the internal lines is arbitrary. The internal lines could also be positioned both above or both below the vertex. In order to get all non-vanishing terms, we have to connect this 1B operator in all possible ways to the rest of the diagram. The application of the 1B operator $\hat{T}$ would, e.g., be depicted as

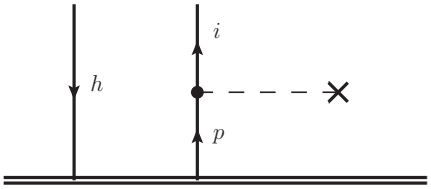

We omitted the implicit δ between the internal and external lines. The 1B operator here would give the factor $t_{p,p'}$, i.e. changing the particle p into p'. By convention, the bra state is associated with the outgoing line and the ket state with incoming line. Since we will be dealing exclusively with Hermitian operators, evaluating it the other way around would nevertheless yield the same result. Of course we can also connect on hole state h with another one h', giving $t_{h,h'}$, or we can build the following diagram

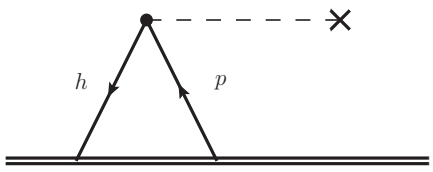

which gives the term $t_{p,h}$. The entire matrix element $\langle \mathrm{HF}^{p'}_{h'}| \hat{T} |\mathrm{HF}^{p}_{h}\rangle = \langle \mathrm{HF}| \hat{a}^\dagger_{h'} \hat{a}_{p'} \hat{T} \hat{a}^\dagger_{p} \hat{a}_{h} |\mathrm{HF}\rangle$ can be covered with the two diagrams

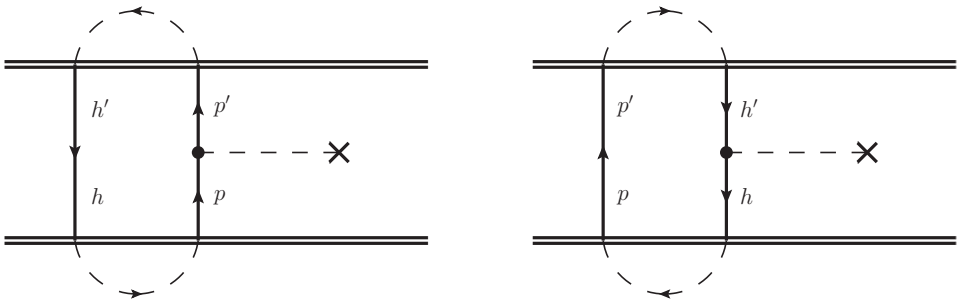

Other combinations are not possible because unconnected lines are not allowed. Lines connecting to external indices without a vertex represent a δ-relation between those indices, i.e., $\delta_{hh'}$ in the left of the above diagrams. The entire left diagram gives, up to a phase factor, $\delta_{hh'} t_{p,p'}$, the right one $\delta_{pp'} t_{hh'}$. We now introduce the phase convention associated with diagrams. The phase of any diagram is given by $(-1)^{n_h - n_l}$ where n_h is the number of hole lines in the entire diagram and n_l is the number of loops (or paths), which are continuously linked sets of lines. Hole lines connected via a δ-relation count as one. With this, for the left diagram we get $(-1)^{1-1} = +1$ and for the right diagram $(-1)^{2-1} = -1$ as phase.

2B operators are denoted by two horizontally aligned half-vertices connected by a dashed interaction line. Each of the half vertices has one incoming and one outgoing line, similar to the 1B case

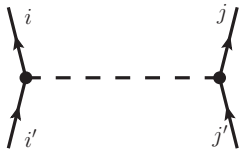

Generally this corresponds to the factor $\sum_{ij,i'j'} v_{ij,i'j'}$ (labels in diagram are omitted). Convention requires the bra state to be given by the outgoing indices and the ket state with the incoming indices. The left half-vertex relates to the first particle, the right half to the second particle. This gives the $\langle$left-out right-out$|\hat{V}|$left-in right-in$\rangle$-scheme. The lines of a 2B operator can in principle be connected in the same way as for the 1B operator. For the full evaluation of a given matrix element containing a 2B operator, all possible connections have to be established and the distinct diagrams identified. Connections can also be made within a 2B (or higher) operator, for 1B operators this could only appear in so-called "bubble" diagrams which we do not cover here. Such an intrinsic connection would look like this

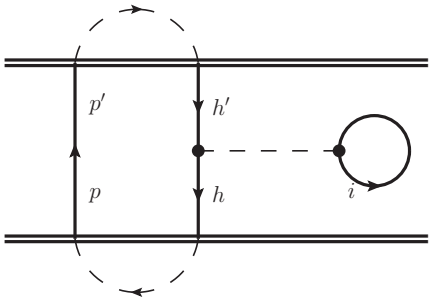

The arrow going down indicates that the corresponding sum of i only runs over hole states. This connection constitutes a loop by its own. Usually the label on these loops is omitted and only an arrow is displayed, the summation index may be chosen at will. For the determination of the phase factor these loops can be neglected since they also consist of only one hole line and therefore give $(-1)^{h+1-l-1} = (-1)^{h-l}$. The above diagram gives $(-1)^{2-1}\delta_{pp'} \sum_i^{\text{occ.}} v_{hi,h'i}$.

As a final comment, we want to stress that this is only a very simplistic introduction to the diagrammatic notation. It is tailored to enable the reader to understand and track the diagrammatic derivations performed in this work. Before starting the derivation of diagrams on one's own, further consultation of e.g. [SB09] is strongly recommended.

C.2 A12 Diagrams

Earlier we defined the matrix A_{12} as $\langle \text{HF}| \left[\hat{\mathcal{A}}_{1,}, [\hat{H}, \hat{\mathcal{A}}^\dagger_{2,j}]\right] |\text{HF}\rangle$. In order to evaluate this on an m-scheme basis, we first get rid of the commutators

$$
\begin{aligned}
(A_{12})_{ij} &= \langle \text{HF}| \left[\hat{\mathcal{A}}_{1,}, [\hat{H}, \hat{\mathcal{A}}^\dagger_{2,j}]\right] |\text{HF}\rangle && \text{(C.2)}\\
&= \langle \text{HF}| \hat{\mathcal{A}}_{1,i} [\hat{H}, \hat{\mathcal{A}}^\dagger_{2,j}] |\text{HF}\rangle && \text{(C.3)}\\
&= \langle \text{HF}| \hat{\mathcal{A}}_{1,i} \hat{H} \hat{\mathcal{A}}^\dagger_{2,j} |\text{HF}\rangle - \langle \text{HF}| \hat{\mathcal{A}}_{1,i} \hat{\mathcal{A}}^\dagger_{2,j} \hat{H} |\text{HF}\rangle && \text{(C.4)}\\
&= \langle \text{HF}| \hat{\mathcal{A}}_{1,i} \hat{H} \hat{\mathcal{A}}^\dagger_{2,j} |\text{HF}\rangle . && \text{(C.5)}
\end{aligned}
$$

The second term in (C.4) vanishes because a one-fold excitation (to the left) of $|\text{HF}\rangle$ cannot be followed by a two-fold de-excitation. Without the commutators we see that A_{12} corresponds to a matrix element of $\hat{H}$ with a 1p1h excitation of HF on the one side and a 2p2h excitation on the other, i.e.

$$
(A_{12})_{ij} \sim \langle \text{HF}^p_h | \hat{H} | \text{HF}^{p_1 p_2}_{h_1 h_2} \rangle . \tag{C.6}
$$

This is a term that we can evaluate using the diagrammatic notation. We start with the 1B part of the Hamiltonian. The only possible diagram type that can be constructed is shown below

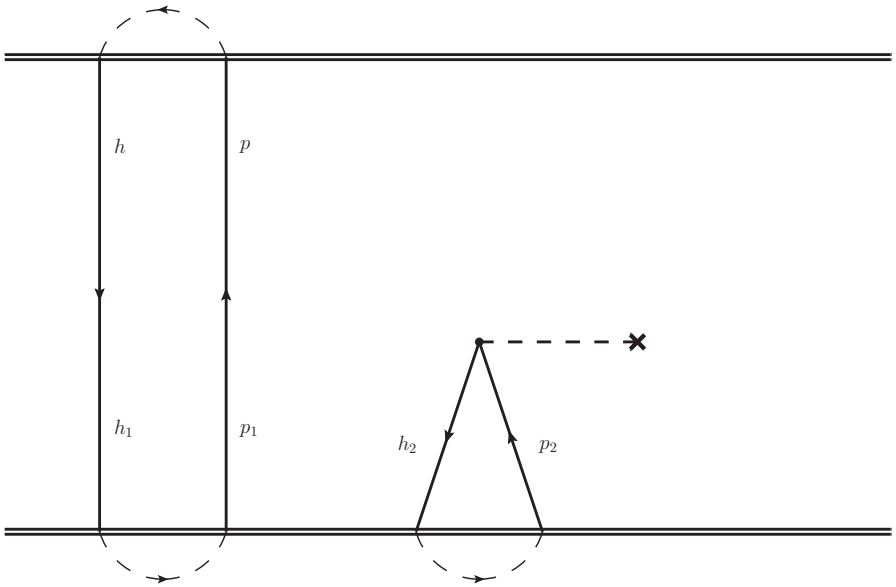

Figure C.1: A_{12}, 1B part.

The two lines of our 1B operator have to be used to "catch" the spare set of ph lines, since only one pair of the two can be compensated by the upper part. The given diagram has two loops and two hole lines, it evaluates to

$$h = 2, l = 2, \tag{C.7}$$
$$\Rightarrow (-1)^{2-2}\delta_{pp_1}\delta_{hh_1}t_{h_2,p_2}. \tag{C.8}$$

In Figure C.1 we randomly chose h_2 and p_2 to interact with our 1B operator. Of course h_1 or p_1 could be applied to this operator just as well, in any combination so long as one particle and one hole line is connected to the 1B operator. In order to get the other, distinct diagrams can simply exchange the p_1 with p_2 (likewise for the holes), using the index exchanging operator $P(1,2)$. This basically corresponds to relabeling the affected particle and hole lines. If we do not want to change the loop structure, we have to take into account that if, e.g., we permuted the particles, the loops given from our initial diagram now indicate a different excitation order. Assuming we started out with the excitation configuration $|\mathrm{HF}^{p_1p_2}_{h_1h_2}\rangle$ this would become $|\mathrm{HF}^{p_2p_1}_{h_1h_2}\rangle = -|\mathrm{HF}^{p_1p_2}_{h_1h_2}\rangle$. We can directly conclude that this permutation produces a minus sign relative to the unpermuted diagram. The remaining, distinct diagrams can be captured by applying the following pattern to the chosen diagram:

$$\begin{aligned}(1 - P(p_1,p_2))(1 - P(h_1,h_2))\delta_{pp_1}\delta_{hh_1}t_{h_2,p_2} =& \delta_{pp_1}\delta_{hh_1}t_{h_2,p_2} \\ &- \delta_{pp_2}\delta_{hh_1}t_{h_2,p_1} \\ &- \delta_{pp_1}\delta_{hh_2}t_{h_1,p_2} \\ &+ \delta_{pp_2}\delta_{hh_2}t_{h_1,p_1}.\end{aligned} \tag{C.9}$$

Since there are no more 1B diagrams, we move on to the 2B part. We start with the diagram given below which is related to the one we just saw.

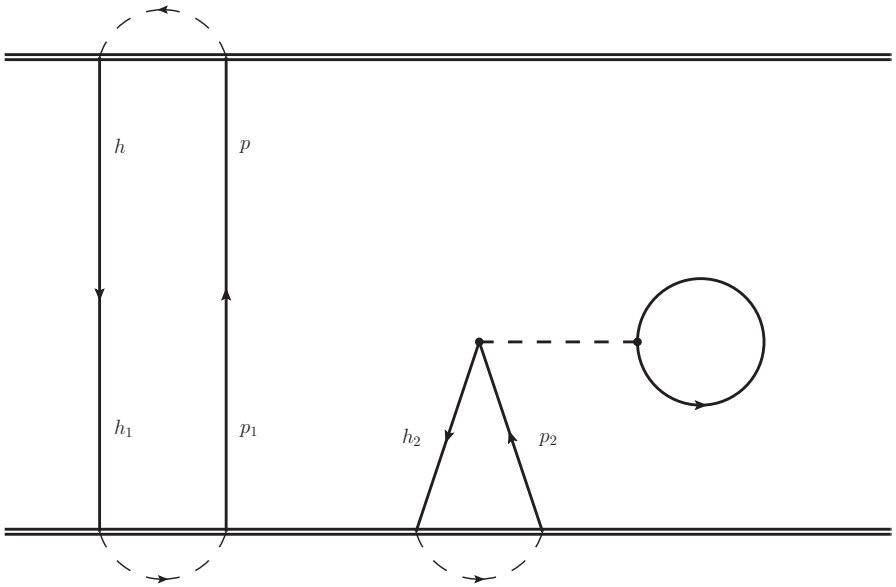

Figure C.2: A_{12}, 2B part, diagram 1.

Since we do not count the intrinsic loop by itself, the shown diagram has two loops and two hole lines, evaluating to

$$h = 2, l = 2 \tag{C.10}$$

$$(-1)^{2-2}\delta_{hh_1}\delta_{pp_1}\sum_{i}^{\text{occ.}} v_{h_2 i, p_2 i}, \tag{C.11}$$

and including permutations we have

$$(1 - P(p_1, p_2))(1 - P(h_1, h_2))\delta_{hh_1}\delta_{pp_1}\sum_{i}^{\text{occ.}} v_{h_2 i, p_2 i}. \tag{C.12}$$

We can now see the relation with the first diagram of Figure C.1. In sum, they give exactly the HF 1B mean-field term of (3.24) (2B case):

$$(1 - P(p_1, p_2))(1 - P(h_1, h_2))\delta_{hh_1}\delta_{pp_1}\left(t_{h_2,p_2} + \sum_{i}^{\text{occ.}} v_{h_2 i, p_2 i}\right) \tag{C.13}$$

$$=(1 - P(p_1, p_2))(1 - P(h_1, h_2))\delta_{hh_1}\delta_{pp_1}\epsilon_{h_2,p_2}. \tag{C.14}$$

Since in HF the mean-field operator is diagonal and particles and holes are disjoint, these terms cancel each other for all combinations ($\epsilon_{ph} = 0$). These diagrams yield no net contribution. In fact, this states that the 1B Hamiltonian, which necessarily occurs when using NO, does not influence the A_{12} matrix.

There are still two possible connection types left. One is to connect the spare ph lines as before, but instead of using the second half-vertex for an intrinsic loop, we can connect it to the two particle lines. The other one is to use the two hole lines. Connecting to the particles gives

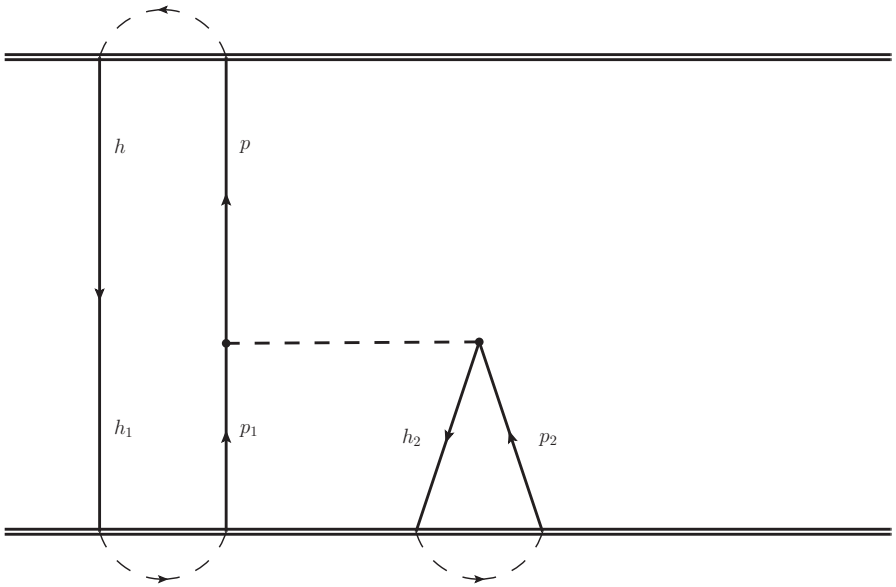

Figure C.3: A_{12}, 2B part, diagram 2.

$$h = 2, l = 2 \tag{C.15}$$

$$(-1)^{2-2}\delta_{hh_1} v_{ph_2,p_1p_2} \tag{C.16}$$

Regarding the permutations, we can see that the exchange of the particles will only yield a multiplicity since $v_{ph_2,p_1p_2} = -v_{ph_2,p_2p_1}$:

$$\begin{aligned}(1 - P(p_1, p_2))(1 - P(h_1, h_2))\delta_{hh_1} v_{ph_2,p_1p_2} =& \delta_{hh_1} v_{ph_2,p_1p_2} \\ &- \delta_{hh_1} v_{ph_2,p_2p_1} \\ &- \delta_{hh_2} v_{ph_1,p_1p_2} \\ &+ \delta_{hh_2} v_{ph_1,p_2p_1} && \text{(C.17)} \\ =& 2\delta_{hh_1} v_{ph_2,p_1p_2} - 2\delta_{hh_2} v_{ph_1,p_1p_2} && \text{(C.18)} \\ =& 2(1 - P(h_1, h_2))\delta_{hh_1} v_{ph_2,p_1p_2} && \text{(C.19)}\end{aligned}$$

However, a multiplicity is not associated with a distinct diagram and therefore we cannot count its contribution. With this, the total value of this diagram results to $(1-P(h_1, h_2))\delta_{hh_1} v_{ph_2,p_1p_2}$.

The last diagram then obviously gives

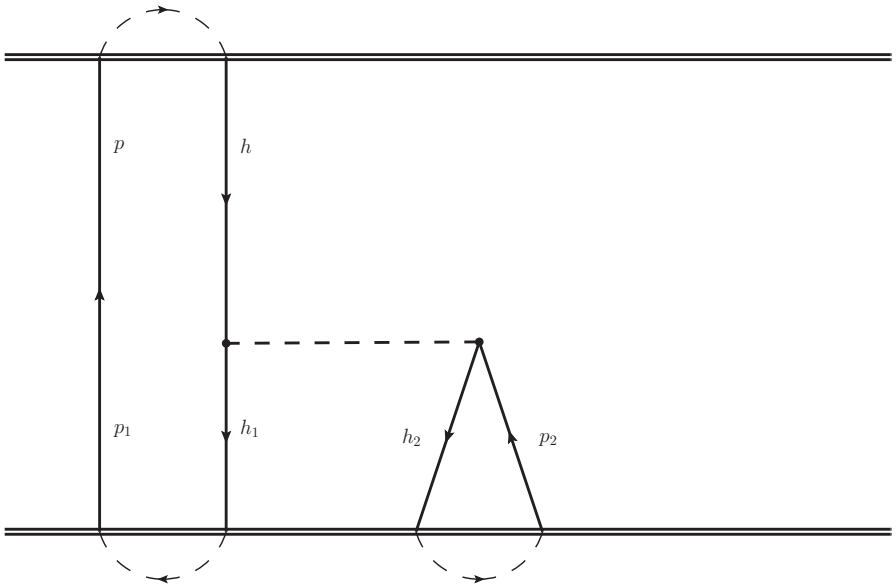

Figure C.4: A_{12}, 2B part, diagram 3.

Here we have one more hole line since connecting both holes to the 2B operator removes the δ-relation between them,

$$h = 3, l = 2 \tag{C.20}$$
$$(-1)^{3-2}\delta_{pp_1} v_{h_1 h_2, hp_2}. \tag{C.21}$$

This time the hole exchange produces the multiplicity:

$$\begin{aligned}(1 - P(p_1, p_2))(1 - P(h_1, h_2))(-1)\delta_{pp_1} v_{h_1 h_2, hp_2} &= -2\delta_{pp_1} v_{h_1 h_2, hp_2} + 2\delta_{pp_2} v_{h_1 h_2, hp_1} &\text{(C.22)}\\ &= -2(1 - P(p_1, p_2))\delta_{pp_1} v_{h_1 h_2, hp_2}. &\text{(C.23)}\end{aligned}$$

A_{12} m-scheme Formula

Combining the non-zero contributions from the diagrams of the last section gives

$$[A_{12}]_{ph;p_1 p_2 h_1 h_2} = (1 - P(h_1, h_2))\delta_{hh_1} v_{ph_2, p_1 p_2} - (1 - P(p_1, p_2))\delta_{pp_1} v_{h_1 h_2, hp_2}. \tag{C.24}$$

C.3 A22 Diagrams

We continue with the derivation of the A_{22} matrix, which we defined earlier (see (3.222)). Omitting the outer, irrelevant commutators and expanding the inner one gives

$$\begin{aligned}A_{22} &\equiv \langle \mathrm{HF}| \, [\hat{\mathcal{A}}_{2,i}, [\hat{H}, \hat{\mathcal{A}}^\dagger_{2,j}]] \, |\mathrm{HF}\rangle &\text{(C.25)}\\ &= \langle \mathrm{HF}| \, \hat{\mathcal{A}}_{2,i} [\hat{H}, \hat{\mathcal{A}}^\dagger_{2,j}] \, |\mathrm{HF}\rangle &\text{(C.26)}\\ &= \langle \mathrm{HF}| \, \hat{\mathcal{A}}_{2,i} \hat{H} \hat{\mathcal{A}}^\dagger_{2,j} \, |\mathrm{HF}\rangle - \langle \mathrm{HF}| \, \hat{\mathcal{A}}_{2,i} \hat{\mathcal{A}}^\dagger_{2,j} \hat{H} \, |\mathrm{HF}\rangle &\text{(C.27)}\end{aligned}$$

The second term here only contributes in the case that $i = j$. However, this is the trivial case of a "bubble" diagram, which we mentioned earlier. In our formalism, we do not have to take its contributions into account since they cancel with an analogous bubble diagram stemming from

the first term. We can therefore effectively assume $A_{22} = \langle \mathrm{HF}^{P_1P_2}_{H_1H_2} | \hat{H} | \mathrm{HF}^{p_1p_2}_{h_1h_2} \rangle$. Consequently, this time we have the same number of lines coming from the bottom as from the top, more specifically we have two particle lines and two hole lines on each side. For the 1B operator one possible diagram is

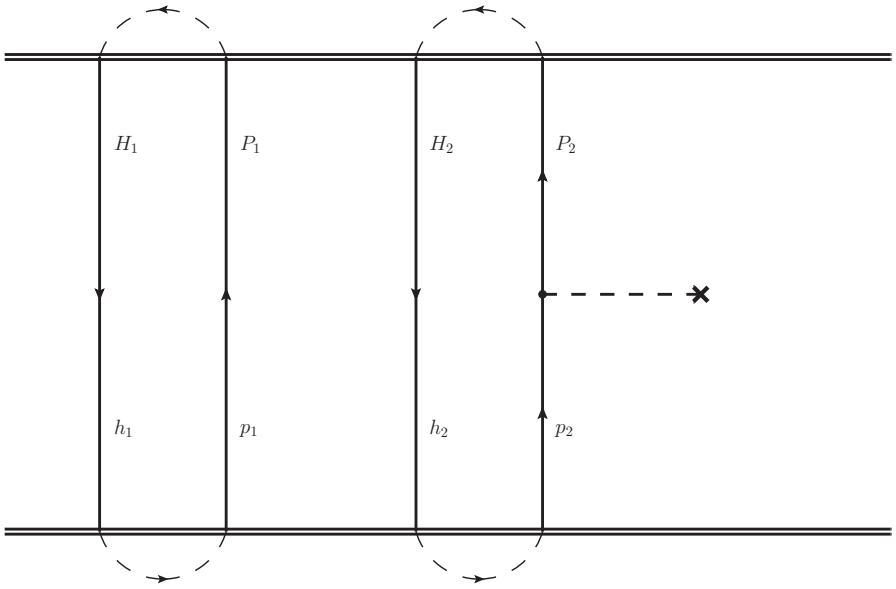

Figure C.5: A_{22}, 1B part, diagram 1.

A diagram with a connection of the 1B operator of the sort of Figure C.1 cannot be constructed without yielding dangling, forbidden lines. Mathematically this diagram corresponds to

$$h = 2, l = 2 \tag{C.28}$$

$$(-1)^{2-2}\delta_{H_1h_1}\delta_{P_1p_1}\delta_{H_2h_2}\, t_{p_2,P_2}. \tag{C.29}$$

Of course we have to take into account all possible permutations, keeping in mind that now both the particles and the holes of the bottom *and* of the top can permute. In A_{12} this was only possible for the bottom part of the diagram since the top had only one ph pair. The complete set of permutations is given by

$$(1 - P(P_1, P_2))(1 - P(H_1, H_2))(1 - P(p_1, p_2))(1 - P(h_1, h_2))\delta_{H_1h_1}\delta_{P_1p_1}\delta_{H_2h_2}\, t_{p_2P_2}. \tag{C.30}$$

Mind that for A_{12} the 1B diagram together with contributions from the 2B part yielded the HF energy. Since the 1B operator connected a particle with a hole state this energy vanished due to off-diagonality. In A_{22} the 1B operator in the above diagram connects two particles.

The same can be done for two hole states. The corresponding diagram is

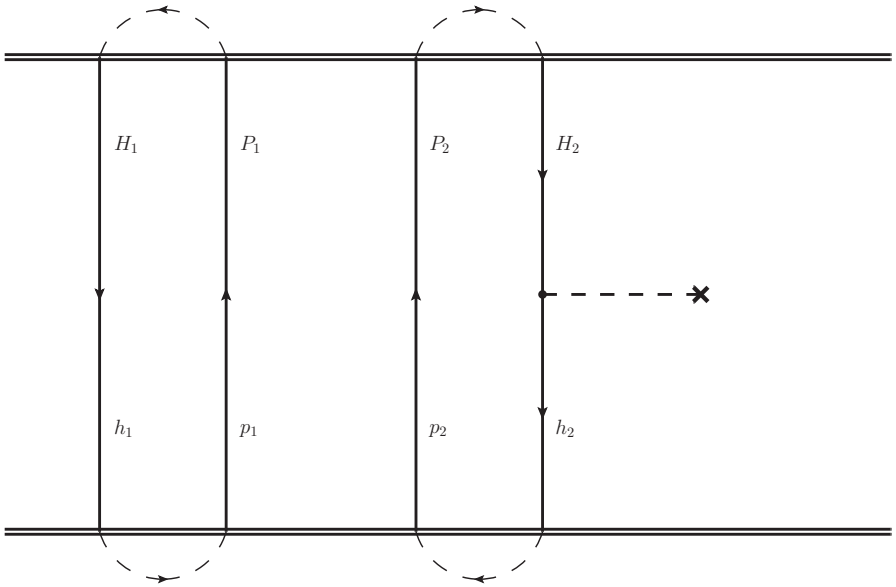

Figure C.6: A_{22}, 1B part, diagram 2.

Mathematically, we get an analogous expression except that the states appearing in the 1B operator now are hole states and we have one additional hole line. This gives

$$h = 3, l = 2 \tag{C.31}$$

$$(-1)^{3-2}\delta_{H_1h_1}\delta_{P_1p_1}\delta_{P_2p_2}\, t_{h_2,H_2}, \tag{C.32}$$

and again the full contribution including all permutations is

$$-(1 - P(P_1, P_2))(1 - P(H_1, H_2))(1 - P(p_1, p_2))(1 - P(h_1, h_2))\delta_{H_1h_1}\delta_{P_1p_1}\delta_{P_2p_2}\, t_{h_2,H_2}. \tag{C.33}$$

For the 2B part we will first consider the corresponding diagrams including the intrinsic loop. In analogy to Figure C.5 we have

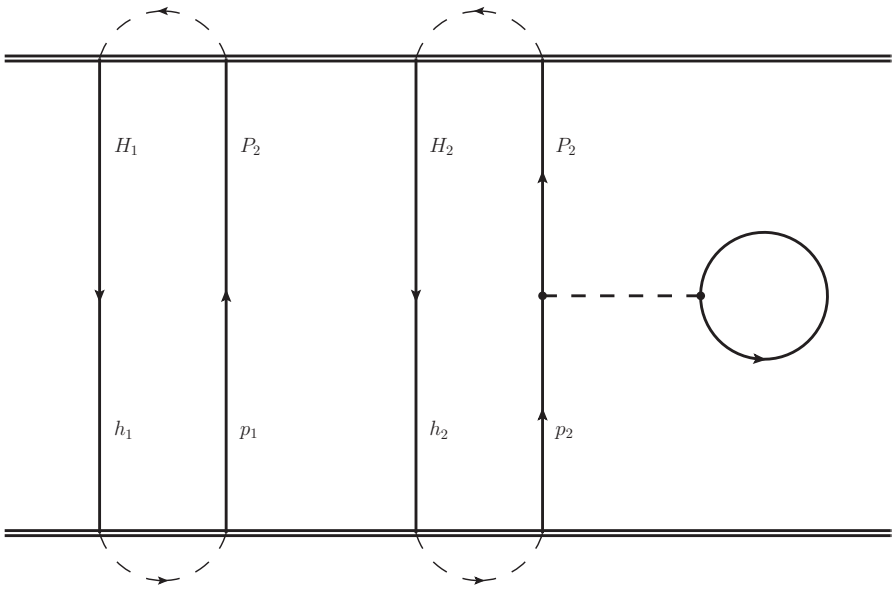

Figure C.7: A_{22}, 2B part, diagram 1.

which translates to (permutations omitted)

$$h = 2, l = 2 \tag{C.34}$$

$$(-1)^{2-2}\delta_{H_1h_1}\delta_{P_1p_1}\delta_{H_2h_2}\sum_{i}^{\text{occ.}} v_{p_2i,P_2i}. \tag{C.35}$$

We will abandon the explicit notation of the permutation terms at this point and return to this issue later on. Together with the 1B part we have

$$\delta_{H_1h_1}\delta_{P_1p_1}\delta_{H_2h_2}\left(t_{p_2,P_2} + \sum_{i}^{\text{occ.}} v_{p_2i,P_2i}\right) \tag{C.36}$$

$$=\delta_{H_1h_1}\delta_{P_1p_1}\delta_{H_2h_2}\epsilon_{p_2,P_2} \tag{C.37}$$

$$=\delta_{H_1h_1}\delta_{P_1p_1}\delta_{H_2h_2}\delta_{p_2P_2}\epsilon_{p_2}. \tag{C.38}$$

The HF energy yields another δ-relation, making it evident that these two diagrams only contribute to the diagonal.

The accompanying 2B diagram to Figure C.6 is

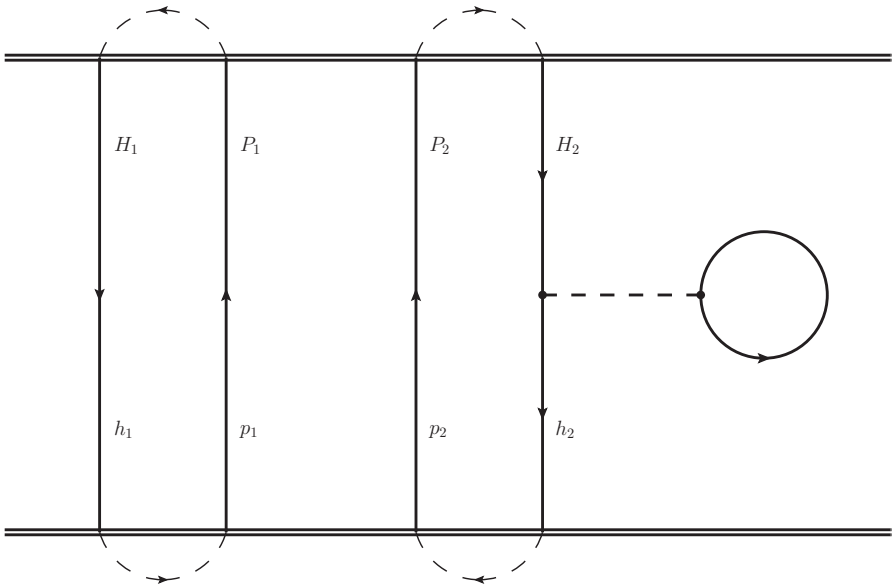

Figure C.8: A_{22}, 2B part, diagram 2.

giving

$$h = 3, l = 2 \tag{C.39}$$

$$(-1)^{3-2}\delta_{H_1h_1}\delta_{P_1p_1}\delta_{P_2p_2}\, v_{h_2i,H_2i}. \tag{C.40}$$

In combination with the 1B terms we get

$$-\delta_{H_1h_1}\delta_{P_1p_1}\delta_{P_2p_2}\left(t_{h_2,H_2} + \sum_{i}^{\text{occ.}} v_{h_2i,H_2i}\right) \tag{C.41}$$

$$=-\delta_{H_1h_1}\delta_{P_1p_1}\delta_{P_2p_2}\epsilon_{h_2,H_2} \tag{C.42}$$

$$=-\delta_{H_1h_1}\delta_{P_1p_1}\delta_{P_2p_2}\delta_{h_2,H_2}\epsilon_{h_2}. \tag{C.43}$$

This is of course also a diagonal contribution. The total diagonal part now reads

$$\delta_{H_1h_1}\delta_{P_1p_1}\delta_{P_2p_2}\delta_{h_2,H_2}(\epsilon_{p_2}-\epsilon_{h_2}). \tag{C.44}$$

This result is very similar to the one of first-order RPA for $A = A_{11}$ (cf. (3.124)). There we also found the HF excitation energies $\epsilon_p - \epsilon_h$ on the diagonal. For SRPA the diagonal again carries the excitation energy. In the above equation this is shown exemplarily for the second index "pair", with the first one giving a likewise contribution stemming from the permutation terms.

Instead of the intrinsic loop we can also connect both half-vertices of the 2B interaction to the external lines. One possible combination for this case is to connect the 2B operator to one particle and one hole from each side, giving the following diagram

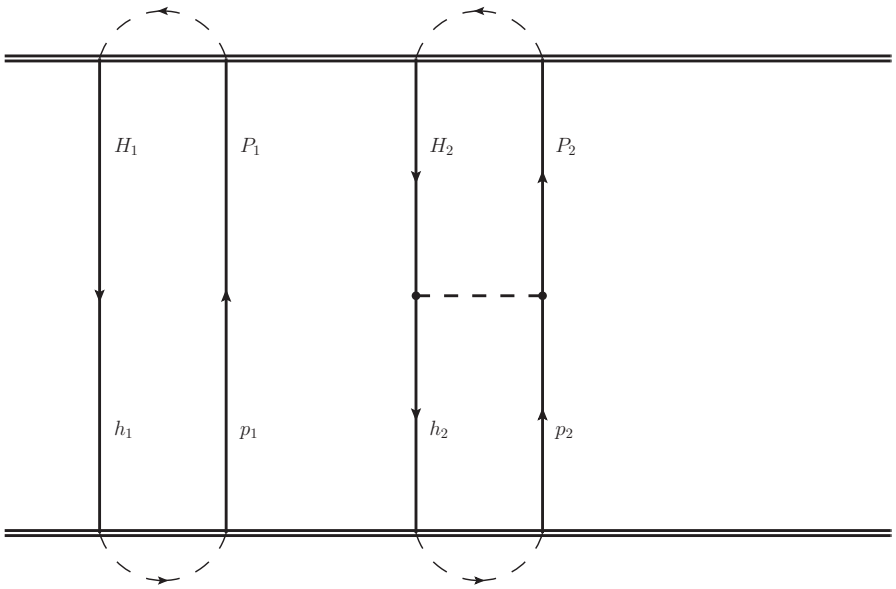

Figure C.9: A_{22}, 2B part, diagram 3.

resulting in

$$h = 3, l = 2 \tag{C.45}$$

$$(-1)^{3-2}\delta_{H_1h_1}\delta_{P_1p_1}\, v_{h_2P_2,H_2p_2}. \tag{C.46}$$

In view of the permutations, we note that $v_{h_2P_2,H_2p_2} \neq v_{h_2P_2,H_2p_1}$, so applying permutations will yield unique terms instead of multiplicities.

Another diagram can be constructed by connecting the 2B operator to all particles lines while simply employing δ-relations between the hole states. The matching diagram is shown in Figure C.10.

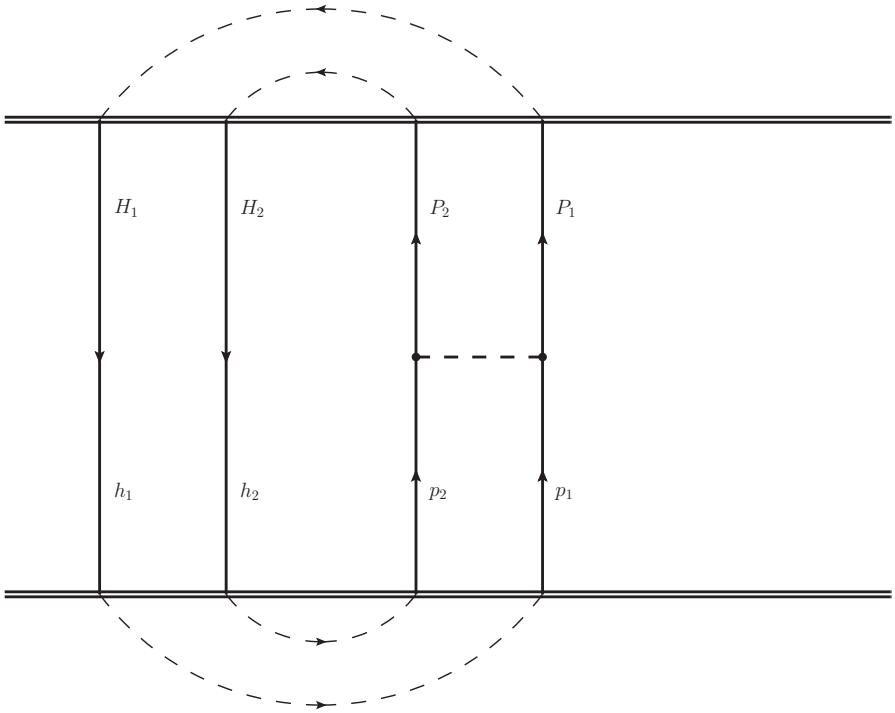

Figure C.10: A_{22}, 2B part, diagram 4.

For the depicted diagram we find the expression

$$h = 2, l = 2 \tag{C.47}$$

$$(-1)^{2-2}\delta_{H_1h_1}\delta_{H_2h_2}\, v_{P_2P_1,p_2p_1}. \tag{C.48}$$

Since $v_{P_2P_1,p_2p_1} = -v_{P_2P_1,p_1p_2}$, the application of the permutations will only yield multiplicities instead of unique contributions.

The last diagram has the same structure as the last one, only now we connect all the hole lines to the 2B operator and use δ-relations for the particle lines

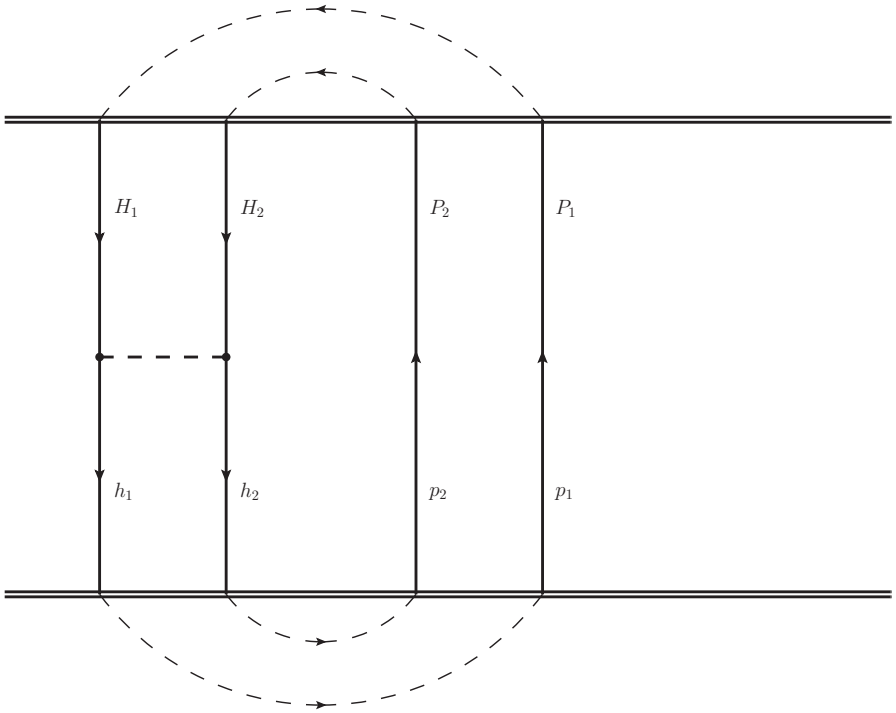

Figure C.11: A_{22}, 2B part, diagram 5.

giving

$$h = 4, l = 2 \tag{C.49}$$

$$(-1)^{4-2}\delta_{P_2p_2}\delta_{P_1p_1}\, v_{h_1h_2,H_1H_2} \tag{C.50}$$

For this diagram the same rules regarding permutations apply as for Figure C.10.

A_{22} m-scheme Formula

In order to build the m-scheme expression for A_{22} we first need to look at the permutations. Normally, for a term of the sort $\delta_{H_1h_1}\delta_{H_2h_2}$ we would expect the following permutations

$$\begin{aligned}(1 - P(H_1, H_2))(1 - P(h_1, h_2))\delta_{H_1h_1}\delta_{H_2h_2} = {}& \delta_{H_1h_1}\delta_{H_2,h_2} - \delta_{H_1h_2}\delta_{H_2,h_1} \\ & - \delta_{H_2h_1}\delta_{H_1,h_2} + \delta_{H_2h_2}\delta_{H_1,h_1}.\end{aligned} \tag{C.51}$$

Keeping in mind that the summation restrictions in the second-order ECO are the following

$$\hat{Q}^\dagger_{2,\omega} = \sum_{\substack{p_1<p_2\\ h_1<h_2}} \left(X^\omega_{p_1h_1,p_2h_2}\, \hat{a}^\dagger_{p_1}\hat{a}_{h_1}\hat{a}^\dagger_{p_2}\hat{a}_{h_2} - Y^\omega_{p_1h_1,p_2h_2}\, \hat{a}^\dagger_{h_1}\hat{a}_{p_1}\hat{a}^\dagger_{h_2}\hat{a}_{p_2}\right) \tag{C.52}$$

we immediately see that while $\delta_{H_1h_2}$ may yield 1, the simultaneous requirement of $\delta_{H_1h_2}$ and δ_{H_2,h_1} vanishes in any case, i.e. $\delta_{H_1h_2}\delta_{H_2,h_1} = 0$. Additionally, the last of the term in (C.51) represents a mere multiplicity and as such no distinct diagram. As a consequence we have to ignore this contribution.

The complete A_{22} matrix without permutations reads

$$\begin{aligned}
[A_{22}]_{p_1p_2h_1h_2;P_1P_2H_1H_2} =& \delta_{H_1h_1}\delta_{P_1p_1}\delta_{P_2p_2}\delta_{h_2,H_2}(\epsilon_{p_2}-\epsilon_{h_2}) && \text{(C.53)}\\
&- \delta_{H_1h_1}\delta_{P_1p_1}\, v_{h_2P_2,H_2p_2} && \text{(C.54)}\\
&+ \delta_{H_1h_1}\delta_{H_2h_2}\, v_{P_2P_1,p_2p_1} && \text{(C.55)}\\
&+ \delta_{P_2p_2}\delta_{P_1p_1}\, v_{h_1h_2,H_1H_2} && \text{(C.56)}
\end{aligned}$$

Applying the permutations consistent with our summation restriction and the requirement of distinctness gives

$$\begin{aligned}
[A_{22}]_{p_1p_2h_1h_2;P_1P_2H_1H_2} =& \delta_{H_1h_1}\delta_{P_1p_1}\delta_{P_2p_2}\delta_{h_2,H_2}(\epsilon_{p_1}+\epsilon_{p_2}-\epsilon_{h_1}-\epsilon_{h_2})\\
&- (1-P(P_1,P_2))(1-P(H_1,H_2))\\
&\times (1-P(p_1,p_2))(1-P(h_1,h_2))\\
&\times \delta_{H_1h_1}\delta_{P_1p_1}\, v_{h_2P_2,H_2p_2}\\
&+ \delta_{H_1h_1}\delta_{H_2h_2}\, v_{P_2P_1,p_2p_1}\\
&+ \delta_{P_2p_2}\delta_{P_1p_1}\, v_{h_1h_2,H_1H_2}. && \text{(C.57)}
\end{aligned}$$

Bibliography

[Ahr+75] J. Ahrens et al. "Total nuclear photon absorption cross sections for some light elements". *Nuclear Physics A* 251.3 (1975), pp. 479–492. ISSN: 03759474. DOI: 10.1016/0375-9474(75)90543-6.

[AL88] S. Adachi and E. Lipparini. "Sum rules in extended RPA theories". *Nuclear Physics, Section A* 489.3 (1988), pp. 445–460. ISSN: 03759474. DOI: 10.1016/0375-9474(88)90006-1.

[AM13] I. Angeli and K. P. Marinova. "Table of experimental nuclear ground state charge radii: An update". *Atomic Data and Nuclear Data Tables* 99.1 (2013), pp. 69–95. ISSN: 0092640X. DOI: 10.1016/j.adt.2011.12.006.

[Bac+14] S. Bacca et al. "Giant and pigmy dipole resonances in He 4, O 16,22, and Ca 40 from chiral nucleon-nucleon interactions". *Physical Review C - Nuclear Physics* 90.6 (2014), pp. 32–40. ISSN: 1089490X. DOI: 10.1103/PhysRevC.90.064619.

[Bar+16] A. Baroni et al. "Nuclear axial currents in chiral effective field theory". *Physical Review C - Nuclear Physics* 93.1 (2016). ISSN: 1089490X. DOI: 10.1103/PhysRevC.93.015501.

[Ber+79] F. Bertrand et al. "Systematics of the isoscalar giant monopole resonance from 60 MeV inelastic proton scattering". *Physics Letters B* 80.3 (1979), pp. 198–202. ISSN: 03702693. DOI: 10.1016/0370-2693(79)90197-7.

[BFS10] S. K. Bogner, R. J. Furnstahl, and A. Schwenk. "From low-momentum interactions to nuclear structure". *Progress in Particle and Nuclear Physics* 65.1 (2010), pp. 94–147. ISSN: 01466410. DOI: 10.1016/j.ppnp.2010.03.001.

[Bin+13] S. Binder et al. "Ab initio calculations of medium-mass nuclei with explicit chiral 3N interactions". *Physical Review C* 87.2 (2013), p. 021303. ISSN: 0556-2813. DOI: 10.1103/PhysRevC.87.021303.

[Bin+14] S. Binder et al. "Ab initio path to heavy nuclei". *Physics Letters B* 736 (2014), pp. 119–123. ISSN: 03702693. DOI: 10.1016/j.physletb.2014.07.010.

[Bin+16] S. Binder et al. "Few-nucleon systems with state-of-the-art chiral nucleon-nucleon forces". *Physical Review C* 93.4 (2016), p. 044002. ISSN: 2469-9985. DOI: 10.1103/PhysRevC.93.044002.

[Bin14] S. Binder. "Coupled-Cluster Theory For Nuclear Structure". PhD thesis. TU Darmstadt, 2014.

[Bir+16] J. Birkhan et al. "Electric dipole polarizability of ^{48}Ca and implications for the neutron skin" (2016), pp. 1–6. arXiv: 1611.07072.

[Bla+09] S. Blanes et al. "The Magnus expansion and some of its applications". *Physics Reports* 470.5-6 (2009), pp. 151–238. ISSN: 03701573.
DOI: 10.1016/j.physrep.2008.11.001.

[Bog+14] S. K. Bogner et al. "Nonperturbative shell-model interactions from the in-medium similarity renormalization group". *Physical Review Letters* 113.14 (2014), pp. 2–6. ISSN: 10797114.
DOI: 10.1103/PhysRevLett.113.142501.

[BW53] K. A. Brueckner and K. M. Watson. "The Construction of Potentials in Quantum Field Theory". *Physical Review* 90.4 (1953), pp. 699–708. ISSN: 0031-899X.
DOI: 10.1103/PhysRev.90.699.

[Cal10] A. Calci. *Ab initio nuclear structure with SRG-transformed chiral NN plus NNN interactions*. 2010.

[Cat+96] F. Catara et al. "Towards a self-consistent random-phase approximation for Fermi systems". *Physical Review B* 54.24 (1996), pp. 17536–17546. ISSN: 0163-1829.
DOI: 10.1103/PhysRevB.54.17536.

[Cat+98] F. Catara et al. "Self-consistent determination of the one-body density matrix and particle-hole excitations". *Physical Review B* 58.24 (1998), pp. 16070–16075. ISSN: 0163-1829.
DOI: 10.1103/PhysRevB.58.16070.

[CDF] CDFE. *Centre for photonuclear experiments data (CDFE)*.

[Číž66] J. Čížek. "On the Correlation Problem in Atomic and Molecular Systems. Calculation of Wavefunction Components in Ursell-Type Expansion Using Quantum-Field Theoretical Methods". *The Journal of Chemical Physics* 45.11 (1966), p. 4256. ISSN: 00219606.
DOI: 10.1063/1.1727484.

[Číž69] J. Čížek. "On the Use of the Cluster Expansion and the Technique of Diagrams in Calculations of Correlation Effects in Atoms and Molecules". *Advances in Chemical Physics* XIV (1969), pp. 35–89. ISSN: 0065-2385.
DOI: 10.1002/9780470143599.ch2.

[CK60] F. Coester and H. Kümmel. "Short-range correlations in nuclear wave functions". *Nuclear Physics* 17 (1960), pp. 477–485. ISSN: 00295582.
DOI: 10.1016/0029-5582(60)90140-1.

[Coe58] F. Coester. "Bound states of a many-particle system". *Nuclear Physics* 7 (1958), pp. 421–424. ISSN: 00295582.
DOI: 10.1016/0029-5582(58)90280-3.

[Col+13] G. Colò et al. "Self-consistent RPA calculations with Skyrme-type interactions: The skyrme_rpa program". *Computer Physics Communications* 184.1 (2013), pp. 142–161. ISSN: 00104655.
DOI: 10.1016/j.cpc.2012.07.016.

[Con30] E. Condon. "Theory of complex spectra". *Physical Review* 36 (1930), pp. 1121–1133.
DOI: https://dx.doi.org/10.1103%2FPhysRev.36.1121.

[CR16] A. Calci and R. Roth. "Sensitivities and correlations of nuclear structure observables emerging from chiral interactions". *Physical Review C - Nuclear Physics* 94.1 (2016), pp. 1–11. ISSN: 1089490X.
DOI: 10.1103/PhysRevC.94.014322.

[CS00] T. Crawford and H. Schaefer III. "An introduction to coupled cluster theory for computational chemists". *Reviews of Computational Chemistry, Volume 14* 14.Ccd (2000), pp. 33–136.
DOI: 10.1002/9780470125915.ch2.

[Dea73] T. J. Deal. "Isoscalar dipole resonances". *Nuclear Physics A* 217.1 (1973), pp. 210–220. ISSN: 03759474.
DOI: 10.1016/0375-9474(73)90634-9.

[DON14] N. M. Dicaire, C. Omand, and P. Navrátil. "Alternative similarity renormalization group generators in nuclear structure calculations". *Physical Review C* 90.3 (2014), p. 034302. ISSN: 0556-2813.
DOI: 10.1103/PhysRevC.90.034302.

[Eck30] C. Eckart. "The Application of Group theory to the Quantum Dynamics of Monatomic Systems". *Reviews of Modern Physics* 2.3 (1930), pp. 305–380. ISSN: 0034-6861.
DOI: 10.1103/RevModPhys.2.305.

[EKM15a] E. Epelbaum, H. Krebs, and U. G. Meißner. "Improved chiral nucleon-nucleon potential up to next-to-next-to-next-to-leading order". *European Physical Journal A* 51.5 (2015). ISSN: 1434601X.
DOI: 10.1140/epja/i2015-15053-8.

[EKM15b] E. Epelbaum, H. Krebs, and U. G. Meißner. "Precision Nucleon-Nucleon Potential at Fifth Order in the Chiral Expansion". *Physical Review Letters* 115.12 (2015), pp. 1–5. ISSN: 10797114.
DOI: 10.1103/PhysRevLett.115.122301.

[Eks+15] A. Ekström et al. "Accurate nuclear radii and binding energies from a chiral interaction". *Physical Review C* 91.5 (2015), p. 051301. ISSN: 0556-2813.
DOI: 10.1103/PhysRevC.91.051301.

[EM03] D. R. Entem and R. Machleidt. "Accurate charge-dependent nucleon-nucleon potential at fourth order of chiral perturbation theory". *Physical Review C* 68.4 (2003), p. 041001. ISSN: 0556-2813.
DOI: 10.1103/PhysRevC.68.041001.

[EMN10] G. Ecker, P. Masjuan, and H. Neufeld. "Chiral extrapolation and determination of low-energy constants from lattice data". *Physics Letters B* 692.3 (2010), pp. 184–188. ISSN: 03702693.
DOI: 10.1016/j.physletb.2010.07.037.

[Erl12] B. Erler. "Mean-Field Approach to Collective Excitations in Deformed sd-Shell Nuclei Using Realistic Interactions". PhD thesis. TU Darmstadt, 2012.

[Ero+03] V. A. Erokhova et al. "Giant resonance in nuclei of calcium isotopes". *Bulletin of the Russian Academy of Science, Physics* 67.10 (2003), pp. 1636–1639.

[Gam+12] D. Gambacurta et al. "Second random-phase approximation with the Gogny force: First applications". *Physical Review C* 86.2 (2012), p. 021304. ISSN: 0556-2813.
DOI: 10.1103/PhysRevC.86.021304.

[GC08] D. Gambacurta and F. Catara. "Particle-hole excitations within a self-consistent random-phase approximation". *Physical Review B* 77.20 (2008), pp. 1–9. ISSN: 1098-0121.
DOI: 10.1103/PhysRevB.77.205434.

[GCR16] E. Gebrerufael, A. Calci, and R. Roth. "Open-shell nuclei and excited states from multireference normal-ordered Hamiltonians". *Physical Review C - Nuclear Physics* 93.3 (2016), pp. 1–6. ISSN: 1089490X.
DOI: 10.1103/PhysRevC.93.031301.

[GGC10] D. Gambacurta, M. Grasso, and F. Catara. "Collective nuclear excitations with Skyrme-second random-phase approximation". *Physical Review C* 81.5 (2010), p. 054312. ISSN: 0556-2813.
DOI: 10.1103/PhysRevC.81.054312.

[GGC11] D. Gambacurta, M. Grasso, and F. Catara. "Low-lying dipole response in the stable

40,48Ca nuclei with the second random-phase approximation". *Physical Review C* 84.3 (2011), p. 034301. ISSN: 0556-2813.
DOI: 10.1103/PhysRevC.84.034301.

[GPR14] A. Günther, P. Papakonstantinou, and R. Roth. "Giant resonances based on unitarily transformed two-nucleon plus phenomenological three-nucleon interactions". *Journal of Physics G: Nuclear and Particle Physics* 41.11 (2014), p. 115107. ISSN: 0954-3899.
DOI: 10.1088/0954-3899/41/11/115107.

[GQN09] D. Gazit, S. Quaglioni, and P. Navrátil. "Three-Nucleon Low-Energy Constants from the Consistency of Interactions and Currents in Chiral Effective Field Theory". *Physical Review Letters* 103.10 (2009), p. 102502. ISSN: 0031-9007.
DOI: 10.1103/PhysRevLett.103.102502.

[GT48] M. Goldhaber and E. Teller. "On Nuclear Dipole Vibrations". *Physical Review* 74.9 (1948), pp. 1046–1049. ISSN: 0031-899X.
DOI: 10.1103/PhysRev.74.1046.

[Gün11] A. Günther. "Nuclear Structure with Unitarily Transformed Two-Body plus Phenomenological Three-Body Interactions". PhD thesis. TU Darmstadt, 2011.

[Hag+07] G. Hagen et al. "Coupled-cluster theory for three-body Hamiltonians". *Physical Review C - Nuclear Physics* 76.3 (2007), pp. 1–11. ISSN: 05562813.
DOI: 10.1103/PhysRevC.76.034302.

[Hag+10] G. Hagen et al. "Ab initio coupled-cluster approach to nuclear structure with modern nucleon-nucleon interactions". *Physical Review C - Nuclear Physics* 82.3 (2010), pp. 1–22. ISSN: 05562813.
DOI: 10.1103/PhysRevC.82.034330.

[HD81] M. N. Harakeh and A. E. L. Dieperink. "Isoscalar dipole resonance: Form factor and energy weighted sum rule". *Physical Review C* 23.5 (1981), pp. 2329–2334. ISSN: 0556-2813.
DOI: 10.1103/PhysRevC.23.2329.

[Her+13a] H. Hergert et al. "Ab initio calculations of even oxygen isotopes with chiral two-plus-three-nucleon interactions". *Physical Review Letters* 110.24 (2013), pp. 1–6. ISSN: 00319007.
DOI: 10.1103/PhysRevLett.110.242501.

[Her+13b] H. Hergert et al. "In-medium similarity renormalization group with chiral two- plus three-nucleon interactions". *Physical Review C* 87.3 (2013), p. 034307. ISSN: 0556-2813.
DOI: 10.1103/PhysRevC.87.034307.

[Her+14] H. Hergert et al. "Ab initio multireference in-medium similarity renormalization group calculations of even calcium and nickel isotopes". *Physical Review C - Nuclear Physics* 90.4 (2014), pp. 1–6. ISSN: 1089490X.
DOI: 10.1103/PhysRevC.90.041302.

[Her+16] H. Hergert et al. "The In-Medium Similarity Renormalization Group: A novel ab initio method for nuclei". *Physics Reports* 621 (2016), pp. 165–222. ISSN: 03701573.
DOI: 10.1016/j.physrep.2015.12.007.

[Her16] H. Hergert. "In-Medium Similarity Renormalization Group for Closed and Open-Shell Nuclei" (2016).
arXiv: 1607.06882.

[HPR11] H. Hergert, P. Papakonstantinou, and R. Roth. "Quasiparticle random-phase approximation with interactions from the Similarity Renormalization Group". *Physical Review C* 83.6 (2011). ISSN: 0556-2813.
DOI: 10.1103/PhysRevC.83.064317.

[HV01] M. N. Harakeh and A. Van Der Woude. *Giant Resonances: Fundamental High-Frequency Modes of Nuclear Excitation*. Oxford science publications. Oxford University Press on Demand, 2001. ISBN: 9780198517337.
DOI: 10.1604/9780198517337.

[JNF09] E. D. Jurgenson, P. Navrátil, and R. J. Furnstahl. "Evolution of Nuclear Many-Body Forces with the Similarity Renormalization Group". *Physical Review Letters* 103.8 (2009), p. 082501. ISSN: 0031-9007.
DOI: 10.1103/PhysRevLett.103.082501.

[Jur+08] E. Jurgenson et al. "Decoupling in the similarity renormalization group for nucleon-nucleon forces". *Physical Review C* 78.1 (2008), p. 014003. ISSN: 0556-2813.
DOI: 10.1103/PhysRevC.78.014003.

[Koc97] V. Koch. "Aspects of Chiral Symmetry". *International Journal of Modern Physics E* 06.02 (1997), pp. 203–249. ISSN: 0218-3013.
DOI: 10.1142/S0218301397000147.

[Kou+96] H. Kouno et al. "Incompressibility of nuclear matter, and Coulomb and volume-symmetry coefficients of nucleus incompressibility in the relativistic mean field theory". *Physical Review C - Nuclear Physics* 53.5 (1996), pp. 2542–2545. ISSN: 05562813.
DOI: 10.1103/PhysRevC.53.2542.

[LCY01] Y.-W. Lui, H. L. Clark, and D. H. Youngblood. "Giant resonances in 16O". *Physical Review C* 64.6 (2001), p. 064308. ISSN: 0556-2813.
DOI: 10.1103/PhysRevC.64.064308.

[LNH87] S. F. LeBrun, A. M. Nathan, and S. D. Hoblit. "Photon scattering in the giant dipole resonance region of ^{16}O". *Physical Review C* 35.6 (1987), pp. 2005–2010. ISSN: 0556-2813.
DOI: 10.1103/PhysRevC.35.2005.

[Lui+11] Y.-W. Lui et al. "Isoscalar giant resonances in ^{48}Ca". *Physical Review C* 83.4 (2011), p. 044327. ISSN: 0556-2813.
DOI: 10.1103/PhysRevC.83.044327.

[Mag54] W. Magnus. "On the exponential solution of differential equations for a linear operator". *Communications on pure and applied ...* VII (1954), pp. 649–673. ISSN: 00103640.
DOI: 10.1002/cpa.3160070404.

[ME11] R. Machleidt and D. R. Entem. "Chiral effective field theory and nuclear forces". *Physics Reports* 503.1 (2011), pp. 1–75. ISSN: 03701573.
DOI: 10.1016/j.physrep.2011.02.001.

[Mio+16] M. Miorelli et al. "Electric dipole polarizability from first principles calculations". 034317 (2016), pp. 1–11. ISSN: 1089490X.
DOI: 10.1103/PhysRevC.94.034317.

[Miş06] Ş. Mişicu. "Interplay of compressional and vortical nuclear currents in overtones of the isoscalar giant dipole resonance". *Physical Review C* 73.2 (2006), p. 024301. ISSN: 0556-2813.
DOI: 10.1103/PhysRevC.73.024301.

[Mon+08] C. Monrozeau et al. "First Measurement of the Giant Monopole and Quadrupole Resonances in a Short-Lived Nucleus: Ni56". *Physical Review Letters* 100.4 (2008), p. 042501. ISSN: 0031-9007.
DOI: 10.1103/PhysRevLett.100.042501.

[MPB15] T. D. Morris, N. M. Parzuchowski, and S. K. Bogner. "Magnus expansion and in-

medium similarity renormalization group". *Physical Review C - Nuclear Physics* 92.3 (2015). ISSN: 1089490X.
DOI: 10.1103/PhysRevC.92.034331.

[Nav07] P. Navrátil. "Local three-nucleon interaction from chiral effective field theory". *Few-Body Systems* 41.3-4 (2007), pp. 117–140. ISSN: 0177-7963.
DOI: 10.1007/s00601-007-0193-3.

[OKe+87] G. O'Keefe et al. "The photonuclear cross sections of 48Ca". *Nuclear Physics A* 469.2 (1987), pp. 239–252. ISSN: 03759474.
DOI: 10.1016/0375-9474(87)90108-4.

[Paa+06] N. Paar et al. "Collective multipole excitations based on correlated realistic nucleon-nucleon interactions". *Physical Review C* 74.1 (2006), p. 014318. ISSN: 0556-2813.
DOI: 10.1103/PhysRevC.74.014318.

[Pap+12] P. Papakonstantinou et al. "Low-energy dipole strength and the critical case of 48Ca". *Physics Letters B* 709.3 (2012), pp. 270–275. ISSN: 03702693.
DOI: 10.1016/j.physletb.2012.02.024.

[Pap07] P. Papakonstantinou. "Reduction of the RPA eigenvalue problem and a generalized Cholesky decomposition for real-symmetric matrices". *Europhysics Letters (EPL)* 78.1 (2007), p. 12001. ISSN: 0295-5075.
DOI: 10.1209/0295-5075/78/12001.

[Pap14] P. Papakonstantinou. "Second random-phase approximation, Thouless' theorem, and the stability condition reexamined and clarified". *Physical Review C* 90.2 (2014), p. 024305. ISSN: 0556-2813.
DOI: 10.1103/PhysRevC.90.024305.

[Pas+09] S. Pastore et al. "Electromagnetic currents and magnetic moments in chiral effective field theory (χEFT)". *Physical Review C* 80.3 (2009), p. 034004. ISSN: 0556-2813.
DOI: 10.1103/PhysRevC.80.034004.

[Pie11] J. Piekarewicz. "Pygmy resonances and neutron skins". *Physical Review C - Nuclear Physics* 83.3 (2011), pp. 1–10. ISSN: 05562813.
DOI: 10.1103/PhysRevC.83.034319.

[PÍS72] J. Paldus, J. Íek, and I. Shavitt. "Correlation problems in atomic and molecular systems. IV. Extended coupled-pair many-electron theory and its application to the BH3 molecule". *Physical Review A* 5.1 (1972), pp. 50–67. ISSN: 10502947.
DOI: 10.1103/PhysRevA.5.50.

[PR09] P. Papakonstantinou and R. Roth. "Second random phase approximation and renormalized realistic interactions". *Physics Letters B* 671.3 (2009), pp. 356–360. ISSN: 03702693.
DOI: 10.1016/j.physletb.2008.12.037.

[PR10] P. Papakonstantinou and R. Roth. "Large-scale second random-phase approximation calculations with finite-range interactions". *Physical Review C* 81.2 (2010), p. 024317. ISSN: 0556-2813.
DOI: 10.1103/PhysRevC.81.024317.

[Pro65] J. da Providência. "Variational approach to the many-body problem". *Nuclear Physics* 61.1 (1965), pp. 87–96. ISSN: 00295582.
DOI: 10.1016/0029-5582(65)90937-5.

[PRP07] P. Papakonstantinou, R. Roth, and N. Paar. "Nuclear collective excitations using correlated realistic interactions: The role of explicit random-phase approximation correlations". *Physical Review C* 75.1 (2007), p. 014310. ISSN: 0556-2813.
DOI: 10.1103/PhysRevC.75.014310.

[PSG08] S. Pastore, R. Schiavilla, and J. Goity. "Electromagnetic two-body currents of one- and two-pion range". *Physical Review C* 78.6 (2008), p. 064002. ISSN: 0556-2813. DOI: 10.1103/PhysRevC.78.064002.

[RNF10] R. Roth, T. Neff, and H. Feldmeier. "Nuclear structure in the framework of the Unitary Correlation Operator Method". *Progress in Particle and Nuclear Physics* 65.1 (2010), pp. 50–93. ISSN: 01466410. DOI: 10.1016/j.ppnp.2010.02.003.

[Ros+13] D. M. Rossi et al. "Measurement of the dipole polarizability of the unstable neutron-rich nucleus Ni68". *Physical Review Letters* 111.24 (2013), pp. 1–6. ISSN: 00319007. DOI: 10.1103/PhysRevLett.111.242503.

[Rot+06] R. Roth et al. "Hartree-Fock and many body perturbation theory with correlated realistic NN interactions". *Physical Review C* 73.4 (2006), p. 044312. ISSN: 0556-2813. DOI: 10.1103/PhysRevC.73.044312.

[Rot+12] R. Roth et al. "Medium-Mass Nuclei with Normal-Ordered Chiral NN+ 3N Interactions". *Physical Review Letters* 109.5 (2012), pp. 1–5. ISSN: 0031-9007. DOI: 10.1103/PhysRevLett.109.052501.

[Row70] D. J. Rowe. *Nuclear Collective Motion*. Methuen, 1970. ISBN: 9780416449600. ISBN: 9780416449600.

[RS80] P. Ring and P. Schuck. *The Nuclear Many-Body Problem*. 3rd ed. Physics and astronomy online library. Berlin, Heidelberg: Springer Berlin Heidelberg, 1980. ISBN: 978-3-540-21206-5. DOI: 10.1007/978-3-642-61852-9.

[SB09] I. Shavitt and R. J. Bartlett. *Many-body methods in chemistry and physics*. Cambridge: Cambridge University Press, 2009.

[SJ03] I. Stetcu and C. W. Johnson. "Tests of the random phase approximation for transition strengths". *Physical Review C* 67.4 (2003), pp. 1–10. ISSN: 0556-2813. DOI: 10.1103/PhysRevC.67.044315.

[Sla29] J. C. Slater. "The theory of complex spectra". *Physical Review* 34.10 (1929), pp. 1293–1322. ISSN: 0031899X. DOI: 10.1103/PhysRev.34.1293.

[Ste+05] I. Stetcu et al. "Effective operators within the ab initio no-core shell model". *Physical Review C* 71.4 (2005), p. 044325. ISSN: 0556-2813. DOI: 10.1103/PhysRevC.71.044325.

[Str+00] S. Strauch et al. "Giant Resonances in the Doubly Magic Nucleus ^{48}Ca from the $(e, e'n)$ Reaction". *Physical Review Letters* 85.14 (2000), pp. 2913–2916. ISSN: 0031-9007. DOI: 10.1103/PhysRevLett.85.2913.

[Suh07] J. Suhonen. *From nucleons to nucleus*. Springer, 2007. ISBN: 9783540488590. DOI: 10.1007/978-3-540-48861-3.

[TBS11] K. Tsukiyama, S. K. Bogner, and A. Schwenk. "In-medium similarity renormalization group for nuclei". *Physical Review Letters* 106.22 (2011), pp. 7–10. ISSN: 00319007. DOI: 10.1103/PhysRevLett.106.222502.

[TBS12] K. Tsukiyama, S. K. Bogner, and A. Schwenk. "In-medium similarity renormalization group for open-shell nuclei". *Physical Review C - Nuclear Physics* 85.6 (2012), pp. 4–7. ISSN: 05562813. DOI: 10.1103/PhysRevC.85.061304.

[Tho60] D. Thouless. "Stability conditions and nuclear rotations in the Hartree-Fock theory". *Nuclear Physics* 21 (1960), pp. 225–232. ISSN: 00295582.
DOI: 10.1016/0029-5582(60)90048-1.

[Tho61] D. Thouless. "Vibrational states of nuclei in the random phase approximation". *Nuclear Physics* 22.1 (1961), pp. 78–95. ISSN: 00295582.
DOI: 10.1016/0029-5582(61)90364-9.

[TMO52] M. Taketani, S. Machida, and S. O-numa. "The Meson Theory of Nuclear Forces, I: The Deuteron Ground State and Low Energy Neutron-Proton Scattering". *Progress of Theoretical Physics* 7.1 (1952), pp. 45–56. ISSN: 0033-068X.
DOI: 10.1143/ptp/7.1.45.

[Tri13] R. Trippel. *Collective Excitations with Chiral NN+3N interactions*. 2013.

[TS04] M. Tohyama and P. Schuck. "Spurious modes in Extended RPA theories". *The European Physical Journal A - Hadrons and Nuclei* 19.2 (2004), pp. 203–213. ISSN: 1434-6001.
DOI: 10.1140/epja/i2003-10110-7.

[Tse13] V. I. Tselyaev. "Subtraction method and stability condition in extended random-phase approximation theories". *Physical Review C* 88.5 (2013), p. 054301. ISSN: 0556-2813.
DOI: 10.1103/PhysRevC.88.054301.

[Ull72] N. Ullah. "On the Reduction of the Generalized RPA Eigenvalue Problem". *Journal of Mathematical Physics* 13.8 (1972), p. 1163. ISSN: 00222488.
DOI: 10.1063/1.1666116.

[UR71] N. Ullah and D. Rowe. "Properties of real RPA matrices and a simple diagonalization procedure". *Nuclear Physics A* 163.1 (1971), pp. 257–264. ISSN: 03759474.
DOI: 10.1016/0375-9474(71)90534-3.

[Van+14] M. Vandebrouck et al. "Measurement of the isoscalar monopole response in the neutron-rich nucleus Ni 68". *Physical Review Letters* 113.3 (2014), pp. 1–5. ISSN: 10797114.
DOI: 10.1103/PhysRevLett.113.032504.

[Van+15] M. Vandebrouck et al. "Isoscalar response of 68Ni α-particle and deuteron probes". *Physical Review C* 92.2 (2015), p. 024316. ISSN: 0556-2813.
DOI: 10.1103/PhysRevC.92.024316.

[Vey+74] A. Veyssière et al. "A study of the photoneutron contribution to the giant dipole resonance of s-d shell nuclei". *Nuclear Physics A* 227.3 (1974), pp. 513–540. ISSN: 03759474.
DOI: 10.1016/0375-9474(74)90774-X.

[Vob14] K. Vobig. *In-Medium Similarity Renormalization Group with Chiral NN + 3N Interactions*. 2014.

[VS81] N. Van Giai and H. Sagawa. "Monopole and dipole compression modes in nuclei". *Nuclear Physics A* 371.1 (1981), pp. 1–18. ISSN: 03759474.
DOI: 10.1016/0375-9474(81)90741-7.

[Wan+12] M. Wang et al. "The A ME 2012 atomic mass evaluation (II). Tables , graphs and references". *Chinese Physics C* 36.12 (2012), pp. 1603–2014. ISSN: 03759474.
DOI: 10.1016/j.nuclphysa.2003.11.002.

[Weg01] F. J. Wegner. "Flow equations for Hamiltonians". *Physics Reports* 348.1-2 (2001), pp. 77–89. ISSN: 03701573.
DOI: 10.1016/S0370-1573(00)00136-8.

[Weg94] F. J. Wegner. "Flow equations for Hamiltonians". *Advances in Solid State Physics 40*. Vol. 3. Berlin, Heidelberg: Springer Berlin Heidelberg, 1994, pp. 133–142.
DOI: 10.1007/BFb0108350.

[Wei79] S. Weinberg. "Phenomenological Lagrangians". *Physica A: Statistical Mechanics and its Applications* 96.1-2 (1979), pp. 327–340. ISSN: 03784371.
DOI: 10.1016/0378-4371(79)90223-1.

[Whi02] S. R. White. "Numerical canonical transformation approach to quantum many-body problems". *Journal of Chemical Physics* 117.16 (2002), pp. 7472–7482. ISSN: 00219606.
DOI: 10.1063/1.1508370.

[Wic50] G. C. Wick. "The Evaluation of the Collision Matrix". *Physical Review* 80.2 (1950), pp. 268–272. ISSN: 0031-899X.
DOI: 10.1103/PhysRev.80.268.

[Wig31] E. Wigner. *Gruppentheorie und ihre Anwendung auf die Quantenmechanik der Atomspektren*. Wiesbaden: Vieweg+Teubner Verlag, 1931. ISBN: 978-3-663-00642-8.
DOI: 10.1007/978-3-663-02555-9.

[Yan87] C. Yannouleas. "Zero-temperature second random phase approximation and its formal properties". *Physical Review C* 35.3 (1987), pp. 1159–1161. ISSN: 0556-2813.
DOI: 10.1103/PhysRevC.35.1159.

[YCL99] D. H. Youngblood, H. L. Clark, and Y.-W. Lui. "Incompressibility of Nuclear Matter from the Giant Monopole Resonance". *Physical Review Letters* 82.4 (1999), pp. 691–694. ISSN: 0031-9007.
DOI: 10.1103/PhysRevLett.82.691.

[YLC01] D. H. Youngblood, Y.-W. Lui, and H. L. Clark. "Isoscalar E0, E1, and E2 strength in ^{40}Ca". *Physical Review C* 63.6 (2001), p. 067301. ISSN: 0556-2813.
DOI: 10.1103/PhysRevC.63.067301.

Acknowledgements

First of all, I would like to thank Prof. Robert Roth for giving me the opportunity to work in his group, and also Prof. Achim Schwenk for agreeing to be the second reviewer of my thesis.

I thank the entire group and my office colleagues for the pleasant atmosphere. In particular, many thanks go to Sven Binder and Klaus Vobig for providing me with the necessary matrix elements for my calculations, and also to Roland Wirth for his ongoing tech support.

Special thanks go to Panagiota Papakonstantinou for helpful discussions about RPA and for providing me with the initial code.

My thanks also go to my family, my friends & Bros and of course Ilka for their continuous support.

Finally, I also would like to thank the Giants for *literally* giving me strength, and last but not least I thank my dear Luke for some nice brewing sessions and for, mayhaps the greatest challenge of all, the incredible niveaulimbo.

PS: It was legen... wait for it... dary.

Lebenslauf

Zur Person

Name:	Richard Trippel
Geburtsdatum:	02.10.1987
Geburtsort:	Langen
Nationalität:	deutsch

Bildungsweg

1998–2007	**Gymnasium**, Dreieichschule Langen
2007–2010	**Bachelorstudium Physik**, TU Darmstadt
2010–2013	**Master Studium Physik**, TU Darmstadt
2013–2016	**Promotionsstudium Physik**, TU Darmstadt

Erklärung zur Dissertation

Hiermit versichere ich, die vorliegende Dissertation ohne Hilfe Dritter nur mit den angegebenen Quellen und Hilfsmitteln angefertigt zu haben. Alle Stellen, die aus Quellen entnommen wurden, sind als solche kenntlich gemacht. Diese Arbeit hat in gleicher oder ähnlicher Form noch keiner Prüfungsbehörde vorgelegen.

Darmstadt, den 22.11.2016

_____

Richard Trippel